Master's Thesis in Aerospace Engineering

Preliminary design of deployable habitat for lunar outpost made by innovative material

Federico Cumino

Polytechnic of Turin
Accademic year 2019/2020

Polytechnic rapporteur	Frulla Giacomo
Polytechnic co-rapporteur	Cestino Enrico
CoRe external supervisors	Giulietti Nicola
	Fossat Eugenio

This page intentionally left blank

Dedicated to all those
who still want to dream.

This page intentionally left blank

Contents

Preface

"The Moon has always held the fascination of man, a symbol of cosmic proportions. It has inspired lovers, poets, writers, and scientists through time. The Apollo missions, by placing man on the moon have not destroyed that inspiration, but have directed it towards people who envision the full utilization of what the moon has to offer to mankind, i.e., lunar bases to house people, resource development, answers to questions on planetary formation and early development of the Earth, etc. Long term exploration of space needs a laboratory for testing out equipment, and human limits, and the closeness of the moon provides an obvious stepping stone to further space exploration in the future. (At the time of this report, Code X at NASA has been dissolved, bringing the Space Exploration Initiative envisioned by President Bush, to a standstill, hopefully only temporarily)."

[Gani B. Ganapathi, Joseph Ferrall and P. K. Seshan. "Lunar Base Habitat Designs: Characterizing the Environment, and Selecting Habitat".]

I have found this poetical introduction in a paper while I was searching material for my thesis. I have been so deeply touched by the beautiful words of the first part of the text, that I thought that my thesis could not begin if not with it.
In the last line it is clearly evident a veil of melancholy. Today I would say to the authors that nothing is really ended; the works and efforts of the past generations will always be a point of progression and inspiration for the new ones, in a continuous cycle that will never stop.
I personally hope that a common goal like the Moon could be the right motivation to become more united as mankind and finally leave our hatred and our conflicts back, in order to concentrate on only one great challenge that could inspire and change each of us. As the American President J. F. Kennedy said: "We choose to go to the Moon in this decade and do the other things, not because they are easy, but because they are hard" and I see in this difficulty the motivation to become better human beings.
Finally I am grateful for this opportunity and I would say to each one of you to never stop dreaming and believe in yourself, because it is the more beautiful capability that a person could have and the spark of our evolution.

Federico Cumino

Abstract

The major limitations in space exploration are the mass and volume of payload, transportable by a launch vehicle. With a view to a future colonization of the Moon, achieved by the transportation of habitats on its surface, this assumes a crucial role. The aim of this thesis is to provide a solution to this problem by using an innovative material for the habitat structure, which has very low weight and the possibility to be rolled in very small radius. Its name is MadFLex. This material has the amazing ability to be flexible on one side and rigid on the other one. Compared to conventional rigid structures, MadFlex would enable the realization of deployable habitat, with considerable savings in volume and weight in the transport phase. The necessary requirements to protect astronauts from space hazards were developed after a first analysis of the Moon environmental features. On this basis, the preliminary configurations were then investigated, in order to understand their feasibility and possibility to be stored in a rolled configuration. The preliminary design was mainly investigated from a structural point of view, providing maximum displacement of the structure in the worst load condition, radius of bending in transport configuration and the total weight.

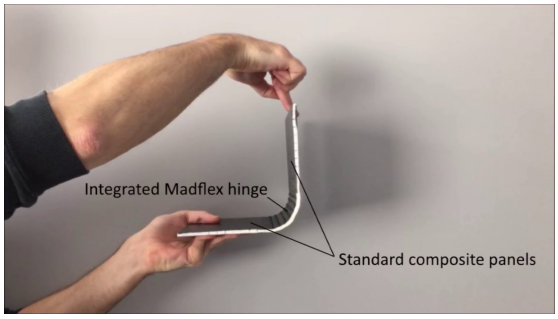

Figure 1: The MadFlex

Chapter 1

Why the Moon

From the 14th December 1972 the mankind never set foot on the Moon again. These efforts in the 1990s were certainly faced due to the constant pressure of the Cold War, which by a fortunate series of events moved its battlefield from Earth to Space. Many new technologies were developed by each of the two part and many of them are still fundamental in everyday life. In the current new sociopolitical-cultural context, that sees the world in a global way, the push to reach the Moon or other planets could represent the simple need for knowledge and new resources. As demonstrated over the past three decades, an international effort could lead to better results than one done by individuals.
Following this idea many goals have been achieved in recent years, including the most important: the construction of the ISS (International Space Station). Fourteen nations were involved in the development of the station and many modules, experiments and people had the honor of docking and being guests of the ISS.
Another mission saw the landing on the red planet, Mars, with the fist rover in the 1997 Sojourner (Mars Pathfinder mission). A good number of other missions also reached the planet: the two twin rovers Spirit and Opportunity (2004),on the two opposite sides of Mars, Curiosity (2012) and the Schiaparelli lander, the first European effort, within the ExoMars mission, ended with a small failure. However precisely on this day, 30 July 2020, a new rover was launched and it will bring the robotic presence of man on Mars: Perseverance.
Other types of mission saw the landing on a comet, Rosetta (2014), the exploration of an asteroid, Hayabusa 2 (2018), and the landing on the dark side of the Moon with the Chang'e 4 mission and the yutu2 rover (2013). If in the past one of the limits of reaching the Moon or Mars was the cost of the launcher, now this problem is almost completely solved. New private companies like Space X have appeared on the space scene and brought the idea, now reality, of a new generation of reusable space vehicle, as the Falcon 9 and Falcon heavy. Now the idea of Elon Musk, the founder of Space X, is to build a vehicle to go to the moon, and the first tests have been already done (Starship).
Space X is not the only private company investing in this business. The concept of Space as an inaccessible place except for a few people is rapidly changing and the idea of commercial travels and space tourism are coming with its good and bad aspects. Other companies are: Blue Origin, Virgin Galactic, Bigelow Aerospace, but they are many more.

In conclusion, the Orion mission and the launcher associated with it, that will bring man back to the moon, is almost ready. The vehicle's name is Space Launch System (SLS) and was designed by NASA after the dissolution of the Constellation program, which was considered too expensive.
Another noteworthy data is the agreement signed with NASA, Roscosmos, ESA and JAXA for the development of a new lunar orbital station: Lunar Orbital Platform-Gateway with the start date of the works scheduled for 2020.
The Moon and Mars are not as far apart as they used to be.
Despite this explanation on the international stage, an answer to the main question used as the title of the chapter, has not been given yet. As the reader can imagine this is not a simple question and a synthesis of all philosophical, scientific and engineering reasoning is needed.
"Why do we need to go to the Moon? Many researchers believe robotic exploration is the best way to conduct most space science. Others disagree. Only humans can properly investigate other worlds, they say, to answer the most pressing questions about the origin and fate of humans and the possibility that life exists elsewhere" [1]. A lot of different opinions are discussed in literature, but following the scheme presented in the paper "Structural Design of a Lunar Habitat" it is possible to provide an almost complete motivation.

Accessibility The Moon is orbiting the Earth at an average distance of 374977 km. As mentioned before, not a great distance with the today possibilities, considering the almost concluded SLS (Space Launch System), which will bring man back to the Moon with the Orion program. The journey with today's technology is three days long and the delay in radio communications is within a tolerable level to allow teleoperation [2].

Inspiration The human being not only has the simple physiological needs, but he also needs to know and understand. Indeed, one of our main characteristics is curiosity. This makes the human being a restless being and it is precisely this characteristic that leads him to evolve and always discover new things, overcoming the sea, air and space with the sole purpose of finding an answer to the fundamental question: who are we?

International Cooperation "There are several reasons why a lunar base project should be an international effort. First, any effort by nations alone would be unnecessarily redundant and limited in scope. Second, it is the intention of the ratified outer space treaties that space development should be a peaceful endeavor, for the benefit of all people. Third, cooperation between nations on lunar base planning, construction, operations and growth, has the potential to create and strengthen peaceful relations between nations" [1], especially in an era of increasing international tension.

Geology With the Apollo mission about 2415 samples with a mass of 382 kg were brought to Earth. However, many questions about the Moon have not been answered yet.
The material from the Moon is not only important for understand the history of the Moon himself, but also the one of the space environment over millions of years. This is possible due to the absence of an atmosphere on the Moon (the

main cause of soil erosion on Earth) and a significant seismic activity.
There will not be advantages in creating a lunar base only for planetary scientists, but also for many other scientists, such as physicists, biologists, paleontologist. It will even bring new knowledge in the field of psychology and sociology.

Astronomy The absence of an atmosphere identifies the Moon as the perfect place to install optical telescopes to observe the universe in a similar way to what the Hubble Space Telescope did. Without the presence of air, the common disturbance of light dispersion, present on Earth, is resolved.
"Moreover Radio telescopes could be placed on the far side of the Moon. There they would be shielded from all the radio noise of Earth" [1].

Energy Production "Sunlight that reaches the lunar surface is constant, predictable, and inexhaustible, and can be converted into electric power by solar panels. Several sites around the South Pole of the Moon always have Earth in view for continuous communications, and receive over 300 days of sunlight per year. The temperature difference between the sunlight and dark areas of the Moon can also be used for the operation of heat engines and for thermal management systems. The produced power could be beamed to Earth or to satellites for distribution around the world" citeStructural Design.

Resources Although the Moon looks like a desolate planet, it has many raw materials and also very rare elements. Example of raw material are iron, aluminium, silicon, titanium, carbon and hydrogen and as rare element: helium 3. These materials could be used both for terrestrial needs, but also to create a self-sustainable colony on our satellite. Furthermore, helium 3 can be used to create energy through nuclear fusion.
Another important element not mentioned before, but fundamental for human life and present on the Moon, is water. It is preserved in the solid state and is conserved in the regolith at the polar region of the planet, but it exists. Oxygen is also contained in the regolith, but combined with other elements. This does not mean that it can not be extrapolated, in fact chemical processes allow it. In this way, hydrogen and oxygen could also be used as fuel for launch vehicles.

Technology All technologies developed for space programs are not only confined to this field but lead also progression and application in numerous terrestrial ones, creating benefits and services, now essential for us. The construction of a habitat on the moon can lead to the same development opportunities as those that occurred for previous space missions, which are summarized on the NASA spin-off.
This is not the only possible scenario. A different one concerns the possibility of using the lunar outpost to carry out new experiments, taking advantage of the scarce presence of atmosphere and the lower constant of gravity.
Lastly the Moon could be used as a test bench for new and innovative technologies for space travel and space habitations.

Commercialization With the new appearance on the space scene of private companies, the Moon could also become a major destination for space tourism,

as envisioned by Elon Musk. As mentioned, this could be a positive or negative thing. As on Earth, tourism creates jobs and it is fundamental for the economy, but also brings with it problems of pollution and disfigurement of places. In the space the problem will not be any different, if some precautions are not taken beforehand.

Steppingstone to Mars and other planets One of the major difficulties for the space exploration is the energy needed to leave the Earth and the relative fuel needed to generate it. The farther the destination is, the greater the fuel consumption and the thrust will be, resulting in an increase in fuel to generate it. This idea is summed up in Tsiolkovski's formula.
The Moon, with its low gravity, allows a lower escape velocity and therefore lower fuel consumption and a rocket with smaller dimensions
As mentioned before, the presence of hydrogen and oxygen allows the production of combustible and comburent immediately on the Moon.

Chapter 2

The lunar environment

The Moon is the only Earth's natural satellite. It has a diameter of 3474,2 km, compared to 12742 km of the Earth and is placed at an average distance of 384400 km form our planet.
By observing one of the numerous photos now available of the Moon, it appears extremely different from the Earth, mainly for its grey colour of the surface but also for the natural constructions present on it.

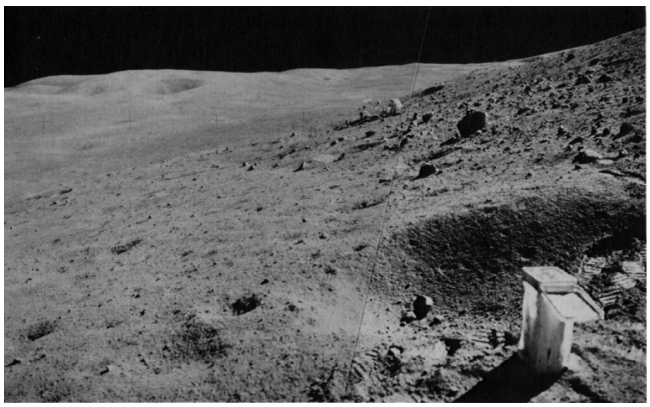

Figure 2.1: The lunar roving vehicle (LRV), parked below a boulder field on Stone Mountain at the Apollo 16 site (NASA Photos AS16-107-17472 and -17473)

Both for the evolution processes and the own characteristics, is clear that the Moon has a very different history than the Earth one. It differs from the blue planet mainly by the lack of atmosphere, lower gravity, very high temperature variation between day and night and a weak magnetic field. Due to the lack of atmosphere the lunar surface is bombarded by millions of micro-meteorites every year. Furthermore, the weak magnetic field allows the ionization radiation to reach the lunar surface. However, these are only a part of the features that make the Moon an inhospitable place to welcome life. Other unfavourable characteristics are the presence of regolith with its high abrasive capabilities and the electrostatically charged dust.

An interesting thing about Moon, but not related to its environments, is the continuous motion away from the Earth. The Moon moves away at a rate of 3.8 cm per year. This calculation is possible thanks to the mirror positioning on the Moon during the Apollo missions. This happens "because the dissipation of tidal energy by bottom friction in Earth's seas (especially shallow seas) has gradually slowed down the Earth's rotation (e.g. Lambeck, 1975). To keep the angular momentum of the Earth-Moon system constant, the Moon slowly moved outward at a speed of a few centimeter per year." [4].

2.1 Temperature and lunar heat flow

2.1.1 lunar heat-flow probe

Important is not only knowing the results and data of an experiment but also understanding how they were found. For this reason, a brief explanation of the instruments used by the astronauts is provided.
The probe used on the Moon to measure the absolute temperature, heat flux and conductivity of the lunar regolith is shown in the following diagram:

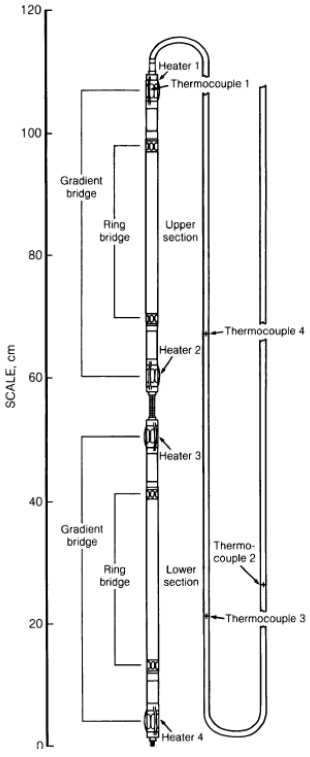

Figure 2.2: Diagram of a lunar heat-flow probe

The instrumentation consisted of two identical probes to the one shown in figure 2.2. They are connected by cables to a common electronic box and placed in holes drilled before, to collect regolith samples. This choice allows to have two independent measurements. Each probe is composed by two thermosensitive parts (50 cm long) and placed in a linear configuration, as shown in the figure on the left. Each temperature-sensing part contains two differential thermometers realized through two Wheatstone-like resistance bridges. These differential thermometers measure the temperature difference between the gradient bridge and ring bridge allowing the measurement of the temperature variation with the depth. The four thermocouples placed in the cable, which connect the probe to the electron box allow instead, the measurement of four absolute temperature values on the surface of the Moon. Conductive measurements are possible thanks to the presence of heaters. The idea is to energize a heater and record the change of temperature perceived by the underlying gradient sensor for 36 hours. The rate of temperature rise is interpreted in terms of conductivity of lunar regolith [4].

2.1.2 Temperature on the Moon

The temperature excursion experienced on the lunar surface just before the lunar dawn to the lunar noon is very high and equals to a mean value of 280 K. Apollo missions 15 and 17 allowed the first experimental measurements about temperatures on the Moon surface. The thermocouples in cables, placed few centimetre above the lunar surface, make possible the recorded of the absolute temperatures. At the landing site of the Apollo 15 mission the temperature ranged between a maximum of 374 K to a minimum of 92 K. At the landing site of Apollo 17 mission the temperatures recorded were 10 degree higher.
These very large excursions recorded on the surface is mainly due to:

- Extremely low thermal conductivity, which inhibits the flow of energy into and out of the subsurface,
- A very low volumetric heat capacity of the regolith,
- A very tenuous atmosphere. [5]

However, the above temperatures are not constant, but they change with the distance of the Moon from the Sun. The noon temperature increases about 6 K from aphelion to perihelion [6].
At a depth of 35 cm the measured temperature for the two mentioned missions is respectively 45 and 40 degree higher compared to the ones on the surfaces (figure 2.3). Instead the average surface temperature recoded during a complete lunar day-night cycle differs for a negative value from the one before.

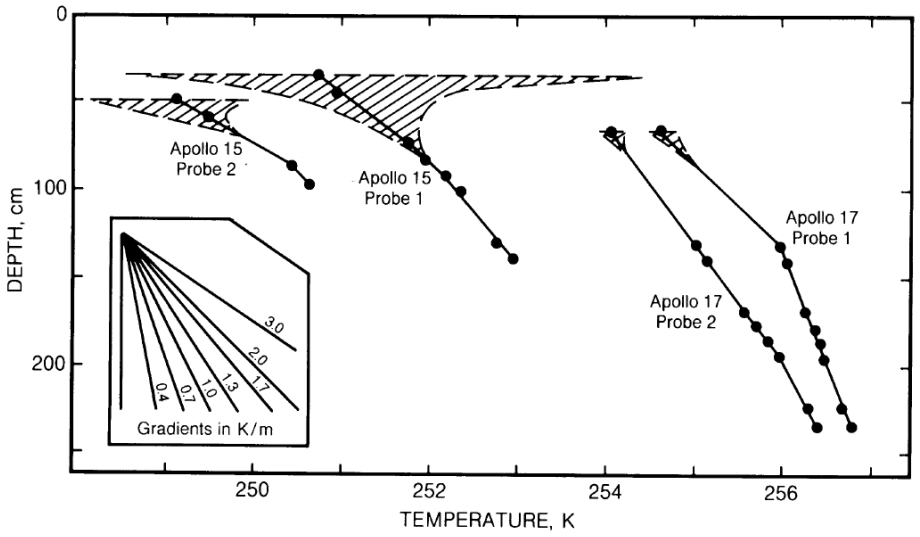

Figure 2.3: Temperature fluctuations in the lunar regolith as a function of depth

The motivation about an higher temperature at a depth of 35 cm than the one on the surface is the following. The average surface temperature is the result of the energy absorbed by the Sun during the lunar day and the energy released by the Moon during the night. Remembering that the radiative heat, transfer between particles is more efficient at hight temperature ($q = \sigma \cdot T^4$), it is easy

to demonstrate that heat adsorbed by the Moon during the day is higher than the one released during the night. The previous considerations lead also to the following feature. The steady-state temperature gradient in the upper few cm of the subsoil can be quite significant [5], as demonstrated by the experimental measurement done during Apollo 15 and 17 missions and reported before. The interesting information in the previous pharaseis: "few centimetre".The greatest variation in temperature in fact, is found in the first, 1 to 2 cm of lunar soil. [4] This information reveals the low thermal conductivity of the lunar soil in the first few centimetres.
Other two important considerations about the graph in figure 2.3 are:

- Below a depth of 80 cm the temperature variation recorded by the probes and due to lunar day-night temperature cycle is negligible.
- Below the same depth, the steady-state temperature gradient is only due to the internal lunar heat flow.

In addiction to the mentioned temperatures, obtained thanks to the Apollo missions, the Lunar Colony Study Group [**?**, **?**] provided some estimates about temperatures in the other regions of the Moon through Earth-base observation. The estimated values are reported in the table below:

	Shadowed Polar Craters	Other Polar Areas	Front Equatorial	Back Equatorial	Limb Equatorial	Typical Mid-Latitudes
Average temp.	40 K (?)	220 K	254 K	256 K	255 K	220<T<255
Monthly range	none	none	± 140 K	± 140 K	± 140 K	± 110 K

2.1.3 Lunar heat flow

"The Moon is a small planetary body, and there is good reason to believe that it has lost most of its initial heat during its first 4.6-b.y. history. Most of the present heat flux is probably generated by radioisotopes (mainly ^{40}K,$^{232}\,Th$,$^{235}\,U$,$^{238}\,U$) present in the interior to a depth of about 300 km." [4].
Thanks to the Apollo mission was possible to measure thermal conductively of the regolith and therefore the precise value of the vertical component of the heat flux. Fore each of the Apollo mission 15, at the Hadley Rille, and 17, at the Taurus-Littrow Valley (the measurement in the 16 was impossible because a broken cable), two probes were located 10 m apart at a depth varying between 1 to 2.36 m due to the different composition of the soil and the relative difficulty of drilling. Using the process involving heaters and explained in the first section of the chapter it was possible to know the thermal conductively of the regolith, which ranges from $1.5 \cdot 10^{-4}\,W/(cm\,K)$ to $2.95 \cdot 10^{-4} W/(cm\,K)$ $\pm 20\%$. Instead the thermal conductivity of the Earth ranges from 1.1 to $2.93 \cdot 10^{-2} W/(cm\,K)$
Generally the experiments have also revealed that thermal conductivity of the regolith increase with depth. The rationale refers to a higher bulk density of the soil due to compaction.
Knowing the steady-state temperature gradient, by means of the differential thermometers, placed in probes at note distance, and the thermal conductively of the regolith, reported before, calculation of the heat flow was possible through the relative governing equation.

$$q_z = -k\frac{dT}{dZ}$$

The value found ranges between 2.5 to $2.8 \cdot 10^{-6}\,W/(cm^2)$. These are the values calculated in the 17 Apollo mission. The large massifs flanking the Taurus-Littrow Valley have a significant effect on the heat flow. It is estimated that a correction from -15% to -20% should be applied; the best value of the resulting heat flux is $2.2 \cdot 10^{-6}\,W/(cm^2) \pm 20\%$
Before the Apollo missions the lunar heat flow measurements were only possible by Earth-base consideration. The evaluation of the thermal emission in the microwave length leaded Krotikov and Troitsky (1964) and Tikhonova and Troitsky (1969) to suppose the heat flow of the Moon around the value of $3.1 \cdot 10^{-6}\,W/(cm^2)$ $\pm 20\%$ which agrees with the values said before. This demonstrates that most of the heat flux is generated by radioisotopes and precisely by ^{40}K,$^{232}\,Th$,$^{235}\,U$,$^{238}\,U$.
In conclusion the upper 1 to 2 cm of lunar regolith must have low thermal conductivities ($1.5 \cdot 10^{-5}\,W/(cm^2)$), while it increases from 5 to 7 times to the depth of 2 cm [4].

2.2 Lunar atmosphere

"Little was known about the lunar atmosphere before the Apollo missions." [5]. However, the data collected through the Apollo Lunar Surface Experiments Package (ALSEP), brought to the Moon in each of the Apollo missions except the 11 and the 13, is not very reliable due to the contamination of the recorded information by the gasses released during the mission.

2.2.1 Data contamination

The level of contamination is easily understandable if we consider that each of the landing manoeuvres releases a quantity of gasses equal at the whole weight of the uncontaminated lunar atmosphere: about 10^4 kg. The latest data leads two considerations: first one, the lunar atmosphere is very tenuous; second one, during the six Apollo missions that touched the Moon, an amount equivalent to six times that of the original atmosphere was released on its surface.
The release of these gasses are evident in the data recorded by the Cold Cathode Gage experiments in Apollo missions 12, 14, and 15. The instrument were easily driven off-scale by the waste gas clouds emitted from the astronauts whenever they approached within a few meters of the experiment [4]. The contamination remained even when the astronauts left the planet. This phenomenon can be observed in the data recorded by the same instrument at the Apollo 14 landing site and reported in the graph below.

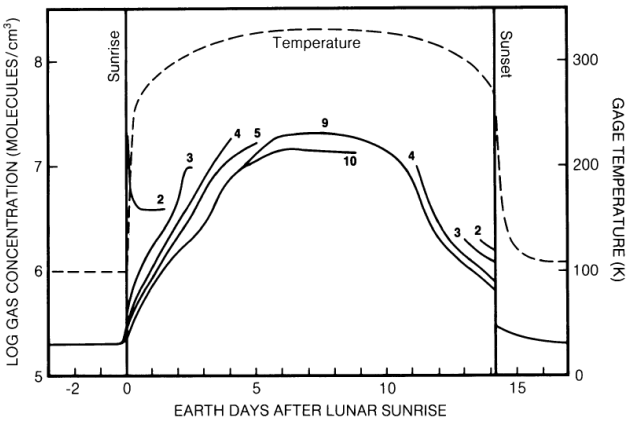

Figure 2.4: Variation in total gas concentration (molecules/cm3) in the near-surface atmosphere at the Apollo 14 landing site,

The graph shows the information collected by the instrument for ten lunar day identified by the numbers from 1 to 10 near the relative curves. Interesting for the previous consideration is the day 2, which represents the first lunar day after the astronauts left. A sharp rise is possible to be identified at the beginning of this curve. The point describes the gas concentration, when the area around the landing site was heated up by the sun. This increments is caused by the exhaust gasses which, once emitted during the ascent phase of the lunar module, were absorbed by the ground and then released by it when the sun rose again.

Now it is easy to understand how the missions affected the data collected by the instruments.

2.2.2 Description of the lunar atmosphere

On the one hand, on the Earth at sea level the atmospheric concentration is of the order of 10^{19} molecules/cm^3. This value decreases to 10^7 molecules/cm^3 at 500 km of altitude and 10^5 molecules/cm^3 at 1500 km from the Earth surface. On the other hand, the value of molecules concentration on the lunar surface is only about 10^5 molecules/cm^3 at the night time and 10^7 molecules/cm^3 at the day. The last value is an upper limit, because it also includes the contamination encountered during the situation explained above and cannot be considered a reliable value. This concentration of particles creates a pressure on the Moon equal to $3 \cdot 10^{-10}$ Pa. It is often said that the Moon has lack of atmosphere, but, as shown above, this is a misstatement, derived from a terrestrial point of view where the atmosphere is 14 order higher than the Lunar one.
The atmosphere is mainly composed by the following elements: neon, hydrogen, helium and argon. Neon and hydrogen are mainly carried by the solar wind. Helium comes from the previous source for the greatest amount and only of 10% from the radiogenic process and lunar origin. Most of the argon occurs in the ^{40}Ar form and derives from the radioactive decay process of lunar ^{40}K. Only the 10% of this element is ^{36}Ar and is transported by the solar wind.
However, the previous information carries inside them a variability and indeterminacy due to the following factors:

- Different temperature from day and night which creates a different level of information contamination by Apollo missions residual gasses as mentioned above;
- The concentration of the solar wind transportes species such as neon and hydrogen is determined by the intensity of the solar wind itself. Since the latter is not constant over time, the species has not the same rate.
- The lunar day-night temperatures differential varies with latitude, precisely decreases with reduction of distance from poles. As better explained afterwards, the atmosphere composition depends to temperature, therefore a lower temperature differential at high latitudes determines a lower diversity in the composition of the atmosphere during the day-night period.

The last consideration is evident in the figure 2.5 which represents the day and night atmosphere concentration of different element at different latitudes. As it is possible to notice, the concentration of the elements and therefore the composition of the lunar atmosphere is not constant along the day-night cycle and even at constant latitude. In particular the behaviour of the Argon during day-night cycle is extremely different from the other ones. This phenomenon is more evident at low latitude where the lunar day-night temperatures differential is higher. It is possible to notice a rapid decrease during the lunar night. This happens because argon is condensable at lunar night temperatures, whereas neon, helium and hydrogen are not [4].

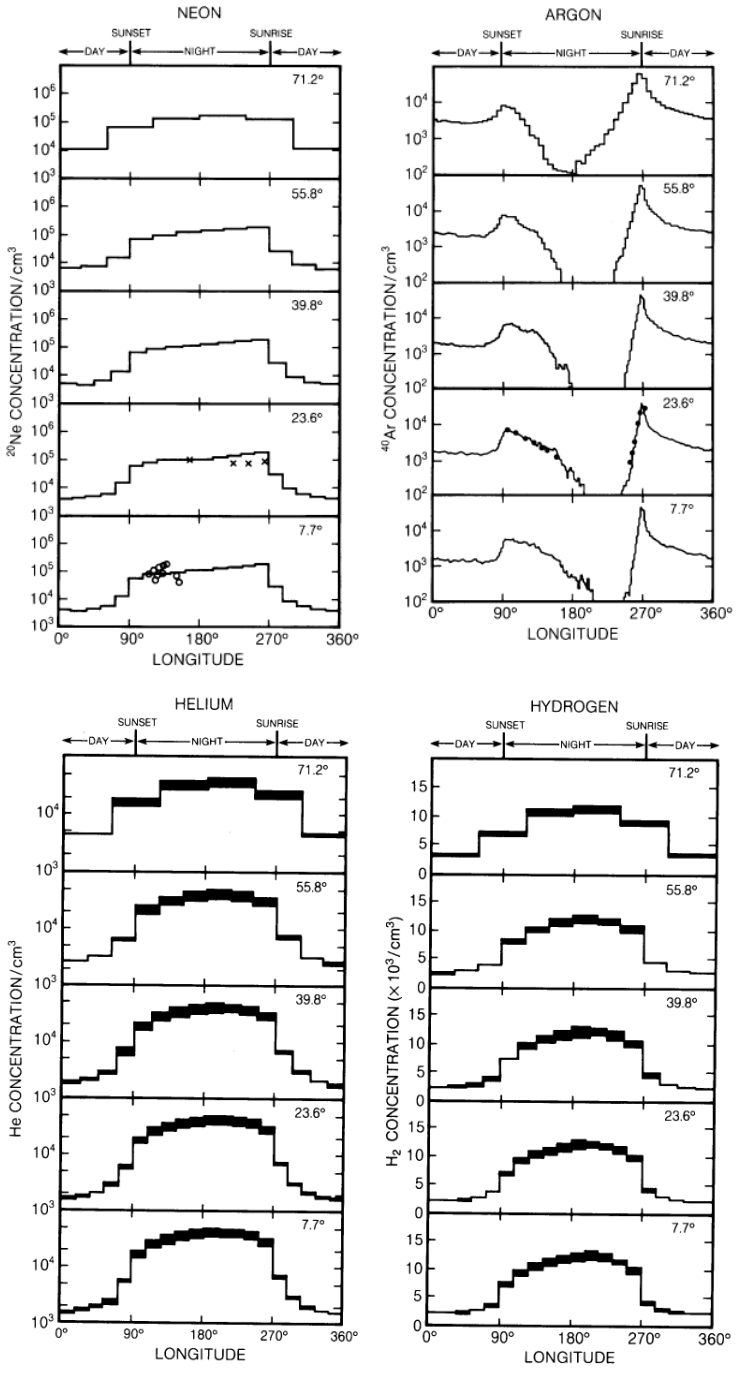

Figure 2.5: Concentration of mainly atmosphere constituents at different latitudes during day-night cycle

2.2.3 Natural and artificial source of the lunar atmosphere

A number of natural and artificial sources of the lunar atmosphere has been listed by G. Jeffrey Taylor and a summary is reported here following the formulation reported by Gani B et al [?, ?].

- Solar wind: Due to the lack of a significant magnetic field the solar wind is able to reach the surface of the Moon and deposits its own particles, principally H and He on it. It is estimated a flow of 50 g/s of particles and precisely 40 g/s of H and 8 g/s of He.
- Meteorite and Comet Volatilization: The lunar soil is constantly bombarded by micro-meteorites. Most of them are volatilized by the energy released by the impacts. A flux of 2 g/s is calculated.
- Internal Degassing: Without the presence of a significant atmospheric pressure, the Moon is constantly subjected to outgassing phenomenon. The flow is in the order of 32 g/s.

Artificial sources of the lunar atmosphere are instead the following:

- Rocket Exhaust: Considering 18 travels every year, Vondrack [9] estimates a flux of 100 g/s of contaminants contaminates released in the lunar atmosphere.
- Habitat Leakage: The structures release a quantity of contaminants in the lunar atmosphere due to outgassing phenomena equal to $2 \cdot 10^{-4}$ g/s. In addition to this value, it is necessary to consider the EVA (Extra Vehicular Activities) done by astronauts which contributes with $7 \cdot 10^{-2}$ g/s.

The most of the gasses present in the lunar atmosphere are carried away by an ionization process caused by the solar wind coupled with the interplanetary electric field. Their escape is due to thermal phenomena, while the reaching thermal speed is a less significant process. These two events determine a continuous renewal of the lunar atmosphere. The average time, during the particles remain in the lunar atmosphere, is about 4 months. Theories show that if the lunar atmosphere were greater than 100 times the current role of the two processes involved in the escape of the gases, it would be reversed. Furthermore, if the total mass of the lunar atmosphere was 10^7 or 10^8 kg, these mechanisms would reach a constant or decreasing rate and the Moon would have a permanent atmosphere [9].

2.3 Seismic activity

From this point of view the Moon is a relatively inert planet. The recorded seismic energy by the Apollo Passive Seismic experiments is about $2 \cdot 10^{10}$ J/yr, compared to 10^{17} or 10^{18} J/yr of the Earth.
The seismic events on the Moon have different sources and different magnitudes, compared to our planet. The forces presented on the Earth and responsible of the creation of faults, folds and mountains are largely absent on the Moon; Indeed, the internal energy released by the tectonic activity is very low on it. Furthermore the energy generated by the earthquakes on the Moon (said moonquakes) is 10^{-12} time lower than the Earth's one (the largest moonquakes recorded correspond at a equivalent Earthquakes of magnitude 4). On the Moon the main seismic activities are the following:

- Monthly deep-focus moonquakes: caused by tidal stresses between Earth and Moon.
- Shallow moonquakes: a few stronger compared to the previous ones but rarer. They may be caused by the tectonic process and meteorite impacts on the lunar surface.
- Thermal moonquakes, they are very small and are caused by the thermal degradation of the boulders located on the edge of young craters.

An interesting property of the Moon is its low attenuation of elastic waves, which propagates through the ground. The wave due to an impact occurred at one point could be carried over a long distance and "heard" in a second point with a great clarity. The low attenuation of the elastic waves also causes a long permanence of vibrations due to the impacts of meteorites or lunar earthquakes around the planet (figure 2.5). This phenomenon gave rise to the phrase "the Moon rings like a bell".

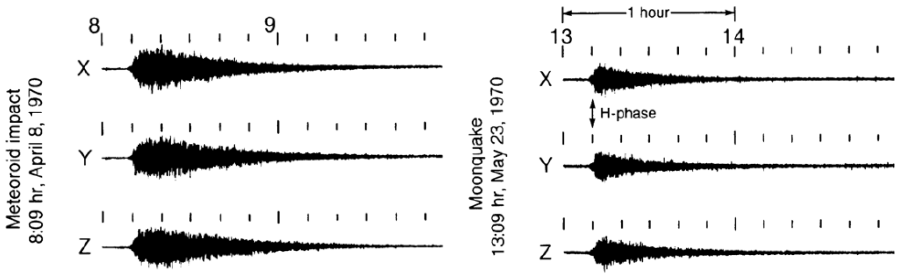

Figure 2.6: Seismic signature of meteorite impacts and moonquakes on the Moon

Finally, the Moon could be defined as a quiet place: moonquakes and meteorite impacts are rare and the lack of atmosphere generates the typical silence of an environment where sound cannot be transported by air.

2.4 Meteoroid Bombardment

On the one hand, direct measurements of meteoroid, impacted near the Moon, were made by the Lunar Orbiters 1 to 5. These space orbiters were made by a series of semi-cylinder metal plates of 0.025 mm thick and equipped with pressure sensitive switches to record perforation by meteoroid. The term meteoroid identifies any solid body, which travels in space and which has not passed through the atmosphere of a planet and therefore has not been collected on its surface.
On the other hand, indirect measurement was largely carried out by examining the samples collected on the lunar surface, during the Apollo programs.

2.4.1 Data about Meteoroid Velocities and Impact Rates

From observation, flux of meteoroids on the lunar surface is mainly composed by solid bodies smaller than 1 μm travelling from the sun to the Moon. Meteoroids of higher dimension ($> \mu$m) and coming from the direction of the Earth's motion are a smaller part [11] [12] [13].
Perforations recorded by the Lunar Orbiter show a perforation rate of $0.16m^2$ per day [10]. This is about half of the perforations encountered by orbiter around the Earth.
The velocity of the meteoroids was instead measured by photographic and radar tracking near the Earth. Using a conversion mechanism, the velocity of meteoroids at the Moon was found between 13, and 18 km/sec [**?**].
In conclusion the part of the Moon more exposed to bombardment of large meteoroids is the one facing the Earth's motion direction.

2.5 Ionization radiation

Before starting the discussion on the ionization radiation present around Moon, a first explanation of what it is could be interesting.
The ionization radiation is the one with enough energy to remove an electron from atom or molecule. In other words, a radiation with an energy equal to or higher than the energy of first ionization. The ionization radiation could be composed by electromagnetic waves, subatomic particles or ions.
The electromagnetic waves able to be ionization radiation are those located in the more energetic part of the electromagnetic spectrum.

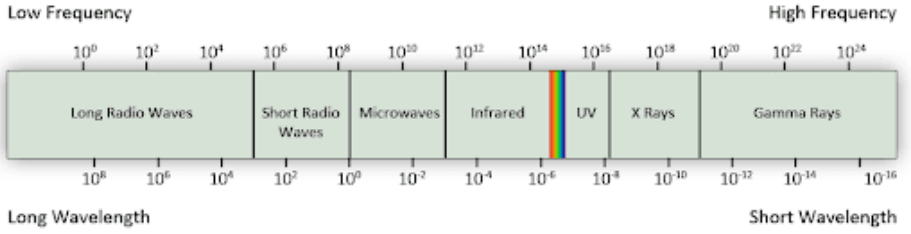

Figure 2.7: Electromagnetic spectrum

Gamma ray, X ray and high-frequency ultraviolet rays are ionization radiation, whereas the low frequency ultraviolet, infrared, microwaves and radio waves are not ionization radiation. The limit located in the ultraviolet radiation between ionization and not-ionization radiation is not a precise value, because the energy of first ionization depends on the atom or molecule considered. A conventional value for this energy is between 10 eV and 33 eV for a photon.
Instead, the sub-atomic particles able to be ionization radiation are for example α particles, β particles an neutrons. Furthermore, almost all radioactive decay products are ionizing, because the energy released by the process is generally higher than the energy of the first ionization. Other natural ionization particles are muons, mesons and positrons, and those particles which compose the secondary cosmic radiation.
On the Earth the main sources of ionization radiation are cosmic rays and the decay of the radioactive isotopes. It is called background radiation. The presence of radioisotopes such as the 14-carbon is attributable again at the cosmic rays and the decay of 14-carbon produces ionizing radiation as mentioned before.
For a better understanding of the composition of the aforementioned particles, a further study is provided below.

Directly ionizing Every particle with a charge and mass can ionize atom through the coulomb's force, if it has a sufficient kinetic energy. For instance, an α particles moving at 0.05c with c the light velocity is ionizing.

- α particles. The α particles are made up by two protons jointed to two neutrons. Substantially they are equal at a nucleus of helium. Generally, the α particles derive from the α decay. They are highly ionizing. If their origins are the radioactive decay, they can be absorbed by the first centimetres of skin. If they arise from ternary fission, they are more penetrating, three time energetic than the previous one, and could reach the deep layers of the human body. As mentioned, cosmic rays are composed by the $10 - 12\%$ of helium nuclei, and they have a higher energy than the α particles produced by nuclear decay, in a way that they can pass through the human and dense body shields.

- Positrons. Positrons are the equivalent of electrons in the antimatter. They have equivalent charge but opposite sign. When a low-energy positron collides with an electron of the same energy level, the entire mass of the two is commuted into energy.

- β particles. The β particles are high-energy electrons or positrons and are produced by radioactive nuclei. They derive from the β decay and precisely there are two form: β^- and β^+ which generate electron and positron respectively. The β particles if pass through matter can produce X ray, known as bremsstrahlung or secondary electrons. Both have a direct ionizing effect. The generation of bremsstrahlung radiation is higher in material with hight atomic number, for this reason shields against β particles are made from material with low atomic number.

- Charged nuclei. They are commonly found in galactic and solar cosmic rays. Skin, cloths or thin layers of shielding are sufficient to stop these

nuclei. The problem are not the nuclei themselves but the secondary radiation and relative biological cascade effect caused by them.

Indirectly ionizing Indirectly ionizing radiation is electrically neutral and so it does not interact strongly with matter. The bulk of the ionization effects are due to secondary ionizations.

- Neutrons. Neutrons have no charge and therefore they cannot directly ionize matter. However, they can ionize atoms with two different processes. Having a mass similar to protons they can ionize other atoms through elastic collision. When a neutron hits a hydrogen nucleus, it transmits its entire momentum to the protons and the atoms become ionized. On the one hand, electron and proton, which are products of the reaction, are highly energetic and represent high ionizing secondary radiation. On the other hand, when a neutron hits an atom heavier than the hydrogen one, only part of its energy is transferred to the other atoms. If this is enough, the atoms are ionized. The second process is called inelastic scattering and consists in the absorption of neutron by nucleus. It is called neutron capture. Factors, which determine the activation of the first or second process, are the scattering section and the neutron velocity.

The following image is a summing-up of the previous concepts. There gamma rays are represented by wavy lines, whereas charged particles and neutrons by straight lines. The small circles show where ionization occurs. Gamma rays were not explained before but it is the name given to photon radiation. They are called gamma rays if produced by a nuclear reaction.

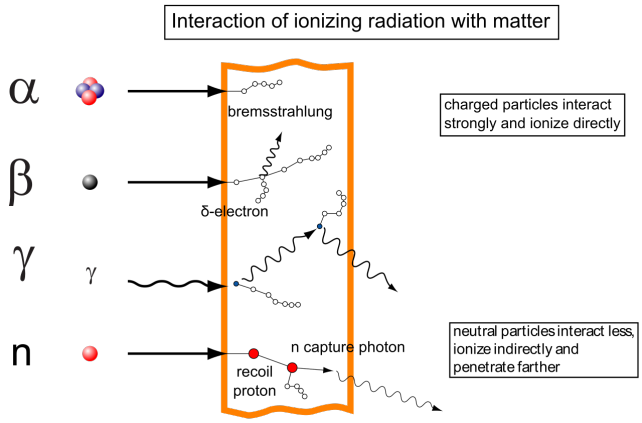

Figure 2.8: Radiation interaction

2.5.1 Ionizing radiation around the Moon

The space around the Moon are characterized by many types of ionizing radiation but unlike the Earth, the Moon has not got a sufficiently dense atmosphere and a significant magnetic field to attenuate or deflect radiations before they

reach its surface. Indeed, the Earth's magnetic field is great enough to trap particles or radiations, inside it in the Van Allen belts and the Earth's atmosphere, with a density equal at 1000 g/cm, has the ability to attenuate the intensity of the incident particles, allowing only weakly interacting muons and few neutrons to reach the Earth's surface.
The ionizing radiation on the Moon is mainly large fluxes of low-energy solar wind particles, smaller fluxes of high-energy galactic cosmic rays, and rare, but occasionally intense, particle fluxes emitted by solar flares [?]. Another types of radiation observed in space around the Earth-Moon system are gamma rays, electrons, antimatter and other charged particles. These radiations have such low fluxes and energies that they are difficult to detect on the lunar surface and some have not yet been well characterized [4]. The radiation energy is traditionally expressed in eV (electron-volt), where $1ev = 1.6021 \cdot 10^{-19} J$ and extends over eight orders of magnitude for the radiation around the Moon. These radiations are mainly composed by electrons, protons, and charged nuclei and their interaction with lunar surface and depth of penetration depends by their energy end composition. The following table summarises the main characteristics of the radiations mentioned, including their energies, fluxes, compositions, and lunar interaction depths.

Type	Solar Wind	Solar Cosmic Rays	Galactic Cosmic Rays
Nuclei energies	~0.3–3 keV/u*	~1 to >100 MeV/u	~0.1 to >10 GeV/u
Electron energies	~1–100 eV	<0.1 to 1 MeV	~0.1 to >10 GeV/u
Fluxes (protons/cm^{2}sec)	~3×10^8	~0–10^{6}†	2–4
Particle ratios‡			
electron/proton	~1	~1	~0.02
proton/alpha	~22	~60	~7
L ($3 \le Z \le 5$)/alpha	n.d.	<0.0001	~0.015
M ($6 \le Z \le 9$)/alpha	~0.03	~0.03	~0.06
LH ($10 \le Z \le 14$)/alpha	~0.005	~0.009	~0.014
MH ($15 \le Z \le 19$)/alpha	~0.0005	~0.0006	~0.002
VH ($20 \le Z \le 29$)/alpha	~0.0012	~0.0014	~0.004
VVH ($30 \le Z$)/alpha	n.d.	n.d.	~3×10^{-6}
Lunar Penetration Depths			
protons and alphas	<micrometers	centimeters	meters
heavier nuclei	<micrometers	millimeters	centimeters

Figure 2.9: Features of mainly ionizing radiation on lunar surface. eV/u = electron volts per nucleon

The table shows averages value of the most probable range of values recorded on the Moon. In fact, these values are not constant but change over time and depend on solar activity, intensity of the galactic cosmic rays and the irregular emission of solar flares. As it is easy to understand from this introduction, the ionizing radiations treated in the following paragraphs are: Solar wind, Solar flare, Galactic cosmic ray.

2.5.2 Solar wind

Coupled with radiant energy, the Sun emits also plasma. The plasma is a state of matter where a gas is highly ionized and most of the atoms are divided into ions and electrons. From a global point of views, however it appears electrically

neutral. The solar wind velocity typically ranges from 300 to 700 km/s and its particles concentration from 1 to 20 particles per cm^3 [15]. The composition of the solar wind is not yet well known. Doubts lie mainly in the composition of heavier nuclei. The long terms alpha particle to proton ratio observation gives a value of 0.037-0.055. The solar wind is also the principal sources of volatile elements in the lunar atmosphere, such as H, He, C and N, as reported in the previous chapter, relating at the lunar atmosphere. The sun is also responsible for the long terms erosion of the lunar surface. However, the main factor remains the bombardment by micro meteorites.

2.5.3 Solar flares

The Sun produces even high flux of energetic charged particles during the major solar flares. These high energy particles are called Solar Cosmic Rays (SCR). SCR are mainly composed by electrons, protons ad heavier nuclei as reported in figure 2.5, where most of the latter are α particles and other elements, which are easier to ionize. However, the composition may vary during the SCR itself and between one SCRs and the other [16].
Solar cosmic ray particles are accelerated in the Sun corona or in the interplanetary space. This acceleration, in the larger flares, can bring particles to relativistic velocity. These can reach the Earth-Moon system in less than a day. For instance, electrons are faster than other particles and those with energy between 0.5 and 1 MeV could reach 1 A.U. within a time of 10 minutes to 10 hours. Protons, which are more massive, with energy of 20-80 MeV usually reach the previous target in 10 hours. However, the precise process of acceleration of GCR particles by solar flares is not yet known. Recent studies and observation have helped us to get a better understanding of them. In several cases particles are accelerated to high velocity by multiple reflection between two converging shock front [17].
There are SCR principally during the period of maximum solar activity, it is strange to record them in different periods and these SCR are usually few. The figure 2.13 shows the major flux of SCR for three 11-year cycles with the vertical line and the sunspot trend with a smoothed cure for the same period for comparison.

The solar activity is often related to the number of sunspot shown by the Sun. These two correlated phenomena recur every 11 year. For this reason, the history of the Sun and solar activity are divided and identified by 11-year cycles. It is clear from the figure 2.13 that major fluxes of SCR appear simultaneously with maximum solar activity period and precisely when the sunspot number is over ~ 50.
Another interesting information is the energy distribution within the particles of SCR. The figure 2.11 shows clearly how the quantity of particles decreases rapidly with increasing energy: most particles have energies below ~ 30 MeV. Few events can have large fluxes of high-energy particles extending to GeV or higher energies [4].

In conclusion it may be useful to create a model to predict SCR for future lunar expeditions, however the small amount of data, due to rarity of these events and the absence of direct measurements with satellite detectors before the 1960, makes this task very difficult.

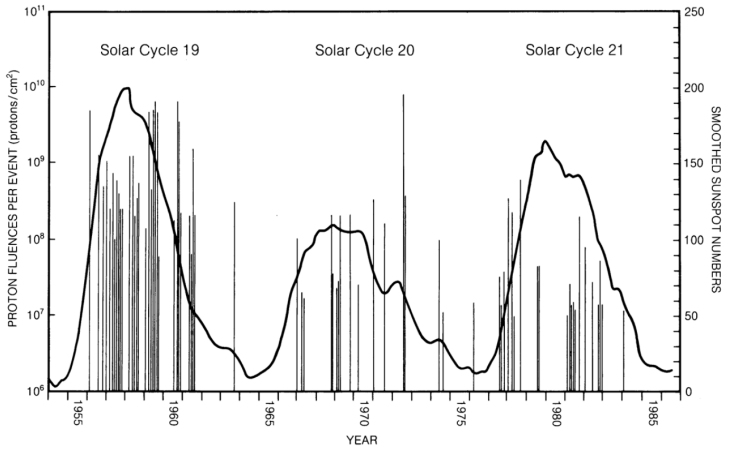

Figure 2.10: Flux of solar cosmic ray, represented with vertical line, and solar activity, related with the sunspot trend and represented with smoothed line fr three 11-year cycle

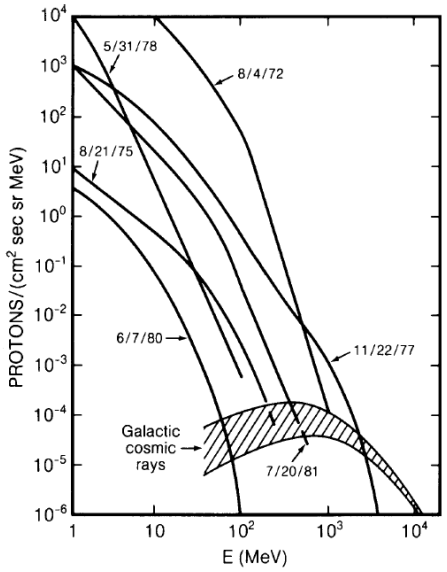

Figure 2.11: Solar-cosmic-ray (SCR) proton fluxes vs. energy

2.5.4 Galactic Cosmic Rays

Galactic Cosmic Rays (GCR) are particles originated outside our solar system. They typically take 10^7 years to reach the Earth-Moon system and during this journey they lost part of their energy due to collisions with other particles in interstellar matter. In these collisions the GCR are also enriched with rare elements, such as: lithium, beryllium and boron.
The energy of these particles can reach 10^{20} eV. However presence of these high energy particles in GCR are very rare.

The fluxes of GCS are not constant over time on the Moon but mainly depend on solar activity. When a solar flare event occurs, the Sun's plasma attenuates the GCR energies, however particles with energies above 10 GeV / u are unaffected by the solar flare event [5]. The energy distribution of protons in GCS flows is shown in the following figure.

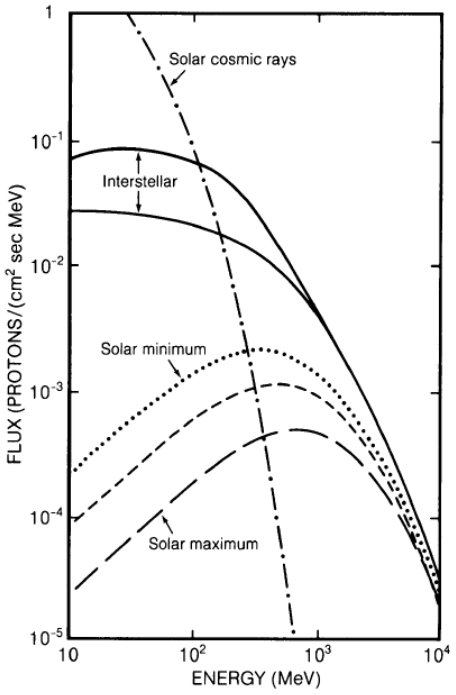

Figure 2.12: Galactic-cosmic-ray proton fluxes vs. energy

As mentioned before, GCR energy spectrum is greater during period of minimum solar activity as shown by the dot line. Instead, the dashed line represents the average between energy spectrum between the maximum and minimum solar activity. The value called "interstellar" shows the energy obtained by GCS in the interstellar space. In conclusion, it is unlikely that CGR energy is higher than the value reported for the interstellar one. The last time that the GCR particles flux was much above the typical range was probably between 1645 to 1715, which was a period of very low solar activity.

2.5.5 Interaction with the Moon

Charged particles described in the previous phenomena interact with lunar soil in different ways, such as through nuclear reactions and ionization processes. These processes and their products were slightly described in the first pages of this chapter, when ionizing radiation was introduced. Most of charged particles loses their energy through ionization process before they can induce a nuclear reaction. The phenomena caused by these interactions are the following:

- Tracks. Tracks are radiation damage effects created by nuclei with Z>20

and so large that these damages can be seen with transmission electron microscopy in some minerals.

- Sputtering. It is a process in which energetic particles can displaced nuclei in matter. If the displaced atom is in the surface layer of the material, it can be removed. It is a process of erosion but less important than micro-meteorite bombardment.

Summarizing:

Solar Wind Solar wind particles have low energy (∼1 keV) and can only interact with the surface layer of the soil, because they era stopped in much less than a micrometer. It is the main cause of sputtering and if the solar wind is intense enough, the crystalline regions on the surface of the grains can be transformed into amorphous ones.

Solar Cosmic Ray Most of the SCR particles are stopped in the first few centimetres of the lunar soil, losing energy due to the ionization process. Particles with a higher mass as heavier nuclei are instead stopped within a depth of a few millimetres and can produce a high density of radiation damage here. The secondary radiations, due to the few reactions induced by SCR, are very small and their flux is much lower than the GCR initially radiation. Depth reached by secondary radiation is not high.

Galactic Cosmic Ray The heavy nuclei of GCR are stopped within ∼10 cm in lunar soil and the damage caused by them is so intense that they can be seen as high tracks density in lunar samples. The lighter nuclei and α particles in GCR are highly penetrating and the secondary radiation produced by them can travel for meters into the lunar surface. The number of secondary particles in GCR cascade is much greater than the number of incident ones.
Galactic-cosmic-ray particles fluxes, both the incident primaries and the secondaries, are shown in the following figure.

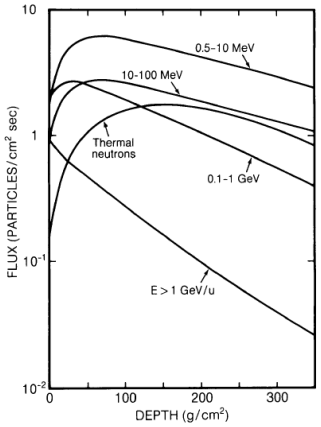

Figure 2.13: Flux of galactic cosmic ray particles.

2.6 Soil properties

On the Moon astronauts have collected samples for a total mass of 381.7 kg. These samples were and are subject of studies and several scientific articles and books are written about the composition, history end creation of our satellite. In this chapter only a brief summary is provided, in order to show the main component and physical properties of the lunar matter. This information will be important in the design phase.
For more information, the book: LUNAR SOURCEBOOK A User's Guide to the Moon of GRANT H. HEIKEN et al.is an excellent and complete handbook.

The top layer of the lunar surface is made up by loose and non-highly bonded rock fragments. The size of these fragments ranges from few microns to millimetres. This blanket of unconsolidated heterogeneous surface deposits, which covers solid rocks, is called regolith. It also includes dust, broken rocks, and other related materials. The term regolith is not exclusive for the Moon, but is used to identify this soil composition also on Earth, Mars, and other planets. It derives from the union of two Greek words: rhegos (blanket) and lithos (rock) and was coined by the American geologist George P. Merrill in 1897.
On the Earth regolith arises from the degradation of bedrock by weathering and biological processes. However, on the Moon these two processes are completely absent and the creation of the regolith is determined by two other factors already mentioned above: micro-meteorites bombardment and a lesser extent by action of solar wind. The regolith layer has a depth of 4 to 5 m in mare areas and from 10 to 15 m in the older highland regions. It appears with a grey colour and is mainly composed by olivine, pyroxene and plagioclase. The bulk density of Moon ranges from 0.9 to 1.1 g/cm^3 in the top few centimetres of surface and increases with depth reaching 1.9 g/cm^3. The average value of density between 0 and 30 cm in depth is 1.58 g/cm^3, whereas from 30 to 60 cm is 1.74 g/cm^3. The increase of this value is caused by the compaction process carried out by upper layers on lower ones due to their weight.
Based on morphological characteristics, the regolith can be divided into [5]:

- Agglutinate: These are particles composed of lithic, mineral, and glass fragments welded together by a glassy matrix containing extremely fine-grained metallic Fe and formed by micrometeorites impact. The energy released by the impacts is in fact sufficient to melt the regolith and create glass. Important observation is that creation of agglutinates are possible thanks to the lack of atmosphere.
- Crystalline, Igneous Rock: Made up of basaltic fragments, which are composed of plagioclase feldspar pyroxene and sometimes olivine.
- Breccias are formed from lithification of crystalline lithic fragments and regolith components, during complex impact driven processes.
- Mineral Fragments: During meteorites impact, lithic fragments are broken, the mineral fragments separate and deposit into the regolith.
- Glass: are formed by impact of meteorites or volcanic eruptions.

Geological characteristics impact on physical properties of the regolith such as porosity, compressibility, shear strength, permeability, diffusivity, ultimate bearing capacity, (static and dynamic), slope stability, trafficability, electrical conductivity, dielectric permittivity, etc. For instance, the shear strength has been extensively studied because it determines the load-bearing capacity and the movement of vehicles on the lunar surface. The most known model is Mohr-Coulomb:

$$\tau = c\sigma \tan \phi$$

where τ is the shear strength, σ normal stress, c the cohesive contribution and ϕ the friction angle. Another interesting value is the maximum slope stability angle which is 36 degree. This value will be important for further consideration in the design phase.
However, the study of the lunar samples was fundamental to understand not only the Moon composition and its creation, but also the Sun's history, galactic and solar cosmic rays composition.

Figure 2.14: Imagines taken during Apollo 11 mission and highlights regolith consistence

2.7 Dust

The Regolith is mainly composed by grain with sizes between 45 to 100 μm. Many of them are sharp and glassy, the result is a highly abrasive material. It has a very low electrical conductivity and dielectric losses; this allow the accumulation of electrostatic charge during ultraviolet irradiation.
The sharp gradient of UV fluxes between day and night can generate electrostatically sustained dust clouds which move around the Moon due to rotation of the latter. Its high capability of accumulate electrostatically charges gives dust a high adhesion properties on equipment and structures causing serious damage.

Chapter 3

Habitat design in literature

Numerous types of habitats are presented in the literature. Before and after the first landing on the Moon on July 20 1969 many engineers and architects developed and designed habitat with the most different characteristics, materials and shapes to better achieve the main goal: design a safety and comfortable place where man can live for a certain period. Many solutions were provided thanks to the great human capacity to think and dream in different ways. However, most of these ideas were developed from a purely architectural point of view and few or no analysis were made from an engineering and strictly structural point of view.
Before analysing the most interesting proposed solutions, a series of concepts is presented in order to classify them.

Figure 3.1: Rendering of a lunar base idea

3.1 Scenario

The document "Stanford" [18] identifies four different type of scenario for future Moon and Mars missions. In this report, the Moon is sometimes considered as a function of Mars. These scenarios differ from each other according to the purpose of the mission, which can be: allow presence of humans on extraterrestrial places, science and exploration and space resource development for the benefit of Earth. In each scenario, the level of scientific efforts, extent of exploration of the planet and level of utilization of local resources are also considered.

- Mars Exploration (Architecture I): Science and Mars exploration are the focus in this scenario while the Moon is considered only as a test bench for equipments and technologies to adopt later on Mars. Exploration of the Moon is a secondary goal for this scenario.
- Science on the Moon and Mars (Architecture 2): The Moon and Mars exploration are equally important in this scenario. In the first phase of lunar exploration, portable tools and equipment are preferred, while larger scientific ones will be used once excellent surface construction and maintenance skills are developed.
- The Moon to Stay and Mars to Explore (Architecture 3): The permanent human presence on the Moon is the focus in this scenario, while Mars becomes only a place for scientific experiments and exploration. Objectives are creation of self-sufficient systems, also called, closed ECLSS to allow life on our satellite. In this scenario high science efforts are required for the previous task.
- Space Resource Utilization (Architecture 4): Space resources utilization to directly supports mission is instead the focus in this last scenario, for instance to develop and support space transports, housing, life science, energy production, construction and many other long term activities. The Moon would be the first step and Mars the second one.

3.2 Development steps of a lunar base

Like cities on Earth, the moon base is also intended to expand over the years. Starting from structures of limited capacity, it will expand to reach large dimensions. In order to make possible this idea, different types of structures are required and in a recent article Cohen MM and Benaroya H. suggest a simple classification to better divide and understand them. The classification is the following and it can also be seen as the actual path to reach the previous cited final goal.

- Class 1: pre-integrated and pre-outfitted module, in composite or metal material for an exploration mission.
- Class 2: pre-fabricated structures made in hybrid or composite material, assembled once reached the planet and designed for a settlement mission.
- Class 3: Structures built with local materials and called, for this reason, In-Situ Resource Utilization (ISRU). Usually realized through 3D printing technology and intended for the colonization of a planet.

3.3 Structural characteristic

The development of new materials and calculation techniques, the conception of new solutions and the desire to achieve different purposes are all elements that influence the structure design. A general classification about structures types is shown in this section. The aim is to provide at the reader a global overview about them in order to better understand the solutions presented in literature. This classification is closely linked to previously mentioned one since the structural knowledge is directly proportional to the development of new technologies and materials, which however require time.

3.3.1 Rigid structures

Rigid structures concerns all the structures which are design to preserve their shape avoiding high deformation and displacement when subjected to the operative loads. They include trusses and frames structures and are usually made by metal or composite material. Until today they represent the most widely used structures in aerospace field. The reason is their high reliability due to the large knowledge about the behaviour of the previously mentioned materials developed in the past years. Rigid structures provides also hight puncture resistance and are designed to keep the desire shape without the need of a secondary structure as happened in the inflatable ones (explanation about them will be provide later). However the penalty is a generally higher mass and the impossibility reduction of their volume during the transport phase.

State of art of rigid structures

The best known example of rigid structures employed as habitat in space are the modules of the international space station (ISS).

Figure 3.2: Tranquillity, module of ISS done by Thales Alenia Space

They are cylinders, closed at the end with two truncated cones where standard interface are placed to allow the connection with the other modulus. The primary structure is composed by cylindrical isogrid stiffened panels welded together to achieve the desired length of the module. The panels are obtained by

machining with machine tools and joined together through friction steel welding process. The secondary structure consists of standard-sized racks, which have the task of accommodating scientific experiments, equipment and facilities for the astronauts. In addition, layers of different materials envelop the module protecting it from the high temperature of the space environment and from micro-meteorites hazard. These layers are not visible in figure 3.2 that shows only the primary structure of the module. All modulus are equipped with the following systems: Environmental Control and Life Supports System (ECLSS), Thermal Control System (TCS) Data Management System (DMS) and Electrical Power System (EPS). To have an idea of module dimensions, the Columbus has a diameter of 4.2 m and a length of 8, with a weight of 10.2 tons and a pressurized volume of 75, m^3. However only 25 m^3 are the free volume when all racks are installed.

3.3.2 Cable and tensegrity structures

The term "tensegral" derives from the crasis of two English word: tensional and integrity and means "integral structures in tension". The most recent and understandable definition about tensegrity structures is given by the professor Renè Motro of the Montpelier university. He said: tensegral is a system in a state of stable self-equilibrium, composed by a discontinuous series of components compressed within a continuum of traction elements. A figure could be however more explicative than any other definitions.

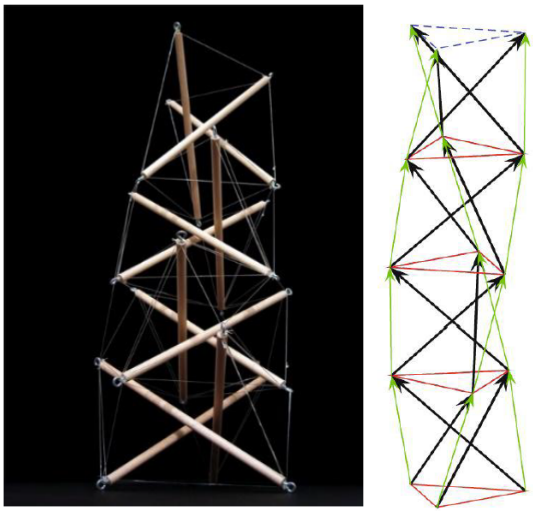

Figure 3.3: Tensegral column generated by the superposition of regular prisms

As shown by the previous image, the compressive elements (bars) create a discontinuous path while the tension elements (cables) make the opposite. However, tensile elements are privileged because the lack of the instability issue allow a lower weigth of the latter. [20]
Tensegrity structures can also change their shape, in other words they can be employed to create deployable structures. The deployment mechanism can be realized by lengthening the bars or pulling the cables. Applying one of the

previous methods it is possible to change structure shape.

State of art of cable and tensegrity structures

There are many structures made with this technique. Examples are covers of stadium or bridges as in figure 3.5

Figure 3.4: Kulirpa Bridge, Brisbane, Australia. Source [20]

In aerospace field, deployable tensegral structures are studied and developed only on an experimental level. An example of their feasible applications in this field is shown in the next figure that represents a deployable tensegral tower, which could by employed as antenna.

Figure 3.5: Tensegral tower. Source [20]

3.3.3 Inflatable structures

Inflatable structures are mainly made with fabrics or membranes. They are able to keep the desired shape and withstand the operative loads only through the help of the internal pressure, presence of a secondary support structure, or both of them. The main reason of interest in this type of structure is their ability to reach small volume and sizes once folded and to ensure large spaces once inflated. "Terms "inflatable" and "deployable" do not have a standard use in the literature, it appears preferable to use inflatable for soft and foldable materials that are balloon-like, and deployable for rigid but storable components that are mostly mechanisms" [21].
Inflatable structures are not very common in the aerospace field, the reasons are mainly two: they are made with newly created exotic material (compared to metal ones) and the deployment process is not linear, presenting high deformations difficult to model mathematically. Furthermore, the first consideration determines a little in-depth knowledge of their behaviour, therefore a lower reliability.

In summary, the main advantages of inflatable structures are:

- hight packaging in folded configuration: they have a 25 percent packaging advantage;
- low mass: they have a 50 percent weight advantage because made by very thin materials;
- low cost: costs reduce to "a factor of ten for structures such as space antennas" [21];
- possibility to be inflated more than one time.

However "the greatest advantage of large inflatable habitats may be the most difficult to quantify: habitability. Habitability is the sum total of those qualities that make an environment a pleasant place to live and a productive place to work Studies have shown that personal space, for work and for leisure, is an important factor in the psychological well-being of isolated groups" [34]
The only disadvantages are:

- not very hight punctual resistance;
- the need of greater attention in the folding phase, because it is necessary to avoid bends in orthogonal direction which could cause high stress during the deployment phase [21].

State of art of inflatable structures

Based on the advantages of these type of structures, many ideas have been developed, but almost none has been realized. In the following paragraph three examples of inflatable structures are reported.

PAGEOS (PAssive Geodetic Earth Orbiting Satellite) One of the first applications of inflatable structures was the PAGEOS. It consist of a balloon like satellite, launched by NASA in the 1966. It has a diameter of 30.48 m, once inflated, and it is composed by a 12.7 μm thick plastic film in mylar, coated by a vapour deposited aluminium. It was used for passive telecommunication thanks to the radio wave reflection done by its surface. PAGEOS' predecessors in satellite triangulation were the Echo 1 (1960, 30 m) and Echo 2 (1964, 40 m) balloons used for the same purpose [24].

Figure 3.6: PAGEOS

TransHab The TransHab was a project developed by NASA in the 1990's with the aim to create an expandable habitat for future interplanetary mission. In fact the name reflects the original intention to design an interplanetary vehicle to transfer humans to Mars: Transit Habitat. However, this purpose was abandoned and the TransHab was designed to replace the rigid modules of the international space station.
Difficulties encountered during the development of the project, delays and increasing cost of the ISS program led to the signature of the House Resolution 1654 in 2000 which forbade NASA to continue the TransHab project. Subsequently the TransHub rights were acquired by the private company: Bigelow Aerospace with the aim of buiding a private space station. The company has already launched the Genesis I, Genesis II, and BEAM pathfinder spacecraft, with plans for additional experimental module such as their BA 330 and the Bigelow Commercial Space Station [25].
The TransHab intended for the ISS have an overall length of 12.19 m and a diameter of 7.28 m, once inflated. These dimensions provide an internal pressurized volume equal at 342 m^2.
The structure is composed by a hard-body cylindrical core made of carbon fibre composite which acts as the backbone of the structure and by a multi-layer inflatable structure which surrounds the previous one as shown in figure 3.7
From an architectural point of view the TransHab is composed by four levels or floors:

- Level 4: The Pressurized Tunnel Area intended to provide a passageway between TransHab and any vehicle to which it is attached.
- Level 3: It hosts the exercise area.
- Level 2: It hosts the crew quarters.
- Level 1: It hosts the kitchen and the common area.

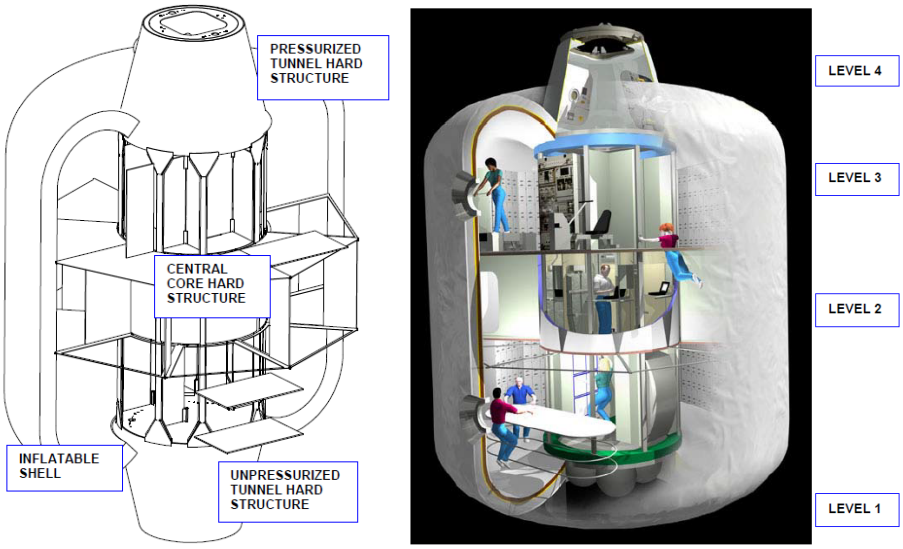

Figure 3.7: TranHab scheme. Source [23]

The TransHab has been designed to reduce its volume at the launch and maximize the available internal space once inflated into orbit. Numerous structural challenges were faced to achieve these goals. One of them is to ensure the same level of protection from space environmental hazards, provided by rigid structures. This objective was reached using several layers of different material, each one, with a precise scope. To describe this solution a figure is more understandable. The following figure 3.8 shows the single layers and and the order in which they are placed. Starting from the external side and going towards the internal one, is possible to encountered:

- One layer of external thermal blanket. It provide thermal insulation of the module, protecting the inner structure and astronauts from the high temperature variation recorded on the external surface (121° on illuminated surfaces and -128° in shadow ones)
- Four layers of bullet-proof materials separated by open-pore foam with the aim to provide a protection against micro-meteorites impacts. Principle behind this concept is the idea of the Whipple shield.
- Multiple layers of Kevlar fabrics with the task to be the primary structure of the inflatable module part. They fix the module shape and withstand the operational load generated by the internal pressure.

- Four layers of Combitherm which make the module air-tight. Combitherm is a material commonly used in the food industry
- An internal cut-resistance and fireproof bladder,to protect the previous layers from accidental scratches and flames [25]

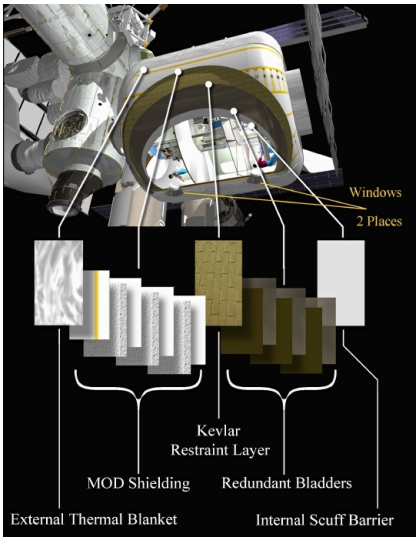

Figure 3.8: TranHab scheme. Source [25]

BEAM (Bigelow Expandable Activity Module) As mentioned at the beginning of the chapter, projects about inflatable structures were numerous, but only few have been really developed. One of these are the BEAM (Bigelow Expandable Activity Module)

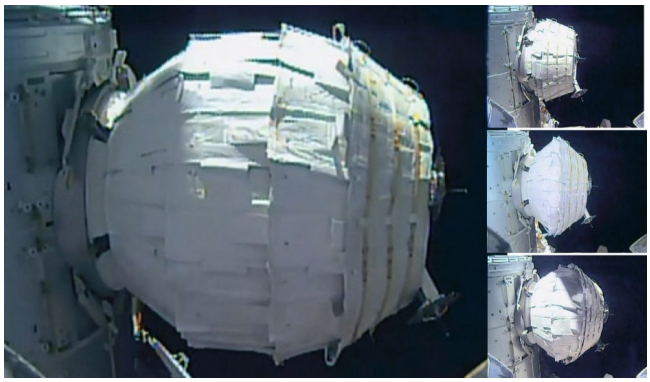

Figure 3.9: BEAM, expansion process

BEAM is an experimental inflatable module, built by Bigelow aerospace for NASA as a temporary module for the International Space Station. It was transported by SpaceX CRS-8 and arrived at the ISS on April 10, 2016. It

was first pressurized on May 26, 2016, but the try failed. The problem was identified in the adhesion between the layers due to the 10 month delay caused by the postponement of the launch. The inflatable process had a better result on May 28 of the same year when the module reached the shape visible in figure 3.9
BEAM is composed of two rigid ends, which allow the connection with the rigid docking interfaces of the ISS and by an external surface in fabric that allows the folding of the module during transport and storage phase. In this configuration BEAM has the following dimensions: 2.16 m in length and 2.36 m of diameter. Once inflated to a final pressure of 101.4 kPa, module can reach 4.01 m in length and 3.23 m of diameter. These dimension allow a pressurized volume of 16 m^3. Inside, module appear as in figure 3.10

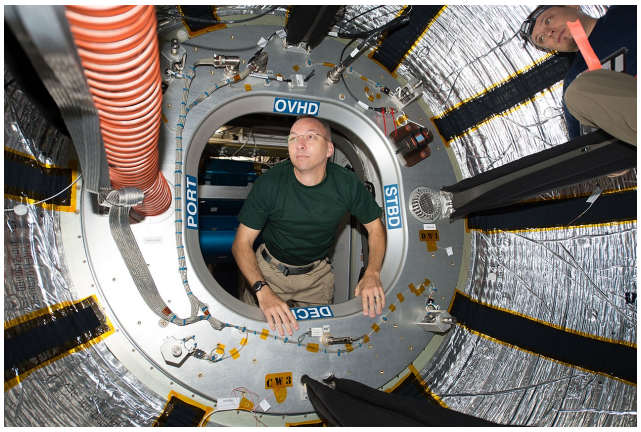

Figure 3.10: BEAM, Inside view

Interesting is the solution adopted by engineers to protect the module and humans from the space environment, such as radiation and micro-meteorites. The primary structure of BEAM is made by flexible Kevlar-like materials, but produced by the company itself, while multiple layers of flexible fabric and closed-cell vinyl polymer foam provide the necessary protection from radiation and micro-meteorites impact. However, this technology is still young and for this reason a series of sensors were placed inside the module to validate model calculations. The closed cell polymer foam structure acts as a shield against micro-meteorites through the Whipple shield principle and also as a radiation shield thanks to the high level of hydrogen contained within the material. A study conducted by NASA in 2002 demonstrated that materials with high level of hydrogen, such as polyethylene, are more efficient to reduce primary and secondary radiation than aluminium **??**.

Whipple shield "The Whipple shield or Whipple bumper, invented by Fred Whipple, is a type of hypervelocity impact shield used to protect crewed and uncrewed spacecraft from collisions with micrometeoroids and orbital debris whose velocities generally range between 3 and 18 kilometres per second (1.9 and 11.2 mi/s).
In contrast to monolithic shielding of early spacecraft, Whipple shields consist

of a relatively thin outer bumper spaced some distance from the main spacecraft wall. The bumper is not expected to stop the incoming particle or even remove much of its energy, but to break up and disperse it, dividing the original particle energy among many fragments that fan out between bumper and wall". Thus "the original particle energy is spread more thinly over a larger wall area, which is more probable to withstand it". [26]

3.3.4 ISRU (In-Situ Resource Utilization) based structures

All the materials exposed to the harsh lunar environment undergoes rapid ageing, with the consequent deterioration of their mechanical characteristics. The materials mainly vulnerable to these conditions are the composite ones. In fact, the polymer matrix, in which the fibers are drowned, is highly sensitive to radiation and humidity, which can lead to fragility and growth of microcracking. Vacuum is also not a favorable condition for them, since it is the cause of the outgassing phenomenon. A solution to these issues could be the use of raw materials already existing on the Moon to create protective structures, for those made of composite materials, or to build new and autonomous ones. This can leads also to the reduction in the number and mass of structures transported from the Earth, decreasing mission cost. However this solution requires advanced robotic manufacturing capabilities.

Figure 3.11: ISRU-based structures

Useful lunar raw materials, from a structural point of view, are magnesium, one of the most pervasive metals in the lunar soil, or simply the regolith. It can be used as concrete if combined with water, or sintered. Sintering is a process in which the material is heated to its melting point and then cast into moulds or used for 3D printing [1]. The aim of this process is to allow the production of artefacts in dry environments. An example of 3D printed structure in shown in figure 3.12.

3.4 Emplacement

Design of lunar habitat can not be decouples from it final emplacement. The location of the habitat, for example below or above the surface, is essential to

Figure 3.12: Structure obtained by 3D printing of lunar simulant, ESTEC

determine the environmental challenges which the structure must face in order to ensure a safe and pleasant environment for human being, and therefore the feature that it must have. Another interpretation of this concept is that a correct decision on its location can reduce issues during the design phase.
In this section different solution are shown.

Above surface The surface of a planet is the easiest place to reach, because no equipments are needed to excavate the soil and all the fundamental resources, such as sunlight, are easily available. However, even if the advantages are numerous and important, the disadvantages are not to be underestimated. An habitat on the lunar surface is exposed to high levels of radiations and also to micro-meteorites bombardment (Chapter 2). Along with the previous disadvantages high temperatures variation exists between lunar day and night and also between the illuminated surface of the structures and those in the shade. These temperature conditions create alternating stresses in the structure giving rise to the consequent fatigue phenomena. All these drawbacks lead to the need of protection systems for the structure, such as anti-radiation screens, micrometeorites and thermal protection systems, which means greater complexity and greater mass to transport, increasing the mission cost.
The alternative option is to bury the structures under a few meters of regolith. Regolith offers an economical alternative to the transport of special materials from Earth. Furthermore, the loose regolith is easy to handle and can also be bagged and piled on top of the habitat. These option are more easily implemented in the mare region, where regolith is many meters thick, than in highlands. The latter regions are also more inaccessible [5].
However only through a precise benefits and drawbacks evaluation is possible to understand if the choice is advantageous or not.

Craters Craters can also be considered as places above the surface, but due to their shape and other characteristics they have some advantages over it. From a radiation point of view, they allow a partial protection of the lateral parts of the habitat from the incoming charged particles moreover if complete close

with a "roof", they allow the creation of large spaces which can be exploited for agriculture, research o Conservation [1].

Lave tube "Lava tubes are natural conduits through which lava travels beneath the surface of a lava flow. Tubes form by the crusting over of lava channels and pahoehoe flows" [29]. Today the Mood a cold planet, and the partial melting zone (lower mantle) has a radius of 587 km, compared to 3484 km of the crust [30]. For this reason lava tubes appear today as empty tunnel. Their existence was hypothesized many years ago, before their effective discovery. The fist lava tube was discovered through data recorded by the JAXA Kaguya in 2008 mission and appear as a 60 m of diameter hole, which was called skylights. Possibility to establish a lunar outpost inside a lava tube has numerous advantages. It provide natural protection against radiation, large temperature variations and micro-meteorites, moreover it is also relatively dust free. In fact it allow a estimate constant temperature of -20° [28]. Ideas developed to take advantage of lava tubes concern transportation of rigid or inflatable structures inside them, or the more ambitious ones: the pressurization of part of them by sealing the ends. In the latter case, the structures do not need to be pressurized, as the whole external environment is.
However, idea of placing habitats inside lava tubes also has drawbacks. The fist is that not all lava tubes are easily accessible, it depends to their orientation and angle of incident with the surface. The second and not less important issue is structural stability of the chosen lava tube.

3.5 Geographic location

The habitat emplacement is not the only factor to consider in the design phase, since its geographic location has an equal importance. This affects both calculations about trajectory and both the habitat external environmental conditions. From a geographic point of view, Moon can be divided in two regions: the Equatorial one and poles.

Poles The temperature of the polar regions is lower and more constant than the equatorial one (temperature variation between lunar day and night is only about pm 10 K), furthermore, in permanently shaded craters they can reach a constant value less than 40 K. These factors can be beneficial to the moon base. The low temperature variation is an excellent factor to avoid alternating stresses in the structures with the origin of consequent fatigue phenomena. However, the polar regions do not allow a homogeneous illumination of the habitat: one side is directly exposed to sunlight and the other remains in shadow. This results in high and different thermal deformation,which can compromise structural integrity.
One of the critical issues for lunar or space base is the internal heat dissipation which is produced by electronics component. The low external temperature of the polar regions is an optimal solution for this issue and it also allows the use of smaller radiators to fulfil this task. This latter consideration leads to a lower mission cost. Additionally, temperature below 40K "could also ease the problem of designing and operating cryogenic equipment consisting of superconductors, cold optics, low-noise photon detectors, and gravitational-wave experiments"

[5].
Another advantage of the polar regions is the possibility of having a perpetual light if the habitat is located on high points such as the edges of large craters or in mountainous areas. This last feature can allow the generation of electricity in a continuously way, adopting solar panels or other technologies related to the sunlight, reducing also the needed of batteries.
However the poles do not have only advantages, the low average temperature in fact requires large insulation system. Another issue is the difficulty of maintaining continuous communication with Earth [5].
However, there is another consideration to take into account. Due to the very small inclination of the Moon's equator (1° 32' respect the ecliptic), J. D. Burke [32] speculated that there may be ice preserved in permanently shaded craters or valleys where temperatures may be relatively constant and as low as 40 K. This additional element could drastically change the habitat design and precisely the life support system (LSS). A more open loop LSS could be used allowing less technological complication. The recovery of oxygen from $C0_2$ would become superfluous and could be extracted, by hydrolysis, from the water. Furthermore, the oxygen and hydrogen obtained from the latter process could be used as rocket propellant for further space missions. However, a method to exact water in a solid state from soil and a second to purify it would be now necessary.
With the NASA's announcement on October 26, 2020 this scenario is becoming more and more real. Thanks at the the Stratospheric Observatory for Infrared Astronomy (SOFIA) it was possible to assert that water is more common on the Moon than previously thought and it is also present in sunlit regions of our satellite, such as the Clavius Crater. As said by Paul Hertz, who leads NASA's astrophysics division "This discovery challenges our understanding of the lunar surface and raises intriguing questions about resources relevant for deep space exploration" [33].

Equatorial region Equatorial regions have mainly disadvantages. The temperatures, as described in chapter 2, have high day-night variation, about ±140 K and generally higher average temperatures than those at the poles. The first feature impacts on the emergence of fatigue phenomena while the second on high thermal stresses and deformations. A solution could be burying the whole structure. However this not solve the needed of heat dissipation. Due to the high temperature radiators should have large surfaces to be efficient and this means large volume and greater mass, increasing mission cost.

3.6 Habitats design

Numerous habitats design were developed by architects and engineers for future lunar settlements. The purpose of this chapter is to show the most interesting ones and to highlight the most ingenious and peculiar features of them in order to draw inspiration for the design of a new one.

The first habitat designs were developed in the post-Apollo era. Companies such as Boeing, Lockheed and Rockwell Intl took part in this challenge.
Boeing in 1963 proposed the LESA (Lunar Exploration System for Apollo). The "initial concept was designed to accommodate six people for six months.

It would hold 46,000 lb of payload, a 10 kW nuclear reactor, a 3765 lb. rover, and equipment to move regolith for shielding use" [21].(figure 3.13)

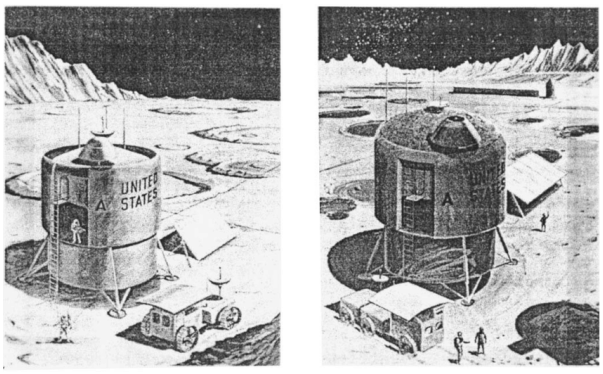

Figure 3.13: The LESA Initial Concept Base Model 2 (Boeing, 1963). Source [21]

The habitat shown below reflect the period from the early 1980s to the present.

Burke, J.D. (1985) The habit proposed by Burke, J.D. (1985), shown in figure 3.14, was designed to be placed in the polar regions and have a rigid structure. As mentioned earlier in the geographic location chapter, these regions could hide frozen water beneath the surface and allow a continuous lighting condition if the habitat is placed in an elevated position. The system used to collect and transport the sunlight inside the structure is particularly interesting: a heliostats, as shown in the figure below. The solution chosen in order to counter the low external temperature and the radiation hazard, was to bury the habitat under a few meters of lunar regolith. The main factors that guided this design and its emplacement were the desire to exploit the Sun as a constant source of light and the possibility of having available water reserves.[5]

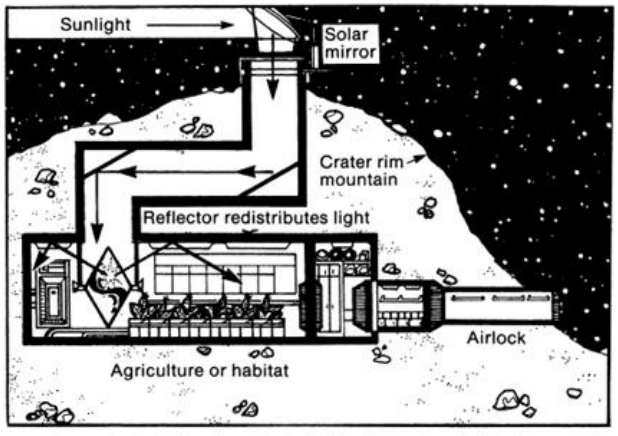

Figure 3.14: Habitat emplaced on lunar pole. (Burke, J.D., 1985). Source [5]

Duke, M.B., et al. (1985) Duke, M.B., et al. had design an habitat able to be modified according to the development level of the base and for three scenarios i.e., scientific research, production, and self-sufficiency. The development steps was identified in:

- Preparatory Exploration
- Research Outpost
- Operational Base
- Advanced Base

The first structures used to begin the construction of the habit could be space station modules, buried under the lunar surface to protect astronauts from radiation. A rigid structure was also used in this project.
Design is shown in figure 3.15.[5]

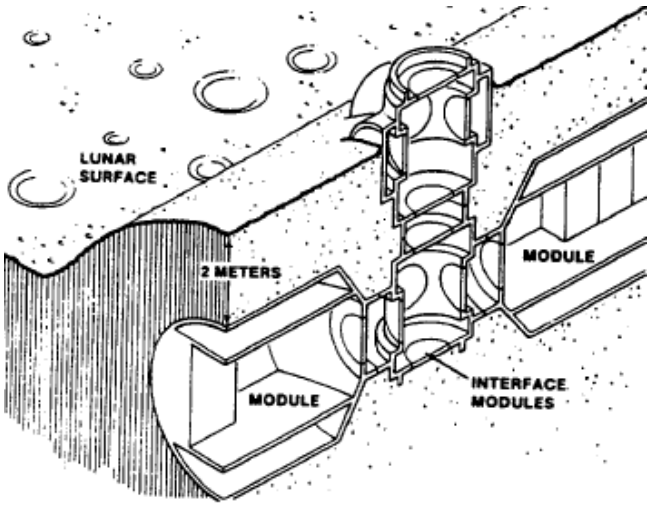

Figure 3.15: Phased Evolution of Lunar Base (Duke, M.B. et al.,1985). Source [5]

Kaplicky, J. and Nixon, D. (1985) This solution for a moon base was developed to accommodate 6 astronaut and the design (figure 3.16) concerns 6 rigid modules of 10 m length and 4.5 m of diameter. The aim of the lunar base was to provide a research outpost with a housing, logistic and laboratory module. The difference from the previous ones, is the way in which modules are buried under the regolith. In this concept, a superstructure is developed. It can be simply deployed manually covering the entire surface of the modules and the thick layer of regolith is placed over it.
The components of the structure once transported by the shuttle to low Earth orbit, would be carried to the Moon with an Earth-Moon transport system. [5]

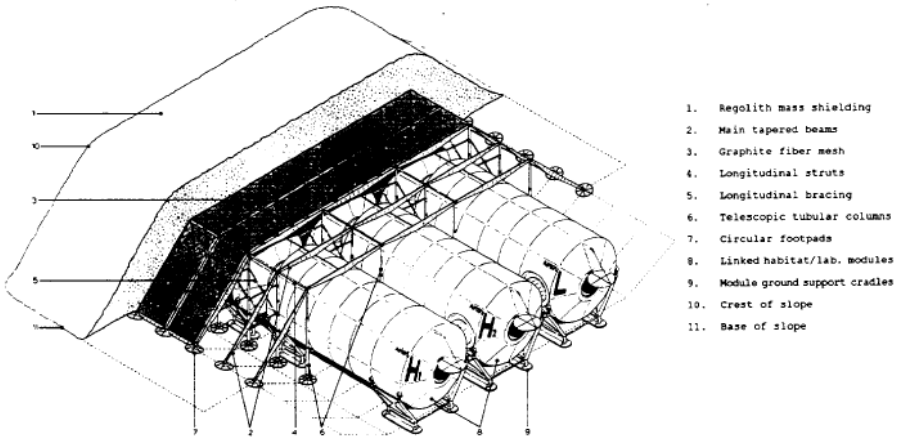

Figure 3.16: Manually deployable superstructure envelope over SSF modules (Kaplicky, J. and Nixon, D., 1985). Source [5]

Three-Hinged Arch Shell Structure The three-hinged arch is a typical structural configuration. It allows an easy calculation of the constraint reactions and of the internal forces, being a statically determined (isostatic) structure and hence it could be an advantageous project for a preliminary sizing calculation. This concept was analysed by Ettouney et al. (1992) [38] and in a modified version by F. Ruess et al. (2006) [1]. Structure shown in this paragraph is the modified version. The habitat proposed has a rise of 5 m and a single storey configuration is chosen. Internal space is exploited as shown in figure 3.17 creating different functional areas.

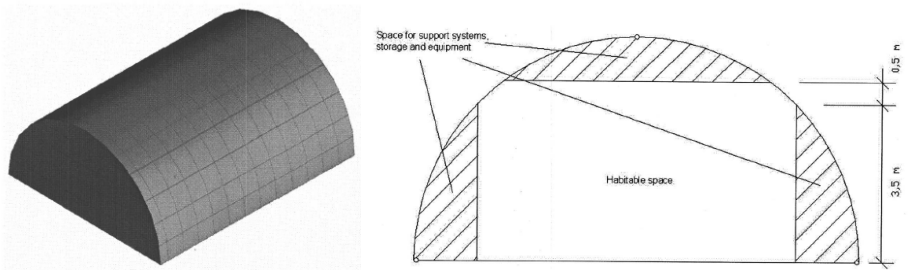

Figure 3.17: Three-Hinged Arch Shell Structure. Source [1]

The cylindrical configuration instead of the parabolic one, was chosen because "On the Moon [...] the governing load is not gravitational. A comparison of parabolic and circular arches under internal pressure loads can be seen in 3.18. It shows clearly that the circular arch is the more suitable structure because no bending moments are introduced in the arch" [1].

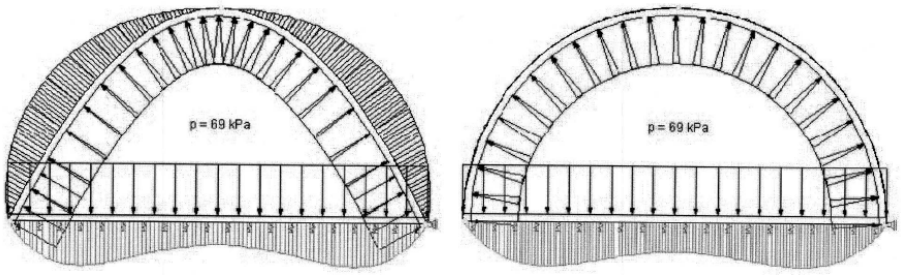

Figure 3.18: Comparison of bending moments for the parabolic and circular arches. Source [1]

Spheric inflatable lunar habitat This habitat was developed for the Lunar Base Systems Study located at the Johnson space Center. The innovative aspect of this habitat consists in being an inflatable structure. It consist of a 16 m diameter sphere with an internal volume of 2145 m^3 when inflated at 101.4 kPa and it is design to accommodate 12 astronauts. The interior space is divided into four floors which allow a walkable area of 594 m^3. The bottom of the sphere gives rise to another plane and could be used as maintenance bay or storage space. The floors are connected by a hexagonal and vertical passage that allows the movement of equipment and people between the levels.
The habitat is composed by a primary structure, a spherical pneumatic envelope, and a secondary one, an internal structure, which supports floors and equipments. The first consists of "a high-strength multi-ply fubric, with an impermeable inner layer and a thermal coating on the outside" [34]. The material selected for the envelope is "Kevlar-29, a high-strength aramid fiber made by the DuPont Chemical Company. DuPont literature indicates that a broadweave fabric of Kevlar-29, with a thickness of 0.114 mm, has a breaking strength of 525 N/cm (Dupont Co., 1976). Based on this material, the envelope has a weight 2200 kg, with a structural safety factor of 5" [34]. The thickness of the envelope was estimated at 5 mm and the total volume around 4 m^3. Considering a packaging ratio of 10:1, therefore, 1 m^3 of material and 9 voids, once folded the structure occupies 40 m^3 of space.
The secondary structure consists of a series of curved beams, placed on the internal side of the envelope and replicating the longitudinal and latitudinal lines of a sphere. In addiction, secondary structure includes also concentric and radial beams with the purpose of supporting floors and equipments. Last but not least purpose of the secondary structure is to support the weight of the habitat with the overlying regolith in case of accidental depressurization, avoiding its collapse. An estimation of the total mass of the habitat is about 16300 kg which includes 9000 kg of primary structures, 6000 kg of floors and 1300 kg of walls. To protect habitat from radiation and micro-meteorites it is half buried and the remainder part covered with regolith "sandbags" with a thickness of 3 m. Covering activity is certainly the main one in the first period of development of the base and great efforts are required. An alternative might be to provide a few inches of shielding to protect the habitat from galactic cosmic radiation, with a separate, smaller, "storm shelter" to protect the crew in the event of a serious solar flare. [34].

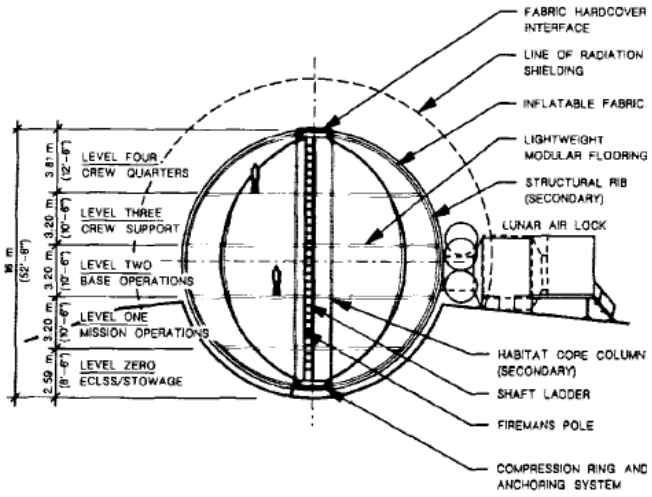

Figure 3.19: Spheric inflatable lunar habitat. Source [34]

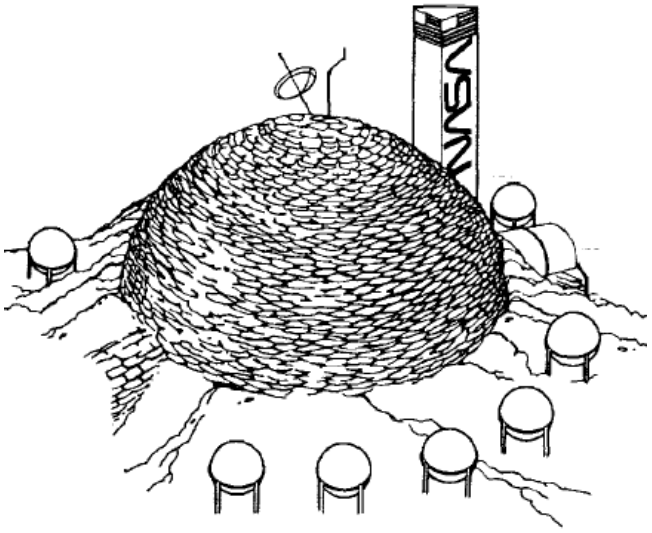

Figure 3.20: Spheric inflatable lunar habitat: Source [34]

Horizontal inflatable habitat for SEI "The spherical shape is the most volumetrically efficient, with the least surface area and mass for a given volume" [34] however, the double curvature of the walls does not allow an optimization of the internal spaces, for example for the equipments location. One possible solution is the one provided by Kriss Kennedy (1992) [35] who proposed a cylindrically shaped inflatable habitat. Habitat has a total length of 43.34 m, when inflated with a pressure of 14.7 psi and a final diameter of 8 m. These dimensions allow a pressurized volume of 2145 m^3 with a walkable area of 547 m^2. It was designed to accommodate 12 astronauts inside. As in the previous habitat,

it is composed of an external pneumatic envelope (primary structure), and two floors supported by an external load-bearing structure (secondary structure). Spherical and cylindrical habitat were developed after a few years since the material chosen for the outer shell is the same: multilayer fabrics of Kevlar, with the addition of Mylar and Spectra. Similarly external enveloped includes also an internal non-permeable bladder and an external thermal coating. The new and interesting solution is the type of structure used to support the second floor of habitat(figure 3.22). Floor is composed by arch-frame structure connected through 40 hard-point to an external exo-structures. To allow the connection, the inflatable envelope is equipped with through holes. Great technological problem of this solution is to guarantee a self internal pressurization, without leakage, in the previous hard-point. The secondary structure have also the task to sustain structure in the event of accidental depressurization [35]

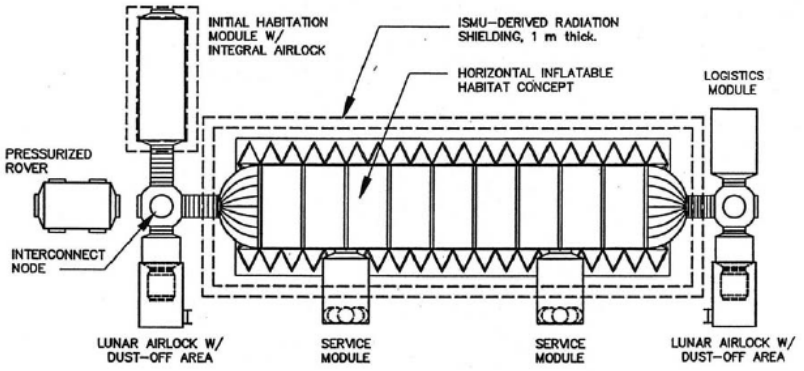

Figure 3.21: Horizontal inflatable habitat for SEI. Source [35]

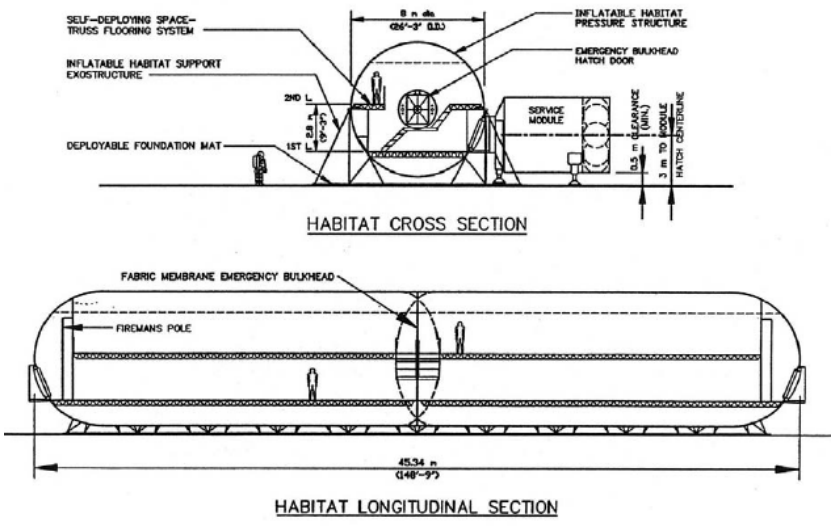

Figure 3.22: Longitudinal and section view. Source [35]

Hypes, W.D. et al. (1992) Hypes, W.D. et al. (1992) proposed three different concepts for a lunar habitat. The first and second one exploit the great knowledge about rigid module and are composed by Space Station Freedom structural elements. Concept 1 (figure 3.23) and 2 (figure 3.24) differ each other in type of method used to create regolith shield against radiation.

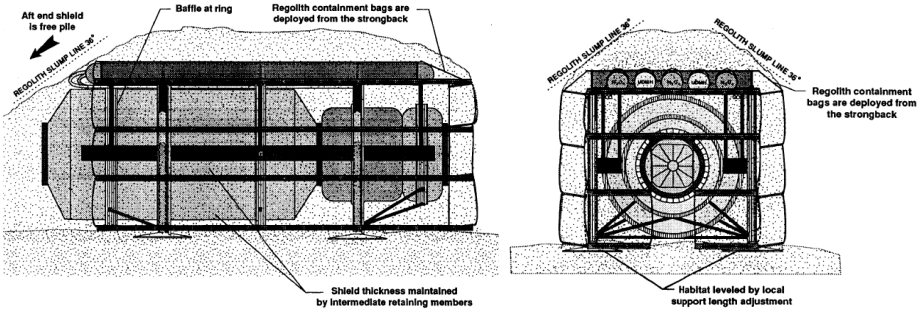

Figure 3.23: Concept 1 with regolith shield. Source [36]

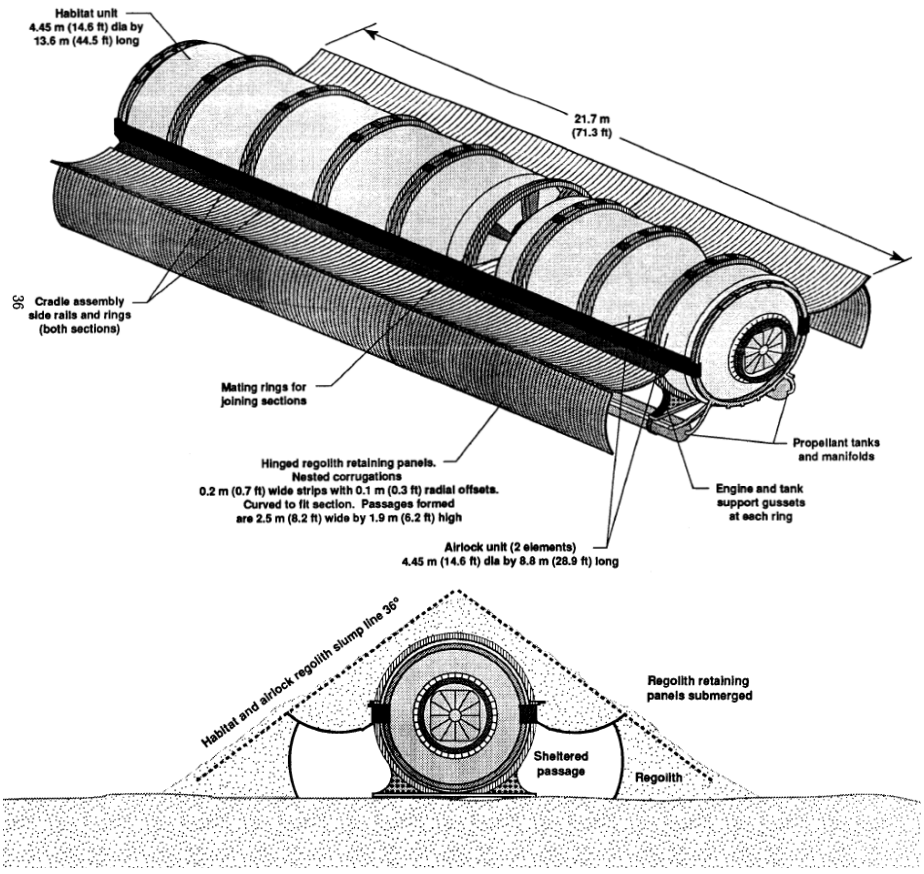

Figure 3.24: Concept 2, At the bottom concept 2 with regolith shielding

However, the most interesting proposed solution is the third (figure 3.25). In this one, an expandable module is coupled with a rigid one. In this way is possible to utilize the most favourable features avoiding the design weaknesses of earlier expandable module. The rigid module consists of a double airlock which allows pressurization cycles avoiding the collapse of the structure in case of depressurization for EVA missions. Before and during the touch-down, expandable part of structures is retracted, and only once on planet, it expands thanks to cradle side rail telescope. Protection from solar flares, GCR and micrometeorites bombardment is provided by a thick layer of regolith [36].

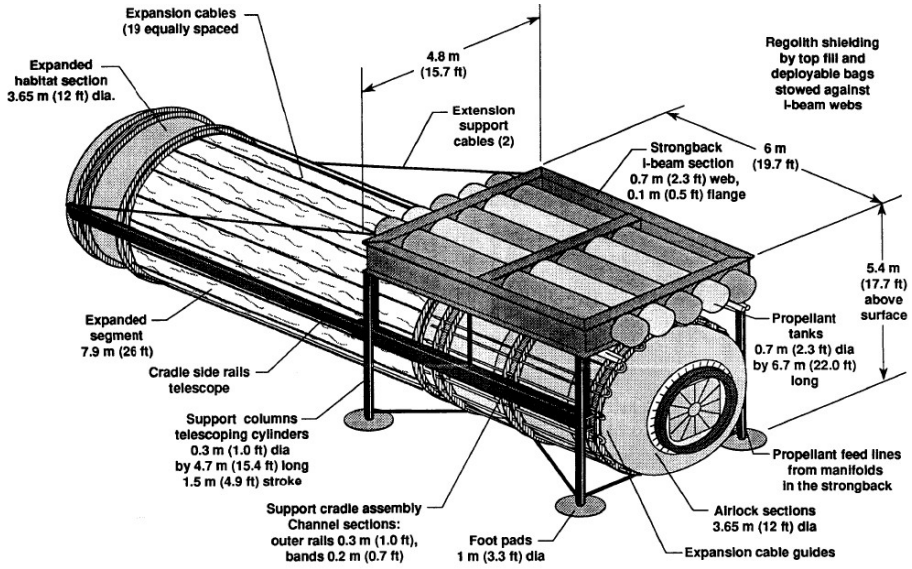

Figure 3.25: Concept 3. Source [36]

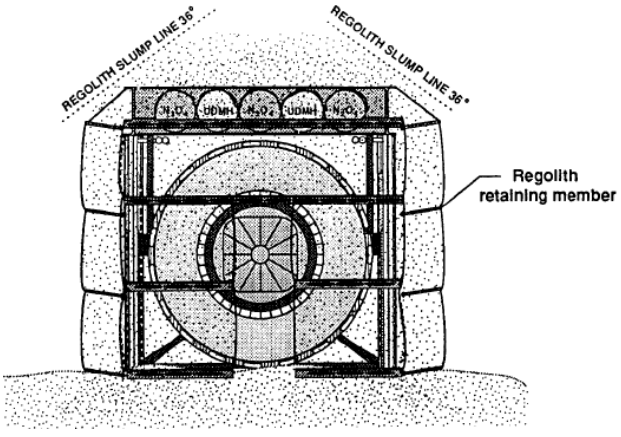

Figure 3.26: Concept 3 with regolith shielding. Source [36]

Genesis II Advanced Lunar Outpost (Moore, G.T. (1991)) If previous concepts were designed to be placed on lunar surface this lunar habitat solution, was thought to exploit natural features of lava tube. A new idea for habitat emplacement was developed. Hybrid rigid-inflatable structures are used for the habitat and this fact highlights how inflatable structures were becoming normal in the in minds of designers. Habitat was designed to accommodate 12 crew members for an indefinite period of time. It provides facilities such as launch and landing sites, solar power array field, habitat and laboratory facilities and a far-side astronomical observatory.
Habitat is composed as follows:

- Level 1: Is composed by two module for EVA missions and provides the stowage and maintenance of space suits. The modules are covered with regolith to protect astronauts from radiation.
- Level 2: It consists in a shuttle-C module which connects element on surface with ones in lave tubes.
- Level 3 & 4: Is composed by two levels inflatable modules, each one placed inside the lava tube, and connecting each others through the shuttle-C previous module. They are made by two kevlar membranes and stiffness of them is achieved through the inflation of structural foam between layers. Intended use of modules is laboratories, shown on the right in figure 3.27 and habitation on the left of the same figure.
- Level 5: It is composed by three modules: the EVA module, Suit Storage and Maintenance Module, and the Crew Support Module. The modules do not touch directly floors of lava tube, but are suspended from the ground by reticular structures to avoid irregularities of the terrain.

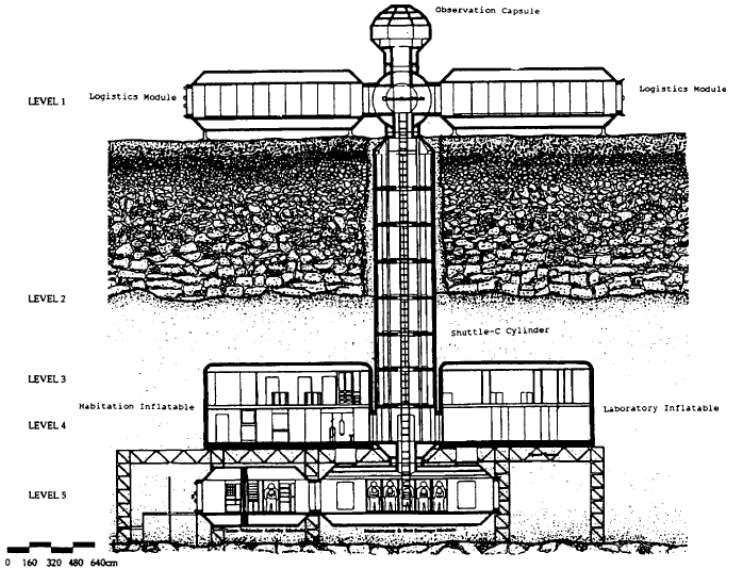

Figure 3.27: Genesis II Advanced Lunar Outpost (Moore, G.T. (1991))

"Tuft Pillow" Inflatable This concept was proposed by Nowak, P.S. et al. (1992). the idea is to provide new shape for inflatable modules that do not concern spherical or cylindrical shapes, with the opportunity of better optimization of floor to volume ratio. The proposed solutions were modules with prismatic shape and the following dimension: 6.1 x 6.1 x 3 m (length, wide, hight), basing on size of normal room on Earth. From a structural point of view they are composed by the following element:

- Four vertical columns with footing. They are made of thin membranes and structural rigidity is reached through inflation of structural foam inside them.
- Four upper and four lower tubular compression arches also made by thin membrane, which give the pillow shape at the structure. Curvature radius of arch is a compromise between the reduction of waste volume (low radius) or induced stresses in arcs (high radius).
- Four external membranes, one for the floor and one for the roof.

The arch and column structures must sustain structure and regolith weight during the operative life and avoid the collapse of the habitat in case of accidental de-pressurization.
The main point of this design is duplicability. Allowing a high modularity, and so different assembling possibility of the lunar base elements, less calculation and analysis are required in the design phases. However, high modularity design have a critical issue: a single design mistake can become a global issue for all the base.
The single modules can be joint together creating a larger structures as shown in figure 3.28 on the left. Management of interior spaces can be perform, removing or leaving wall membranes between modules.
The most interesting idea, employed in this design and the previous one is the use of foam to make rigid, structured made in fabrics.
Preliminary mass calculations speculates a value of approximately 195 kg for each module using the kevlar 49 as material for the walls and other structural components [1].

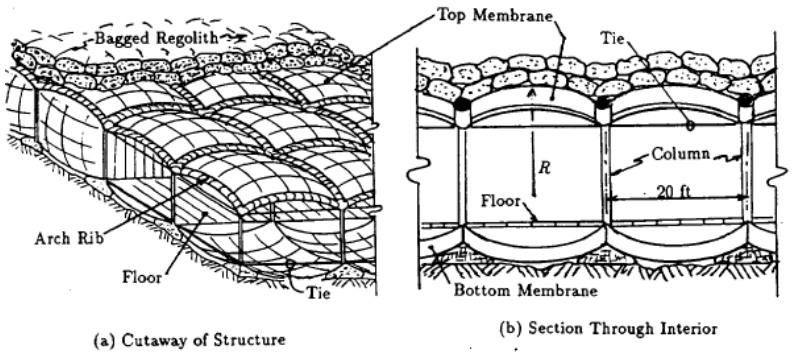

Figure 3.28: "Tuft Pillow" Inflatable: Source [1]

Claims Harrison, R.A. (1992) The structure shown in figure 3.29 is only an example and not a totally developed concept of a cylindrical habitat. It provides an idea of an interesting solution for primary structure proposed by Claims Harrison, R.A. (1992) [37]. "The fabric could be fashioned into cylindrical tubes, creating Cylindrical Fabric-Confined Soil (CFCS) structures" [5] as one shadowed in the figure. Consequently is possible to have arches, beams or other primary structures able to withstand the operative load and avoid the collapse of the habitat due to accidental de-pressurization.

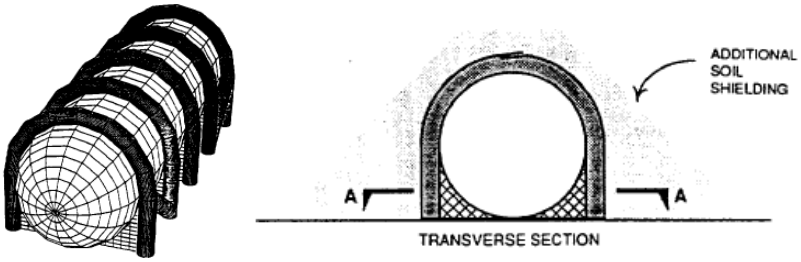

Figure 3.29: Cylindrical inflatable design, with the shaded region indicating regolith coverage. Source [5]

Kopernikus Lunar Base The kopernikus Lunar Base was proposed by a group of students during the Lunar Base Design Workshop, hosted by ESA/ESTEC in 2002. It consists of a linear set of modules connecting together and elevated from ground thanks to an external support structure. The rigid modules are connected end to end, like the ones of the International Space Station, giving rise at the beck bone of the habitat. "Crew cabins, command structure and the medical station are attached to the sides of the backbone hull" [39]. However these latter modules are not made by rigid structure, but through hybrid ones. Parts of these are inflatable allowing space saving in transportation and storage phases and a larger available volume once deployed through pressurization.

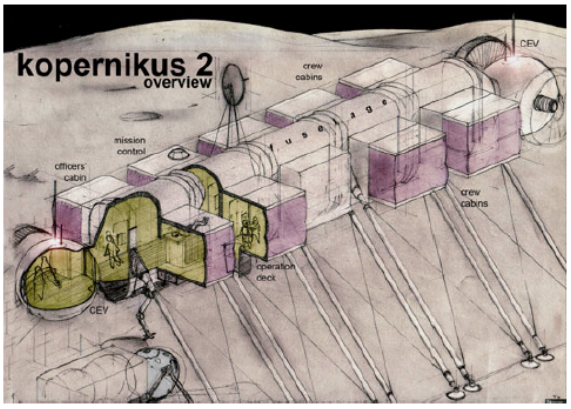

Figure 3.30: Kopernikus Lunar Base. Source [39]

Tycho Rolling Lunar Base This design was also proposed during the previous contest at ESA/ESTEC. The mainly aspect is its capability to move on lunar surface. Habitat was designed for scientific research and mining process of Helium 3. For this motivation spherical shape was chosen, allowing the rolling movement of the habitat. It is compose by three concentric spheres as shown in figure 3.31. The inner and firs one contains the habitat, the second one water use as slider liquid and the third (external one) acts as a radiations protection thanks to lunar-water and by-products of mining process stored inside it. Movement is allowed through air-cushions, which are inflated on one side and deflated in the other. This process is supported by motion of water stored in the second sphere, which changes the center of gravity allowing a displacement of few metres at week [39].

Figure 3.31: Tycho Rolling Lunar Base. Source [39]

Concrete habitats using lunar resources Last but not leas there are ISRU base structures. As described in the chapter 3.3.4 they are made by raw material present on Moon. Possible examples of regolith, as construction material, are the ones proposed by Bialla, P., et al. (1992) in his paper [40]. Regolith can be used to create concrete. The idea is to extract calcium silicate and oxygen from regolith. The first one can be used as cement and the oxygen adding at the hydrogen Earth-delivered could provide the required water. The obtained concrete can be used to create prefabricate structures with optimal capabilities of thermal insulation, shielding against radiation and micro-meteorites.

Fused regolith habitat The use of regolith to create concrete is not the only solution to build ISRU base structures. Another one is to fuse regolith through concentrated solar radiation. In this way is possible to reach temperature of 900-1000 ° as proposed by Cliffton, E.W. (1990). [41] The compressive and tensile properties of the fused regolith material is comparable to concrete.

Many habitat designs were not mentioned in this chapter due to the large number of them present in literature. If the reader wishes to learn more about these unmentioned designs, from a strictly architectural point of view, the scientific article "Deployable Lunar Habitation Design", written by Sandra Häuplik-Meusburger and Kürsad Özdemir in 2012 is a detailed and optimal text.

Chapter 4

Study about protection from high temperature gradient, micro-meteorites and radiations

The aim of this chapter is to report studies about possible solutions for protection against lunar environment and their efficacy. In addition to this some informations about consequence of harsh environment on lunar habitat design will be explained.

4.1 Temperature fluctuation due to diurnal cycle

Temperature gradient on Lunar surface during day-night cycle is very high. As mentioned in Chapter 2 it reaches a mean value of 280 K. This feature has a crucial importance on the habitat design.
The main problem, relative to the high temperature gradient, is the birth of fatigue phenomena which constrain the size of uncovered surface and the geometry of the structure. For structures or parts of them directly exposed to this gradient, a high elasticity material is required.
Another problem, due to the high temperatures present on the Moon, concerns the coupling system between modulus. They can generate high thermal deformation, which can differ from material to material, making more complicated the joining of two parts of the same module or that between two modules [42].
Nevertheless, thermal excursion 80 cm below the lunar surface is almost irrelevant as shown by figure 2.3. If the habitat would be buried below 30 cm of regolith, this thickness would be sufficient to damp out the 280 K of lunar surface temperature fluctuation to a value of only 6 K [4]. Moreover "it is sufficient to have a regolith covering of just 50 cm to 100 cm over the habitat to damp out the diurnal extremes experienced on the lunar surface" [5]. This shows how a buried habitat could be a good solution to protect astronauts and structure from high temperature excursion avoiding fatigue phenomena for the latter. Moreover using regolith as shield would not be necessary transport of material from

Earth, reducing the mission cost. The only disadvantage in this solution is to find an efficient method to reject the internal heat produced by the electronic devices.

4.2 Meteoroid Bombardment

The probability that a meteorite strikes an astronauts is in the order of 10^8 considering a cumulative time of one year. The probability is therefore very low. However it is not possible to assert the same for a lunar base. A lunar base has a larger surface than an astronaut and it would be exposed to micro-meteorites bombardment for all its life.
Risk is not only the probability that something could happen, but also the critical consequences of it. Probabilities of meteorites' impacts is well know however in not possible to assert the same about the precise impact zone. The level of hazard varies if the target is a vital support system or a simple inert structure. The effective risk could be calculated only when habitat design is defined.
The rate of perforations per day in lunar orbit is shown in figure 4.1 for a Be-Cu plate as the one used in spacecraft meteoroid detectors. The black curve represents the Whipple's (1963) predicted curve.

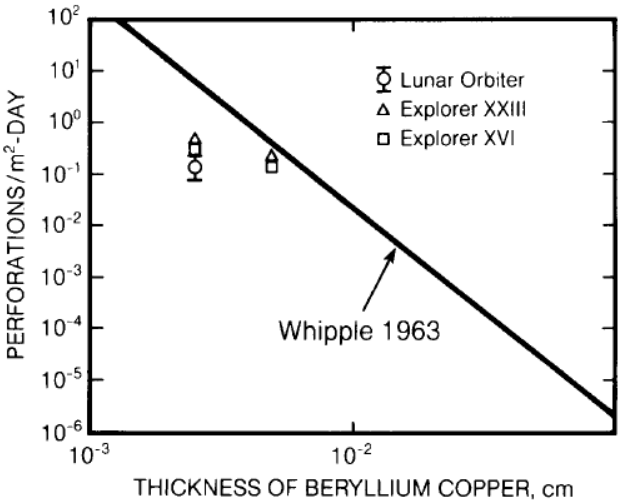

Figure 4.1: Hazards of perforation by meteoroids in lunar orbit as a function of metal thickness. Source [4].

The important data are however the following. Meteorites can have different masses, from micrograms to grams. Micro-meteorites of about 10^{-6} g can produce craters of 500 μm diameter in metal materials. The depth of damages is in general comparable with the diameter, but in brittle material damage can reaches greater depths. To shield habitats or spacecraft from meteorites of these dimensions, two or three millimetres of tough composite material is sufficient [4]. Micrometeorites with masses in the grams order are more dangerous and damage would be in the centimetre scale.

Even if the section about protection from radiation is the subsequent, an interesting comment is the following: "for all practical purposes, if the habitat is protected for radiation, it will be adequately protected for micrometeorite damage" [5].

4.3 Ionizing radiation

This chapter summarizes and show the most important informations contained in three scientific article about how protect the astronauts and the structure from ionizing radiation.

Solar-Flare Shielding With Regolith at a Lunar-Base Site [43] This article written by John E. Nealy et al. provides initial estimates of dose level induced by large solar proton event for more probable configurations of lunar habitats shielded by regolith. The model used to calculate the transport of nucleons through layered shielding material is the Langley Baryon Transport computer code BRYNTRN [44]. Only solar proton flares are implemented in the model since is focused on radiation effect for lunar short-duration missions (2 or 3 month) where the most energetic sources are the solar flares, and precisely the proton "Solar flares may also contain X rays and gamma rays, electrons, neutrons and some heavier charged particles as well as protons. However, examination of the previous observations of large flare radiation fluxes indicates that if the shielding against the high-energy protons is effective, the absorbed dose against the other solar radiation are probable not significant" [43].
The examined solar flares in the article are three and have been chosen because of anomalous large solar proton events.

- Flare of August 1972. It was characterized by the higher numbers of protons, but many of the particles have energy below 150 MeV.
- Flare of February 1956. It produces one-tenth of protons of the previous event but most of them have energy far above 200 MeV.
- Flares of November 1960. It ranks for the number of protons and its energy at an intermediate value compared to the two previous events.

The figure 4.2 shows the protons flux spectra for the three flares presented before.

The results reported in this paper are very interesting. The first one shows the rem dose at 5 cm depth in tissue as a function of regolith slab thickness for the three flares under consideration. Figure 4.3 shows the results. The depth of 5 cm is chosen because it represents the most important radiation dose for human and because it is one of the reference value used in the normative. These aspects about normative and requirements will be treated in detail in the next chapter (Chapter 5) but in order to better understand the following results, normative recommends the Ionization Radiation Exposure Limits at 35 rem/month and 50 rem/year at 5 cm of depth.

The 1972 flare with large low-energy protons without shielding protection releases a dose near the lethal one (about 500 rem at 5 cm depth is the lethal dose), while with a 50 cm of regolith shielding the computed dose is below 1

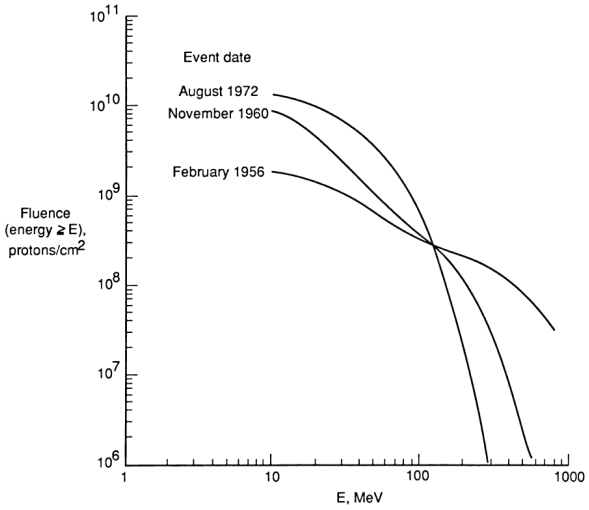

Figure 4.2: Time-integrated proton flux spectra for three anomalously large solar proton events. Source [43]

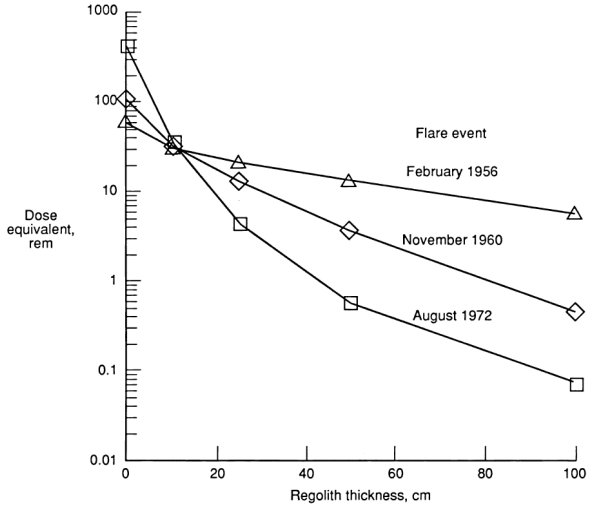

Figure 4.3: Predicted 5 cm tissue dose equivalent for slab thickness between 0 and 100 cm in simulated lunar regolith. Source [43]

rem. Different are the results calculated for the flare with the greatest number of high-energy particles. If without shielding the rem dose is about the limit established by normative, with a 50 cm of regolith shielding the value does not change drastically as in the previous case. This trend is due to the high energy of the protons that results in a higher penetration capability. The 1960 flares have a calculated behaviour equal at the average of the others.
Also results about the rem dose variation with depth and thickness of regolith shield is computed and highlight differences of it from eyes to BFO (blood-forming organs), but the more interesting information for the thesis is the one

presented below.
The data base generated with the transport code is applied to determine radiation fields inside simple geometric structures that represent lunar habitation modules shielded by regolith layers. The structures investigated are the cylinder and sphere. Cylinder is leant on the lunar soil and for this motivation, thickness of regolith is not constant from ground to upper part of the structures. Regolith configuration is showed in figure 4.4

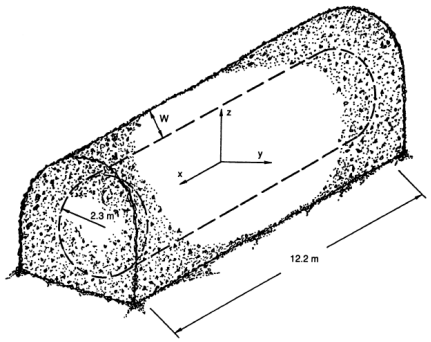

Figure 9. Depiction of regolith shield around cylindrical module on lunar surface. (Configuration used for dose map calculations of figs. 10 and 11.) W = Overhead regolith thickness.

Figure 4.4: Depiction of regolith shield around cylindrical module on lunar surface. Source [43]

This figure reports also the dimension of the cylindrical structures used in the simulation. The sphere instead is half-buried and has a diameter of 15.2 m. Dimensions are different from the ones that will be chosen for the Medflex lunar habitat but this calculation can give an approximative idea of the equivalent dose of radiation inside a structure with 50 cm of regolith shield and furthermore zones with an higher magnitudes dose. Isodose contour plots for cylinder structures are calculated for planes positioned horizontally at three different heights: one meter above the centerline, at the centerline and one meter below the centerline. The same is for the sphere.
Figure 4.5 shows the three isodose contour plots for the 1960 flare event, while figure 4.6 represents results of the same flare but with a top regolith thickness of 100 cm. The rem dose calculated for the three planes are not very different and the point of maximum dose is located at two third from center to the end. Figure 4.7 shows the isodose contour plot for the 1960 flare while figure 4.8 for the 1956 one. The point of maximum dose is at approximately one-third of the radius, near the top of the sphere.
This information, interpreted in a qualitative way, is important to understand which places have to be avoided by astronauts during solar flare events.
In conclusion the scientific article explains that "While 50 cm of regolith thickness may provide adequate flare protection, larger thicknesses may be more desirable." However, as mentioned above, only dose caused by solar flares protons are considered, because the time mission taken into consideration is only about 2 or 3 months, but the objective of this thesis is not to design an habitat for short-duration mission, but for a permanent settlement. For this purpose also the GCRs dose must be considered. Even GCR fluxes are low compared to solar flares and they are constant over time. Moreover, as mentioned by the

article, "The problem of protection from the very high-energy galactic cosmic rays are different from those associated with solar flares in many respect." The precedent results are however interesting to have a general idea about the needed thickness of regolith to protect astronauts during the first month of permanence on the Moon. For example while design thickness of the regolith cover is not reached yet.

Lunar Base Habitat Designs: Characterizing the Environment, and Selecting Habitat Designs for Future Trade-offs This paper, already mentioned in the previous chapters, is less precise for what concern the distribution of radiation dose level inside a structure but reports the thickness of regolith needed to keep it below 5 rem. It says: "Using their transport model, Silberberg et al. (1985) have derived the minimum thickness of the lunar regolith for radiation protection to be 400 g cm^{-2} if the annual dose equivalent is to be less than 5 rem, which is the permissible limit for radiation workers". 400 g/cm^2 is equivalent at a thickness of 2.50m of lunar regolith considering a regolith density of 1.6 g/cm^3

Interaction Depth [g/cm^3] The unit of measurement g/cm^3 could be strange especially if it is used to represent a distance. The motivation is explained below. While charged particles travels through matter, their energy gradually decreases and it is released to the latter through ionization processes. A measure of the path length to predict the absorption by the matter is necessary. This path is proportionally to the density of the matter times the path length. "If density has units of g/cm^3 and path length is in units of cm, then this Interaction Depth, has units of g/cm^2. This unit of measurement allows the comparison of absorption through km of atmosphere to few centimetre of water [46].

In conclusion also the paper "Structural Design of a Lunar Habitat" written by F. Ruess, J. Schaenzlin, and H. Benaroya and already mentioned above says: "It appears that at least 2.5 m of regolith cover would be required to keep the annual dose of radiation at 5 rem, which is the allowable level for radiation workers".

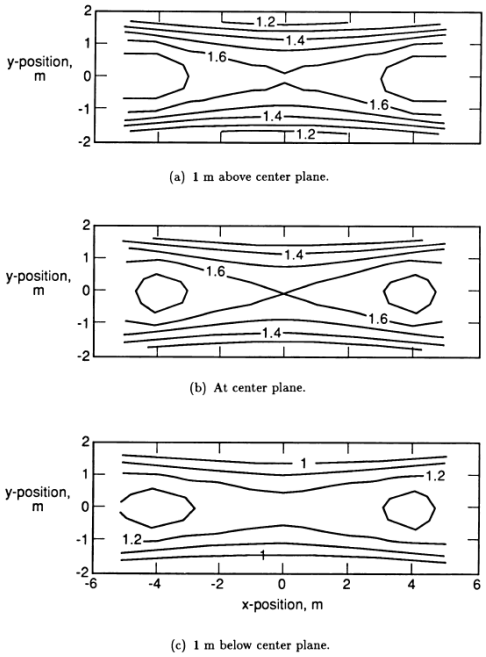

(a) 1 m above center plane.

(b) At center plane.

(c) 1 m below center plane.

Figure 4.5: Isodose maps for cylindrical module for top shield thickness of 50 cm for flare of November 1960. Doses are in rem for 5-cm tissue depth (BFO dose); Contour interval = 0.1 rem. Source [43]

(a) 1 m above center plane.

(b) At center plane.

(c) 1 m below center plane.

Figure 4.6: Isodose maps for cylindrical module for top shield thickness of 100 cm for flare of November 1960. Doses are in rem for 5-cm tissue depth (BFO dose); Contour interval = 0.01 rem. Source [43]

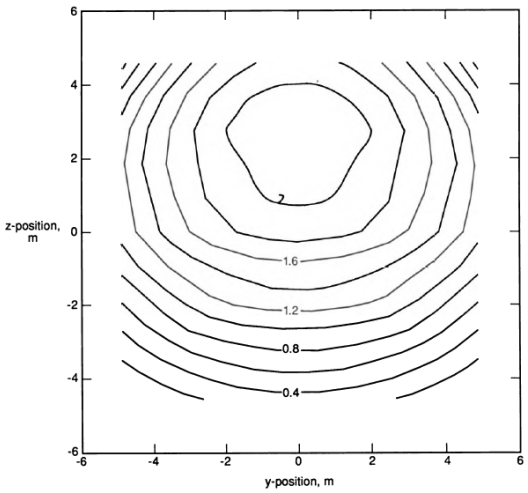

Figure 4.7: Portion of isodose map for half-buried sphere of 15.24-m diameter with top shield thickness of 50 cm. Doses are in rem at 5-cm tissue depth (BFO dose). Source [43]

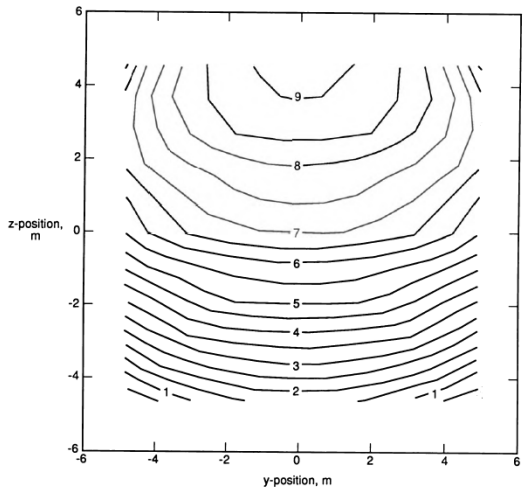

Figure 4.8: February 1956 flare. Source [43]

Chapter 5

Habitat requirements

Requirements represent the guide line for each project. This chapter summaries and justifies the chosen ones, through the explanation of their origins. It includes architectural, internal environmental, structural and launcher requirements. They will be the basement of this study, leading to the choice for the preliminary design and being the comparison parameter for the achieved results.

5.1 Architectural requirements

As M. Roberts says "As used here, the term architectural refers to those factors that influence the volume and form of the habitat. The physical and psychological needs of humans in a confined environment must be balanced against the physical limitations of a pneumatic structure." [34].

5.1.1 Needed habitable volume per person

The term volume here means the available free space which does not include occupied volume by equipments or secondary structures. As learned by Gemini missions, the available free space per crew members can be of 0.57 m^3. If this value is sufficient for short-duration missions, where astronauts are also retrained to a seat most of the time, a different value must be adopted for longer ones. Figure 5.1 shows historical data about specific volume per person compared to mission duration.
The NASA's document NASA-STS-3000 [47] provides a guideline for the habitable volume estimation per crew member as a function of mission duration and performance level. Figure 5.2 shows the graph extrapolated from it. As it can be seen, for mission duration longer than 5 months the optimal performance level is obtained around $20m^3$ per crew member. However graph's values are based on an original study carried out by Celentano, Amorelli and Freeman, who analyse a samples of 18 subject, living in simulated condition for a maximum duration of 7 day [50]. As explain by Kriss Kennedy, author of the mentioned paper, "these data was somewhat questionable, given that they were based on (1) a very small subject pool, (2) under limited simulated conditions,(3) with extrapolations to 12 months drawn from seven days of testing".
For these reasons a free volume per crew member of 120m^3 is proposed, includ-

ing living and working areas. This value is similar to the actual available volume per person on the the ISS.

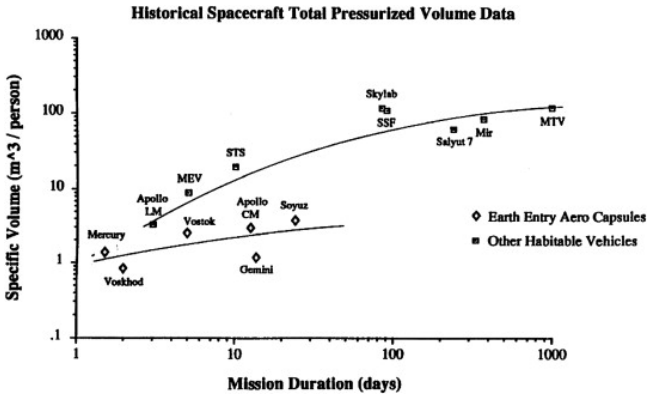

Figure 5.1: Specific volume per crew member

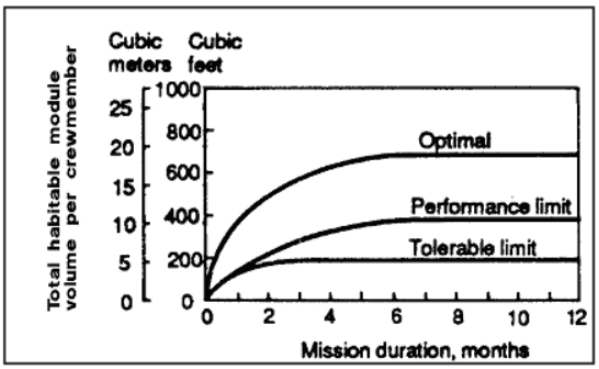

Figure 5.2: Performance level about crew member as function of mission duration. Source [47]

5.1.2 Height of the habitat

"Proposed floor heights for lunar habitats range from 2.44 m (Vanderbilt et al. 1988) to 4.0 m (Chow and Lin 1989; Kennedy 1992)" [1]. Height of the habitat is important on the Moon because the gravity constant is 1/6 of the Earth one, therefore movements made by astronauts would be more similar to jumps rather than to steps of a walk on Earth. Another factor to keep in mind is the thickness of equipments such as light and air conduits placed at the top of the module, which reduce the effective available height in the module. This thickness can go from 0.5 to 1 m.
By analysing the mentioned consideration a total height equal at 3.5 m is chosen for the preliminary design. Motivations are the following:

- Considering an equipments thickness of 0.5 m, a free height of 3 m is available, allowing movements of the astronauts into the module.

- In the half-cylindrical and dome configurations, the base of the habitat has a length double of the height, therefore, higher height leads to a module with larger base an therefore heavier structure to sustain the regolith load.

5.1.3 Length of the Habitat

As mentioned in chapter 3, length of a typical ISS module, as the Columbus is 8 m. It could be a reasonable dimension also for a lunar module. Adding 1 m at the length of the Columbus, a value of 9 m is chosen for the longitudinal dimension of the habitat in the design phase.

5.1.4 Total Needed floor area per person

To size the total needed floor area per person the process explained by F. Ruess et al. [1] is followed. Considering a free volume of 120 m^3 per crew member, an effective available height of 3 m and using the approximation of the habitat free space to a parallelepiped, the available floor per person is 40 m^2. Adding the 20% of the previous value, which is occupied by equipments, the total floor surface is around 48 m^2. Multiplying this latter value for the number of the crew members a preliminary estimation of the total floor area is provided. Based on this estimation the total needed surface of the bases can be calculated, knowing the required number of modules to reach it.

5.1.5 Habitat shape

The habitat geometry coupled with the MadFlex orientation along the thickness must allow the folding of the structure, exploiting the better feature of the MadFlex: flexibility if loaded on one side and rigidity if loaded on the other one. In other words the structure must be deployable.

5.2 Environmental requirement (ECLS)

Since this structure is designed to host humans, other requirements are needed to guarantee a suitable environment for them. This includes, the proper pressure, temperature, humidity and all the other features which are indispensable to allow human life. However these features are fundamental, they represent additional requirements that the habitat structure has to satisfy.

5.2.1 Internal pressure

To understand this requirements the knowledge of the Dalton's Law, which explain that the total pressure of a mixture of non-reacting gases is equal at the sum of the partial pressure of the individual gasses is important. Partial pressure is the pressure reached by a single gas of the mixture, when is alone in the same volume occupied by the mixture.
To allow the respiration and maintenance of normal functions of the human body the partial pressure of oxygen is fundamental and not the barometric pressure (total pressure) of the surrounding environment. For this motivation, attention must be focused on this value, which must be higher than 0,114 atm (1.68 psi). To understand the origin of the previous value a brief explanation

is provided below. The minimum barometric pressure which prevents ebullism, the spontaneous boiling of body tissues is 0,06 atm (0.9 psi). This value represents the saturated vapour pressure of water at body temperature. However oxygen is not the only gas presents in the blood, the other one is the carbon dioxide. To allow the respiration and so the gas exchange across the alveolar membrane the required pressure inside the lungs must be higher than the sum of the oxygen partial pressure 0,06 atm (0.9 psi) plus the carbon dioxide one, which is 0,048 atm (0.7 psi), because a pressure gradient must exist. The result is indeed an ambient pressure higher than 0,114 atm (1.68 psi). This pressure could be provide by oxygen alone, leading a single gas environment or by multiple gas as happens in the Earth's atmosphere. However, as mentioned above the partial pressure of the oxygen is important and not the environment barometric pressure. Therefore in a multiple gas environments the barometric pressure is higher than one composed only by oxygen.
For the reasons explained before an environmental suitable pressure for human life can be reached with a single-gas atmosphere or with a more complicated dual-gas atmosphere (oxygen-nitrogen). At the beginning of the space history a single gas-atmosphere was adopted in NASA's programs as the Apollo one. The motivation to prefer this solution to the others is that "it permits a lower habitable atmospheric pressure, thus decreasing the risk of decompression sickness during EVA; it minimizes the required strength of the spacecraft hull since it will not need to withstand a higher internal pressure; and it requires smaller stores of gas." [?]. However a single gas environment does not have only benefits it indeed leads to a numerous problematics. "While the single gas environment simplified the atmospheric control system for these early space vehicles, there were concerns about the effects of prolonged hypobaric pressures on the crewmembers as well as the increased danger of fire in oxygen-enriched environments, particularly if the barometric pressure were raised above the hypobaric level. This was the case in the Apollo 1 disaster, where a 100% oxygen cabin environment was temporarily raised to 16 psi for a test on the launch pad. In the resulting fire, Ed White, Virgil "Gus" Grissom, and Roger Chaffee died." [?]. Today the idea of a single-gas environment is abandoned and all the modern vehicle's cabin and modules have a dual-gas oxygen-nitrogen atmosphere. This requires a higher internal barometric pressure, "International Space Station make use of a 14.7 psi normal cabin barometric pressure, as this requires the least adaptation by crewmembers and avoids confounding of scientific experiments that might be affected by atmospheric pressures different from the terrestrial standard". ISS atmosphere is composed by oxygen for the 21% and by nitrogen for the complementary percentage.
In conclusion, for the reasons mentioned above a dual-gas atmosphere with an internal pressure of 1 atm (14.7 psi) is chosen for the preliminary design.

5.2.2 Temperature and Humidity

Temperature and humidity are two features closely linked between them because the perceived temperature strongly depends on the humidity level.

Temperature

"Ambient temperatures on current spacecraft are usually kept at “shirtsleeve” conditions, i.e. around 23.9°C (75°F), though launch and landing temperatures are usually 5° cooler, to improve comfort when wearing Launch and Entry System pressure suits". Also Russians consider the range of 22.2°C - 23.9°C (72°F - 75°F) as the ideal condition for a working environment [?].

Humidity

As explained above humidity has a strong influence on the perceived temperature and on the human comfort. As it happen in the desert vs. jungle, temperature may be very similar but the second is more uncomfortable than the first one. The motivation is the different level of humidity. At a comfortable temperature, this effect is less noticeable, but with the raising or decreasing of it, humidity assumes a fundamental role. At high temperatures a low level of humidity is preferable, promoting evaporative cooling adopted by the body, while at low temperatures high humidity is convenient to reduce evaporation and facilitate heat retention.
The cabin environment is usually maintained at about 60% relative humidity (corresponding to approximately 0.2 psi of water vapour pressure) [?]. "If the relative humidity rises above 70%, there is an increased risk of microorganism growth, corrosion, and/or spontaneous condensation", while "Under lower humidity, other problems exist; crew comfort can be compromised and chapped lips, dry skin, and increased upper respiratory infections may be seen." [?].

5.2.3 Noise and vibration

Not considering the launch ad re-entry phases vibrations are not the major health concern for crew members of a space module or of a space launcher. The main source of vibration such as turbulences are absent in space, due to the lack of atmosphere. Therefore, even if vibration could be an issue for certain payloads, they are not an issue for manned operations. Differently from vibrations, noise is instead a bigger concern in space.
"A major source of both noise and vibration in the spaceflight environment is the avionics and other equipment: pumps, fans, compressors, and so on." [?].

Noise

Individual level of noise tolerance is variable, however some general considerations can be done by analysing a large sample of people. "At noise levels above 50 dB, most people must raise their voices to be heard and find the ambient noise annoying. Above 65 dB, temporary threshold shifts are seen and sleep is impaired. Above 75 dB, performance degradation is seen. Obviously, for space travellers – especially those on long duration missions – noise and vibration control mechanisms can be very important for long term health and mood." [?].
The operation effects due to noise are a issue for astronauts and obviously their risk depends from duration and intensity of it. "Audio frequencies are typically 15 Hz -20,000 Hz, with spoken words between 200-6000. While loud chronic ambient noise can eventually damage hearing, short-burst noise, if loud enough, can also be dangerous. Even if not at a level that will lead to auditory damage,

unpredictable, short duration noise can still pose a hazard to crew concentration and could cause distraction at a dangerous time." [?]. In addiction to that a constant level of noise decreases the level of attention of the crew towards the mission critical communications and alarms.
On the ISS the most silent environment is the US lab with a noise level around the 60 dB, while the loudest is the Russian Service Module with a level of 76 dB.
For long duration missions, as a lunar base one, the level of noise must be reduced. The optimal condition would be to set this level below the 50 dB, threshold value above which, people usually raise their voice to be heard. For This reason the previous value of 50 dB is chosen as the highest admissible level of noise for the habitat preliminary design.

Vibration

"Low frequency (0.1-0.63 Hz) whole body vibration frequently provokes motion sickness, while higher frequencies (1-30 Hz) cover the resonant frequencies of the human body." However, once reached the orbit or the Moon surface, the only present vibrations are the ones caused by payload, avionic system and crew members.

5.2.4 Ventilation

In microgravity conditions fluxes of gasses have a different behaviour than ones experienced on the Earth. This happens because forces generated by the gravity and/or breezes, local airflows, and weather are absent inside a space module. In order to replace these phenomena an artificial ventilation must be implemented. The more precise motivation are the following:

- Carbon dioxide is heavier than oxygen and in presence of gravity force it falls away from the face, allowing the presence of new oxygen near the mouth and the nose. In space, where gravity and the other phenomena mentioned above are absent, the previously explained movement of gasses is impossible and leads to the creation of pockets of carbon dioxide around the face, making the normal process of breathing difficult and leading to hypercarbia and hypoxia.
- The absence of ventilation can also lead to a non uniform atmosphere with an heterogeneous distribution of the oxygen and carbon dioxide inside the cabin. In addiction to the previously mentioned pockets of carbon dioxide this can also cause the creation of zones of pure oxygen, increasing fire hazard.
- An heterogeneous micro-environment is also disadvantageous for the detection of undesirables level of harmful contaminants such as carbon dioxide, particulates, carbon monoxide and the other released by on board materials.

"For sea level dual gas environments, ventilation systems usually operate at flow rates of 0.08-0.2 m/s, though they must have the capacity to regulate this level depending upon the crew activities. If a number of crew occupy the

same module, then temperature and carbon dioxide levels will rise more rapidly, necessitating greater ventilation." [?].
For the reasons above the mentioned values are chosen for the requirements about ventilation for the habitat preliminary design.

5.2.5 Ionizing radiation

Once that astronauts leave the Earth to reach the ISS or the lunar surface, they are subjected to a larger radiation dose, due to the lack of atmosphere (for the ISS) and the magnetic protective field (for the Moon). Due to this risks the space agency adopted guideline for the maximum radiation exposure for its astronauts. These exposure limits are based on the recommendation of the National Council on Radiological Protection and Measurements (NCRP). "Exposure to large solar flares or long-term exposure to cosmic rays can exceed these limits. Note that these limits are considerably above those for non-space workers." [57, ?]. These value are shown in figures 11.4.2 and 11.4.2

Organ specific equivalent dose limits	
Exposure interval	**BFO (Sv)**
30 days	0,25
Annual	0,50
For references, see Annex C .	

Figure 5.3: Current ionizing radiation equivalent dose limits. Source [57].

Exposure interval	Bone marrow (Sv)	Eye (Sv)	Skin (Sv)
30 days	0,25	1,0	1,5
Annual	0,50	2,0	3,0
Career	-	4,0	6,0
For references, see Annex C .			

Figure 5.4: Organ dose limits for deterministic effects (all ages). Source [57].

"The career depth equivalent dose limit is based upon a maximum 3% lifetime excess risk of cancer mortality and has additional components of detriment associated with it, namely the risk of heritable effects (0,6%) and of non-fatal cancer (also 0,6%) for a total detriment of 4,2%." [57, ?].

	Age of exposure			
Sex	**25**	**35**	**45**	**55**
Male	0,7	1,0	1,5	3,0
Female	0,4	0,6	0,9	1,7
NOTE 1: Based on 3% excess lifetime risk on fatal cancer in Sv. NOTE 2: For references, see Annex C .				

Figure 5.5: Current career exposure limits. Source [57].

5.2.6 Previous ECLS flight data

Parameter	Earth [a]	Skylab (1973-4) [b]	MIR (1986-) [c]	SSF (1992) [d]	STD-3000 (1995) [e]	ISS (1996) [f]
-	-	84 day max. stay	365 day max. stay	90+ day design stay	-	90+ day design stay
Total pressure, kPa	101,3	34,5	88,0-114,7	100,0-102,7	100,0-102,7	97,9-102,7
O_2 partial pressure, kPa	21,0	22,8-26,9	20,0-26,7	19,5-23,1	19,5-23,1	19,5-23,1
CO_2 partial pressure, Pa	31-100	670 (nominal)	≤ 800	≤ 400	≤ 400	Average < 707, peak < 1 013
Diluent gas	N_2/Ar	N_2	N_2	N_2	N_2	N_2
Temperature, °K	292,5-300,5	285,9-305,4	291,1-301,1	291,5-299,8	291,5-299,8	291,5-302,6
Dew point, °K	274,9-289,9	280,9-288,7	-	277,6-288,7	277,6-288,7	277,6-288,7
Relative humidity, %	20-85	25-85	30-70 [g]	25-70	25-70	25-70
Ventilation, m/s	< 0,1	-	0,2-0,5	0,076-0,203	0,076-0,203	0,051-0,203
Particles (> 0,5 µm), particles/m³	-	-	-	< 3,5E6	≤ 3,5E6	Average < 3,5E6, peak < 7,1E7
Particles (> 0,5 µm), µg/m³	8-9 (nominal)	-	-	-	-	Average < 50, peak < 1 000
Microorganisms [h], CFU/m³	200-600	-	-	≤ 1 000	≤ 500	Average < 1 000
Trace contaminants	Variable	-	see ref. (c)	≤ SMAC [i]	≤ SMAC [i]	≤ SMAC [i]

a Total pressure, O_2 partial pressure and lower bound on CO_2 partial pressure are based on ambient, sea-level conditions (Lide, 1995). Upper bound on CO_2 partial pressure is considered a nominal-to-high indoor value based on the ASHRAE standard for indoor-outdoor air exchange (ASHRAE, 1989) (indoor values as high as 300 Pa are reported). Temperature, dew point, relative humidity, and ventilation ranges are based on bounds of the ASHRAE indoor comfort zones (ASHRAE, 1989). Particulate levels are indoor values (for particulates > 2,5 µm) reported by Liu, et al. (1991). Microorganism levels are indoor values (for manufacturing areas) reported in the ISS ECLS requirements document (D684-10508-1-4, 1996).

b Ref: Wieland, 1994.

c Ref: D684-10508-2-3, 1996.

d Ref: JSC-31000, 1992; SSP-30000, 1992; NASA-STD-3000, 1991.

e Ref: NASA-STD-3000, 1995. Based on values reported in customary units.

f Ref: D684-10508-1-1, 1996; D684-10508-1-2, 1996; D684-10508-1-4, 1996, D684-10508-2-1 ,1996.

g At 293,1 K. Water vapour partial pressure is reported to be 1,3 ⊕ 0,7 kPa.

h CFU = Colony forming units.

i SMAC = Spacecraft maximum allowable concentration.

Figure 5.6: Previous ECLS flight data. Source [57].

5.3 Structural requirements

This section summarizes and provides all the requirements closely linked at the structure such as safety factor, load condition and maximum stresses allowable in each MadFlex layer.

5.3.1 Safety Factor

Safety Factor (SF) is one of the most important structural parameters since it represents the previous knowledge and experience that engineers have about material's behaviours chosen for the structure, and about environmental features which determine the external load conditions. "The range for the factor of safety on Earth is [...] approximately between 1.7 and 3.5. All of the problems and uncertainties on the Moon will certainly require higher safety factors, so factors of safety of 4.0 or higher seem reasonable." [1].
Relying on the consideration mentioned before a SF of 4 is chosen for the design phase.

5.3.2 Load condition

This represents the most important structural requirement. The structure must withstand the following load conditions satisfying both sturdiness and stiffness criterion. Requirements about this latter criterion are listed in the next paragraph.

Load conditions:

1. Internal pressure of 1 atm ($1.013 \cdot 10^5$ Pa) only;
2. Internal pressure of 1 atm ($1.013 \cdot 10^5$ Pa), plus regolith cover load (regolith thickness: 2.5 m);
3. Regolith cover load only (regolith thickness: 2.5 m) [1];
4. Load used to keep the habitat in the folding configuration.

The last load condition represents the most restrictive condition to satisfy. Structure must withstand the regolith load without any help from the internal pressure. This requirement is fundamental since it describes an emergency or planned de-pressurization of the module where structure have to avoid the habitat collapse, with the following crushing of astronauts.

5.3.3 Sturdiness criterion

Sturdiness means the capabilitie of the structure to withstand the ultimate load without breaking. Ultimate load is the maximum expected load of the structure during its operational life multiplied by prescribed factors of safety.
This requirement imposes to verify that the internal stresses of the structure, generated by the ultimate loads for each load condition, are lower than the ultimate strength of each material of which the structure is composed.

However materials behaviour and type of breakdown are different when materials are in traction or in compression, therefore specifically requirements are necessary for each of them.

Dyneema

- Tensioned: Internal stresses generated by ultimate load must be lower than the ultimate tensile strength reported on material's data sheet.
- Compressed: When compressed, Dyneema layers in the MadFlex reach the buckling condition, therefore no compressive Sturdiness requirement is needed.

Foam

- Tensioned: Internal stresses generated by ultimate load must be lower than the ultimate tensile strength reported on material's data sheet.
- Compressed: Internal stresses generated by ultimate load must be lower than the ultimate compressive strength reported on material's data sheet.

Carbon

- Tensioned: Internal stresses generated by ultimate load must be lower than the ultimate tensile strength reported on material's data sheet.
- Compressed: Since MadFles has a sandwich configuration, when compressed, the carbon layers break due to "face wrinkling" phenomenon, before reaching the ultimate compressive strength. Therefore, internal stresses generate by ultimate load must be lower than critical buckling stress ($\sigma_{b,i,x}$ or σ_{Ho}) of the carbon.
  This latter value is calculated with the following two empirical formulas:

  1. First empirical formula:

  $$\sigma_{b,i,x} = \frac{2}{3} \cdot \left(E_{c,i,x} \cdot E_{3,z} \cdot \frac{t_i}{t_3} \right)^{0.5}$$

  "wherein: t_i is the thickness of the outer layer (carbon). E_c, i, x is the compression elasticity module of the same outer layer [...]; t_3 is the thickness of the intermediate layer (foam) and $E_{3,z}$ is the compression elasticity module of the intermediate layer, in the direction of the thickness in accordance with ASTM C365 / C365M standard" [52].

  2. Second empirical formula:

  $$\sigma_{Ho} = 0.5 \cdot (E_f \cdot E_c \cdot G_c)^{\frac{1}{3}}$$

  Where the subscript "f" means the face of the sandwich, while the subscript "c" the core of it [53].

To satisfy the previous requirement about critical buckling stress of the carbon layers, stresses inside the carbon must me lower than only one the two previous value calculated through the empirical formula.

5.3.4 Stiffness requirements

Stiffness is the capability of a structure to avoid large deformation under ultimate load.
This requirement is composed by two sub-requirements, one concerning the arch and one concerning the floor or tie of the arch.

- Arch: Under the ultimate load, the deformation of the structure must allow the movement of the astronauts inside it and avoid the sliding of the regolith bags, compromising the radiation shielding.
- Tie of the Arch: It musts have a adequate stiffness to avoid an excessive deformation of habitat floor under ultimate load proper of second load condition. An excessive curvature of the floor could lead to equipment stability problems inside the module.

5.4 External environmental requirements

This section summarizes the requirements concerning structure and external environment (Lunar environment) interaction.

5.4.1 Regolith abrasion

Regolith is highly abrasive. Even if regolith is collected in polyethylene bags, perforation hazard of the latter exists. To protect the internal layer of the structure from it, avoiding damages, Madflex orientation is fundamental.
This requirement is composed by two sub-requirements, one concerning the vault of the structure and one concerning the floor of the structure.

- Vault of the structure: The MadFLex layer in contact with the regolith, placed on the top of the habitat, must be the rigid one because it is more resistant to abrasive phenomena caused by regolith. Although regolith is contained in bags, this additional requirement has to be satisfied because damage to the outer layer of the material is almost impossible to be reached and repaired as it is buried under 2.5 m of regolith.
- Floor of the structure: For the same motivation of abrasion properties of regolith and lower punctual resistance of the flexible layer compared to the rigid one, the necessary configuration of MadFlex for the floor is with the rigid layer facing the lunar soil.

5.4.2 Vibration

Vibrations produced by the movement of astronauts inside the habitat or by the payloads and equipments must be mitigated, avoiding their transmission at the regolith bags through the primary and secondary structure. Movement of the regolith can produce laceration and degradation of the bags and structure below, because of its abrasive capabilities.

5.5 Payload requirements

This section summarizes all the requirements which a payload must satisfy to be transported on board of a launcher. This includes maximum size, volume and weight. The launcher considered is the Space Launch System (SLS). "The Space Launch System (SLS) is a super heavy-lift expendable launch vehicle, which has been under development by NASA [...]. It will be the primary launch vehicle of NASA's deep space exploration plans, including the planned crewed lunar flights of the Artemis program and a possible follow-on human mission to Mars." [54].
These requirements are fundamental, because the size and weight of the habitats must be optimized in order to allow the stowage of the greatest number of habitats inside the launcher. The reasons is that the lower is the number of launches needed to bring all the base modules to the moon, the lower is the cost of the program.

5.5.1 faring diameter

With a big approximation, the diameter of the faring represents the maximum transversal dimension that a payload can have. Applying this consideration to the lunar habitats, fairing diameter represents a limit of habitat dimensions and number of them that can be stowed on the same transversal plane.
"Impacts of Launch Vehicle Fairing Size on Human Exploration Architectures" provides three different fairing concepts for exploration missions which the SLS launcher can fit:

1. SLS block 1B cargo & 2: 8.4 m (27.6 ft) with an internal diameter (value of interest) of 7,5 (24.6 ft);
2. SLS block 1B cargo & 2: 8.4 m (27.6 ft) with an internal diameter (value of interest) of 7,5 (24.6 ft);
3. SLS block 2: 10 m (32.8 ft) with an internal diameter (value of interest) of 9,1 m (29.9 ft) [55].

If the values reported in the first and second points of the previous list, could seem a repetition, these two fairing concepts differs instead in other parameters such as height and volume. These values are shown in figure 5.7, the ones mentioned in the previous scientific article.

5.5.2 Fairing height

With a big approximation also the height of the faring represents the maximum longitudinal dimension that the payload can have.
Faring heights of the SLS launcher, provided by the previously mentioned article for the three different faring concepts, are:

1. SLS block 1B cargo & 2: 19,1 m (62.7 ft);
2. SLS block 1B cargo & 2: 27,4 m (90 ft);
3. SLS block 2: 27,4 m (90 ft) [55].

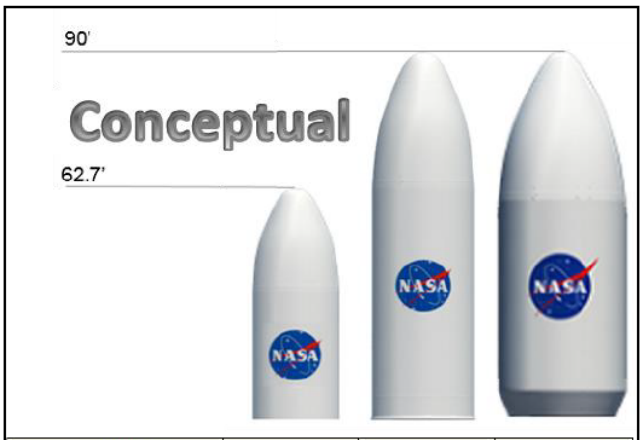

Payload Accommodation	8.4m Short	8.4m Long	10m
Type	8.4m PLF	8.4m PLF	10m PLF
SLS Block Effectivity	1B & 2	1B & 2	2
Length	62.7 ft	90 ft	90 ft
Diameter	27.6 ft	27.6 ft	32.8 ft
Internal Diameter	24.6 ft	24.6 ft	29.9 ft

Figure 5.7: SLS fairing concepts for exploration missions. Source [55].

5.5.3 Fairing volume

The whole available volume for the payload, in the three mentioned configuration is:

1. SLS block 1 cargo: 229.9 m^3 (8118 ft^3);
2. SLS block 1B cargo: 621.1 m^3 (21930 ft^3);
3. SLS block 2: 988 m^3 (34910 ft^3)

The same value are shown in figure 5.8 with same additional details.

5.5.4 Maximum transportable mass

The maximum transportable mass corresponds to the maximum payload's mass and depends on the available trust of the launcher and the mission target (Moon L2, Mars or other planet). The maximum mass for the three mentioned launcher configurations are:

1. SLS block 1 cargo: 27 t (59.5k lbs);
2. SLS block 1B cargo: 42 t (92.5k lbs);
3. SLS block 2: 46 t (101.4k lbs) [56].

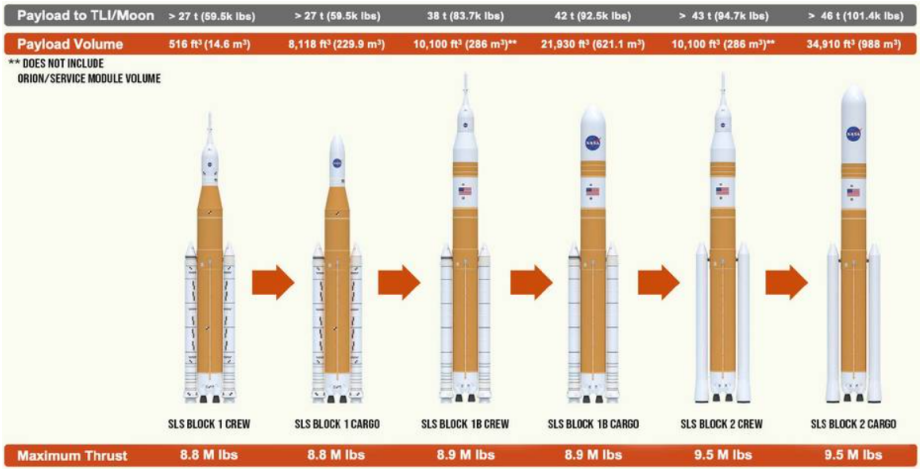

Figure 5.8: SLS evolution

5.5.5 Vibrations

During the flight, turbulence, engines' turbo-pumps and other numerous factors generate vibrations. These vibrations can interfere with the resonance frequency of the payload leading to damages or catastrophic rupture of the latter. To avoid these accidents, resonance frequency of the payload must be far from the ones generated by launcher and atmospheric phenomena.

5.6 Thermal protection requirement

This section focuses on how protect the structure and astronauts from the extreme lunar temperature and its variation from day to nigh.

5.6.1 Thickness of regolith shield

Based on the considerations of in Chapter 4, "it is sufficient to have a regolith covering of just 50 cm to 100 cm over the habitat to damp out the diurnal extremes experienced on the lunar surface." [5].

5.7 Micro-meteorites protection requirements

This section focuses on how protect the structure from micro meteorites bombardment

5.7.1 Thickness of regolith shield

Based on comment in Chapter 4: "for all practical purposes, if the habitat is protected for radiation, it will be adequately protected for micrometeorite damage." [5].

5.8 Radiation protection requirements

This section focuses on how protect the structure and astronauts from ionizing radiation such as solar wind, Solar Cosmic Ray (SCR) and Galactic Cosmic Ray (GCR).

5.8.1 Thickness of regolith shield

Based on the scientific article, mentioned in Chapter 4 "2.5 m of regolith cover would be required to keep the annual dose of radiation at 5 rem, which is the allowable level for radiation workers." [1].

5.9 Summary of Requirements

Architectural requirements	
Item	**Requirement**
Volume per person	120 m^3
Habitat height (radius)	3.5 m
Habitat length	9 m
Floor area per person	40 m^2
Habitat shape	Habitat must be deployable

Environmental requirement (ECLS)	
Item	**Requirement**
Internal pressure	1 atm (14.7 psi) dual-gas atmosphere (oxygen (21%, nitrogen)
Temperature	22.2°C - 23.9°C (72°F - 75°F) (295,35 K - 297,05 K)
Humidity	60% relative humidity (corresponding to approximately 0.2 psi of water vapour pressure)
Noise	$<$ 50 dB
Ventilation	Forced ventilation is required with an air flow rates of 0.08-0.2 m / s.
Ionizing radiation	See tables in paragraph 5.2.5

Structural requirements	
Item	**Requirement**
Safety Factor	4

Load conditions	1. Internal pressure only; 2. Internal pressure plus regolith cover load; 3. Regolith cover load only; 4. Load used to keep the habitat in the folding. configuration.
Sturdiness criterion	Internal stresses of the structure generated by the ultimate loads must be lower than the ultimate strength of each material of which the structure is composed.
Stiffness criterion	• Arch: Under the ultimate load, the deformation of the structure must allow the movement of the astronauts in it and avoid the sliding of the regolith bags, compromising the radiation shielding. • Tie of the Arch: It must have an adequate stiffness to avoid an excessive deformation of habitat floor under ultimate load proper of second load condition.

External environmental requirements	
Item	**Requirement**
Regolith abrasion	• Vault of the structure: The MadFLex layer in contact with the regolith, placed on the top of the habitat, must be the rigid one because it is more resistant to abrasive phenomena caused by regolith. • Floor of the structure: The MadFlex layer facing downwards must be the rigid one because of its high abrasive and punctual resistance.

Vibration	Vibrations produced by the movement of astronauts inside the habitat or by the payloads and equipments must be mitigated, avoiding their transmission at the regolith bags since movement of the latter can produce laceration and degradation in the bags and structure below.

Payload requirements	
Item	**Requirement**
faring diameter	7.5 m (24.6 ft) or 9.1 m (29.9 ft)
Fairing height	19,1 m (62.7 ft) or 27,4 m (90 ft)
Fairing volume	1. SLS block 1 cargo: 229.9 m^3 (8118 ft^3); 2. SLS block 1B cargo: 621.1 m^3 (21930 ft^3); 3. SLS block 2: 988 m^3 (34910 ft^3).
Maximum transportable mass	1. SLS block 1 cargo: 27 t (59.5k lbs); 2. SLS block 1B cargo: 42 t (92.5k lbs); 3. SLS block 2: 46 t (101.4k lbs)
Vibrations	resonance frequencies of the payload must be far from the ones generated by the launcher and atmospheric phenomena.

Thermal protection requirements	
Item	**Requirement**
Thickness of regolith shield	50 to 100 cm

Micro-meteorites protection requirements	
Item	**Requirement**
Thickness of regolith shield	if the habitat is protected for radiation, it will be adequately protected for micrometeorite damages

Radiation protection requirements	
Item	**Requirement**
Thickness of regolith shield	2.5 m of regolith cover would be sufficient to keep the annual dose of radiation at 5 rem

Chapter 6

The Madflex

The Madflex is a material with an innovative configuration created by the Composite Research (CoRe). It is a composite material having a sandwich-like structure which has the unique feature to be crushproof if loaded on one side and flexible, even rollable, if loaded on the other one. The following figure shows its dual behaviour under the two differer load conditions.

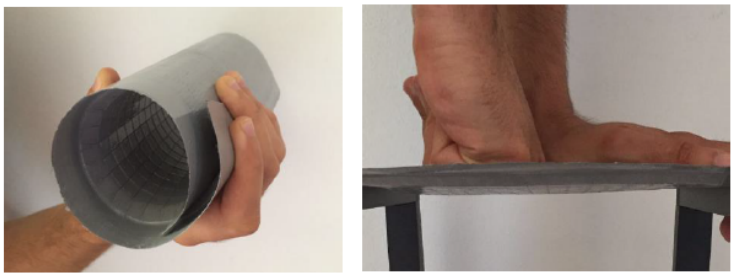

Figure 6.1: Madflex's behaviour. Source [48].

The materials employed for the realization of the two skins can be different such as carbon fibres, Kevlar, aramidic fibres and many others.
The advantages of the MadFlex are the following ones:

- Structural strength: If loaded on the rigid side, it allow hight structural strength. Figure 6.2 shows a representative values about MadFlex mechanical properties.

	Bending stiffness rigid side	Bending stiffness rollable side	Tensile strength	Flexural strength	Flatwise compressive strength
	[N·m2/m]	[N·m2/m]	[kN/m]	[MPa]	[MPa]
TEST METHOD	ASTM D7250/D7250M	ASTM D7250/D7250M	ASTM D3039/D3039M	ASTM D7250/D7250M	ASTM C365/C365M
Max value configurations	250	2,0	700	450	2,4
Min value configurations	13	0,1	350	95	1,2

Figure 6.2: MadFlex Mechanical Properties. Source [48].

- Lightness: Compared to rigid materials, for example alluminium, it provides the same deflection, under the same load (200 Kg) with a total weight of only 1.7 kg compared to 7.8 kg of the aluminium. Moreover "It is 5-6 times lighter than a sheet of ABS (polymer material) of the same flexural rigidity and 3-4 times lighter than a sheet of ABS of the same flexural resistance"[48]. Figure 6.3 shows the mentioned data.

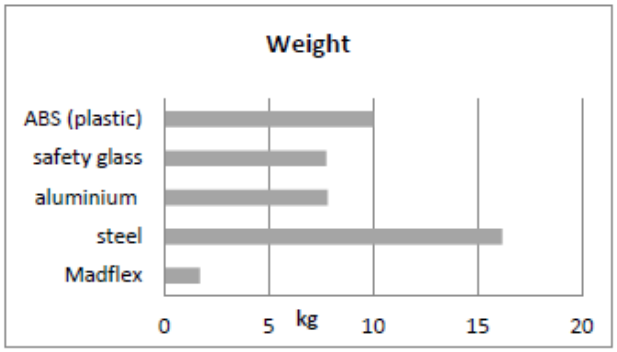

Figure 6.3: Lightness of 1 m^2 sheets in different materials and with the same deflection under a load of 200 N. Source [48].

- Thermic insulating: Its insulating capacity are over 5 times higher than an ABS panel as shows in figure 6.4.

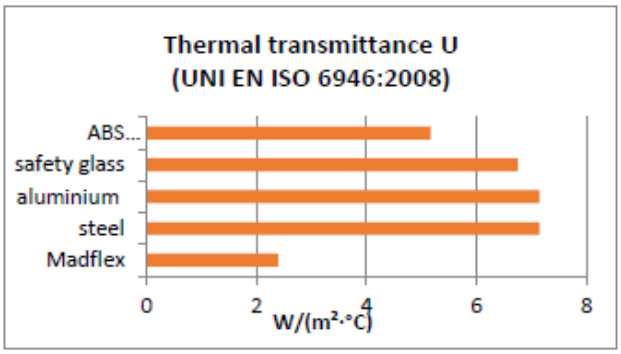

Figure 6.4: Thermal trasmittance of 1 m^2 sheets in different materials and with the same deflection under a load of 200 N. Source [48].

- Environmental friendly material: the Co_2 released during the production process of this material is very low. The greenhouse gases delivered to the environment are about half of those released to produce an ABS panel with equivalent mechanical properties.
- Thermoformable: It possible to provide to the Madflex the desired shape, simply using moulds. An example is shown in figure 6.6
- Easy to transport: Thanks to its properties to be rollable on one side it can be stored and transported in very small volume.

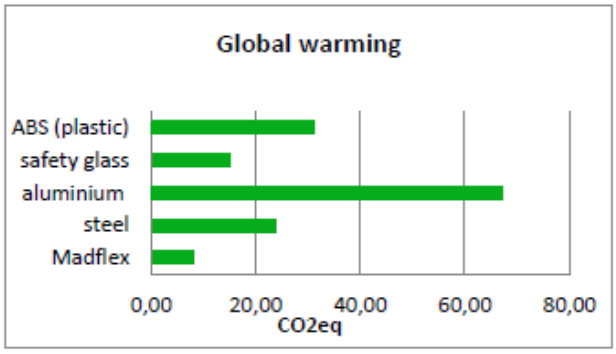

Figure 6.5: CO_2 emitted for the production of 1 m^2 sheets in different materials and with the same deflection under a load of 200 N. Source [48].

Figure 6.6: My colleague while making a Madflex curved panel.

- Temperature resistant.
- Anti-seismic.
- Resistant to chemical agents.
- Fireproof.
- Endless surface finishing

As mentioned before Madflex can be made with different materials in order to satisfy the design requirements of each project. For this motivations the types of Madflex developed are numerous and the table below shows the mechanical properties of only a part of them. The data about the other MadFlex types are reported in the MadFlex sample Book 6.2.

MadFlex 1.0 It is the first type of Madflex developed by CoRe and led to the filing of the MadFlex patent.

	Unit	Typical value	test
Thickness	mm	5	
Areal weight	kg/m^2	1.3	
Tensile strength	kg/m	500	ASTM D3039/D3039M
Failure bending moment	Nm/m	170	ASTM D7250/D7250M
Bending stiffness "rigid side"	Nm^2/m	30	ASTM D7250/D7250M
Bending stiffness "rollable side"	Nm^2/m	0.5	ASTM D7250/D7250M
Flatwise compressive strength	MPa	1.7	ASTM C365/C365M
Heat transfer coefficient	W/m^2K	7.5	DIN52612

Maximum Structural Performances It is able to replace structural metallic part.

	Unit	Typical value	test
Thickness	mm	11	
Areal weight	kg/m^2	1.8	
Tensile strength	kg/m	700	ASTM D3039/D3039M
Failure bending moment	Nm/m	480	ASTM D7250/D7250M
Bending stiffness "rigid side"	Nm^2/m	240	ASTM D7250/D7250M
Bending stiffness "rollable side"	Nm^2/m	1.5	ASTM D7250/D7250M
Flatwise compressive strength	MPa	1.5	ASTM C365/C365M
Heat transfer coefficient	W/m^2K	3.6	DIN52612

Cut Resistant it is able to withstand to cut and perforation damages

	Unit	Typical value	test
Thickness	mm	6	
Areal weight	kg/m^2	1.65	
Tensile strength	kg/m	450	ASTM D3039/D3039M
Failure bending moment	Nm/m	230	ASTM D7250/D7250M
Bending stiffness "rigid side"	Nm^2/m	40	ASTM D7250/D7250M
Bending stiffness "rollable side"	Nm^2/m	0.6	ASTM D7250/D7250M
Flatwise compressive strength	MPa	1.7	ASTM C365/C365M
Heat transfer coefficient	W/m^2K	6.2	DIN52612

Another Madeflex's version cut resistant has the following mechanical properties:

	Unit	Typical value	test
Thickness	mm	5.5	
Areal weight	kg/m^2	1.75	
Tensile strength	kg/m	500	ASTM D3039/D3039M
Failure bending moment	Nm/m	225	ASTM D7250/D7250M
Bending stiffness "rigid side"	Nm^2/m	55	ASTM D7250/D7250M
Bending stiffness "rollable side"	Nm^2/m	0.4	ASTM D7250/D7250M
Flatwise compressive strength	MPa	1.7	ASTM C365/C365M
Heat transfer coefficient	W/m^2K	7.2	DIN52612

6.1 In structural terms

The Madflex is a asymmetrical sandwich material. The asymmetry is due to three different factors:

- Different materials for the upper and lower skins of the sandwich.
- Different thickness of the skins, for equal type of material.
- Both of the previous consideration.

Madflex can be classified as an asymmetric material for the third explanation mentioned before. The different behaviour in traction and compression of the skins confers to the MadFlex the capabilities to be rollable on one side and rigid from the other one. in more detail:

- One skin is made from materials with significant elastic modulus, both in traction and in compression, therefore the skin is able to develop high resistance in this two configurations. Materials used to realize this skin is principally Carbon fiber reinforced polymer, and glass fibers.
- The other skin is made from materials able to develop high resistance to traction but to oppose a very low one when compressed. The way in which these materials are able to have this two different behaviour is detailed at the end of this chapter because it is not due to a simply mechanical feature. Materials used to realize this skin are mainly dyneema and aramidic fiber.

Analysing the mechanical behaviour of the whole MadFlex in bending configuration, two load cases can be identified:

- If the asymmetric sandwich is loaded on the rigid side as in figure 6.7, the rigid skin (green) is in compression and the flexible one (red) in traction. This allow at the sandwich to withstand high loads due to the high compression resistance of the rigid skin and the high resistance to traction of the other one. In this load condition the flexible skin contributes to the overall flexural stiffness of the system.

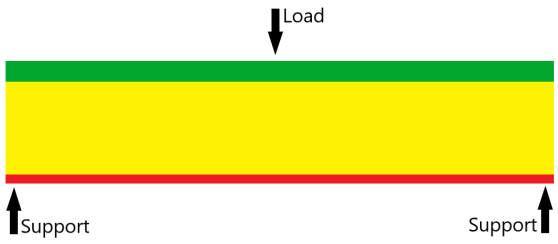

Figure 6.7: First load configuration with rigid side in compression and flexible one in traction

- If sandwich is loaded on the flexible side, rigid skin is in traction while the flexible one in compression. However, the flexible skin does not have the ability to withstand the compression end therefore the sandwich folds, under very low loads. In this load configuration, the flexural stiffness of

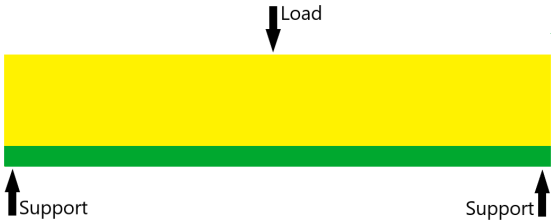

Figure 6.8: Second load configuration with rigid side in traction and flexible one in compression

the flexible skin can be neglected when it is calculated the overall one. The sandwich can be thought as composed by only two layers.

In conclusion if the first load configuration, allows to support high loads, the second one, allows at this material to be rolled. This is possible thanks to the translation of the flexural neutral axis or the centroid near or inside the rigid skin allowing smaller radii of curvature than the ones shown in the first load conditions.
In other word, each material subjected to a bending moment, develop a curvature as shown by the following expression:

$$M = EI \cdot k$$

where M is the bending moment, EI the flexural stiffness and k the curvature equal at 1/r. This expression is referred at the Eulero-Bernulli beam theory for a homogeneous and isotropic material.

The entity of the curvature is due at the flexural stiffness if the bending moment are constant, for this reason, stiffer materials develop lower curvature with higher bending radii, while less stiffness materials develop high curvature with small bending radii. Materials we are usually dealing with have only one value of flexural stiffness and developing the same curvature if loaded on one side or on the other, the Madflex, instead is able to have this dual behaviour thanks to the possibility to develop two different value of flexural stiffness depending on the load condition, which determines the contribution or not of the flexible skin at the overall flexural stiffness. Therefore the curvatures and the radii developed are different.

6.2 How the MadFlex works

In the previous section the double behaviour of the MadFlex was addressed in structural terms, but how is possible to develop these feature using the existing materials?

The flexible skin The low resistance developed by the flexible skin once in compression is due at the possibility to make a skin supple. This can be achieve exploiting something that is usually consider a defect or issue to avoid in the

design phase of a material: the local buckling of a skin.

A sandwich skin can fail due to the following local instability:

- Dimpling: "A sandwich with a honeycomb core may fail by buckling of the face where it is unsupported by the walls of the honeycomb" [49].

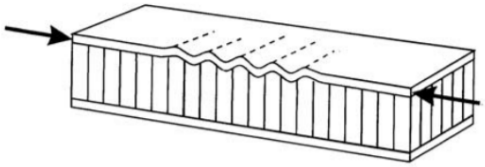

Figure 6.9: Dimpling. Source [49].

- Wrinkling: "Face wrinkling is a buckling mode of the skin with a wavelength greater than the cell width of the honeycomb" [49],in other word: when the core yields under compression due to the load transmitted by the face.

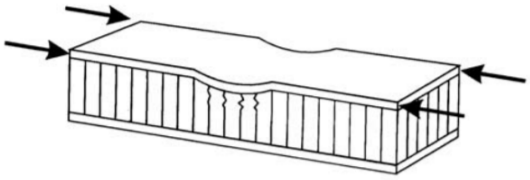

Figure 6.10: Wrinkling. Source [49].

The cave in of the skin can be facilitated by the following factors:

- an elastomeric matrix to allow the fiber deformation;
- a lower thickness of the compressed skin;
- a lower density of the core.

The reversible buckling is the main factor that leads to the double mechanical behaviour shown by the Madflex. It can be obtained applying the previous concepts in a intentional and controlled manner. Figure 6.11 and figure 6.12 show the previously mentioned concept applied to the MadFlex.

The rigid skin To better explain the behaviour of the rigid skin, a clarification is needed. The materials, which rigid skin is made, have a high resistance in compression, but, as all panels or beams with small thickness, the critical issue is the global buckling load, which occurs before the ultimate compressive strength. To avoid this phenomenon the foam and the junction glue, have a fundamental role. Thanks to them the rigid skin can overtake the buckling load and withstand higher load once compressed. However, because MadFlex is a

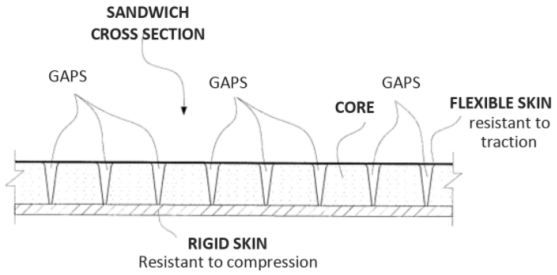

Figure 6.11: MadFlex, section view. Source [48].

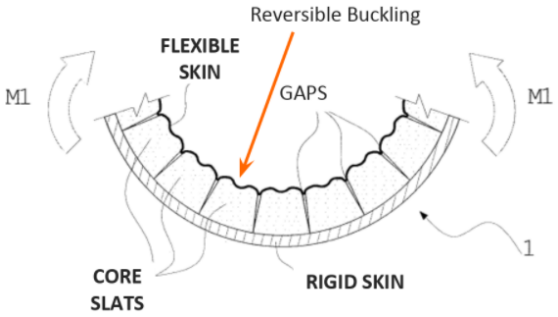

Figure 6.12: MadFlex, section view in bending configuration. Source [48].

sandwich-like material a great attention is also needed for the other skin failure modes mentioned in the previous paragraph, especially when they are not intentional. The most critical failure mode for the rigid skin joined to a foam is the wrinkling which limits the maximum applicable compressive load.

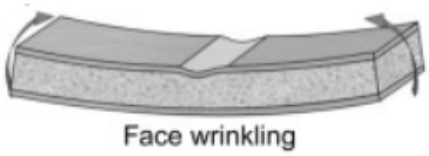

Figure 6.13: Face wrinkling.

Chapter 7

Preliminary designs

Before starting the in-depth structural analysis, it is needed to develop a preliminary design which uses the MadFlex as the main material and it is able to satisfy the most important requirement, mentioned in Chapter 5:

"The habitat geometry coupled with the MadFlex orientation along the thickness must allow the folding of the structure, exploiting the better feature of the MadFlex: flexibility if loaded on one side and rigidity if loaded on the other one. In other words the structure must be deployable."

The word deployable is the key for the following designs. Even if the MadFLex shows the great ability to be flexible on one side and rigid on the other side, is not an easy task using it to design a deployable habitat.
In order to decide which designs have the better features to be analysed in the next phase (preliminary structural analysis), the concept proposed will be evaluated according to these criteria:

- Packaging: ability of the structure proposed to reduce its volume once stored in the launcher faring;
- Ease of deployment: simplicity to deploy the proposed structure;
- Available volume: volume available to astronauts;
- Volume optimization: Quantity of available volume compared to the external surface of the structure;
- Feasibility of the folding process: simplicity to roll and fold the structure in the stored configuration with industrial process (personal consideration, based on not enough experience in this field);
- Constructive simplicity: simplicity to realize and build the presented structure with the modern technologies (personal consideration, based on not enough experience in this field);
- Note: general consideration about issues or advantageous aspect of the structure.

7.1 Deployable habitat

7.1.1 Brief explanation

All the designs shown below are based on the following concepts. Th next figure shows a cylindrical module with a cross plain $A-A$ that cuts the cylinder along the transverse direction. The section is shown in figure 7.2.

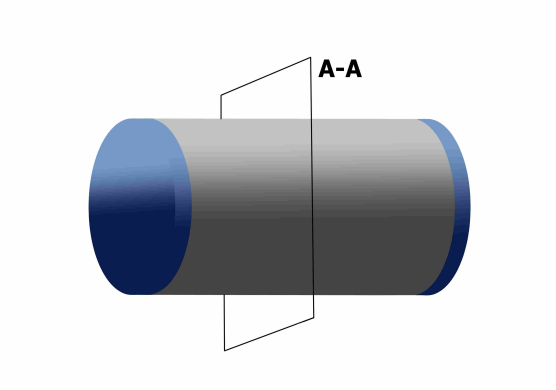

Figure 7.1: hypothetical cylindrical habitat

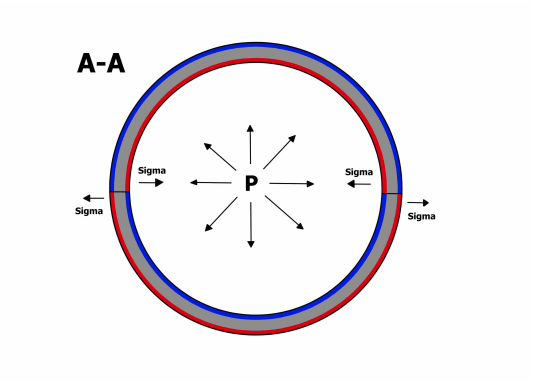

Figure 7.2: A-A section

The idea is a cylinder where the half-cylindrical upper part of it is made by a MadFlex oriented with the flexible skin facing inwards and the rigid skin facing outwards. Therefore the mentioned part can bend inwards and not in the opposite direction. The arrows referred to this part (sigma) mean the reaction forces produced by the material if it is bended upwards. The flexible part is represented in red and the rigid one in blue.
The opposite concept is applied for the lower part of the cylinder. The MadFlex is oriented with the flexible skin facing outward and rigid skin facing inwards. Therefore the mentioned part can bend downwards and not in the opposite direction. The arrows referred to this part mean the resistant forces produced by the material if it is bended upwards. The flexible part is represented again in

red and the rigid one in blue.
This concept allows the lower part to bend downwards and place itself in contact with the upper part, replicating its shape. Once the previous step is done, the overall structure can be rolled inwards, getting a cylinder with a smaller radius. Some proposed configurations are also based on the opposite idea or on an hybrid one, where the MadFlex can change its orientation along the perimeter of the upper or lower part. Many figures are shown in the paragraph below to better explain the previous concepts.

7.1.2 Mechanism of deployment

All the habitats of this category unfold thanks to the inflation of air. The presence of the pressure is favourable for the following three reason:

- it ensures 1 atm of pressure for the life of the astronauts;
- it acts as a mechanism to deploy the habitat once located in the mission site;
- it keeps the habitat in the right position and shape and helps the structure to withstand the weight of the regolith above the structure. The latter are fundamental to shield the habitat from the cosmic rays and solar storms. A clarification about the role of the pressure to "withstand" the regolith weight is explained in the next chapter.

7.1.3 Regolith and pressure

Since the gravity on the Moon is a $\frac{1}{6}$ of the gravity on Earth, a 2.5 m thick regolith cover has a lower weight than we usually think. Therefore, the higher loads introduced in the structure arise from the internal pressure and not from the regolith cover. This is the reason of the previous affirmation. To provide a quantitative example "a 101.4-kPa internal pressure is capable of supporting 40 m of soil on the Moon, assuming a soil density of 1.6 g per cubic centimetre." [34].

Half-cylindrical habitat (M1)

This habitat has a half-cylindrical shape. The explanation about the example at the beginning of this section can be adapted for this structure considering the lower part of it as a flat surface and not semi-cylindrical.

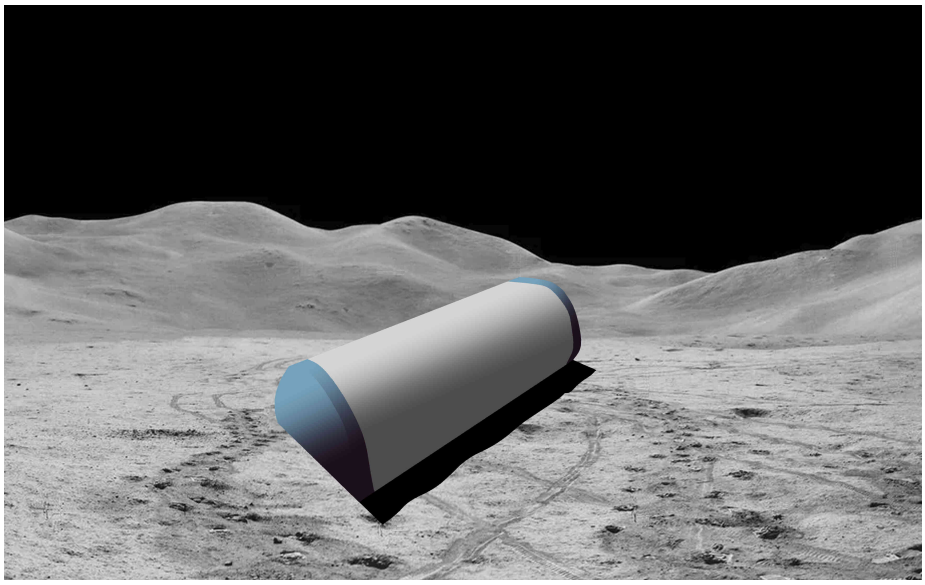

Figure 7.3: semi-cylindrical habitat

This habit can be deployed as shown below.

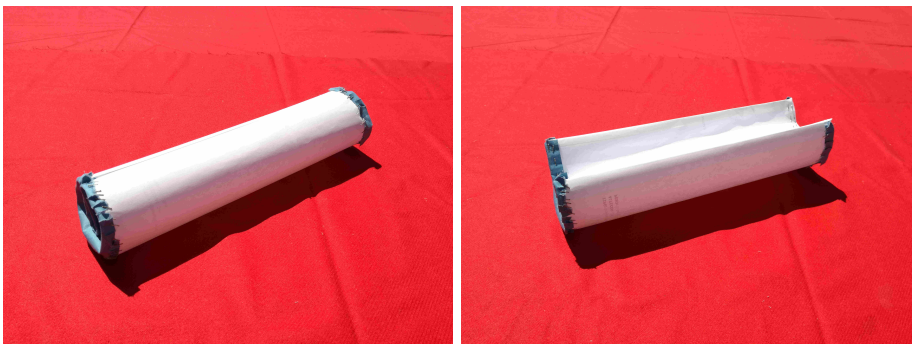

Figure 7.4: Phases 1-2

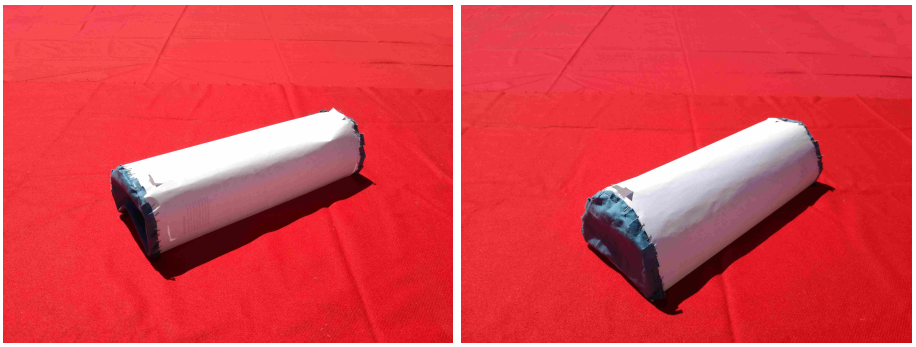

Figure 7.5: Phases 3-4

Once deployed it is necessary to rotate it in the right position. This could be done with a rover or a robotic arm placed on the lander module. The low gravity favours this manoeuvre.

Properties

Property	Considerations
Packaging	medium low
Ease of deployment	hight
Available volume	medium low
Volume optimization	medium hight
Feasibility of the folding process	medium hight
Constructive simplicity	medium hight
Note	It has medium-low packaging since the ends membranes not allow high curvature radius in the folded configuration

Half-cylindrical habitat with 1/4-spheres to the ends (M2)

This concept is similar to the previous one but has one-quarter of sphere at the ends. The example mentioned at the beginning of the section can be adapt to this module as done for the previous one.

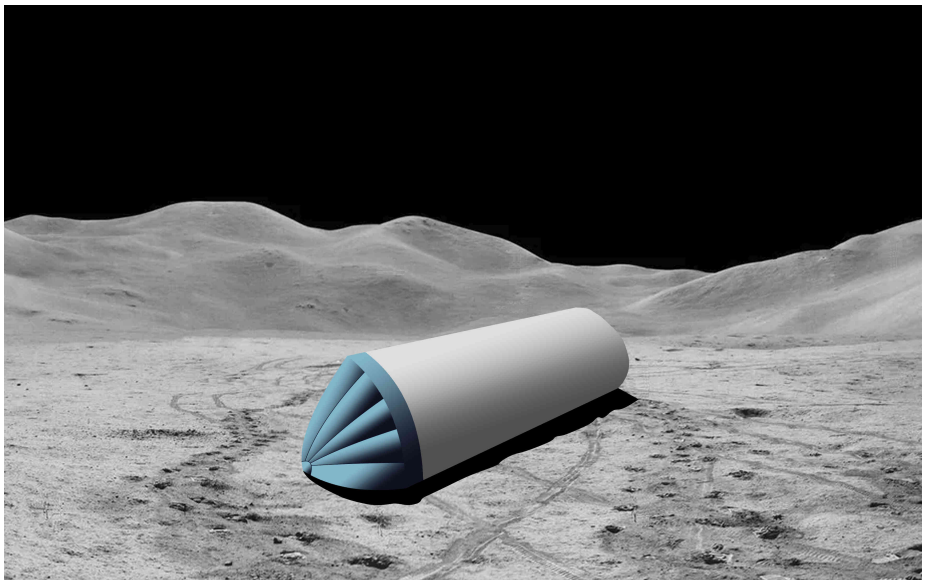

Figure 7.6: semi-cylindrical habitat with two semi-spheres

This habit can be deployed as shown below.

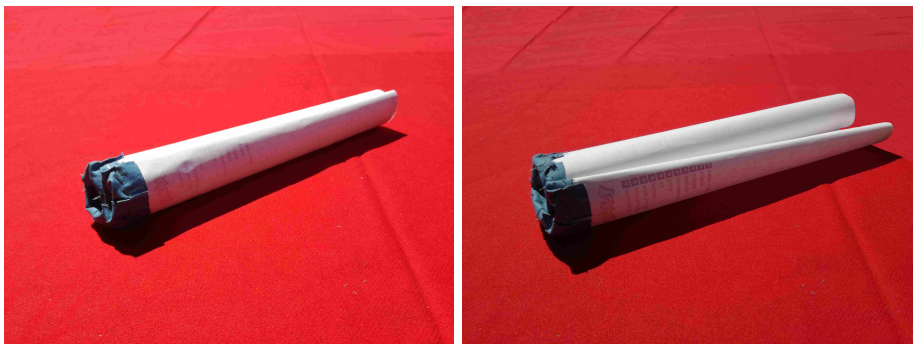

Figure 7.7: Phases 1-2

Once deployed it is necessary to rotate it in the right position. This could be done with a rover or a robotic arm placed on the lander module. The low gravity favours this manoeuvre.

Properties

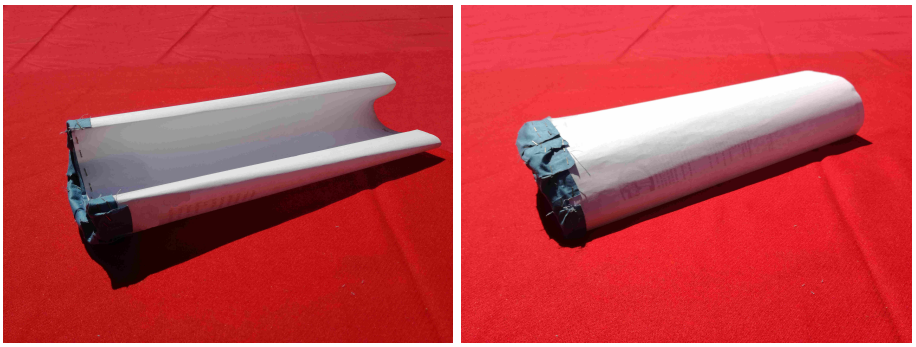

Figure 7.8: Phases 3-4

Figure 7.9: Phase 5

Property	Considerations
Packaging	medium hight
Ease of deployment	hight
Available volume	medium hight
Volume optimization	medium hight
Feasibility of the folding process	medium hight
Constructive simplicity	medium hight
Note	the packaging capability of the structure is higher than the one of the previous module because of the presence of the two one-quarter-spheres at the ends which allow wider surface to bend the ends membrane.

General consideration As reported in the *Note* a structure ended with semi-spherical surfaces or one-quarter-spherical surfaces has better capability to be folded. The latter consideration leads to a lower volume in the stored configuration.
In the following designs the option with two one-quarter-spherical ends is not implemented due to the difficulties to create a real model with this shapes. However the previous observation is valid for all the structure proposed.

Ω SHAPE (M4)

This concept has a cylindrical shape. The name of this habitat comes from the shape assumed by the structure in the folded configuration: it shows indeed a Ω (figure 7.11). In this case the initial example can be perfectly adapted at this model.

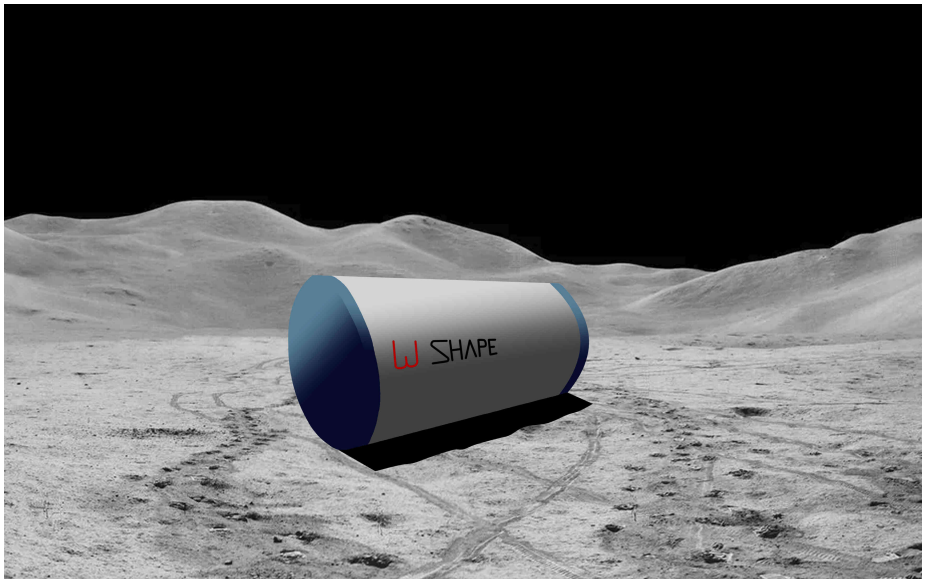

Figure 7.10: Ω SHAPE habitat

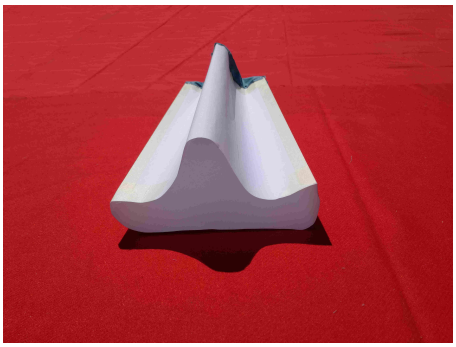

Figure 7.11: Ω SHAPE

Idea behind the deployment process The idea behind the deployment of this structure is the following:

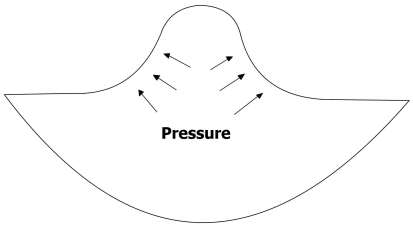

Figure 7.12: Deployment explanation

The air introduced inside the habitat produces a pressure that acts equally on the interior surfaces of the structure. However, the deployment is advantaged by the structural instability of areas pointed by arrows. This mechanism allows an easier process of deployment.

This habit can be deployed as shown below.

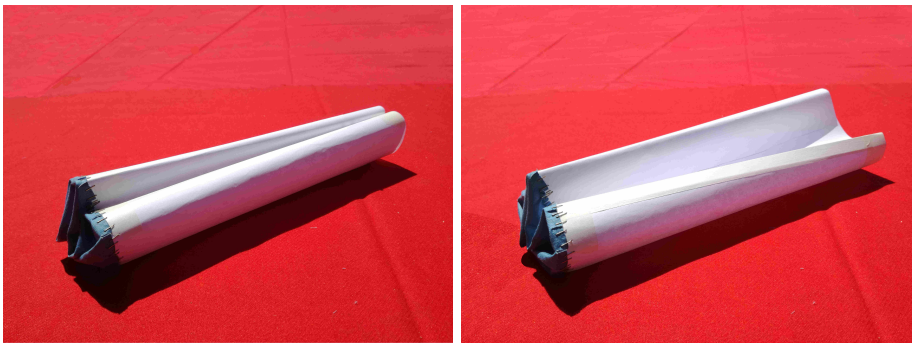

Figure 7.13: Phases 1-2

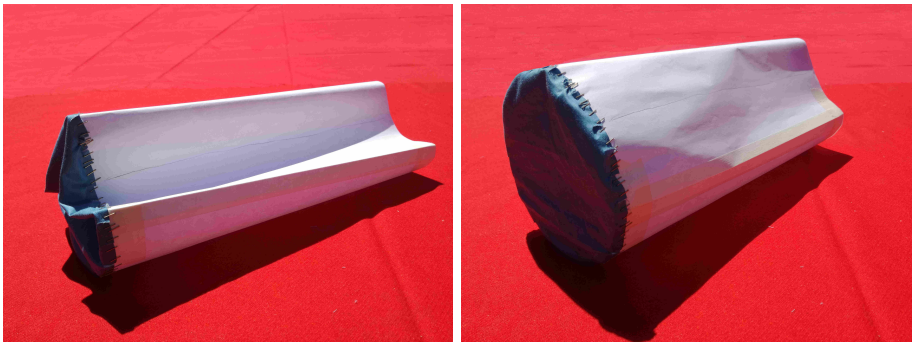

Figure 7.14: Phases 3-4

Once deployed it is necessary to rotate it in the right position. This could be done with a rover or a robotic arm placed on the lander module. The low gravity favours this manoeuvre.

Properties

Property	considerations
Packaging	hight
Ease of deployment	hight
Available volume	very hight
Volume optimization	very hight
Feasibility of the folding process	medium hight
Constructive simplicity	medium hight
Note	a structure ended with semi-spherical surfaces or one-quarter-spherical surfaces has a better ability to be folded therefore a lower volume in the stored configuration can be reached.

Another considerations

- necessity to create for this design an anchoring system to avoid undesired rotations of the habitat.
- the present concept allows a larger available volume for the astronauts. It allows also to exploit the lower part of the cylinder to place all the equipments necessary to the life support system leaving the floor free from them.
- this folded shape is better intended for an habitat with large dimension, because the presence of two unstable areas needed for the deployment process. A larger surface in the lower part of the cylinder makes easier the folding of the material in two points.

S SHAPE (M5)

This concept arises from the need to design a smaller habitat then the previous one using the same mechanism for the deployment: the instability of the shape. The name of this habitat derives from the shape assumed by the structure in the folded configuration: it shows indeed an S (figure 7.16).

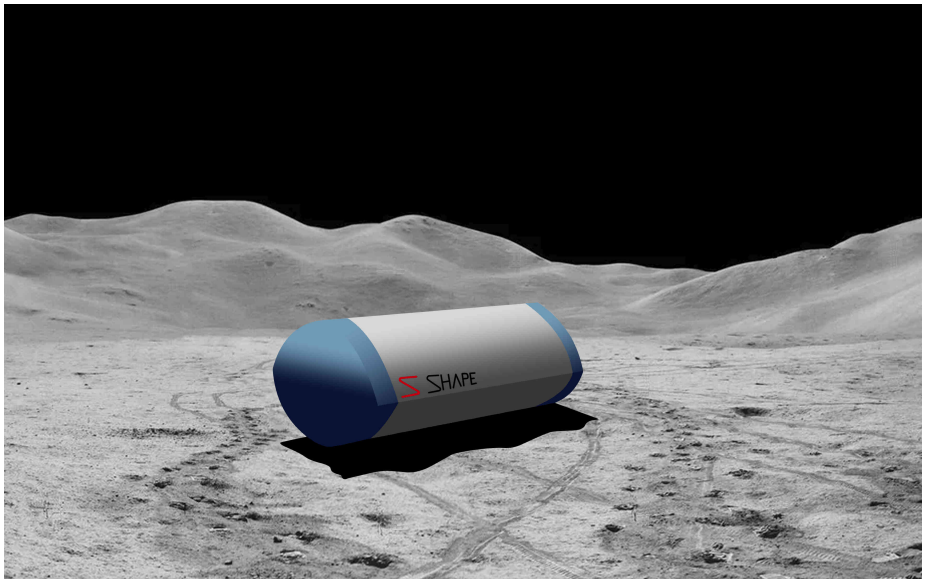

Figure 7.15: S SHAPE habitat

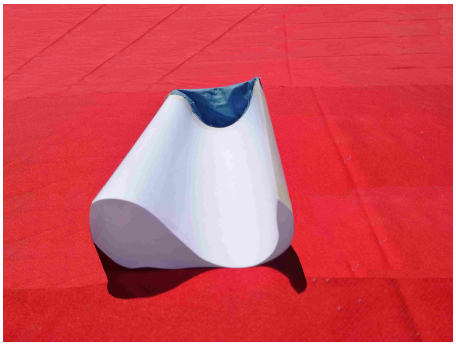

Figure 7.16: S SHAPE

Idea behind the deployment process The idea to behind the deployment of this structure is the following:

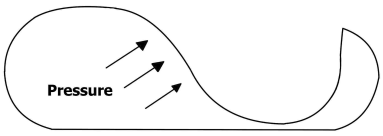

Figure 7.17: Deploying explanation

The deployment is facilitated by the structural instability of the surface indicated by arrows. This mechanism allows an easier process of deployment.

This habit can be deployed as shown below.

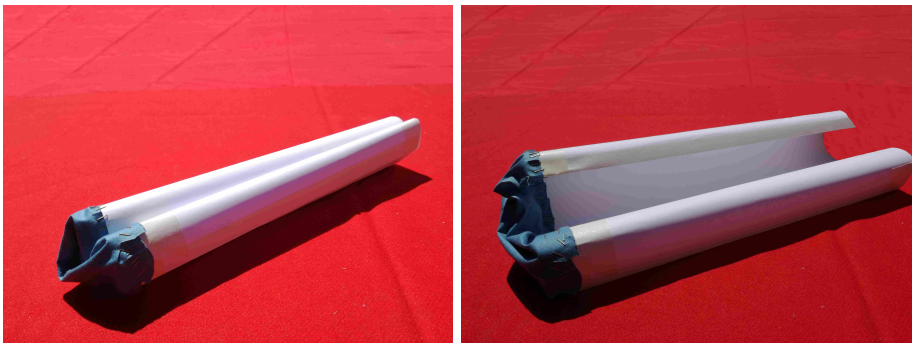

Figure 7.18: Phases 1-2

Figure 7.19: Phases 3-4

Figure 7.20: Phase 5

Once deployed it is necessary to rotate it in the right position. This could be done with a rover or a robotic arm placed on the lander module. The low gravity favours this manoeuvre.

Properties

Property	considerations
Packaging	hight
Ease of deployment	hight
Available volume	hight
Volume optimization	very hight
Feasibility of the folding process	medium hight
Constructive simplicity	medium hight
Note	a structure ended with semi-spherical surfaces or one-quarter-spherical surfaces has better capability to be folded therefore a lower volume in the stored configuration.

Another consideration

- necessity to create for this design an anchoring system to avoid undesired rotations of the habitat.
- the present concept allows a larger available volume for the astronauts. It allows also to exploit the lower part of the cylinder to place all the equipments necessary to the life support system leaving the floor free from them.

7.2 Deployable origami Habitat

7.2.1 Brief explanation

The following concepts arise from the idea to create an habitat with a larger space along the longitudinal direction, once deployed, and not along the transversal one, as achieved by the precedent solution. This goal is reached with the use of deployable structure with features similar to the origami.
The folds in the structure can be created by inserting MadFlex hinges in the material.

7.2.2 Mechanism of deployment

Deployment of the following design can be achieve through the pressurization of the habitat coupled with the action of a mechanical system . The latter is needed to act contemporary in many points, where the action of the pressurization does not provide the right contribution.

Prismatic habitat (M6)

This habitat has the easiest shape in the folded configuration: the square.

Figure 7.21: Prismatic habitat

This habit can be deployed as shown below.

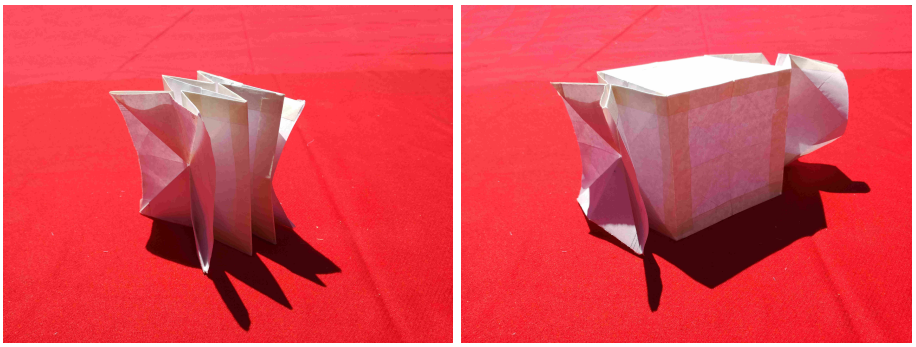

Figure 7.22: Phases 1-2

Figure 7.23: Phase 3

Properties

Property	considerations
Packaging	very hight
Ease of deployment	very low
Available volume	hight
Volume optimization	very hight
Feasibility of the folding process	very low
Constructive simplicity	low

Consideration

- An integral structure with many bending points can be difficult to realise.
- It shows a lot of edges which are critical point for the development of high stresses in the structure.

Cylindrical origami habitat (M7)

This habitat is developed to solve the problem of the edges in the structure. The only figure that has no edges is the circle. A good idea is to verge on this shape. Realising the following design we can have a circular section of the module. In the folded configuration it appears as the external part of the Composite Research's logo.

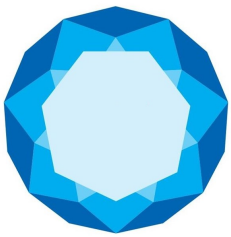

Figure 7.24: CoRe's logo

Because of the difficult to realise all the circular section with this method, only a segment is built with a paper model to test the ease of deployment.

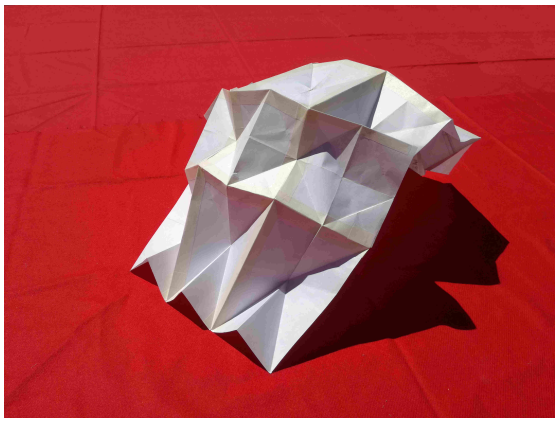

Figure 7.25: Cylindrical origami habitat

This habit can be deployed as shown below.

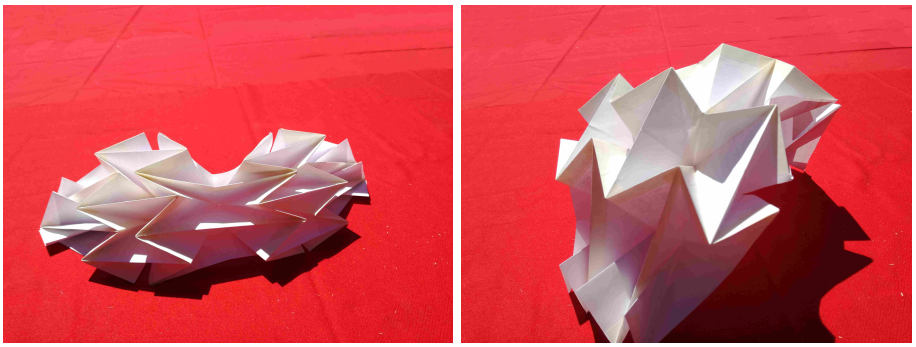

Figure 7.26: Phases 1-2

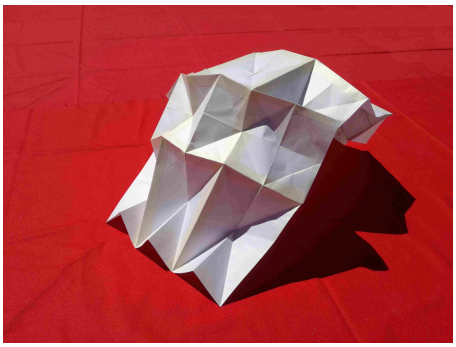

Figure 7.27: Phase 3

Properties

Property	considerations
Packaging	very hight
Ease of deployment	low
Available volume	hight
Volume optimization	very hight
Feasibility of the folding process	very low
Constructive simplicity	low

Consideration

- An integral structure with many bending points can be difficult to realise.
- It shows however, a lot of edges which are critical zones for the development of high stresses in the structure.

Hexagonal surface (M8)

Another solution to design a cylinder able to be bended in a planar configuration is to consider the external surface composed by hexagonal elements. An example is reported below.

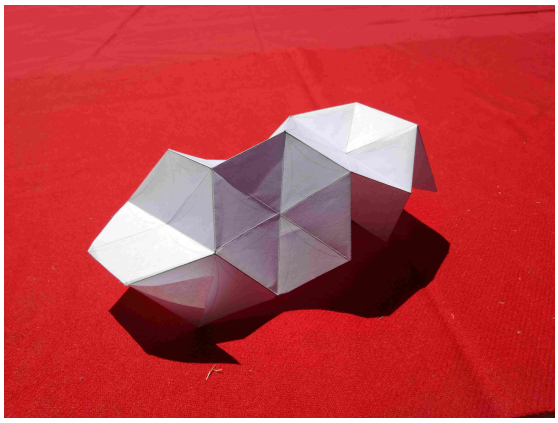

Figure 7.28: Hexagonal surface

Consideration

- I have not found the way to bend this planar surface in a circular shape in other words to create a circle shape of the section, once in the folded configuration.

Umbrella habitat (M9)

This concept consists of an umbrella-shaped structure. It does not have a half-sphere shape therefore it allows a better exploitation of the volume ensuring an almost constant hight for all the habitat floor.
The mechanism of deployment could be similar at the ones of a normal umbrella. The difference could be only the following: internal branches of the "umbrella" are pushed upwards through the rotational motion of a threaded column which allows the upward translation of a ring where the previous mentioned branches are connected.

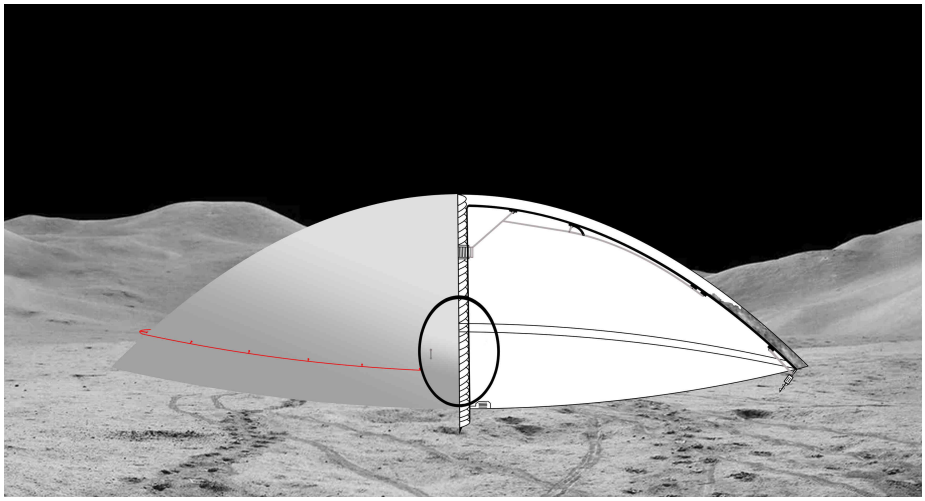

Figure 7.29: Umbrella habitat

A paper model, as in the previous cases, is realized to understand how to bend the surface of the umbrella with single and defined bends.
This bends could be created inserting MadFlex hinges in the bending edges. Once the habitat (umbrella) is close, it can also be rolled around its central column to minimize its volume.
This habit can be deployed as shown below.

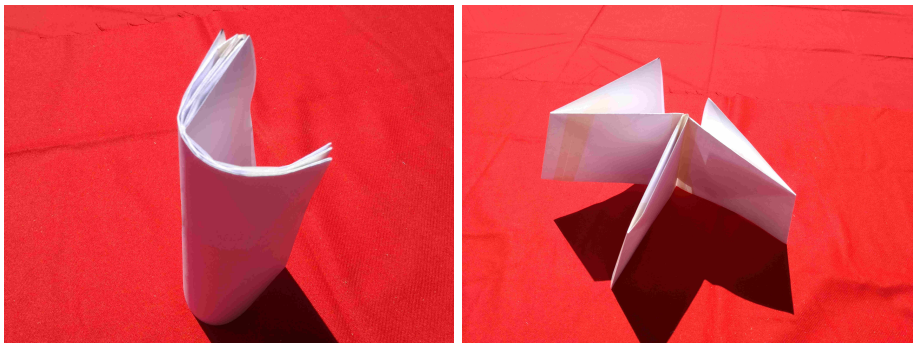

Figure 7.30: Phases 1-2

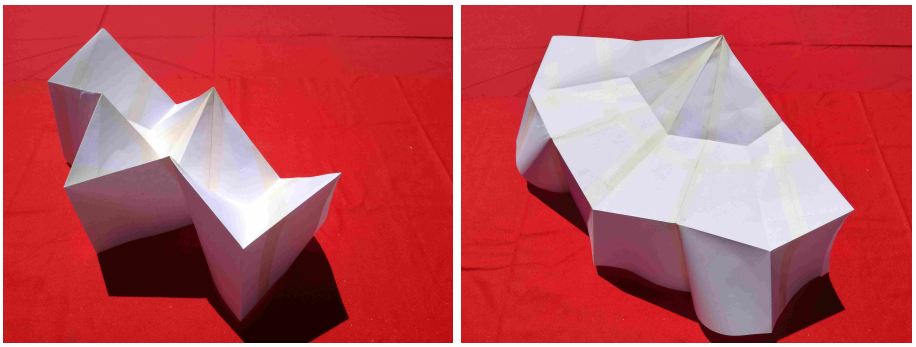

Figure 7.31: Phases 3-4

Figure 7.32: Phases 5-6

Properties

Property	considerations
Packaging	very hight
Ease of deployment	very hight
Available volume	hight
Volume optimization	hight
Feasibility of the folding process	hight
Constructive simplicity	medium hight

Another consideration

- the umbrella in the folded configuration is rolled around its principal axis. The issue of reproducing this configuration is to create MadFlex hinges able to allow both the closing of the habitat and the bending in the orthogonal direction.

CoRe Space Antenna

This concept was developed by CoRe in order to realize a deployable space antenna. It has a half-spherical shape and consists in four branches made in MadFlex, which are connected together through a fabrics in order to reach a continuous surface. The multi-layers fabric acts as a membrane, able therefore to withstand only axial forces and not the bending moment or transversal shear. The MedFlex orientation along the thickness of the branches allows them to bend inwards. They are kept in the extend position through a cables mechanism which connects each branch to a ring able to move along a road placed at the apex of the antenna. The following figure shows a prototype of it.

Figure 7.33: CoRe Space Antenna

Even if this design is developed for an antenna, the same concept can be used to create a deployable dome for a lunar base by placing the antenna as in the previous figure. The cables mechanism can also be replaced with a less bulky one.

This habit can be deployed as shown below.

Properties

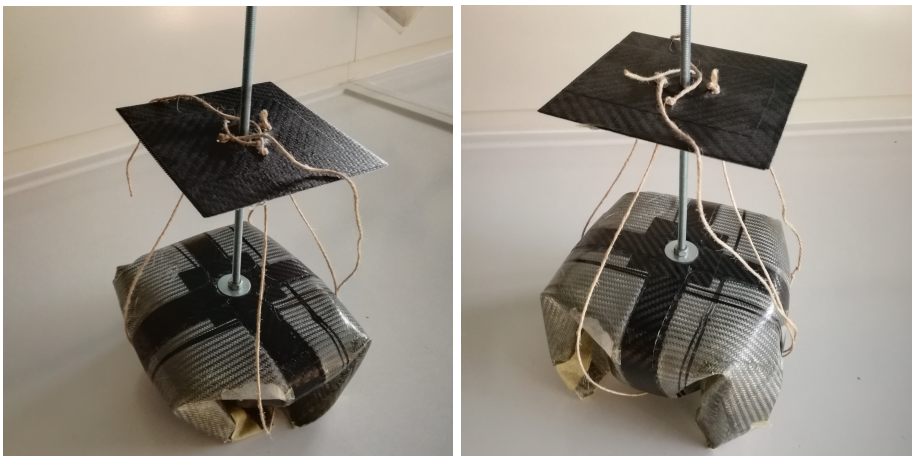

Figure 7.34: Phases 1-2

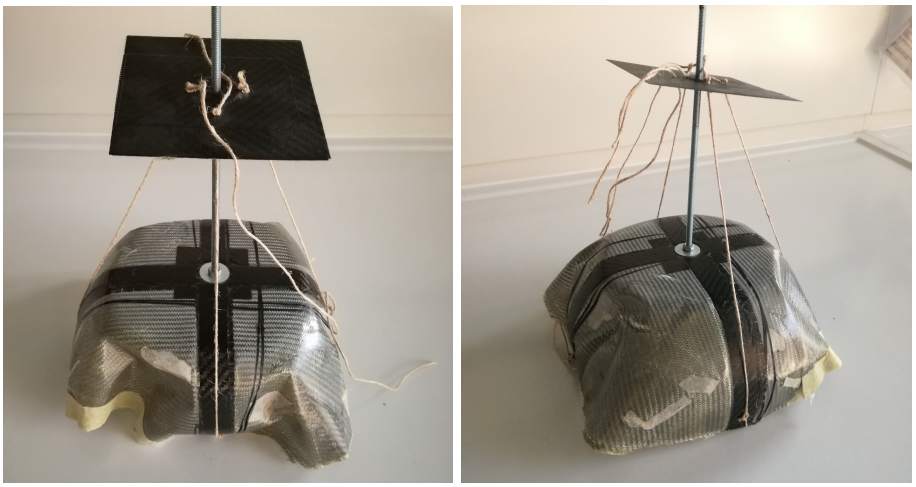

Figure 7.35: Phases 3-4

Property	considerations
Packaging	very hight
Ease of deployment	very hight
Available volume	very hight
Volume optimization	hight
Feasibility of the folding process	very hight
Constructive simplicity	very hight

7.3 Conclusion

The evaluations provided in this chapter are only intended to understand the concepts which better satisfy the requirement about the deployment of the habitat. Other concepts are developed during the structural analysis to better satisfy the structural requirements.

In conclusion the habitats which better satisfy the requirement about deployability are:

- The Ω SHAPE

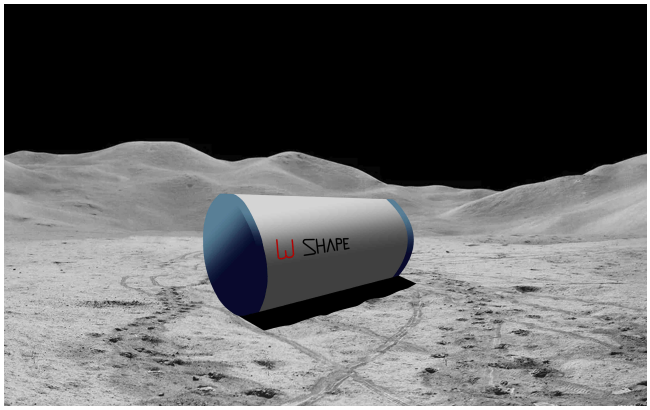

Figure 7.36: Ω SHAPE habitat

- The S SHAPE

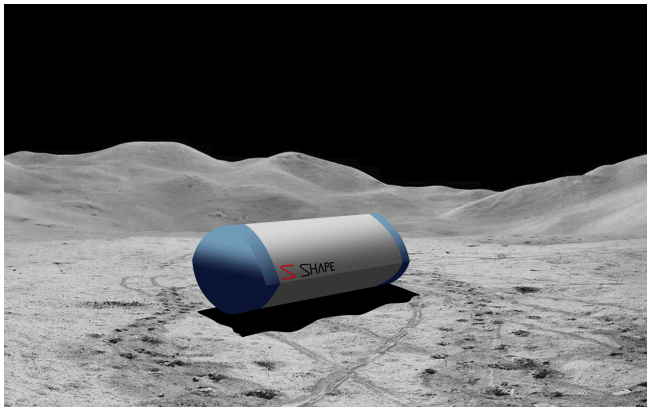

Figure 7.37: S SHAPE

- The Umbrella habitat

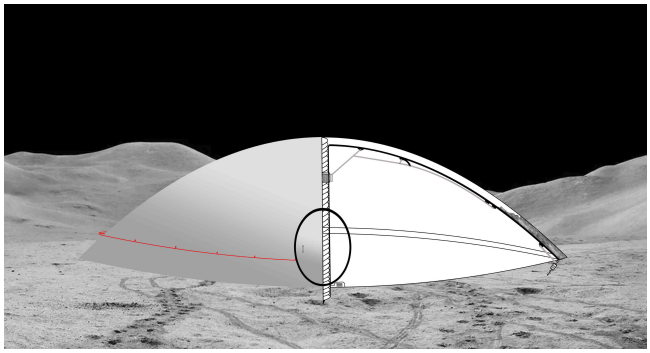

Figure 7.38: Umbrella habitat

- CoRe Space Antenna

Figure 7.39: CoRe Space Antenna

Chapter 8

The MadFlex Moon base

This chapter shows an idea of a feasible lunar base design, composed by habitats made in Madflex. The introduction of this chapter has the aim to provide a greater contextualization to this project in order, to make it a part of a broad and complete idea. If this is the main motivation the second one is to better understand the structural needs of a module into a more complex contest: the base. It includes for example type of connections between modulus, necessary systems for their transport and the assembly procedure steps of the lunar base.

8.1 Global description of the lunar base

The main global criteria followed for its development were:

- : Standardization of module's global features: in order to simplify the construction of the lunar base, for example through standard docking system between modules, and to reduce costs and efforts in the design and production phases of the habitat.
- : Diversification of scope of the modules based on the shape. In other words, different shapes for different uses.

Following the first criterion two types of habitat configurations are considered: hemispherical and semi-cylindrical. Adopting the second criterion, the results are the following:

- The domed assumes the role of connecting node between the semi-cylindrical modules that are placed in radial pattern around it. Another intended use for the dome, including the galley and wardroom could be a social and meeting place.
- The semi-cylinder habitat could be used for different intended use as: greenhouses, crew quarters, laboratories and airlocks.

The lunar base could assume the following configurations: figure 8.1 from above while figure 8.2 from a lateral view

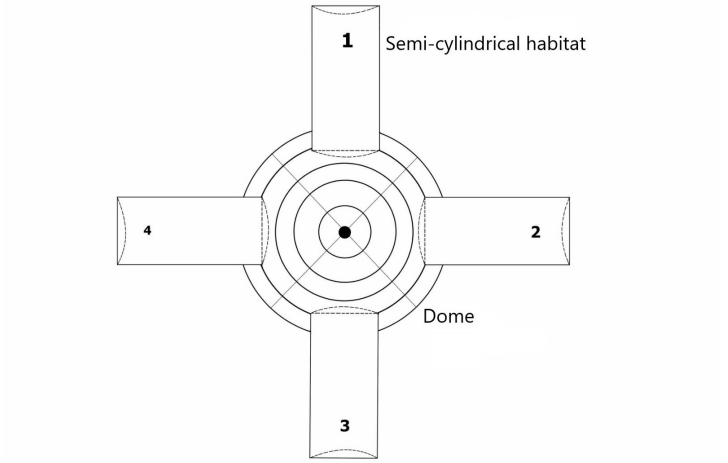

Figure 8.1: Lunar base seen from above

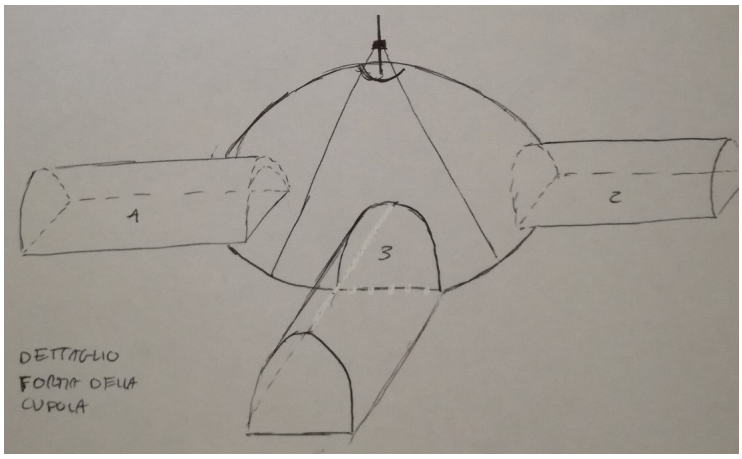

Figure 8.2: Lunar base from lateral view

The lateral walls of the semi-cylindrical habitat can have a planar geometry when the connection with a semi-spherical habitat is planed or a 1/4 of sphere when it is considered dead branch of the structure. In the latter case, a 1/4 end allows a better folding capacity and a larger internal space.

8.2 Architectural consideration about habitat

Seen from above the dome appears as in figure 8.4. In this case if the upper coverage of the semi-cylindrical modules are perfect semicircle, in the section view, the "D" distance in the image is greater than the "d" one. To avoid that, if it will be a problem for structural integrity, the upper coverage must have a low arch shape.

8.3 Generic consideration about habitat shape

From an architectural point of view a semi-cylindrical habitat has a more optimized volume compared to the hemispherical one due to the single curvature of the top. Maximum constant height is not achieves in a single point as in the hemisphere configuration, but along a line, the symmetry one. For this motivation a differentiation of the intended use of the habitat based on the shape is essential.
Interesting it is also an investigation of the optimal curvature that the upper part of the semi-cylindrical or hemispherical habitat should have to better support the final load configuration: internal pressure plus regolith load. As mentioned in the third chapter about Three-Hinged Arch Shell Structure, a semi circular arch is more convenient compared to a parabolic one because the principal load on the Moon is the pressure and not the gravitational load. Considering this new notion a in-depth analysis it is essential to understand if a semi-cylindrical module with a perfect semicircular shape in the section view is more convenient than a "D" distance equal at the "d" one in the dome.

8.4 Preliminary discussion about habitat design

After the considerations about the volume and shape of the habitats another preliminary observation about how to satisfy the less technical requirements for the different orientations of the Madflex in the structure can be done. The less technical requirements are the following:

- Even if it could be a predictable requirement the orientation of the MadFlex coupled with the geometry of the habitat can allow the folding of the structure, exploiting the better feature of the MadFlex: flexibility if loaded on one side and rigidity if loaded on the other one. In other words the structure must be deployable.
- The MadFLex layer in contact with the regolith, placed on the top of the habitat, must be the rigid one because it is more resistant to abrasive phenomena caused by regolith. Although regolith is contained in bags, this additional requirement has to be satisfied because damage to the outer layer of the material is almost impossible to be reached and repaired as it is buried under 2.5 m of regolith.
- For the same motivation of abrasion properties of regolith and lower punctual resistance of the flexible layer compared to the rigid one, the necessary configuration of MadFlex for the floor is with the rigid layer facing the lunar soil.

semi-cylindrical habitat In case of semi-cylindrical habitat the possible configurations in relation to the Madflex orientations are mainly two and both satisfy the first requirement, thanks to the single curvature of the cylinder. The two configurations are the following:

- Rigid layer of Madflex facing outwards. In this case the habitat can be rolled up downwards and do not need an additional coverage because this design satisfy the first requirement mentioned above.

- Rigid layer of Madflex facing inwards. The habitat can be rolled up upwards, but now the habitat needs an additional coverage to protect the flexible layer from abrasion phenomena

In both previous cases, the floor can be in MadFex too, or in membrane, but an additional protection between the membrane and the soil is required in the second option. It could be another sheet of Madflex with rigid layer facing downwards, in order to satisfy the second requirement.

hemispherical habitat If the semi-cylindrical habitat possible configurations were mainly two, now the possible configuration is only one. This happens because if MadFlex orientation shows the rigid side facing inwards the double curvature of the hemisphere does not allow the folding of the habitat upwards. Specifying, the upward bending in this configuration is possible as far as the deformations endured by all the materials of the dome remain in the elastic field. If deformation limit is excised, initial dimensions can not be reached again by material, while for fragile one, this causes the breaking of the layers. Therefore to make it possible a dome with low height and large base diameter is necessary. The second and more probable configuration is the one that sees the rigid layer facing outside. In this case the folded configuration of the dome can be the following:

Figure 8.3: Deployment of the dome

In this case, the dome seen from above will has the configuration shown in figure 8.4

Therefore the dome can not be made by arches, jointed together at the top as in figure 8.3, leaving at the membrane the purpose of jointing spaces between them, but it will appear as an almost continuous semi-spherical surface made

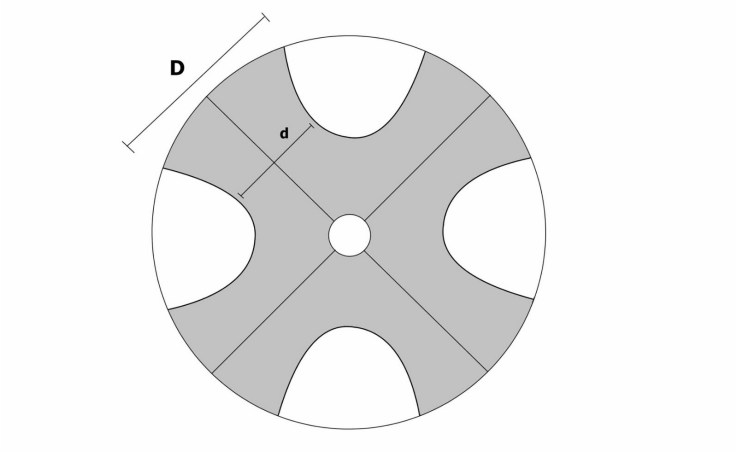

Figure 8.4: Dome seen from above

of rigid material. This because it is necessary to avoid or limit the membrane's surface exposed to the regolith, as explained in the previous second requirement. The non shaded zones are made of membrane, but represent the areas where the semi-cylindrical modulus will be jointed at the dome.

Another configuration called "umbrella configuration" is available in order to make a dome deployable but its design cannot be included in the previous classification. However the implementation difficulties are much greater for the umbrella configuration, which must have an internal rigid structure.

The consequence of material orientation on the technical structural requirements as the resistance at the regolith load in case of accidental de-pressurization, or regolith load plus internal pressure of 1 atm, will be discussed in the next chapters with a more accurate structural analysis.

8.5 How to keep habitat in folding position

The issue is not only to keep the habitat in the folded configuration, that is favourable during the transport phase of the mission, but also to allow its deployment once the Moon is reached. The solutions developed are two:

- keep the habitat in folded configuration through belts, with an unhook mechanism, that allows the opening of the habitat. This mechanism can concern the use of small pyrotechnic mechanism or it can be realised through other type of options that do not need big mass or any source of external power. Another idea could be the use of piezoelectric materials.
- Dome's branches can be keep in bended configuration through electro magnets connecting the end of them with the habitat's top, but this needs an external source of power for forces generation. For this reason it is a very heavy mechanism.

8.6 Docking mechanism between habitats

One of the most critical manoeuvre in space between two modulus is the docking. Numerous are the issues during this phase, such as the perfect alignment of the two modulus along the desired direction, the union without rise of damages and the perfect sealing of the contact surfaces avoiding de-pressurization phenomena. During assembly operations of a Moon base all these issues are present, but dealing with deployable modules arises an additional one: the interfaces between modulus are less precise than in a rigid one as on the ISS, because they has a greater mobility. A solution to the latter issue, useful to solve also the cited ones before, is shown in figure 8.5.

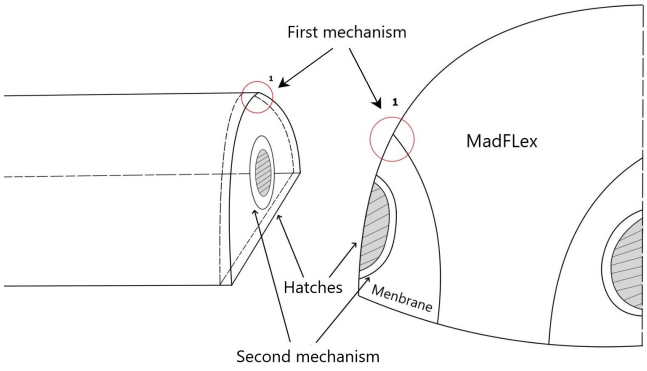

Figure 8.5: Alignment of the habitat

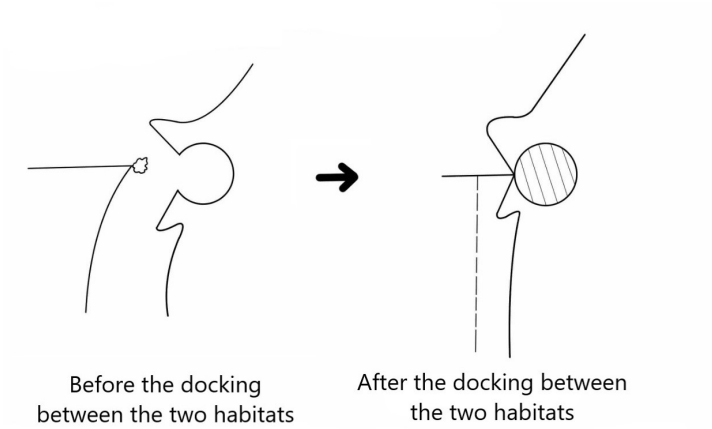

Figure 8.6: First docking mechanism

Since the most important requirement is the deployment possibility of these habitat, the presence of rigid docking mechanism or hatches at the ends, as on the ISS, is not allowed because it prevents the folding of the structure. Therefore a different solution is necessary. The docking system is composed

by two mechanisms. The first is placed at the contour of the semi-cylindrical habitat and on the contour of the rigid material of the dome, while the second around the area where the hatches should be.

First mechanism It consists in two parts: an inflatable membrane located on the contour of the semi-cylindrical habitat, as shown in figure 8.6 on the left, and an inlet located on the contour of the rigid part of the dome, shown on the right. When the habitats are aligned the semi-cylindrical will be translated horizontally until its contour and inflatable membranes are inside the inlet of the dome. When this is obtained, the membrane will be inflated with air if connection would be temporary, or with expandable foam if permanent, allowing the sealed connection between them.

Second mechanism As the previous one it consists in two parts too. The mechanism is the same but in this case the inflatable membranes and the inlet are placed on the contour of the hatch zone.

However in previously described situations, module is still not equipped with rigid hatches, these will be placed at the arrival of the astronauts. The motivation is the impossibility to fold the habitat with rigid hatches at the ends. The sequence of actions assumed to locate the hatch is described in the next section.

8.6.1 Hatch placement

For hatches placement on the module ends, the idea is to take advantage of the semi-cylindrical modules already designs to be used as airlock, because of the presence of two separate spaces and the ability to support load during depressurization. The second statement needs a comment: when astronauts will arrive on Moon base will be assembled and completely covered by the regolith shield. Motivation will be explained in the next section.

The airlock Airlock design is the following:

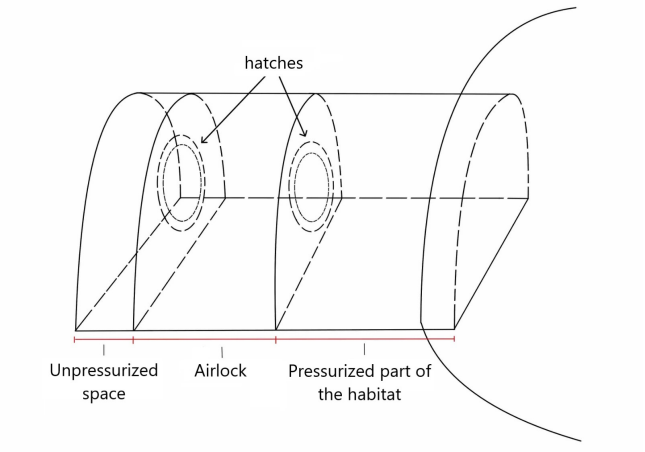

Figure 8.7: The airlock

Starting from the left side, the fist space is a porch. It is not pressurized and in contact with the lunar environment. Its purpose is to provide a first shelter for the astronauts from micro meteorite and radiation hazard. On its right is placed the real airlock chamber where astronauts can take off their suits and regolith is removed through a process similar to the one used for the aspiration of asbestos fibers. Once ready, astronauts can open the last hatch on the right and get into the habitat. A valve between the two internal room allows passage and pressure compensation in the deployment phase. Once the process is finished the valve is closed.

Operation for hatches placement in chronological, order are the following:

1. Astronauts arrive on Moon with the rigid hatches. Base is already assembled, module are pressurized and covered by regolith.
2. On the external side of the free end of the ailock semi-cylindrical module, there is an inflatable membrane along the contour of the future opening while the hatch has an inlet in the same position. The mechanism is the same used for the docking mechanism between modules.
3. Astronaut places the hatch in order to allow membrane entrance in the inlet. Once happened, the membrane is inflated with expandable foam and joint is realized.
4. Now, only the airlock chamber is de-pressurized and the external membrane, inside the hatch opening, is cut.
5. Astronauts enter in the airlock with two new hatches. The external and fist hatches is closed, regolith removed from inside the module, and room pressurized again.
6. The second hatch is placed in the same way as the first
7. Now astronauts are at the end of the semi-cylindrical module, which is separated by two membranes from the dome internal space. Hatch zones, between membranes are already jointed through the second docking mechanism. A third hatch is placed in the some way of the previous two, cutting the two membranes.
8. Joint between hatches and membranes could be reinforced with an added rig of equal dimension of the hatch and connected to it with a mechanical system. Membrane will be entrapped between hatch and correspondent ring, allowing a second redundancy joint.

8.7 protection from high temperature gradient, micro-meteorites and radiations

The chosen solution for this preliminary study, about environmental issue, is the one concerning a 2.5 m coverage of the habitat as suggest by studies and papers mentioned in chapter 4. The mainly issue is how to collect, transport and placed the regolit on the habitat top, keeping constant the radial thickness at 2.5 m and avoiding the sliding of the regolit on the lateral side as in the following design proposed by Hypes, W.D. et al. (1992)and mentioned in Chapter 3:

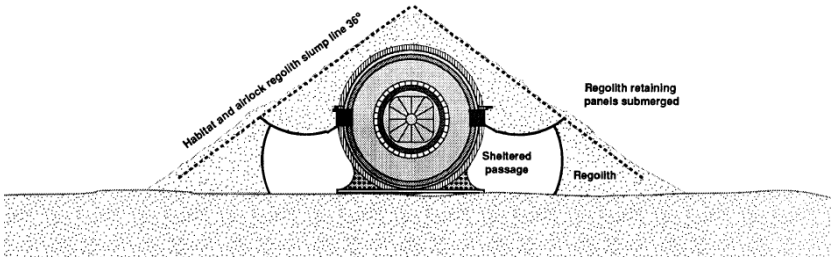

Figure 8.8: Hypes, W.D. et al. (1992)

The idea was to pack the regolit inside sand bags as proposed in the "Spheric inflatable lunar habitat" developed at Johnson space Center and mentioned in Chapter 3 and to transport them on the top of habitats. If the issue about sliding has been solved, the other ones as the collection and the transportation remain,. The solution investigates is the possibility to use a rover to carry out these tasks.

8.7.1 The lunar rover

The mainl feature of the Moon is that constant gravity of the planet is 1/6 compared to the Earth's one. This is convenient for some tasks, but very unfavourable if the objective is to drill the soil. On Earth, excavators can work because their weight is high enough to contrast the reaction force developed by the terrain during the excavation process. On the moon, the weight of each object is 1/6 of the Earth's one, so during this process the rover could be unable to carry out the task. A feasible solution is to design a rover not able to take great quantities of regolith in a single point, but great along long distance. Following this idea the rover could be based on the same principle used by the terrestrial agricultural machinery developed for the creation of the round bales. It will have a short blade under it, able to excavate lunar soil within the first 15 cm, where regolith is less dense. Once that regolith is excavated, a conveyor belt transports it inside a compactor where it will be packed into polyethylene bags. Figure 8.9 shows a sketch of this idea.
It will be also equipped with a mechanical arm, as the Mobile Servicing System placed on the ISS for the subsequent placement of regolith bags on the structure and a trailer to transport bags.

Rover operations for regolith packaging This paragraph shows the rover operation for regolith packaging in chronological order:

1. The rover moves on the lunar surface, collects regolith in polyethylene bags, each one with a precise shape in order to fill a pre-determinate position in the coverage as bricks in an igloo. For this reason they are marked with a symbol as QR code;

2. Through their gps position, or other systems, rover recovers all the bags;

3. It transports them to the habitat location, with its trail, using its mechanical arm to load them on the latter.

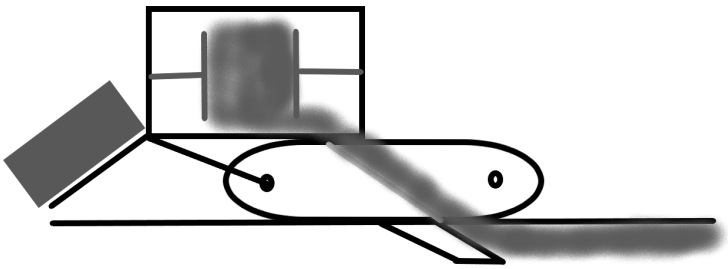

Figure 8.9: The lunar rover

4. Through its mechanical arm it places the bags of regolith in the right position using the QR code recognition mechanism

8.8 Mission profile

This is only a general and hypothetical mission profile, but the main aspect is the importance to assemble and build the base before astronauts arrival. Mission profile is subdivided in two mission's subroutines. The chronological steps to transport the payload from Earth to the Moon surface and the activities on the lunar surface to assembly the base.

Material transport from Heart to the Moon The transport of material from Earth to the Moon is realized in two steps: From Earth to lunar orbit, and than from the latter to the lunar surface. These two steps are done by two different transport vehicles: one could be a rocket similar to the SLS, developed by NASA and the second a vehicle able to withdraw material from the Moon orbit and bring it to the surface
Chronological steps:

1. The first launch includes only the second transport vehicle as payload and leave it on the lunar orbit.
2. The second launch includes the rover and the dome habitat as principal elements and other semi-cylindrical habitat if possible.
3. The second transport vehicle in the orbit withdraws the payload and brings it on the Moon surface. Then it returns at its initial position.
4. Subsequent payload consists in all the other habitats necessary to built the bases, and the process to transport them on the Moon surface is the same described in the previous points.
5. When base is finished the first human mission can be done.

assembly of the lunar bases This paragraph illustrates the chronological steps for the moon base assembly. The scenario begins with the second transport system landed on the Moon with rover, its trail and dome.

1. The rover descends the transport vehicle's ramp, and with its mechanical arm recuperates the trail and hook the latter to it.
2. Dome habitat is taken by the rover through the mechanical arm left on the trail.
3. Trail and dome are transported to Lunar base emplacement by the rover. Then it leaves the habitat on the Moon surface, covers it with a protection layer, unhooks the trail and begins the Regolite collection operation described in the paragraph: "Rover operations for regolith packaging"
4. After the placement of all the regolith bags in a single area, the rover cleans the soil from the bigger rocks and puts the protection layer in MadFlex for the habitat's floor.
5. Rover takes the habitat through a hook placed at the ends of dome legs and lifts it off the ground.
6. Now the habitat can be pressurized without touching the soil and avoiding regolith abrasion.
7. Habitat is placed on the MadFlex protection layer with the desired orientation and the rover waits for the arrival of the new habitats.
8. Once arrived, it takes the cylindrical habitat from the inside of the transport vehicle, lift it off the ground and once inflated, begins the alignment procedure necessary for the docking between modules.
9. The following processes of base assembly are the replication of the previous described ones.

The total assembly of the base before humans arrive could be favourable, because precesses of collecting regolith and docking of modules need a lot of time. Maybe two rovers would be useful to reduce time.

Chapter 9

Structural preliminary analysis

This chapter summarises and shows how the preliminary structural analysis is carried out. The Chapter explains the method applied to solve the Three-Hinged and Two-Hinged Arch, the examined load conditions and especially the Matlab® script implemented to carry out the preliminary structural analysis. A comparison between the results obtained by the script and the FEM analysis is also shown at the end of the Chapter in order to validate the program implemented in Matlab ®.

9.1 Analysed structure

The half-cylinder and the dome are the habitat designs chosen for the development of the MadFlex Moon base. A half-cylindrical section with a depth of 0.5 m is analysed in order to carry out a single structural analysis able to include both the designs mentioned above. This section represents a slice of the half-cylindrical module, while for the dome it represents the shape assumed by two consecutive structural branches with a width equal to the depth of the section. Figure 9.1 shows the standard half-cylindrical section.

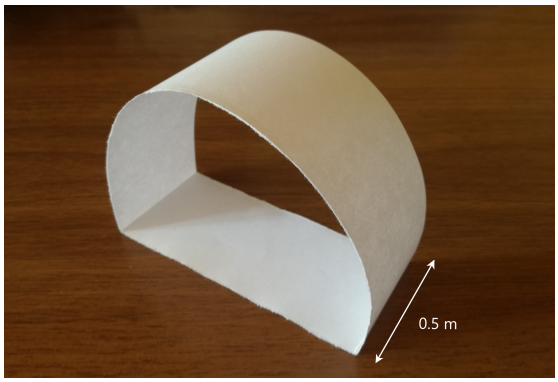

Figure 9.1: Standard half-cylindrical section

9.2 Analysed configurations

The half-cylindrical section mentioned above can be realised in many ways such as Hingeless Arch, Two-Hinged Arch or a Three-Hinged Arch. These different configurations lead to different displacement, deformation and internal stresses. Moreover, also the solution process is different if they are solved analytically. The analysed configurations are the following:

- Three-Hinged Arch. It is a statically determinate structure (isostatic). For this reason it is the easiest configuration to solve analytically.

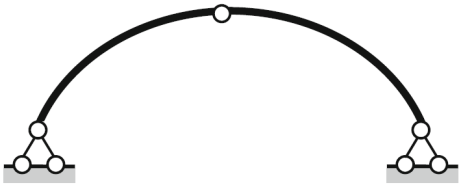

Figure 9.2: Three-Hinged Arch. Source [58]

- Two-Hinged Arch. It is a statically indeterminate structures. For this reason, it requires a more complex analytical resolution.

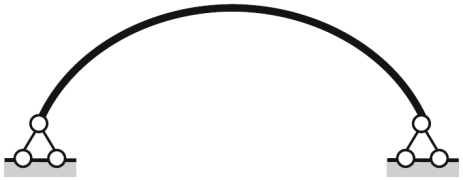

Figure 9.3: Two-Hinged Arch. Source [58]

Arches with four or more hinges were not considered because they become statically underdetermined structures.

9.3 Load conditions

The analysed load conditions are the ones reported in paragraph 5.3.2 except for the first one which is the less critical. The other three are analysed for the following reasons (each number of the list below corresponds to the relative load condition mentioned in paragraph 5.3.2)

2. Internal pressure of 1 atm plus regolith cover load. It is the nominal operative load which the structure must withstand during its entire operative life.

3. Regolith cover load only. It is the most critical load condition, due to the lack of the internal pressure, which has a mitigating effect on the bending moment induced by regolith. For this reason, the largest displacements of the habitat top is expected in this load condition.

4. Load used to keep the habitat in the folding configuration. This load condition provides the greatest limitation about the curvature of the habitat in the folded configuration. The highest stresses in the foam are expected under this load.

9.4 Structural theory

The Allen's beam theory is used in the analysis since the MadFlex is a composite material panel having a sandwich-like structure. This theory assumes that:

- The overall shear deformation is absorbed by the core of the sandwich, therefore the equivalent shear stiffness is:

$$GA^* = G \cdot \frac{d^2 b}{h_c}$$

where the factor mentioned above are explain in this figure:

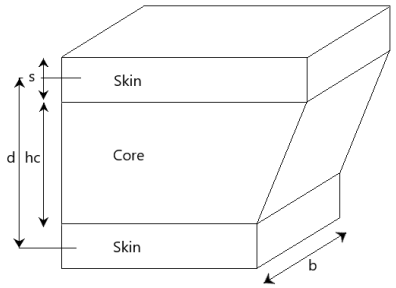

Figure 9.4: Sandwich scheme

- All the layers of the sandwich take part at the overall flexural stiffness, which is calculated as the one in the Eulero-Bernulli beam

$$EI = 2E_f \left(\frac{bs^3}{12} + bs\frac{d^2}{2} \right) + E_c \frac{bh_c^3}{12}$$

This theory was chosen in order to not neglect the shear contribution in the calculation of the displacements.

9.5 Script for preliminary structural analysis in Matlab®

The purpose of this script is to provide a preliminary tool able to analyse the previous structure configurations and allow the discernment about their feasibility. Information about the displacement and the stresses and strain developed under the defined loads are also output data of the script. It could be also employed for the optimization of the materials thickness and their properties in

order to get the lightest and most resistant structure.

The load conditions are analysed in the script with the following order:

- Load condition 3 Analysed in the First Script;
- Load condition 4 Analysed in the First Script;
- Load condition 2 Analysed in the Second Script.

It is possible to view the first and the second script in the Appendix A and B of the Thesis.

9.5.1 Script explanation

Explanations about the composition of the script and how it works are provided in the following paragraphs.

Input Data The program's input data are listed below. The names assumed by the variables in the program are shown in brackets.

- Geometrics input data
  - Habitat radius, 3.5 [m] (r) ;
  - Thickness of the regolith (s_r);
  - Depth of the analysed section, 0.5 [m] (b)
- Physic input date
  - Gravity constant of the Moon, 1/6 of the the terrestrial one (g_l)
- Program's parameters
  - Number of discretization points (N). They are equally spaced points along the curvilinear coordinate of the arch, named s. Their number must be odd and they will be used to discretize the distributed but non-uniform load of the regolith. A more detailed explanation will be provided in the next paragraph.
    To better understand how the script works a number N=9 of discretization point is consider from now on. The following figure shows this discretization.

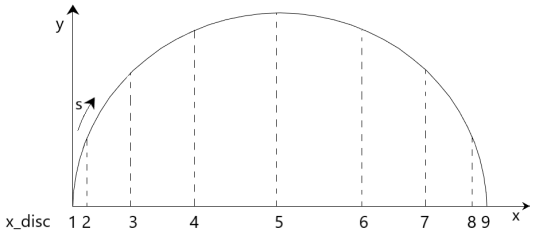

Figure 9.5: Discretization points (N)

The coordinates of the equally spaced points along the curvilinear coordinate are contained in a vector called ds_disc, while their coordinates in the Cartesian axis are contained in the vectors x_disc and y_disc.

- Regolith properties
  - Density, 1600 kg/m^3
- Safety factor, 4 (SF)

Material properties. It includes the mechanical properties of each material which MadFLex is composed.

- Carbon layers
  - Fiber layering, [deg] (theta_c)
  - Thickness of each layer [m] (s_c)
  - Elastic longitudinal modulus in traction [N/m^2] (E_Lc_t)
  - Elastic longitudinal modulus in compression [N/m^2] (E_Lc_c)
  - Elastic transversal modulus [N/m^2] (E_Tc)
  - Shear modulus [N/m^2] (G_LTc)
  - Poisson's coefficient (ni_LTc)
  - Density [Kg/m^3] (rho_c)
  - Ultimate strength [Pa] (sigma_rc_t)
- Foam
  - Foam orientation, [deg] (theta_s)
  - Thickness of the layer [m] (s_s)
  - Elastic modulus in traction [N/m^2] (E_s_t)
  - Elastic modulus in compression [N/m^2] (E_s_c)
  - Shear modulus [N/m^2] (G_s)
  - Density [Kg/m^3] (rho_s)
  - Ultimate strength in traction [Pa] (sigma_rs_t)
  - Ultimate strength in compression [Pa] (sigma_rs_c)
- Dyneema layers
  - Fiber layering, [deg] (theta_d)
  - Thickness of each layer [m] (s_d)
  - Elastic longitudinal modulus in traction [N/m^2] (E_Ld_t)
  - Elastic longitudinal modulus in compression [N/m^2] (E_Ld_c)
  - Elastic transversal modulus [N/m^2] (E_Td)
  - Shear modulus [N/m^2] (G_LTd)
  - Poisson's coefficient (ni_LTd)
  - Density [Kg/m^3] (rho_c)
  - Ultimate strength [Pa] (sigma_rd_t)

Load Condition 3: Regolith load

Discretization of the regolith load Once the habitat is deployed and the regolith shield placed above it, the module is buried under 2.5 m of regolith, as imposed by the requirements to allow an adequate protection against ionizing radiation.
Regolith load above the habitat is a distributed, but non-uniform load, for this reason, a discretization of it is needed for the carrying out of an analytical structural analysis. The distributed load is therefore converted in concentrated loads equal to the volume of the regolith between two discretization points and multiplied by the lunar density and the lunar constant of gravity. The result is N-1 concentrated load, in [N] and placed in the middle of the distance between the discretization points. Figure 9.6 shows graphically this concept.

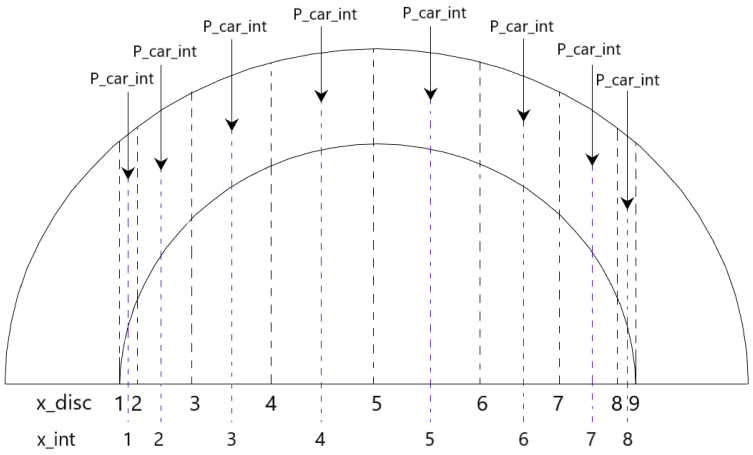

Figure 9.6: Discretization loads

Obviously, the application point of the concentrated loads is not precisely the middle point between two discretization points along s, however increasing N this imprecision becomes negligible. 19 points are enough to provide a negligible variation of the internal forces. All the coordinates relative to the application points of the concentrated loads are saved with the subscript "int".
The load distribution appears as in figure 9.7.

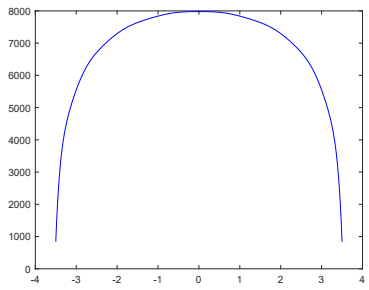

Figure 9.7: Loads, x axis: arch span [m], y axis: Concentrated loads [N]

Solution of Three-Hinges-arch For the analytically solution of the two analysed structural configuration (Three-Hinged-arch and Two-Hinged-arch) the book Theory of Arched Structures, written by Igor A. Karnovsky is used.

Constraint reactions In arch structures the horizontals reactions (H_a and H_b) are named thrust and are equal in magnitude but opposite in direction.
Referring to the Figure 9.9

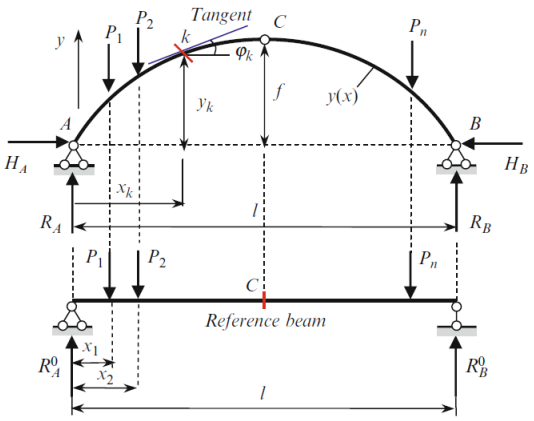

Figure 9.8: Three-Hinged Arch. Source [58].

The horizontal reactions can be calculated with the equilibrium of the flexural moment at the upper hinge and established that is equal to zero.

$$M_c = \underbrace{R_A \frac{l}{2} - P_1\left(\frac{l}{2} - x_1\right) - P_2\left(\frac{l}{2} - x_2\right)}_{M_c^0} - H_A \cdot f = 0$$

Therefore

$$H = \frac{M_c^0}{f}$$

"The vertical reactions of three-hinged arches carrying the vertical loads have same values as the reactions of the reference beam" [58] and can be obtained with a simply equilibrium equation of the moment in the points A or B.

Internal forces Referring to the convention shown in Figure 9.9 the Bending Moment M_k, Shear Q_k, and axial forces N_k at each section k can be obtained considering the equilibrium of free body diagram of the left or right part of the arch. Referring to the left part:

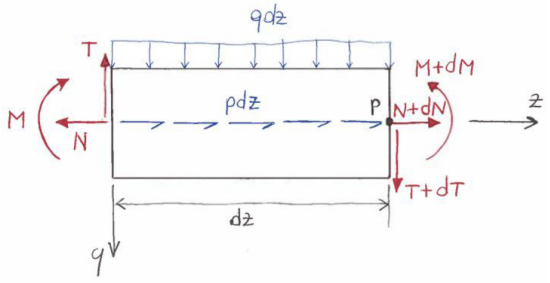

Figure 9.9: Rectilinear elementary beam segment. Source [59]

$$M_k = R_A x_k - \sum_{\text{left}} P_i(x_k - x_i) - Hy_k$$

$$Q_k = \left(R_A - \sum_{\text{left}} P\right) cos\varphi_k - H\, sin\varphi_k$$

$$N_k = -\left(R_A - \sum_{\text{left}} P\right) sin\varphi_k - H\, cos\varphi_k$$

Where φ is the angle between the tangent to the arch center line at the section k and the horizontal line.

As reported in the book "Theory of Arched Structures": " In order to calculate the bending moment in any cross section of the three-hinged arch, the bending moment at the same section of the reference beam should be decreased by the value Hy_k. Therefore, the bending moment in the arch less than that of in the reference beam. This is the reason why the three-hinged arch is more economical than simply supported beam, especially for large-span structures."

MadFlex work cases, membrane stiffness, flexural stiffness and shear stiffness To calculate the membrane and flexural stiffness of the MadFLex, its orientation and the mechanical properties of each materials related to the work conditions must be kept in mind. The previous considerations are explained below.

- Mechanical properties of each materials related to the work conditions: As mentioned in Chapter 6, the MadFlex have a dual behaviour, thanks to the different one developed by the dyneema in traction or in compression. Likewise, the mechanical properties of the carbon change if it is in traction or compression. For this motivation, four different values of flexural stiffness arise from this consideration.

Work case	Upper skin	Lower skin
Case 1	Carbon in **Traction**	Dyneema in **Traction**
Case 2	Carbon in **Compression**	Dyneema in **Traction**
Case 3	Carbon in **Traction**	Dyneema in **Compression**
Case 4	Carbon in **Compression**	Dyneema in **Compression**

- MadFlex orientation. The highest membrane and flexural stiffness of the MadFLex is reached when the Dyneema is in traction, however it is not possible to know which zones of the arch are in traction or in compression before the end of the analysis. If we want to optimize the membrane and flexural stiffness of the MadFlex, having always the Dyneema in traction, another 4 work cases must be consider.

Work case	Upper skin	Lower skin
Case 5	Dyneema in **Traction**	Carbon in **Traction**
Case 6	Dyneema in **Traction**	Carbon in **Compression**
Case 7	Dyneema in **Compression**	Carbon in **Traction**
Case 8	Dyneema in **Compression**	Carbon in **Compression**

In conclusion, there are 8 possible work cases, which generate 8 different membrane and flexural stiffness.
Membrane and flexural stiffness for the 8 work cases are calculated as follow, adopting the theory of the plate
Referring to the following figure, where the coordinates L and T represent the longitudinal and transversal direction along the fiber and belonging to the reference system, named "p".

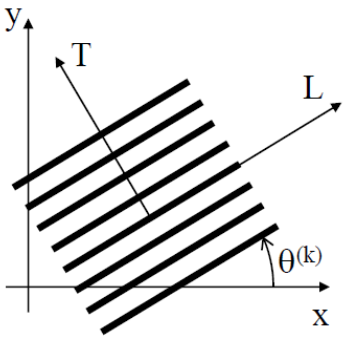

Figure 9.10: Orthotropic reference system and global reference system. Source [60]

the reduced stiffness matrix for a single layer of a orthotropic material can be obtained as:

$$[Q_p^{(k)}] = \begin{bmatrix} \frac{E_L}{1-\nu_{LT}\cdot\nu_{TL}} & \frac{\nu_{TL}E_T}{1-\nu_{LT}\cdot\nu_{TL}} & 0 \\ \frac{\nu_{LT}E_T}{1-\nu_{LT}\cdot\nu_{TL}} & \frac{E_T}{1-\nu_{LT}\cdot\nu_{TL}} & 0 \\ 0 & 0 & G_{LT} \end{bmatrix}$$

If the reference system p is rotated of an angle θ with respect to the global reference system, the directional cosines matrix $[\Lambda^{(k)}]$ needs to be introduced.

$$[\Lambda^{(k)}] = \begin{bmatrix} cos^2(\theta^{(k)}) & sen^2(\theta^{(k)}) & cos(\theta^{(k)}) \cdot sin(\theta^{(k)}) \\ sin^2(\theta^{(k)}) & cos^2(\theta^{(k)}) & -2cos(\theta^{(k)}) \cdot sin(\theta^{(k)}) \\ -cos(\theta^{(k)}) \cdot sin(\theta^{(k)}) & cos(\theta^{(k)}) \cdot sin(\theta^{(k)}) & cos^2(\theta^{(k)}) - sin^2(\theta^{(k)}) \end{bmatrix}$$

The reduced stiffness matrix in a rotated coordinate system can be finally calculated as:

$$[Q^k] = [\Lambda^{(k)}]^{-1} \cdot [Q_p] \cdot \left([\Lambda^k]^{-1}\right)^T$$

Then, the membrane stiffness matrix [A], the coupling matrix [B] and the flexural stiffness matrix [D] of the plate can be obtained as follow:

$$[A] = \int_{-\frac{h}{2}}^{+\frac{h}{2}} [Q]\, dz = \sum_{k=1}^{NS} [Q^{(k)}] \int_{z^{k-}}^{z^{k+}} dz = \sum_{k=1}^{NS} [Q^{(k)}]\, (z^{k+} - z^{k-}) = \sum_{k=1}^{NS} h^{(k)}\, [Q^{(k)}]$$

$$[B] = \int_{-\frac{h}{2}}^{+\frac{h}{2}} z[Q]\, dz = \sum_{k=1}^{NS} [Q^{(k)}] \int_{z^{k-}}^{z^{k+}} z\, dz = \sum_{k=1}^{NS} [Q^{(k)}] \left(\frac{(z^{k+})^2}{2} - \frac{(z^{k-})^2}{2} \right)$$

$$[D] = \int_{-\frac{h}{2}}^{+\frac{h}{2}} z^2[Q]\, dz = \sum_{k=1}^{NS} [Q^{(k)}] \int_{z^{k-}}^{z^{k+}} z^2\, dz = \sum_{k=1}^{NS} [Q^{(k)}] \left(\frac{(z^{k+})^3}{2} - \frac{(z^{k-})^3}{2} \right)$$

where z^{k+} and z^{k-} are the coordinates along the thickness of the upper and lower side of each layer referred to a coordinate system placed in the middle of the overall thickness of the plate. On the other hand, NS represents the number of layers of which the material is composed.

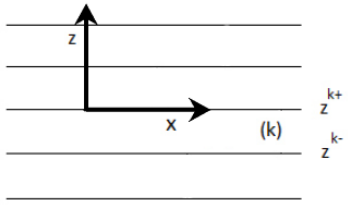

Figure 9.11: Coordinate system placed in the middle of the overall thickness and indication about z^{k+} and z^{k-}

Because the theory used for the analysis is the one referred at the beam, only the element $(1,1)$ of the matrices [A], [B] and [D] are considered and saved by the program. Even if the flexural stiffness D(1,1) is different from the one used in the theory of the beam because the value relative to $Q_p^{(k)}(1,1)$ is equal only to E_L and not $\frac{E_L}{1-\nu_{LT}\cdot\nu_{TL}}$, the different is negligible. Moreover this process allows a quick and tested calculation of the three stiffness matrices for a layered material with a different fiber orientation.

However, a B(1,1) value equal to zero is worthwhile to ease the analytical solution about displacement, which utilizes the Virtual Working Principle, also called Force Method in the book "Theory of Arched Structures". B(1,1)=0 allows the decoupling of the membrane phenomena from the flexural ones. For the previous reason, the translation of the reference material system from the middle of the plate's thickness to the centroid is needed. The centroid is the intersection point of material neutral axes. Points along these axes have only membrane strain (ϵ^0) and the absence of the curvature(k) contribution to the overall strain (ϵ).
To avoid a redundant notation the term (1,1) of the previous matrix will be indicated with the subscript 1.

The centroid can be calculated starting from the constitutive equations of the beam:

$$\begin{Bmatrix} \{N\} \\ \{M\} \end{Bmatrix} \begin{bmatrix} A_1 & B_1 \\ B_1 & D_1 \end{bmatrix} \begin{Bmatrix} \epsilon_0 \\ k \end{Bmatrix}$$

and imposing that the curvature k is equal to zero is possible to find the z coordinate of the centroid:

$$z = \frac{B_1}{A_1}$$

Now the membrane and flexural stiffness referred to the centroid position can be obtained repeating the process mentioned above paying attention to consider the material layers position with respect to it. This process allows the decoupling of the membrane effects from the flexural ones and therefore the simplification of the equation used in the Virtual Working Principle.

Internal stresses and strain The input data of this process are the bending moment and axial force values, calculated in the paragraph referred to the solution of the Three-Hinged Arch. Inserting these values in the constitutive equation of the beam, it is possible to obtain the membrane strain and the curvature.

$$\begin{Bmatrix} \epsilon_0 \\ k \end{Bmatrix} \frac{1}{A_1 D_1 - B_1^2} \begin{bmatrix} D_1 & -B_1 \\ -B_1 & A_1 \end{bmatrix} \begin{Bmatrix} \{N\} \\ \{M\} \end{Bmatrix}$$

The overall strain ϵ can be obtained as:

$$\{\epsilon\} = \{\epsilon_0\} + z\{k\}$$

In conclusion, applying the material constitutive equation is possible to calculate the internal stresses.

$$\{\sigma\} = [Q]\{\epsilon\}$$

However, the previously explained process provides a perfect result for standard material, but fails with the Madflex. As mentioned before, behaviour of the MadFlex changes according to the load condition; therefore, the stiffness matrices are not constant, but they are influenced by the load. This material

introduces a new relation which links the material properties to the load condition making the system underdetermined. How is it possible to solve this situation? Solution is an iterative process. Starting the process with a test solution, the desired information can be obtained repeating this process for a finite number of times until it converges. The number of iterations depends by the chosen condition about the exit from the loop.

Implementation in the program This paragraph explains how the previous iterative process is implemented in the Matlab script. Some concepts and consideration need to be introduced first to better understand the following flowchart.

- Stresses and strains calculations are carried out about the structure in the standard configuration. The term "standard" denotes the structure which have the carbon layer facing outwards and the Dyneema layer facing inward along the arch length.
- The vector named "j" contains work cases assumed by the MadFlex in each point of discretization of the structure. For this reason, it has a length equal at the number N. The terms j is followed by the subscript, proper of each analysed structure. In this case, the subscript is _is for *is*ostatic structure.
- The term "t_it_max" represents the maximum number of iterations set by the user. If the process does not converge, it avoids an infinity number of iterations.
- The variable "flag" assumes the value 1 when desired precision between the previous iterative sigma and the new one is reached. The desired precision or tolerance is named "toll_sigma"

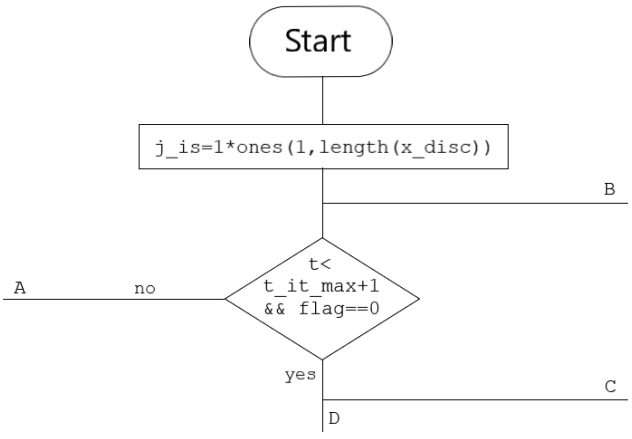

Figure 9.12: First part of the flowchart showing the iterative loop

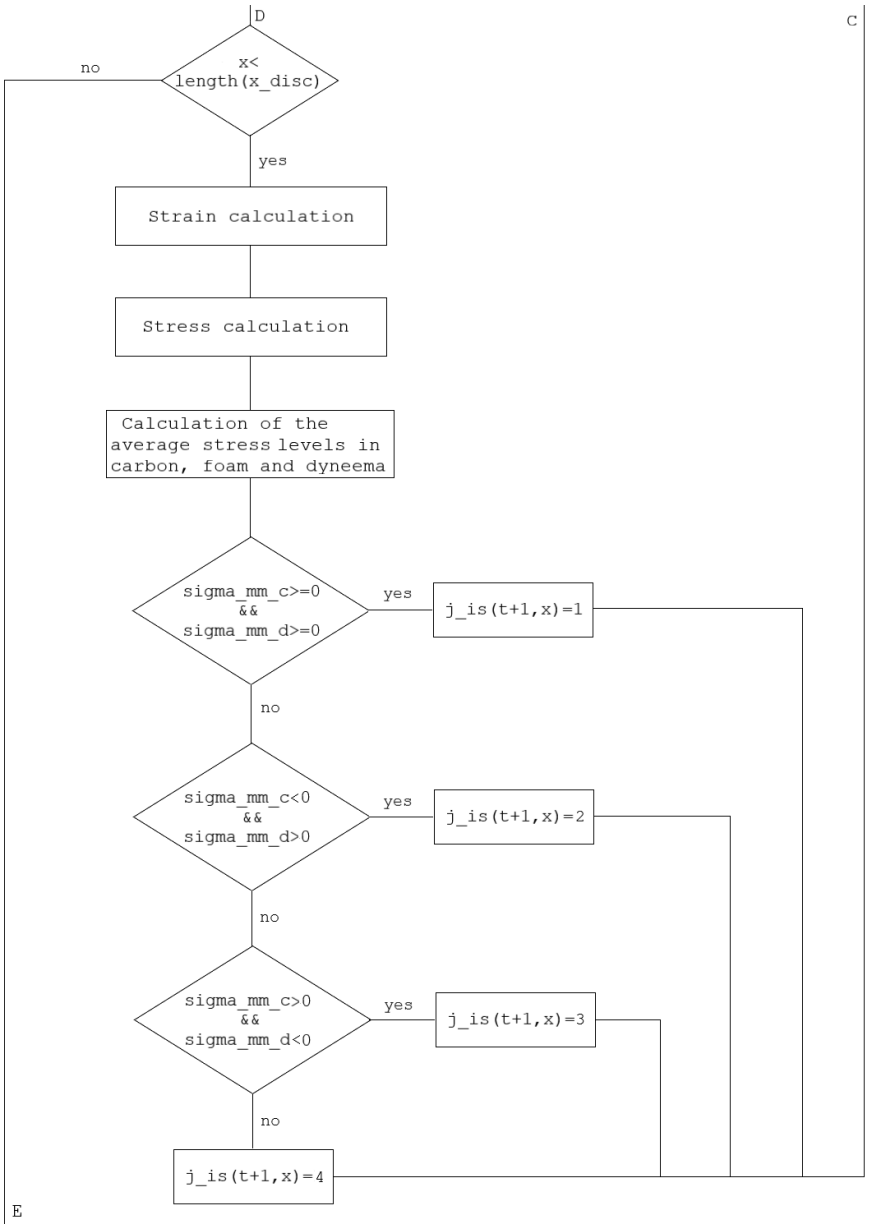

Figure 9.13: Second part of the flowchart showing the loop assigned to the assembling of the vector j_is

The values of vector J, which corresponds to the material work case under the regolith load in each discretization point, are assigned through the comparison between the average sigma developed by the carbon layer to the one developed by the Dyneema. The nested "if" carries out the task for each point.

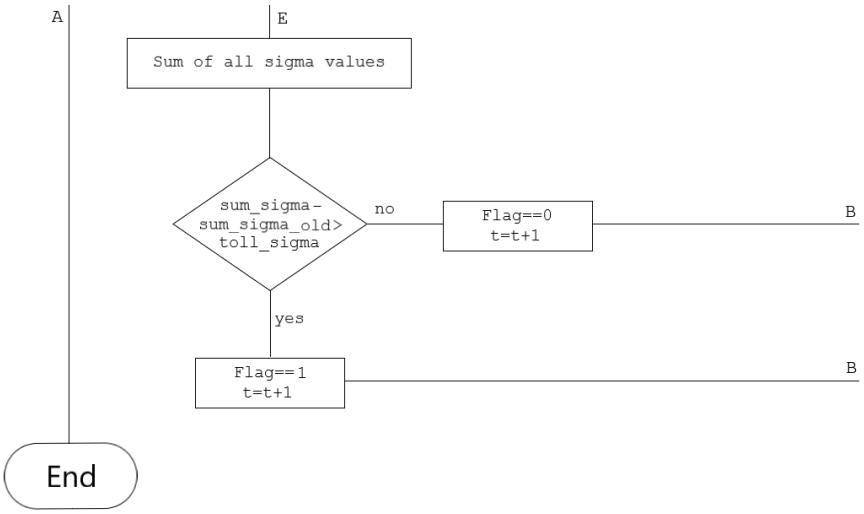

Figure 9.14: Third part of the flowchart showing the end of the iterative loop

The loop ends when the number of iterations is greater than the value imposed by the user and when the flag is equal to one. However, part of the process not shown in the flowchart calculates also the axial force resultant and the bending moment resultant comparing them with the initial value introduced in the process to avoid calculation or programming mistakes.
The process returns in this way the real work case of each discretization point of the structure which cannot be known at first.
Increasing the number of discretization point is possible to have a more precise knowledge about the work case of the material and therefore a more precise solution.

Overturning of the material As mentioned in the previous paragraph, "The highest membrane and flexural stiffness of the MadFLex is reached when the Dyneema is in traction". However, it could happen that this situation is not present in all the structures. To obtain that, an overturning of the material in sections that have not the previously mentioned behaviour is needed. This action allows an optimization of the material properties.
The following flowchart show this process, however some information must be presented first.

- The vector "flag_rib" is used to save in which discretization points, therefore, in which section the material is overturned. If the structure in the standard configuration shows the carbon facing outwards, and the Dyneema facing inwards applying the overturning of the material the carbon is now facing inwards and the Dyneema is facing outwards. The work case of material from 1 to 4 is used in the standard configuration, while the cases 5 to 8 is used in the overturned configuration.
- The variable "n_it_max_rib" denotes the number of overturns chosen by the user. Its value can be only 0 or 1.
- j_is is saved as j_old before the beginning of the overturn process.

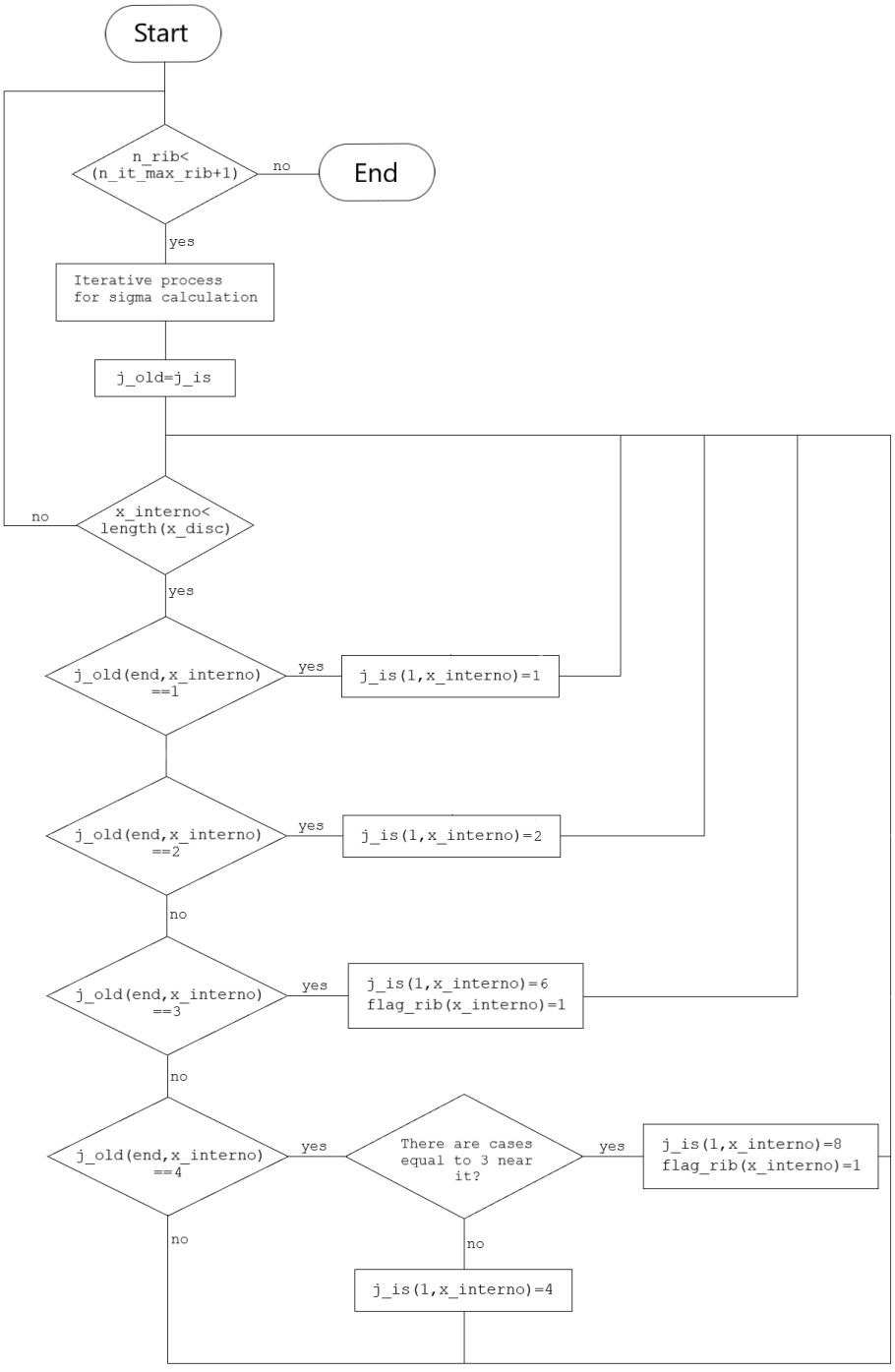

Figure 9.15: Loop for the overturning of the material

Displacement calculation for the Three-Hinged Arch Virtual Working Principle, also called "Force method" in the book "Theory of Arched Structures" is used for the calculation of the structure displacement.

"The Virtual Work principle establishes the equivalence between external virtual work L_v^e and internal virtual work L_v^e for a structure subject to two independent systems: the (a) balanced system (external forces and internal tensions) and the congruent system (b) (displacements and strain)" [59].

$$L_v^e = L_v^i$$

The internal virtual work is defined for a deformable structure as:

$$L_v^i = \int_V \{\sigma^{(a)}\}\{\epsilon^{(b)}\}\, dV$$

Referring to the beam of De Saint Venant, the contribution of bending moment, transversal shear and axial force to the internal virtual work for a flat beam in the plane x,z can be written as follows:

$$L_v^i = \int_L \left(\frac{N^{(a)}N^{(b)}}{EA} + \frac{M^{(a)}M^{(b)}}{EI} + \frac{T^{(a)}T^{(b)}}{KGA} \right) dx$$

where EA is the membrane stiffness of the beam, EI is the flexural stiffness of the beam, GA is the shear stiffness ad k the shear correction factor.
The external virtual work can be instead expressed as:

$$L_v^e = \int_V \{f^{(a)}\}^T\{\eta^{(b)}\}\, dV + \int_V \{M^{(a)}\}^T\{\varphi^{(b)}\}\, dV$$

where f is an external force, η the displacement induced by it, M the external moment and φ the rotation induced by it.
The congruent system (b), mentioned above, can be chosen as the real system (r), while the balance system (a) as the "primary system" (u) (as called in the book "Theory of Arched Structures") for the displacement calculation. Only one force with value equal to one ($f^{(a)} = 1$) is presented in the primary system (u). This allow to have the following expression:

$$|\{\eta\}| = \int_L \left(\frac{N^{(u)}N^{(r)}}{EA} + \frac{M^{(u)}M^{(r)}}{EI} + \frac{T^{(u)}T^{(r)}}{KGA} \right) dx \tag{9.1}$$

$$|\{\varphi\}| = \int_L \left(\frac{N^{(u)}N^{(r)}}{EA} + \frac{M^{(u)}M^{(r)}}{EI} + \frac{T^{(u)}T^{(r)}}{KGA} \right) dx \tag{9.2}$$

The previous relations are also valid for beams where material properties and section change along it (but for limited variations). In fact, material properties (E and G) and the ones related to the section (area, moment of inertia and shear corrective factor) are kept within the integral in the previous expressions. [59]

Primary system A vertical force equal to one and placed at different time in the discretization points is chosen as the exploratory force for the primary system. This allows to know the vertical displacement of each discretization point. The knowledge of the latter information is fundamental to understand the residual habitat height when an accidental or planned de-pressurization happens. Figure 9.16 shows the position of the exploratory forces.

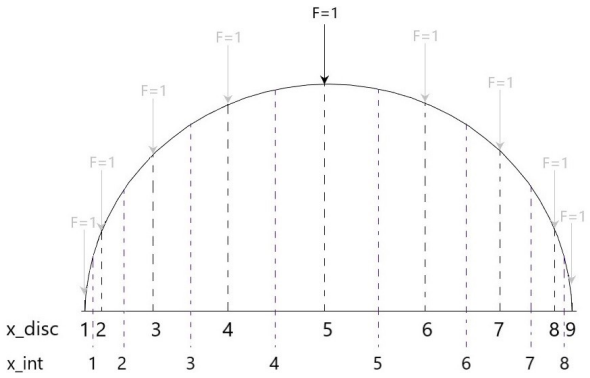

Figure 9.16: Exploratory force for the 9 primary system

Implementation in the program As mentioned before, the Virtual Working Principle expressions are valid for material where its mechanical and geometrical properties can change along it. However, how is it possible to implement it with a "for" loop? The integral of the previous expression can be carried out as the sum of finite number of integrals equal to the one of zones where the materiel properties are constant. Therefore, it is needed to couple the functioning of the numerical method for the integral resolution to the knowledge about material work case. The numerical method implemented for the integral resolution is the trapezoid one, which can be applied only between equispaced points, while the information about work case of the material arise from the vector j_is. The work case of the MadFlex is known in the discretization points. To allow the calculation, this information was extended up to the two points named with the subscript "_int" near to each discretization point.

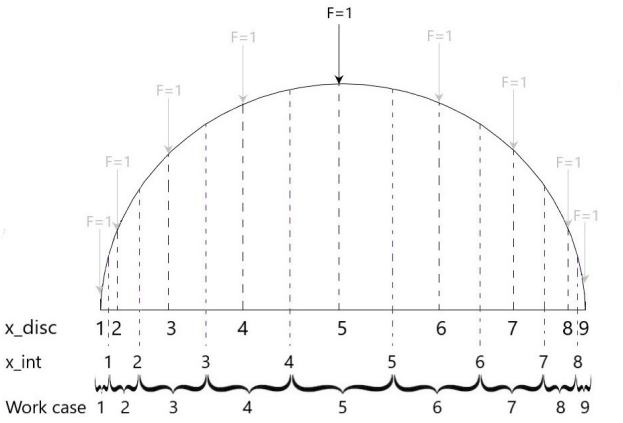

In each cycle, the "for" loop calculates the numerical integrals along the domain identified by a single and constant work case. In order to have a better approximation, each integral domain is divided into two sub domains with a length equal to the distance between a discretization and "_int" point. The contributions of the segments at the end cannot be included in the "for" loop because the domain of integration is half of the others. Therefore, they are added to the loop results when the loop is ended.

```
for J=1:length(x_disc)-2  % I decrease the number of
    points by two not to consider the end segments
     caso=j_is(end,J+1);

     % Contribution of the bending moment
     w_M=d_ds_plv(1)/(2*D_cnu(caso))*[1; 2; 1];
     I_t_M(k,J)=[M_plv_r(2+(J-1)*2)*M_plv1_u(k,2+(J-1)
         *2) M_plv_r(3+(J-1)*2)*M_plv1_u(k,3+(J-1)*2)
         M_plv_r(4+(J-1)*2)*M_plv1_u(k,4+(J-1)*2)]*w_M;
end
```

In the part of script mentioned before only the calculation about moment contribution is shown. The same is done with the transversal shear and the axial force. The displacement of the point of application of the exploratory force is obtained summing up all the contribution provided by the internal forces and geometrically, by the standard domain of integration plus the contribution of the end segments. Repeating this process for the other exploratory forces is possible to obtain the vertical displacement of all the discretization point of the structure.

Solution of the Two-Hinged Arch The Virtual Working Principle can also be used to solve statically indeterminate structure such as the Two-Hinged Arch. In this configuration, the constrain reaction cannot be obtained with the three equilibrium equations, because their number is equal to four. The system allows infinite solution, but only one make the system balanced and congruent. The missing equation can be written by the Virtual Working Principle. The first step is to chose a constrain reaction as "Primary unknowns" (X) and replace it with a active force, obtaining an equivalent statically determinate structure. The latter system is equal to the statically indeterminate one, only if the displacement caused by the active force is equal to zero. [59] The value X of the Primary unknown can be calculated applying the Virtual Working Principle in the following manner. At first it is needed to identify which system is the real system (r) and which is the primary one (u).

- Real system (r): The system with all the applied load is the real one. It is convenient to employ the real system in the equivalent statically determinate structure. Applying the principle of superposition, it is possible to express it as the sum of two systems, named (0) and (1). A possible choice about systems (0) and (1) to solve the Two Hinged Arch is the following:

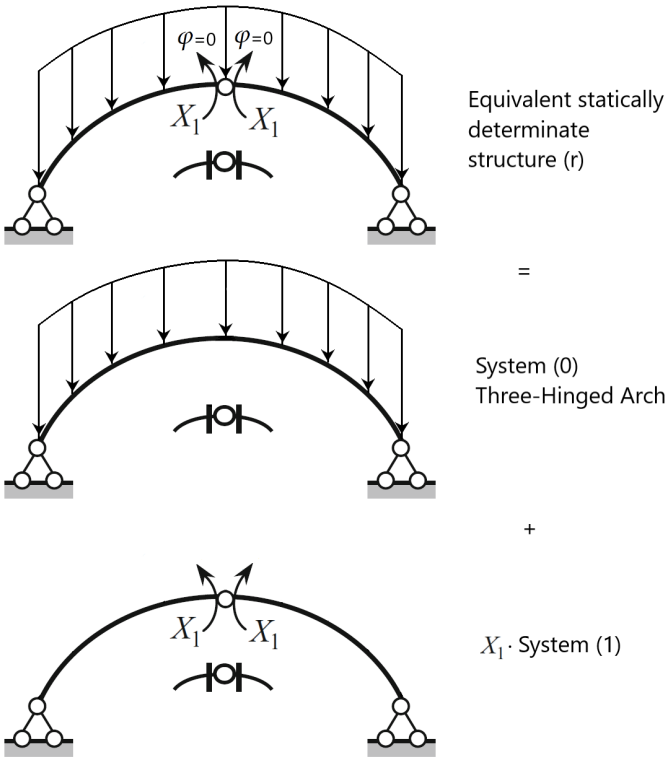

Figure 9.17: Decomposition of the real system (equivalent statically determinate structure) in the system (0) and (1)

where the system (0) is the Three-Hinged Arch already solved and the system one is the structure where only the primary unknown is applied. Therefore:

$$\begin{cases} H_a^{(r)} = H_a^{(0)} + X \cdot H_a^{(1)} \\ \dots \\ M^{(r)} = M^{(0)} + X \cdot M_a^{(1)} \\ \dots \end{cases} \tag{9.3}$$

- The primary system (u) must have the same constrain reaction of (r) and an exploratory force placed in the point where the displacement is needs to be calculated. Therefore, the system (u) corresponds to the system (1).

Imposing that the rotation at the upper hinge is zero in the (9.2), the primary unknown X can be obtained as:

$$X = -\frac{\int_L \frac{N^{(0)}N^{(1)}}{EA}\,dx + \int_L \frac{M^{(0)}M^{(1)}}{EI}\,dx + \int_L \frac{T^{(0)}T^{(1)}}{KGA}\,dx}{\int_L \frac{N^{(1)}N^{(1)}}{EA}\,dx + \int_L \frac{M^{(1)}M^{(1)}}{EI}\,dx + \int_L \frac{T^{(1)}T^{(1)}}{KGA}\,dx} \tag{9.4}$$

In conclusion, the constrain reactions and the internal forces of the Two-Hinged Arch can be obtained applying the relations 9.3.

Internal Stress and Strain in the Two-Hinged Arch The internal stresses and strains for the Two-Hinged Arch are calculated with the same process implemented for the Three-Hinged one. The overturning of the material is also applied as done in the first analysed configuration for the MadFlex optimization. However, work cases assumed by the material in the discretization points are different from the one developed by the Three-Hinged Arch. For this reason, the previous vector is named now "j_ip". The same subscript _ip used to distinguish the variable of the Two-hinged configuration from the Three-Hinged one.

Displacement calculation for the Two-Hinged Arch The same expression 9.2 used for the displacement calculation of the Three-Hinged Arc can be used to calculate the ones of the statically indeterminate structure (Two-Hinged Arch). However, attention to the choice of the system (r) and (u) must be done. For the Two-hinged Arch:

- The (r) system is the Two-Hinged structure under the regolith load, which was solved, in turn, with the Virtual Working Principle in the paragraph before.
- As mentioned by the Virtual Working Principle, the statically indeterminate structure with only one load equal to one should be the (u) system. However, the (u) system must be only balance and not necessarily congruent to the one analysed. Therefore, the (u) system can be the statically determinate structure with a unitary exploratory force. This means that the primary 9 systems used for the Three-Hinged Arc can be employ again for the displacement calculation of the Two-Hinged one.

Load Condition 4: Load used to keep the habitat in the fold configuration

The load needs to bend the habitat from the flexible side in order to roll it in the folded configuration are analysed in this section. The flexural stiffness of the 8 work case of the MadFlex and refer to the centroid of it have already been calculated in the previous section. The moment required to bend it in this load configuration can be obtain as follows:

- The first step is to change the work cases saved in the vector j with their opposite both for the Three-Hinged and the Two-Hinged Arch. The values inside the vectors are now referred to the mechanical properties of the material loaded on the flexible side. This can be done with the process shown by the flowchart in the next page.
- Applying the constitutive equation of a beam and using the mechanical properties referred to the centroid, it is possible to obtain the bending moment for different input values of the curvature in the following manner:

$$M = -EI \cdot k \quad \text{where} \quad k = \frac{1}{r}$$

- Then the program allows the user to choose a single radius of curvature. The stresses and strains induced by it are calculated with the aforementioned iterative process explained in figures 9.12, 9.13 and 9.14

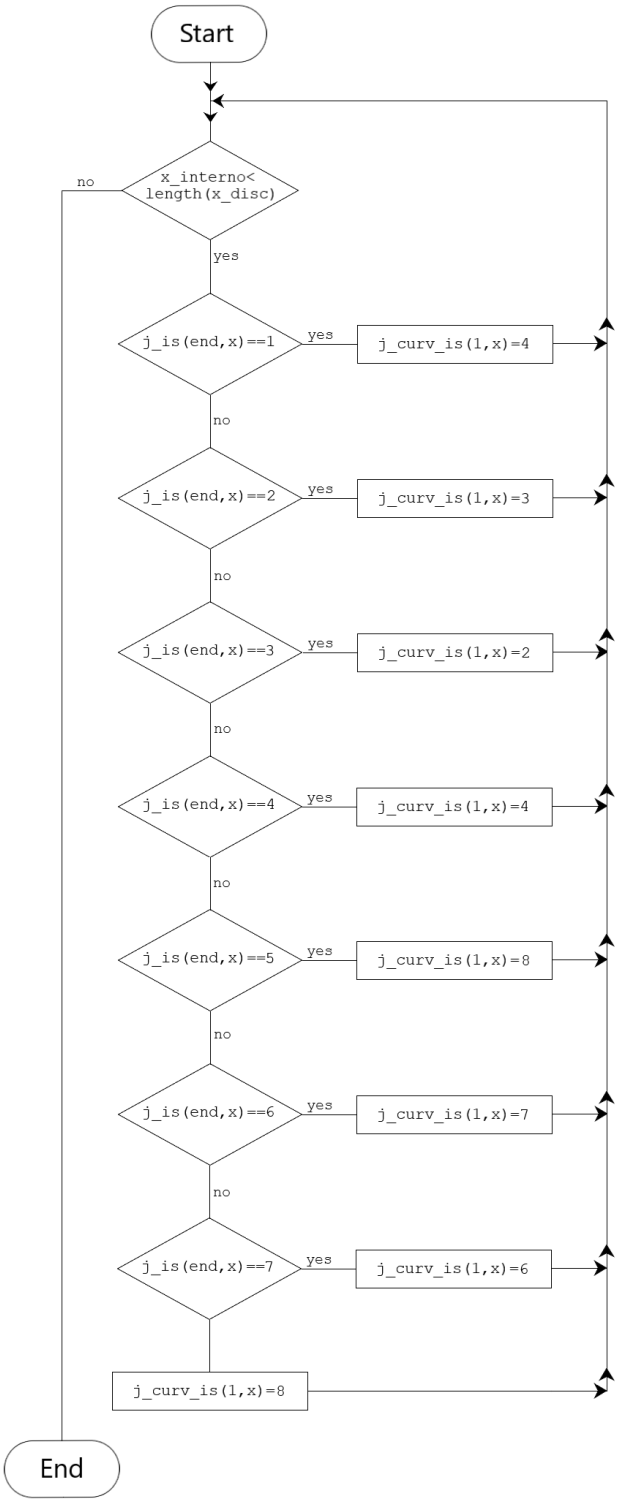
Start
x_interno< length(x_disc)
no
yes
j_is(end,x)==1
yes
j_curv_is(1,x)=4
no
j_is(end,x)==2
yes
j_curv_is(1,x)=3
no
j_is(end,x)==3
yes
j_curv_is(1,x)=2
no
j_is(end,x)==4
yes
j_curv_is(1,x)=4
no
j_is(end,x)==5
yes
j_curv_is(1,x)=8
no
j_is(end,x)==6
yes
j_curv_is(1,x)=7
no
j_is(end,x)==7
yes
j_curv_is(1,x)=6
j_curv_is(1,x)=8
End

Habitat mass The calculation of the habitat mass is carried out as the sum of the masses of each single material. The latter can be obtained multiplying the surface, shown by the material in the section view, by the depth of the half-cinder section (b=0.5 m) and by its density. The aim of this paragraph is to provide data in order to allow:

- disquisition about requirement relative to the maximum load allowed by the launcher.
- the knowledge about the dead weight of the habitat. It can be obtained multiplying the habitat mass by the gravity constant of the Moon (g_l)

Safety factor, sturdiness criteria and critical buckling stress The part of the script explained in this paragraph is implemented to understand if the sturdiness criteria mentioned in Chapter 5 are satisfied by the input data chosen by the user for each material and for the previously analysed load conditions (2 and 3) is the purpose of this part of the script.

Load condition 3, regolith load

- **Rigid skin (carbon)** As mentioned in Chapter 6, the most critical failure mode for the rigid skin in compression is the wrinkling. This failure mode affects the maximum stress tolerable by the material, decreasing it from the ultimate compressive strength to the critical buckling stress of wrinkling. As stated in Chapter 5, the critical buckling stress of wrinkling is calculated with the two following expressions:

  1. First empirical formula (sigma_b1):

  $$\sigma_{b,i,x} = \frac{2}{3} \cdot \left(E_{c,i,x} \cdot E_{3,z} \cdot \frac{t_i}{t_3} \right)^{0.5}$$

  "wherein: t_i is the thickness of the outer layer (carbon). E_c, i, x is the compression elasticity module of the same outer layer [...]; t_3 is the thickness of the intermediate layer (foam) and $E_{3,z}$ is the compression elasticity module of the intermediate layer, in the direction of the thickness in accordance with ASTM C365 / C365M standard" [52]. This value is saved in the program with the variable name sigma_b1.

  2. Second empirical formula (sigma_b2):

  $$\sigma_{Ho} = 0.5 \cdot (E_f \cdot E_c \cdot G_c)^{\frac{1}{3}}$$

  Where the subscript "f" represents the face of the sandwich, while the subscript "c" the core of it [53]. This value is saved in the program with the variable name sigma_b2.

  Then, the stresses developed by the rigid skin in the Three-Hinged Arch (sigma) and by the Two-Hinged one (sigma_is) are multiplied by SF=4 to allow the comparison with the critical buckling stress of wrinkling previously calculated. This part was implemented in the program as follows:

```
Mat_b1_sigma_is=sigma<-sigma_b1; % I check that
    stresses in the three-hinged arch are lower
    than the value obtained with the first
    empirical formula for the wrinkling.
Mat_b2_sigma_is=sigma<-sigma_b2; % I check that
    stresses in the three-hinged arch are lower
    than the value obtained with the second
    empirical formula for the wrinkling,

Mat_b1_sigma_ip=sigma_ip<-sigma_b1; % I check that
     stresses in the two-hinged arch are lower than
     the value obtained with the first empirical
    formula for the wrinkling.
Mat_b2_sigma_ip=sigma_ip<-sigma_b2; % I check that
     stresses in the two-hinged arch are lower than
     the value obtained with the second empirical
    formula for the wrinkling.
```

If the matrix on the left of the equal returns all zeros, it means that the requirement is satisfied. Instead, the matrix returns one where this does not happens.

- **Foam** The same process is implemented for the foam to verify if the absolute value of compression and tensile stresses developed in the two structural configuration are respectively lower than the ultimate compressive and tensile strength.
- **Flexible skin (Dyneema)** The same process implemented for the foam and for the rigid skin is used to verify that the tensile stresses developed in the two analysed configuration are lower than the ultimate tensile strength of the flexible skin.

  Checks about tensile strength of the carbon are not provided because the process of material overturning allows working condition of the carbon only in compression. This allows the optimization of the material with the Dyneema always in traction.

Load condition 4, Load to keep the habitat in the folded configuration

- **Rigid skin (Carbon)** The same process explained before is implemented to verify if the stresses developed by the rigid skin under this load condition for the two analysed structure configuration is lower than the ultimate tensile strength of the material.
- **Foam** The same process is implemented for the foam to verify if the absolute value of the compression and tensile stresses developed in the two structural configuration are respectively lower than the ultimate compressive and tensile strength.

Checks about compression stresses of the flexible skin (Dyneema) are not provided because as mentioned in Chapter 5 "When compressed, Dyneema layers in the MadFlex, reach the buckling condition, therefore no compressive Sturdiness requirement is needed."

Input value for analysis about load condition 1 The aim of this part of the script is to provide the input load values for analysis about load condition 2. The latter is composed by the sum of the following load:

- Regolith load: It has already been calculated at the beginning of this script
- Internal pressure of 1 atm ($1.013 \cdot 10^5$ Pa): This uniform and distributed load is turned into concentrated loads in order to allow its application in the same _int points used for the regolith one. Moreover, it is also divided in its vertical and horizontal components in order to ease the calculation of the constrain relations and vertical displacement in load configuration 1. The latter values are saved in the program with the relative variable names F_pressure_arc_y and F_pressure_arc_x.
- Dead load of the structure: Mass of the total structure is divided in N-1 parts and multiplied by g_l in order to allow its application in the _int points as done for the previous loads. The latter values are saved in the program with the variable name F_tot_ds_y

The previous vectors of loads are added together in order to get the total loads in the y and x direction for the load condition one. The latter values are saved in the program with the relative variable names F_arc_tot_y and F_arc_tot_x

This represents the contents of the first script.

Load Condition 2: Internal pressure plus the regolith load

This load condition is analysed in the Second script present in the Appendix B of the Thesis. The input data of the First and Second script must be the same in order to carry out a correct and coherent analysis.
As mentioned before, the Second script uses some values, calculated by the First one, such as:

- F_arc_tot_y;
- F_arc_tot_x
- j_is: work case of the Madflex in the Three-Hinged Arch
- flag_rib_is: vector in which the information about the overturning of the material in the Three-Hinged Arch is saved.
- j_ip: work case of the Madflex in the Two-Hinged Arch
- flag_rib_ip: vector in which the information about the overturning of the material in the Two-Hinged Arch is saved.

This Second script is composed by the same parts and processes of the First one until the paragraph "Displacement calculation for the Two-Hinged Arch". The only difference from the First script is the absence of the overturning process of the material for both the analysed configurations. The optimization of the material is fundamental with the regolith load only while, as mentioned in Chapter 7 "a 101.4-kPa internal pressure is capable of supporting 40 m of soil on the Moon, assuming a soil density of 1.6 g per cubic centimetre" [34] therefore, the work cases assumed by the MadFLex is almost certainly the number 1 or 5, with all the material layer in traction. These are the best cases because offer the highest membrane and flexural stiffness: therefore, they are already optimized.

9.6 Script validation

The validation of the script was carried out comparing the results obtained by it with the ones provided by the Fem analysis.

9.6.1 Isotropic structure and Virtual Working Principle

The first step of the validation was carried out verifying that the Principle of Virtual Work, applied for the displacement calculation, was implemented correctly in the script. This task was conducted comparing the results obtained by the script for an aluminum arch with the ones provided by the Fem for the same structure. This allowed to verify the accuracy of the script avoiding:

- the issues about the simulation of the MadFlex behaviour, such as the calculation of the membrane and flexural stiffness for the 8 work case of the material.
- the complexity about the determination of the work cases of the MadFlex for the Virtual Working Principle application. This simplification avoid also the stress and strain calculation and the implementation of the overturning of the material for both the structure configurations.

Geometrical features of the structure and mechanical properties of the material are shown below:

Geometrical features		
Item	**Value**	**Unit**
Arch radius	3.5	m
g	9.81	m/s^2
Section height	0.05	m
Section width	0.05	m
N (discretization points)	9	
Mechanical properties		
Elastic modulus	70	GPa
ν	0.33	
Load condition		
Load condition	uniform load of 100 Kg	

Three-Hinged Arch This paragraph shows the results obtained by the script and by the Fem for the vertical displacement of the Three-Hinged Arch.

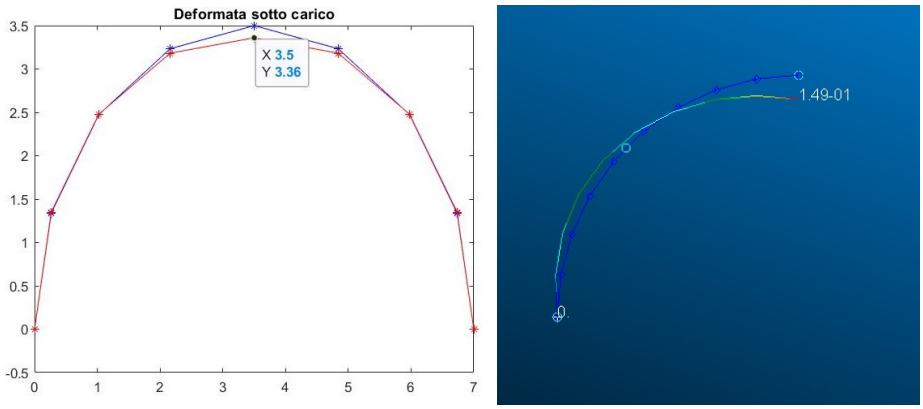

Figure 9.18: Vertical displacement of the Three-Hinged Arch. Script solution on the left (unit of measurement of both the axes [m]), Fem solution on the right

Considerations:

- Fem solution: the result shown in the figure is expressed in [m] and it represents the vertical displacement because the constraint imposed at the end impedes the horizontal displacement.
- Script solution: The not deformed structure is shown in the figure with the blue curve, while the deformed one with the red curve. The value shown in the box is the height reached by the structure under the mentioned loads and is expressed in [m].
  The vector of the displacement for the 9 points is the following:

$$it\_tot = 0.0000,\ -0.0105,\ -0.0051,\ 0.0517,\ 0.1404,\ 0.0517,\\ -0.0051,\ -0.0104,\ 0.0000 \quad [m]$$

  If the number of discretization point is increased in order to reach a better accuracy the displacement of the upper hinge is: 0.1425 [m]

Two-Hinged Arch This paragraph shows the results obtained by the script and by the Fem for the vertical displacement of the Two-Hinged Arch (Figure 9.19).

Considerations:

- Fem solution: the result shown in the figure is expressed in [m] and it represents the vertical displacement because the structure is symmetrical.
- Script solution: Information about this image are the same mentioned before.
  The vector of the displacement for the 9 points is the following:

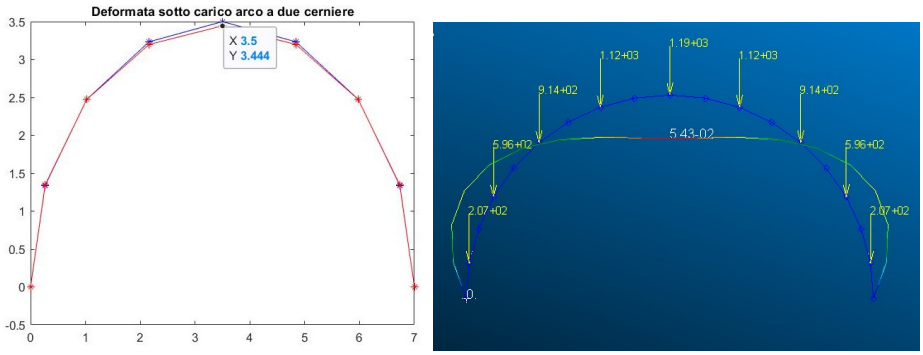

Figure 9.19: Vertical displacement of the Two-Hinged Arch. Script solution on the left (unit of measurement of both the axes [m]), Fem solution on the right

$$it\_ip\_sptot = 0.0000,\ -0.0063,\ 0.0014,\ 0.0351,\ 0.0558,\ 0.0351$$
$$0.0014,\ -0.0063,\ 0.0000 \quad [m]$$

If the number of discretization point is increased in order to reach a better accuracy the displacement of the upper hinge is: 0.0559 [m]

9.6.2 MadFLex structure with all the material in tension

The second step of the validation was carried out verifying that the Principle of Virtual Work, the process for the membrane and flexural stiffness calculation and the simplified process for the stresses and strains calculation was implemented correctly in the script. This task was conducted comparing the results obtained by the script for a MadFLex structure with all the materials in traction with the ones provided by the Fem for the same structure and condition. The work case with all the material in traction was chosen randomly in order to test the membrane and flexural stiffness calculation process. This allowed to verify the accuracy of the script avoiding:

- the complexity about the determination of the work cases of the MadFlex for the Virtual Working Principle application. This simplification avoid also the stress and strain calculation and the implementation of the overturning of the material for both the structure configurations.

Geometrical features of the structure and mechanical properties of the material are shown below:

Geometrical features		
Item	**Value**	**Unit**
Arch radius	3.5	m
g _l	9.81	m/s^2
Section width (b)	0.5	m
N (discretization points)	37	

Mechanical properties and thickness of each layer are the following:

Rigid skin (Carbon)		
Item	**Value**	**Unit**
Fiber orientation	0	degree
Thickness of each ply	1	mm
Tensile Longitudinal Elastic Modulus	150	GPa
Compression Longitudinal Elastic Modulus	135	GPa
Transversal Elastic Modulus	2.9	GPa
Shear Modulus	5.5	GPa
Poisson's ratio	0.3	

Foam		
Item	**Value**	**Unit**
Fiber orientation	0	degree
Thickness of the foam	8	mm
Tensile Elastic Modulus	60	MPa
Compression Elastic Modulus	54	MPa
Shear Modulus	30	GPa

Flexible skin (Dyneema)		
Item	**Value**	**Unit**
Fiber orientation	0	degree
Thickness of each ply ply	3	mm
Tensile Longitudinal Elastic Modulus	100	GPa
Compression Longitudinal Elastic Modulus	0.1	Pa
Transversal Elastic Modulus	0.1	GPa
Shear Modulus	0.2	GPa
Poisson's ratio	0.05	

Load condition	
Load condition	uniform load of 100 Kg

Two-Hinged Arch This paragraph shows the results obtained by the script and by the Fem for the vertical displacement of the Two-Hinged Arch (Figure 9.20). The validation was carried out only for the statically indeterminate structure to ease the process because the resolution of it is based on the statically determinate one.

Considerations:

- Fem solution: the result shown in the figure is expressed in [m] and it represents the vertical displacement because the structure is symmetrical.
- Script solution: The not deformed structure is shown in the figure with the blue curve, while the deformed one with the red curve. The value shown in the box is the height reached by the structure under the mentioned loads and is expressed in [m].
  The displacement of the apex of the arch considering only the bending moment contribution is: 0.4046 [m],

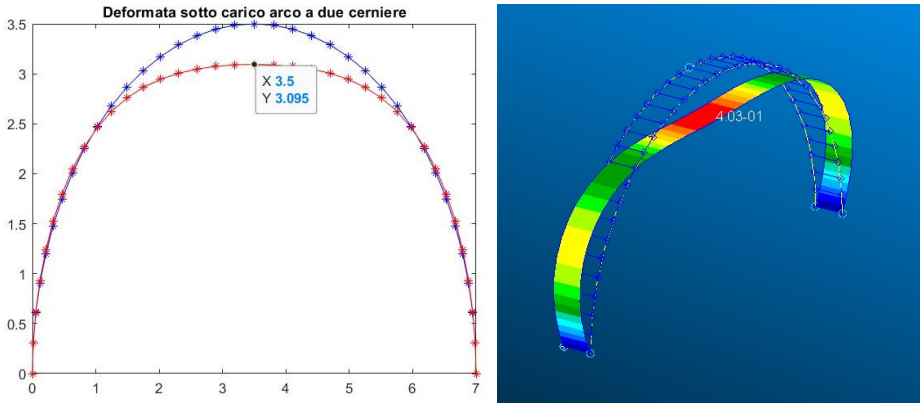

Figure 9.20: Vertical displacement of the Three-Hinged Arch. Script solution on the left (unit of measurement of both the axes [m]), Fem solution on the right

9.6.3 MadFLex structure

The third and final step of the validation was carried out verifying the accuracy of each process implemented in the script. This task was conducted comparing the results obtained by the script for a MadFLex structure with the ones provided by the Fem for the same structure. This paragraph allows the validation of the overall script and therefore the calculation of the displacements and stresses and strain really developed by the structure under the regolith load considering the double behaviour of the MadFlex and the overturning of the material.
The bilinear behaviour of a material was not implemented in the Fem analysis, therefore the work case of the structure are provided by the Matlab script.

Geometrical features of the structure and mechanical properties of the material are shown below:

Geometrical features		
Item	**Value**	**Unit**
Arch radius	3.5	m
Thickness of the regolith cover	0.5	m
g _l	1.635	m/s^2
Section width (b)	0.5	m
N (discretization points)	19	

Rigid skin (Carbon)		
Item	**Value**	**Unit**
Fiber orientation	[0 90]	degree
Thickness of each ply	0.12	mm
Tensile Longitudinal Elastic Modulus	150	GPa
Compression Longitudinal Elastic Modulus	135	GPa
Transversal Elastic Modulus	2.9	GPa
Shear Modulus	5.5	GPa
Poisson's ratio	0.3	

Foam		
Item	**Value**	**Unit**
Fiber orientation	0	degree
Thickness of the foam	50	mm
Tensile Elastic Modulus	60	MPa
Compression Elastic Modulus	54	MPa
Shear Modulus	30	GPa

Flexible skin (Dyneema)		
Item	**Value**	**Unit**
Fiber orientation	[90 0]	degree
Thickness of each ply	0.12	mm
Tensile Longitudinal Elastic Modulus	100	GPa
Compression Longitudinal Elastic Modulus	0.1	Pa
Transversal Elastic Modulus	0.1	GPa
Shear Modulus	0.2	GPa
Poisson's ratio	0.05	

Load condition	
Load condition	Half-circular cover of regolith (shape of the operative condition)

Two-Hinged Arch This paragraph shows the results obtained by the script and by the Fem for the vertical displacement of the Two-Hinged Arch (Figure 9.21). The validation was carried out only for the statically indeterminate structure to ease the process because the resolution of it is based on the statically determinate one.

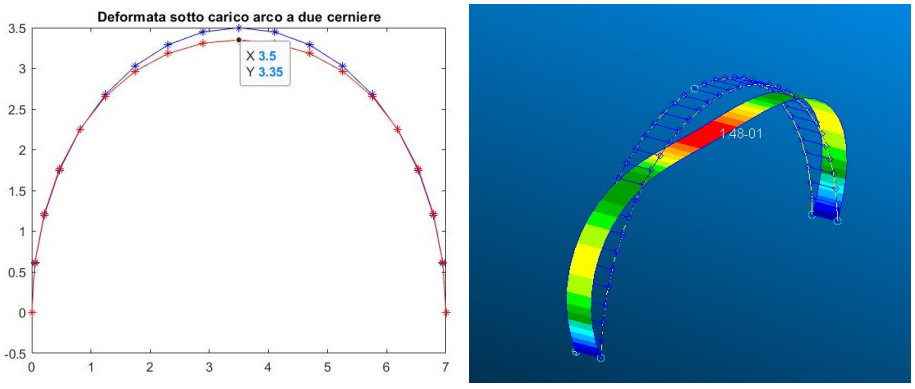

Figure 9.21: Vertical displacement of the Three-Hinged Arch. Script solution on the left, Fem solution on the right

Considerations:

- Fem solution: the result shown in the figure is expressed in [m] and it represents the vertical displacement because the structure is symmetrical.

- Script solution: The not deformed structure is shown in the figure with the blue curve, while the deformed one with the red curve. The value shown in the box is the height reached by the structure under the mentioned loads and is expressed in [m].
  The displacement of the apex of the arch considering only the bending moment contribution is: 0.1497 [m],

The purpose of this script is not only to provide to the user a preliminary tool for understand the structural feasibility of a desired configuration, but also to provide information about the real work case developed by the material under the different load conditions for the Fem analysis.

Chapter 10

Comments and results

Changing the input parameters leads to different results in the Matlab script, in this chapter I present and analyse those results. The aim of this analysis is to provide a support for the structural preliminary analysis showing how each parameter affects the final result and therefore to better satisfy the initial requirements. I only varied the materials properties and their thickness, because the other initial parameters are setted by the architectural requirements.

10.1 Comparison Input data and Results

A first analysis is carried out with the input data mentioned below in order to calculate the real load condition 3 explained in chapter 9 with 2.5 m of regolith. The results reported in this chapter are only useful to highlight the impact of the initial parameters on the stress and displacements of the structures and they are meant to allow a better comprehension of the model created in this thesis.

Input parameters

The input parameters of the configuration are reported in four different tables. The geometrical features of the structure and the mechanical properties of the material are:

Geometrical features		
Item	**Value**	**Unit**
Arch radius	3.5	m
Thickness of the regolith cover	2.5	m
g _l	1.635	m/s^2
Section width (b)	0.5	m
N (N° discretization points)	19	

Mechanical properties and thickness of each layer are the following:

Rigid skin (Carbon)		
Item	**Value**	**Unit**
Fiber orientation	[0 90 0 90]	degree
Thickness of each ply	0.2	mm
Tensile Longitudinal Elastic Modulus	150	GPa
Compression Longitudinal Elastic Modulus	135	GPa
Transversal Elastic Modulus	2.9	GPa
Shear Modulus	5.5	GPa
Poisson's ratio	0.3	
Density	$1.60 \cdot 10^3$	Kg/m^3

Foam		
Item	**Value**	**Unit**
Fiber orientation	0	degree
Thickness of the foam	60	mm
Tensile Elastic Modulus	60	MPa
Compression Elastic Modulus	54	MPa
Shear Modulus	30	GPa
Density	130	Kg/m^3

Flexible skin (Dyneema)		
Item	**Value**	**Unit**
Fiber orientation	[90 0 90 0]	degree
Thickness of each ply	0.2	mm
Tensile Longitudinal Elastic Modulus	100	GPa
Compression Longitudinal Elastic Modulus	0.1	Pa
Transversal Elastic Modulus	0.1	GPa
Shear Modulus	0.2	GPa
Poisson's ratio	0.05	
Density	$0.98 \cdot 10^3$	Kg/m^3

Load condition	
Load condition	Half-circular cover of regolith (shape of the operative condition)

Results

The results relative to these input data are shown in the pages below. To have a better understanding of the results, the following information are needed:

- **Tables of the Material Work Cases (WC)**. In the pages below the reader can see multiple two line tables. In these tables, the second line report the work case developed by the material in the discretization points for the specified load condition. The discretization points are reported in the first line. Only the work cases related to the left part of the arch, including the apex of it, are shown because the load and the structure are symmetrical. A summary of the possible material work cases is shown

below. This table is fundamental to understand the results shown in each paragraph referring to the stresses developed by the material.

Work case	Upper skin	Lower skin
Case 1	Carbon in **Traction**	Dyneema in **Traction**
Case 2	Carbon in **Compression**	Dyneema in **Traction**
Case 3	Carbon in **Traction**	Dyneema in **Compression**
Case 4	Carbon in **Compression**	Dyneema in **Compression**
Case 5	Dyneema in **Traction**	Carbon in **Traction**
Case 6	Dyneema in **Traction**	Carbon in **Compression**
Case 7	Dyneema in **Compression**	Carbon in **Traction**
Case 8	Dyneema in **Compression**	Carbon in **Compression**

- **Tables of stresses**. For better clarity, the tables report only the stresses developed by the left part of arch, including the apex. The meanings of the columns and line are the following:
  - Column: Each column represents the stresses developed by the materials along the thickness of the structure in the discretization point. The number of the column represents the number of the discretization point considered. The first column represents the stresses in the first discretization point, while the last one (discretization point number 10), represents the stresses developed at the apex of the arch.
  - Line: Each line shows the stresses developed by each material layer in its upper or lower side. Their stratification is consistent with the reference system used; the z axis is facing up. Therefore the first line represents the stress developed by the upper side of the first layer facing outwards and the second one the stress developed by the lower side of the first layer facing outwards. Observing the working case developed by the material for the relative chosen discretization point is necessary to understand the order of the material reported in the table. For example, if the work case for the desired discretization point is 6, the fist eight values refer to the Dyneema, while the last eight to the carbon and the two in the middle to the foam.
- **Tables of bending moment to keep the habitat in the folded configuration**. The values shown in these paragraph represent the needed moment to fold the MadFLex with the specified radius of curvature. Each value of the moment shown along the second line of the table is referred to the relative work case developed by the material in each discretization point.

Three-Hinged Arch results

Load Condition 3. Regolith load only

- Displacement: The displacement of the apex of the arch is: 0.4011 [m]

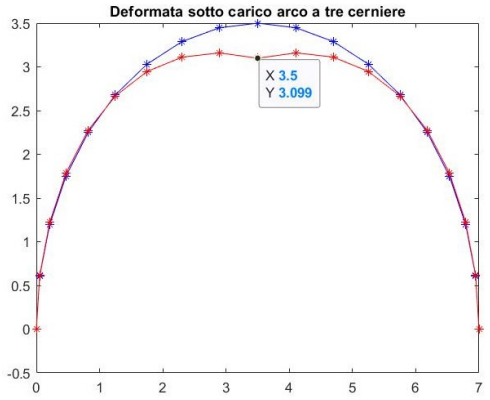

Figure 10.1: Vertical displacement of the Three-Hinged Arch. Unit of measurement of both the axes [m].

- Material work cases (j_is)

$\mathbf{N}^{\circ}_{disc}$	1	2	3	4	5	6	7	8	9	10
$\mathbf{WC}_{3H}$	8	6	6	6	6	6	6	6	6	8

- Stresses: (sigma)

```
 1.0e+08 *

Columns 1 through 12

  0.0000    2.0978    3.4122    3.7669    3.3972    2.5812    1.5985    0.6984    0.0759    0.0000
  0.0000    2.0845    3.3914    3.7443    3.3768    2.5655    1.5885    0.6937    0.0747    0.0000
  0.0000    0.0021    0.0034    0.0037    0.0034    0.0026    0.0016    0.0007    0.0001    0.0000
  0.0000    0.0021    0.0034    0.0037    0.0034    0.0025    0.0016    0.0007    0.0001    0.0000
  0.0000    2.0711    3.3706    3.7216    3.3564    2.5499    1.5786    0.6890    0.0736    0.0000
  0.0000    2.0577    3.3499    3.6990    3.3360    2.5343    1.5686    0.6842    0.0724    0.0000
  0.0000    0.0021    0.0033    0.0037    0.0033    0.0025    0.0016    0.0007    0.0001    0.0000
  0.0000    0.0020    0.0033    0.0037    0.0033    0.0025    0.0016    0.0007    0.0001    0.0000
 -0.0066    0.0012    0.0020    0.0022    0.0020    0.0015    0.0009    0.0004    0.0000   -0.0030
 -0.0001   -0.0012   -0.0017   -0.0019   -0.0017   -0.0013   -0.0009   -0.0004   -0.0002   -0.0001
 -0.0062   -0.0573   -0.0842   -0.0906   -0.0815   -0.0631   -0.0414   -0.0216   -0.0079   -0.0029
 -0.0051   -0.0577   -0.0848   -0.0912   -0.0821   -0.0636   -0.0416   -0.0217   -0.0080   -0.0023
 -0.2359   -2.6869   -3.9483   -4.2469   -3.8234   -2.9600   -1.9388   -1.0105   -0.3708   -0.1081
 -0.1819   -2.7050   -3.9764   -4.2775   -3.8510   -2.9811   -1.9522   -1.0169   -0.3724   -0.0834
 -0.0039   -0.0581   -0.0854   -0.0919   -0.0827   -0.0640   -0.0419   -0.0218   -0.0080   -0.0018
 -0.0027   -0.0585   -0.0860   -0.0925   -0.0833   -0.0645   -0.0422   -0.0220   -0.0080   -0.0013
 -0.1279   -2.7232   -4.0045   -4.3081   -3.8786   -3.0023   -1.9657   -1.0234   -0.3739   -0.0586
 -0.0740   -2.7413   -4.0326   -4.3388   -3.9062   -3.0234   -1.9791   -1.0298   -0.3755   -0.0339
```

Figure 10.2: Stresses of the Three-Hinged Arch, load condition 3. Unit of measurement [Pa].

Load condition 4. Load used to keep the habitat in the folding configuration This paragraph shows the developed material work case, stresses and needed bending moment to reach a curvature radius of 1.5 m.

- Material work cases (j_curv_es_is). The following table shows the material work cases developed by the structure in the discretization points under the previously mentioned load.

$\mathbf{N}^{\circ}_{disc}$	1	2	3	4	5	6	7	8	9	10
$\mathbf{WC}_{3H}$	7	7	7	7	7	7	7	7	7	7

- Bending moment to keep the habitat in the folded configuration (M_curv_es_is). As done for the sigma, only the moment of the left part of the arch are shown. Unit of measure [Nm].

$\mathbf{N}^{\circ}_{disc}$	1	2	3	4	5	6	7	8	9	10
$\mathbf{M}_{3H}$[Nm]	1415	1415	1415	1415	1415	1415	1415	1415	1415	1415

- Stresses (sigma_curv).

```
  1.0e+08 *

Columns 1 through 12

   0.0000    0.0000    0.0000    0.0000    0.0000    0.0000    0.0000    0.0000    0.0000    0.0000
   0.0000    0.0000    0.0000    0.0000    0.0000    0.0000    0.0000    0.0000    0.0000    0.0000
   0.0000    0.0000    0.0000    0.0000    0.0000    0.0000    0.0000    0.0000    0.0000    0.0000
   0.0000    0.0000    0.0000    0.0000    0.0000    0.0000    0.0000    0.0000    0.0000    0.0000
   0.0000    0.0000    0.0000    0.0000    0.0000    0.0000    0.0000    0.0000    0.0000    0.0000
   0.0000    0.0000    0.0000    0.0000    0.0000    0.0000    0.0000    0.0000    0.0000    0.0000
   0.0000    0.0000    0.0000    0.0000    0.0000    0.0000    0.0000    0.0000    0.0000    0.0000
   0.0000    0.0000    0.0000    0.0000    0.0000    0.0000    0.0000    0.0000    0.0000    0.0000
  -0.0235   -0.0235   -0.0235   -0.0235   -0.0235   -0.0235   -0.0235   -0.0235   -0.0235   -0.0235
   0.0005    0.0005    0.0005    0.0005    0.0005    0.0005    0.0005    0.0005    0.0005    0.0005
   0.0232    0.0232    0.0232    0.0232    0.0232    0.0232    0.0232    0.0232    0.0232    0.0232
   0.0270    0.0270    0.0270    0.0270    0.0270    0.0270    0.0270    0.0270    0.0270    0.0270
   1.3987    1.3987    1.3987    1.3987    1.3987    1.3987    1.3987    1.3987    1.3987    1.3987
   1.5991    1.5991    1.5991    1.5991    1.5991    1.5991    1.5991    1.5991    1.5991    1.5991
   0.0309    0.0309    0.0309    0.0309    0.0309    0.0309    0.0309    0.0309    0.0309    0.0309
   0.0348    0.0348    0.0348    0.0348    0.0348    0.0348    0.0348    0.0348    0.0348    0.0348
   1.7994    1.7994    1.7994    1.7994    1.7994    1.7994    1.7994    1.7994    1.7994    1.7994
   1.9998    1.9998    1.9998    1.9998    1.9998    1.9998    1.9998    1.9998    1.9998    1.9998
```

Figure 10.3: Stresses of the Three-Hinged Arch, load condition 4. Unit of measurement [Pa].

Two-Hinged Arch results

Load Condition 3. Regolith load only

- Displacement: The displacement of the apex of the arch is: 0.1630 [m]

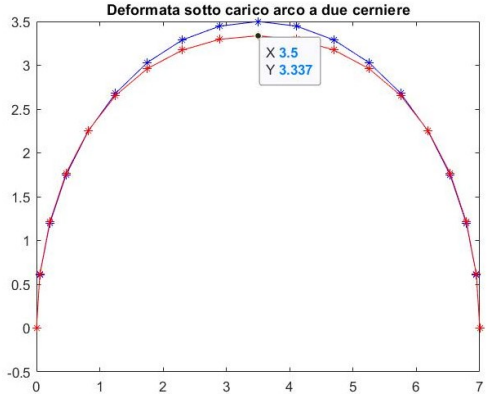

Figure 10.4: Vertical displacement of Two-Hinged Arch. Unit of measurement of both the axes [m].

- Material work cases (j_ip).

$\mathbf{N}^{\circ}_{disc}$	1	2	3	4	5	6	7	8	9	10
$\mathbf{WC}_{2H}$	8	6	6	6	6	6	2	2	2	2

- Stresses: (Sigma_ip)

```
1.0e+08 *

Columns 1 through 12

   0.0000    1.6829    2.5948    2.5720    1.8611    0.7505   -0.4662   -1.5372   -2.2642   -2.5209
   0.0000    1.6718    2.5787    2.5562    1.8494    0.7452   -0.4642   -1.5268   -2.2480   -2.5026
   0.0000    0.0017    0.0026    0.0026    0.0018    0.0007   -0.0100   -0.0328   -0.0483   -0.0538
   0.0000    0.0017    0.0026    0.0025    0.0018    0.0007   -0.0099   -0.0326   -0.0479   -0.0534
   0.0000    1.6608    2.5626    2.5403    1.8377    0.7400   -0.4622   -1.5163   -2.2318   -2.4844
   0.0000    1.6498    2.5464    2.5244    1.8261    0.7348   -0.4602   -1.5058   -2.2156   -2.4662
   0.0000    0.0016    0.0025    0.0025    0.0018    0.0007   -0.0099   -0.0323   -0.0476   -0.0530
   0.0000    0.0016    0.0025    0.0025    0.0018    0.0007   -0.0098   -0.0321   -0.0472   -0.0526
  -0.0066    0.0010    0.0015    0.0015    0.0011    0.0004   -0.0002   -0.0007   -0.0010   -0.0011
  -0.0001   -0.0010   -0.0014   -0.0014   -0.0010   -0.0005    0.0001    0.0007    0.0012    0.0013
  -0.0062   -0.0486   -0.0670   -0.0654   -0.0492   -0.0245    0.0001    0.0012    0.0020    0.0022
  -0.0051   -0.0489   -0.0675   -0.0658   -0.0495   -0.0247    0.0001    0.0012    0.0020    0.0022
  -0.2359   -2.2766   -3.1402   -3.0654   -2.3046   -1.1499    0.1085    1.2234    1.9782    2.2444
  -0.1819   -2.2915   -3.1620   -3.0869   -2.3204   -1.1570    0.1100    1.2311    1.9902    2.2579
  -0.0039   -0.0492   -0.0679   -0.0663   -0.0498   -0.0249    0.0001    0.0012    0.0020    0.0023
  -0.0027   -0.0495   -0.0684   -0.0668   -0.0502   -0.0250    0.0001    0.0012    0.0020    0.0023
  -0.1279   -2.3065   -3.1838   -3.1083   -2.3362   -1.1641    0.1115    1.2388    2.0021    2.2714
  -0.0740   -2.3214   -3.2056   -3.1298   -2.3520   -1.1712    0.1129    1.2466    2.0141    2.2848
```

Figure 10.5: Stresses of the Two-Hinged Arch, load condition 3. Unit of measurement [Pa].

Load condition 4. Load used to keep the habitat in the folding configuration This paragraph shows the developed material work case, stresses and needed bending moment, for a curvature radius of 1.5 m.

- Material work cases (j_curv_es_ip). The following table shows the material work cases developed by the structure in the discretization points under the previously mentioned load.

$\mathbf{N}^{\circ}_{disc}$	1	2	3	4	5	6	7	8	9	10
$\mathbf{WC}_{2H}$	7	7	7	7	7	7	3	3	3	3

- Bending moment to keep the habitat in the folded configuration (M_curv_es_ip). As done for the sigma only the moment of the left part of the arch are shown. Unit of measure [Nm].

$\mathbf{N}^{\circ}_{disc}$	1	2	3	4	5	6	7	8	9	10
$\mathbf{M}_{2H}$[Nm]	1415	1415	1415	1415	1415	1415	-1415	-1415	-1415	-1415

- Stresses (sigma_ip_curv).

```
1.0e+08 *

Columns 1 through 12

   0.0000    0.0000    0.0000    0.0000    0.0000    0.0000    1.9998    1.9998    1.9998    1.9998
   0.0000    0.0000    0.0000    0.0000    0.0000    0.0000    1.7994    1.7994    1.7994    1.7994
   0.0000    0.0000    0.0000    0.0000    0.0000    0.0000    0.0348    0.0348    0.0348    0.0348
   0.0000    0.0000    0.0000    0.0000    0.0000    0.0000    0.0309    0.0309    0.0309    0.0309
   0.0000    0.0000    0.0000    0.0000    0.0000    0.0000    1.5991    1.5991    1.5991    1.5991
   0.0000    0.0000    0.0000    0.0000    0.0000    0.0000    1.3987    1.3987    1.3987    1.3987
   0.0000    0.0000    0.0000    0.0000    0.0000    0.0000    0.0270    0.0270    0.0270    0.0270
   0.0000    0.0000    0.0000    0.0000    0.0000    0.0000    0.0232    0.0232    0.0232    0.0232
  -0.0235   -0.0235   -0.0235   -0.0235   -0.0235   -0.0235    0.0005    0.0005    0.0005    0.0005
   0.0005    0.0005    0.0005    0.0005    0.0005    0.0005   -0.0235   -0.0235   -0.0235   -0.0235
   0.0232    0.0232    0.0232    0.0232    0.0232    0.0232    0.0000    0.0000    0.0000    0.0000
   0.0270    0.0270    0.0270    0.0270    0.0270    0.0270    0.0000    0.0000    0.0000    0.0000
   1.3987    1.3987    1.3987    1.3987    1.3987    1.3987    0.0000    0.0000    0.0000    0.0000
   1.5991    1.5991    1.5991    1.5991    1.5991    1.5991    0.0000    0.0000    0.0000    0.0000
   0.0309    0.0309    0.0309    0.0309    0.0309    0.0309    0.0000    0.0000    0.0000    0.0000
   0.0348    0.0348    0.0348    0.0348    0.0348    0.0348    0.0000    0.0000    0.0000    0.0000
   1.7994    1.7994    1.7994    1.7994    1.7994    1.7994    0.0000    0.0000    0.0000    0.0000
   1.9998    1.9998    1.9998    1.9998    1.9998    1.9998    0.0000    0.0000    0.0000    0.0000
```

Figure 10.6: Stresses of the Two-Hinged Arch, load condition 4. Unit of measurement [Pa].

Critical buckling stress of wrinkling This paragraph shows the values provided by the two empirical formulas for the critical buckling stress of wrinkling. The adjectives "first" and "second" refer to the order in which they are presented in Chapter 9 and 5.

- First empirical formula (sigma _b1): 2.0785e+08,
- Second empirical formula (sigma _b2): 3.0124e+08.

10.2 Modification of the input parameters

As mentioned at the beginning of this chapter the input parameters are modified to understand their effect on the results. This section shows the advantages and the disadvantages of each modification. In all the paragraphs below only the results concerning the increasing of the input values are shown in order to streamline the discussion.

10.2.1 Rigid skin (Carbon)

Longitudinal Elastic Modulus in traction and in compression

Rigid skin (Carbon)			
Item	**Original Value**	**Modified Value**	**Unit**
Tensile Longitudinal Elastic Modulus	150	400	GPa

Advantages of increasing the input values

- Lower deformation of the structure under the load condition 3, both for the Three-Hinged Arch and the Two-Hinged one.

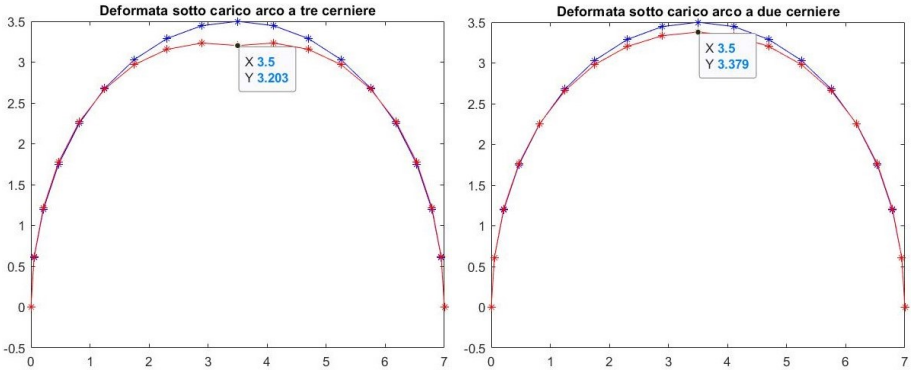

Figure 10.7: Vertical displacement of the Three-Hinged Arch (on the left) and the Two-Hinged Arch (on the right) with modified input data, load condition 3. Unit of measurement of both the axes [m].

- Higher critical buckling stress of wrinkling. Reason of its increasing can be easily understood observing the empirical formula about the critical buckling stress of wrinkling in Chapter 5 and 9.
  - First empirical formula (sigma _b1): 3.3941e+08,
  - Second empirical formula (sigma _b2): 4.1774e+08.
- Higher stability of the structure. The buckling load factor provided by the Fem analysis is not shown, but previous analysis validated this behaviour.

Disadvantages of increasing the input values

- Higher values of compression stress in the rigid skin (carbon) both for the Three-Hinged Arch and the Two-Hinged one for the load condition 3.

$\mathbf{N}^{\circ}_{disc}$	1	2	3	4	5	6	7	8	9	10
$\mathbf{WC}_{3H}$	8	6	6	6	6	6	6	6	6	8
$\mathbf{WC}_{2H}$	8	6	6	6	6	6	2	2	2	2

```
 1.0e+08 *

Columns 1 through 12

  0.0000    2.0733    3.3761    3.7281    3.3623    2.5541    1.5807    0.6892    0.0725    0.0000
  0.0000    2.0640    3.3613    3.7119    3.3477    2.5430    1.5738    0.6860    0.0719    0.0000
  0.0000    0.0021    0.0034    0.0037    0.0033    0.0025    0.0016    0.0007    0.0001    0.0000
  0.0000    0.0021    0.0033    0.0037    0.0033    0.0025    0.0016    0.0007    0.0001    0.0000
  0.0000    2.0547    3.3466    3.6958    3.3332    2.5319    1.5668    0.6828    0.0713    0.0000
  0.0000    2.0454    3.3319    3.6796    3.3186    2.5208    1.5598    0.6796    0.0707    0.0000
  0.0000    0.0020    0.0033    0.0037    0.0033    0.0025    0.0016    0.0007    0.0001    0.0000
  0.0000    0.0020    0.0033    0.0037    0.0033    0.0025    0.0016    0.0007    0.0001    0.0000
 -0.0066    0.0012    0.0020    0.0022    0.0020    0.0015    0.0009    0.0004    0.0000   -0.0030
 -0.0001   -0.0005   -0.0007   -0.0007   -0.0006   -0.0005   -0.0003   -0.0002   -0.0001   -0.0000
 -0.0042   -0.0218   -0.0319   -0.0343   -0.0309   -0.0239   -0.0157   -0.0082   -0.0030   -0.0019
 -0.0030   -0.0220   -0.0324   -0.0348   -0.0313   -0.0243   -0.0159   -0.0083   -0.0031   -0.0014
 -0.3762   -2.7359   -4.0167   -4.3194   -3.8886   -3.0110   -1.9732   -1.0299   -0.3799   -0.1724
 -0.2313   -2.7694   -4.0698   -4.3776   -3.9411   -3.0510   -1.9983   -1.0415   -0.3820   -0.1060
 -0.0019   -0.0223   -0.0328   -0.0353   -0.0317   -0.0246   -0.0161   -0.0084   -0.0031   -0.0009
 -0.0007   -0.0226   -0.0332   -0.0357   -0.0322   -0.0249   -0.0163   -0.0085   -0.0031   -0.0003
 -0.0864   -2.8028   -4.1228   -4.4358   -3.9936   -3.0911   -2.0235   -1.0530   -0.3841   -0.0396
  0.0585   -2.8363   -4.1759   -4.4940   -4.0460   -3.1311   -2.0486   -1.0645   -0.3862    0.0268
```

Figure 10.8: Sigma values for the Three-Hinged Arch with modified input data, load condition 3. Unit of measurement [Pa].

```
 1.0e+08 *

Columns 1 through 12

  0.0000    1.6622    2.5663    2.5443    1.8405    0.7405   -0.4792   -1.5906   -2.3450   -2.6114
  0.0000    1.6546    2.5550    2.5331    1.8323    0.7370   -0.4763   -1.5711   -2.3141   -2.5765
  0.0000    0.0017    0.0026    0.0025    0.0018    0.0007   -0.0038   -0.0127   -0.0186   -0.0208
  0.0000    0.0016    0.0025    0.0025    0.0018    0.0007   -0.0038   -0.0125   -0.0184   -0.0205
  0.0000    1.6471    2.5437    2.5220    1.8241    0.7335   -0.4735   -1.5515   -2.2832   -2.5415
  0.0000    1.6395    2.5324    2.5108    1.8160    0.7300   -0.4707   -1.5319   -2.2522   -2.5066
  0.0000    0.0016    0.0025    0.0025    0.0018    0.0007   -0.0038   -0.0123   -0.0181   -0.0202
  0.0000    0.0016    0.0025    0.0025    0.0018    0.0007   -0.0038   -0.0122   -0.0179   -0.0199
 -0.0066    0.0010    0.0015    0.0015    0.0011    0.0004   -0.0001   -0.0003   -0.0004   -0.0004
 -0.0001   -0.0004   -0.0005   -0.0005   -0.0004   -0.0002    0.0001    0.0007    0.0012    0.0013
 -0.0042   -0.0185   -0.0254   -0.0248   -0.0187   -0.0093    0.0001    0.0012    0.0020    0.0022
 -0.0030   -0.0187   -0.0257   -0.0251   -0.0189   -0.0094    0.0001    0.0012    0.0020    0.0022
 -0.3762   -2.3193   -3.1961   -3.1197   -2.3463   -1.1729    0.1058    1.2159    1.9674    2.2325
 -0.2313   -2.3465   -3.2369   -3.1600   -2.3758   -1.1855    0.1066    1.2213    1.9760    2.2422
 -0.0019   -0.0189   -0.0261   -0.0255   -0.0191   -0.0096    0.0001    0.0012    0.0020    0.0022
 -0.0007   -0.0191   -0.0264   -0.0258   -0.0194   -0.0097    0.0001    0.0012    0.0020    0.0023
 -0.0864   -2.3737   -3.2777   -3.2003   -2.4052   -1.1981    0.1074    1.2268    1.9846    2.2519
  0.0585   -2.4010   -3.3185   -3.2405   -2.4346   -1.2107    0.1082    1.2322    1.9932    2.2616
```

Figure 10.9: Sigma values for the Two-Hinged Arch with modified input data, load condition 3. Unit of measurement [Pa].

- Higher value of the bending moment to fold the MadFlex for both for the Three-Hinged Arch and the Two-Hinged one for the load condition 4.

  Work case for load condition 4 are shown in the following table:

N°_{disc}	1	2	3	4	5	6	7	8	9	10
$\mathbf{WC}_{3H}$	7	7	7	7	7	7	7	7	7	7
$\mathbf{WC}_{2H}$	7	7	7	7	7	7	3	3	3	3

N°_{disc}	1	2	3	4	5	6	7	8	9	10
$\mathbf{M}_{3H}$[Nm]	1454	1454	1454	1454	1454	1454	1454	1454	1454	1454
$\mathbf{M}_{2H}$[Nm]	1454	1454	1454	1454	1454	1454	-1454	-1454	-1454	-1454

- Higher values of tensile stress in the rigid skin (carbon) both for the Three-Hinged Arch (Figures 10.10) and the Two-Hinged one (10.11) for the load condition 4.

```
  1.0e+08 *

 Columns 1 through 12

   0.0000    0.0000    0.0000    0.0000    0.0000    0.0000    0.0000    0.0000    0.0000    0.0000
   0.0000    0.0000    0.0000    0.0000    0.0000    0.0000    0.0000    0.0000    0.0000    0.0000
   0.0000    0.0000    0.0000    0.0000    0.0000    0.0000    0.0000    0.0000    0.0000    0.0000
   0.0000    0.0000    0.0000    0.0000    0.0000    0.0000    0.0000    0.0000    0.0000    0.0000
   0.0000    0.0000    0.0000    0.0000    0.0000    0.0000    0.0000    0.0000    0.0000    0.0000
   0.0000    0.0000    0.0000    0.0000    0.0000    0.0000    0.0000    0.0000    0.0000    0.0000
   0.0000    0.0000    0.0000    0.0000    0.0000    0.0000    0.0000    0.0000    0.0000    0.0000
   0.0000    0.0000    0.0000    0.0000    0.0000    0.0000    0.0000    0.0000    0.0000    0.0000
  -0.0239   -0.0239   -0.0239   -0.0239   -0.0239   -0.0239   -0.0239   -0.0239   -0.0239   -0.0239
   0.0001    0.0001    0.0001    0.0001    0.0001    0.0001    0.0001    0.0001    0.0001    0.0001
   0.0032    0.0032    0.0032    0.0032    0.0032    0.0032    0.0032    0.0032    0.0032    0.0032
   0.0071    0.0071    0.0071    0.0071    0.0071    0.0071    0.0071    0.0071    0.0071    0.0071
   0.9804    0.9804    0.9804    0.9804    0.9804    0.9804    0.9804    0.9804    0.9804    0.9804
   1.5141    1.5141    1.5141    1.5141    1.5141    1.5141    1.5141    1.5141    1.5141    1.5141
   0.0110    0.0110    0.0110    0.0110    0.0110    0.0110    0.0110    0.0110    0.0110    0.0110
   0.0148    0.0148    0.0148    0.0148    0.0148    0.0148    0.0148    0.0148    0.0148    0.0148
   2.0478    2.0478    2.0478    2.0478    2.0478    2.0478    2.0478    2.0478    2.0478    2.0478
   2.5814    2.5814    2.5814    2.5814    2.5814    2.5814    2.5814    2.5814    2.5814    2.5814
```

Figure 10.10: Sigma values for the Three-Hinged Arch with modified input data, load condition 4. Unit of measure [Pa].

Advantages of the decreasing of the input value It can be convenient to slightly decrease the longitudinal elastic modulus for the following reasons:

- to obtain lower compression stresses in the rigid skin (carbon) when the structure has to withstand load condition 3 in order to satisfy the rigid skin's sturdiness criteria;

- to obtain lower tensile stresses in the carbon layer when the structure has to withstand load condition 4 in order to satisfy the rigid skin's sturdiness criteria.

```
 1.0e+08 *

Columns 1 through 12

  0.0000    0.0000    0.0000    0.0000    0.0000    0.0000    2.5814    2.5814    2.5814    2.5814
  0.0000    0.0000    0.0000    0.0000    0.0000    0.0000    2.0478    2.0478    2.0478    2.0478
  0.0000    0.0000    0.0000    0.0000    0.0000    0.0000    0.0148    0.0148    0.0148    0.0148
  0.0000    0.0000    0.0000    0.0000    0.0000    0.0000    0.0110    0.0110    0.0110    0.0110
  0.0000    0.0000    0.0000    0.0000    0.0000    0.0000    1.5141    1.5141    1.5141    1.5141
  0.0000    0.0000    0.0000    0.0000    0.0000    0.0000    0.9804    0.9804    0.9804    0.9804
  0.0000    0.0000    0.0000    0.0000    0.0000    0.0000    0.0071    0.0071    0.0071    0.0071
  0.0000    0.0000    0.0000    0.0000    0.0000    0.0000    0.0032    0.0032    0.0032    0.0032
 -0.0239   -0.0239   -0.0239   -0.0239   -0.0239   -0.0239    0.0001    0.0001    0.0001    0.0001
  0.0001    0.0001    0.0001    0.0001    0.0001    0.0001   -0.0239   -0.0239   -0.0239   -0.0239
  0.0032    0.0032    0.0032    0.0032    0.0032    0.0032    0.0000    0.0000    0.0000    0.0000
  0.0071    0.0071    0.0071    0.0071    0.0071    0.0071    0.0000    0.0000    0.0000    0.0000
  0.9804    0.9804    0.9804    0.9804    0.9804    0.9804    0.0000    0.0000    0.0000    0.0000
  1.5141    1.5141    1.5141    1.5141    1.5141    1.5141    0.0000    0.0000    0.0000    0.0000
  0.0110    0.0110    0.0110    0.0110    0.0110    0.0110    0.0000    0.0000    0.0000    0.0000
  0.0148    0.0148    0.0148    0.0148    0.0148    0.0148    0.0000    0.0000    0.0000    0.0000
  2.0478    2.0478    2.0478    2.0478    2.0478    2.0478    0.0000    0.0000    0.0000    0.0000
  2.5814    2.5814    2.5814    2.5814    2.5814    2.5814    0.0000    0.0000    0.0000    0.0000
```

Figure 10.11: Sigma values for the Two-Hinged Arch with modified input data, load condition 4. Unit of measurement [Pa].

Layering

Rigid skin (Carbon)			
Item	**Original Value**	**Modified Value**	**Unit**
Fiber orientations	[0 90 0 90]	[30 -30 30 -30]	Degree

Advantages of changing the input value

- Lower deformation of the structure under the load condition 3, both for the Three-Hinged Arch and the Two-Hinged one.

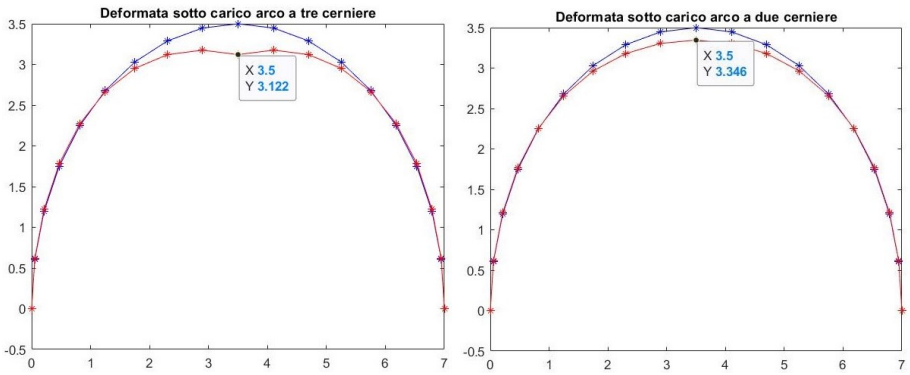

Figure 10.12: Vertical displacement of the Three-Hinged Arch (on the left) and the Two-Hinged Arch (on the right) with modified input data, load condition 3. Unit of measurement of both the axes [m].

- More homogeneous compression stress values in the rigid skin for load

condition 3, avoiding critical stresses in some layers (the previous one with 0° of orientation) and involving all layers to withstand the load both for the Three-Hinged Arch and for the Two-Hinged one.

$\mathbf{N}^{\circ}_{disc}$	1	2	3	4	5	6	7	8	9	10
$\mathbf{WC}_{3H}$	8	6	6	6	6	6	6	6	6	8
$\mathbf{WC}_{2H}$	8	6	6	6	6	6	2	2	2	2

```
 1.0e+08 *

Columns 1 through 12

   0.0000    2.0966    3.4104    3.7650    3.3955    2.5799    1.5976    0.6980    0.0757    0.0000
   0.0000    2.0842    3.3910    3.7438    3.3764    2.5652    1.5883    0.6936    0.0747    0.0000
   0.0000    0.0021    0.0034    0.0037    0.0034    0.0026    0.0016    0.0007    0.0001    0.0000
   0.0000    0.0021    0.0034    0.0037    0.0034    0.0026    0.0016    0.0007    0.0001    0.0000
   0.0000    2.0717    3.3715    3.7226    3.3573    2.5506    1.5790    0.6892    0.0736    0.0000
   0.0000    2.0592    3.3521    3.7014    3.3382    2.5359    1.5697    0.6848    0.0726    0.0000
   0.0000    0.0021    0.0034    0.0037    0.0033    0.0025    0.0016    0.0007    0.0001    0.0000
   0.0000    0.0020    0.0033    0.0037    0.0033    0.0025    0.0016    0.0007    0.0001    0.0000
  -0.0066    0.0012    0.0020    0.0022    0.0020    0.0015    0.0009    0.0004    0.0000   -0.0030
  -0.0001   -0.0010   -0.0015   -0.0016   -0.0015   -0.0011   -0.0007   -0.0004   -0.0001   -0.0000
  -0.1450   -1.3721   -2.0156   -2.1678   -1.9517   -1.5110   -0.9899   -0.5162   -0.1898   -0.0664
  -0.1126   -1.3822   -2.0313   -2.1850   -1.9671   -1.5228   -0.9974   -0.5198   -0.1906   -0.0516
  -0.1126   -1.3822   -2.0313   -2.1850   -1.9671   -1.5228   -0.9974   -0.5198   -0.1906   -0.0516
  -0.0803   -1.3923   -2.0470   -2.2021   -1.9826   -1.5347   -1.0049   -0.5233   -0.1914   -0.0368
  -0.0803   -1.3923   -2.0470   -2.2021   -1.9826   -1.5347   -1.0049   -0.5233   -0.1914   -0.0368
  -0.0480   -1.4024   -2.0627   -2.2192   -1.9980   -1.5465   -1.0124   -0.5269   -0.1923   -0.0220
  -0.0480   -1.4024   -2.0627   -2.2192   -1.9980   -1.5465   -1.0124   -0.5269   -0.1923   -0.0220
  -0.0157   -1.4124   -2.0784   -2.2364   -2.0134   -1.5583   -1.0199   -0.5304   -0.1931   -0.0072
```

Figure 10.13: Sigma values for the Three-Hinged Arch with modified input data, load condition 3. Unit of measurement [Pa].

```
 1.0e+08 *

Columns 1 through 12

   0.0000    1.6819    2.5934    2.5707    1.8601    0.7500   -0.2398   -0.7922   -1.1671   -1.2995
   0.0000    1.6716    2.5784    2.5559    1.8492    0.7452   -0.2387   -0.7863   -1.1580   -1.2893
   0.0000    0.0017    0.0026    0.0026    0.0018    0.0007   -0.2387   -0.7863   -1.1580   -1.2893
   0.0000    0.0017    0.0026    0.0025    0.0018    0.0007   -0.2376   -0.7805   -1.1490   -1.2791
   0.0000    1.6613    2.5633    2.5410    1.8383    0.7403   -0.2376   -0.7805   -1.1490   -1.2791
   0.0000    1.6510    2.5482    2.5262    1.8274    0.7354   -0.2365   -0.7746   -1.1399   -1.2689
   0.0000    0.0017    0.0025    0.0025    0.0018    0.0007   -0.2365   -0.7746   -1.1399   -1.2689
   0.0000    0.0016    0.0025    0.0025    0.0018    0.0007   -0.2355   -0.7688   -1.1308   -1.2587
  -0.0066    0.0010    0.0015    0.0015    0.0011    0.0004   -0.0002   -0.0006   -0.0008   -0.0009
  -0.0001   -0.0009   -0.0012   -0.0012   -0.0009   -0.0004    0.0001    0.0007    0.0012    0.0013
  -0.1450   -1.1628   -1.6033   -1.5651   -1.1768   -0.5875    0.0001    0.0012    0.0020    0.0022
  -0.1126   -1.1711   -1.6155   -1.5770   -1.1856   -0.5914    0.0001    0.0012    0.0020    0.0022
  -0.1126   -1.1711   -1.6155   -1.5770   -1.1856   -0.5914    0.1087    1.2241    1.9794    2.2458
  -0.0803   -1.1794   -1.6276   -1.5890   -1.1944   -0.5954    0.1100    1.2314    1.9906    2.2584
  -0.0803   -1.1794   -1.6276   -1.5890   -1.1944   -0.5954    0.0001    0.0012    0.0020    0.0023
  -0.0480   -1.1877   -1.6398   -1.6010   -1.2032   -0.5993    0.0001    0.0012    0.0020    0.0023
  -0.0480   -1.1877   -1.6398   -1.6010   -1.2032   -0.5993    0.1113    1.2386    2.0018    2.2710
  -0.0157   -1.1959   -1.6520   -1.6130   -1.2120   -0.6032    0.1127    1.2458    2.0130    2.2837
```

Figure 10.14: Sigma values for the Two-Hinged Arch with modified input data, load condition 3. Unit of measurement [Pa].

- More homogeneous tensile stress values in the rigid skin for load condition 4 avoiding critical stresses in some layers and involving all layers to withstand the load. This happens both for the Three-Hinged Arch and for the Two-Hinged one.

$\mathbf{N}^{\circ}_{disc}$	1	2	3	4	5	6	7	8	9	10
$\mathbf{WC}_{3H}$	7	7	7	7	7	7	7	7	7	7
$\mathbf{WC}_{2H}$	7	7	7	7	7	7	3	3	3	3

```
 1.0e+08 *

Columns 1 through 12

  0.0000    0.0000    0.0000    0.0000    0.0000    0.0000    0.0000    0.0000    0.0000    0.0000
  0.0000    0.0000    0.0000    0.0000    0.0000    0.0000    0.0000    0.0000    0.0000    0.0000
  0.0000    0.0000    0.0000    0.0000    0.0000    0.0000    0.0000    0.0000    0.0000    0.0000
  0.0000    0.0000    0.0000    0.0000    0.0000    0.0000    0.0000    0.0000    0.0000    0.0000
  0.0000    0.0000    0.0000    0.0000    0.0000    0.0000    0.0000    0.0000    0.0000    0.0000
  0.0000    0.0000    0.0000    0.0000    0.0000    0.0000    0.0000    0.0000    0.0000    0.0000
  0.0000    0.0000    0.0000    0.0000    0.0000    0.0000    0.0000    0.0000    0.0000    0.0000
  0.0000    0.0000    0.0000    0.0000    0.0000    0.0000    0.0000    0.0000    0.0000    0.0000
 -0.0236   -0.0236   -0.0236   -0.0236   -0.0236   -0.0236   -0.0236   -0.0236   -0.0236   -0.0236
  0.0004    0.0004    0.0004    0.0004    0.0004    0.0004    0.0004    0.0004    0.0004    0.0004
  0.6304    0.6304    0.6304    0.6304    0.6304    0.6304    0.6304    0.6304    0.6304    0.6304
  0.7493    0.7493    0.7493    0.7493    0.7493    0.7493    0.7493    0.7493    0.7493    0.7493
  0.7493    0.7493    0.7493    0.7493    0.7493    0.7493    0.7493    0.7493    0.7493    0.7493
  0.8682    0.8682    0.8682    0.8682    0.8682    0.8682    0.8682    0.8682    0.8682    0.8682
  0.8682    0.8682    0.8682    0.8682    0.8682    0.8682    0.8682    0.8682    0.8682    0.8682
  0.9871    0.9871    0.9871    0.9871    0.9871    0.9871    0.9871    0.9871    0.9871    0.9871
  0.9871    0.9871    0.9871    0.9871    0.9871    0.9871    0.9871    0.9871    0.9871    0.9871
  1.1059    1.1059    1.1059    1.1059    1.1059    1.1059    1.1059    1.1059    1.1059    1.1059
```

Figure 10.15: Sigma values for the Three-Hinged Arch with modified input data, load condition 4. Unit of measurement [Pa].

```
 1.0e+08 *

Columns 1 through 12

  0.0000    0.0000    0.0000    0.0000    0.0000    0.0000    1.1059    1.1059    1.1059    1.1059
  0.0000    0.0000    0.0000    0.0000    0.0000    0.0000    0.9871    0.9871    0.9871    0.9871
  0.0000    0.0000    0.0000    0.0000    0.0000    0.0000    0.9871    0.9871    0.9871    0.9871
  0.0000    0.0000    0.0000    0.0000    0.0000    0.0000    0.8682    0.8682    0.8682    0.8682
  0.0000    0.0000    0.0000    0.0000    0.0000    0.0000    0.8682    0.8682    0.8682    0.8682
  0.0000    0.0000    0.0000    0.0000    0.0000    0.0000    0.7493    0.7493    0.7493    0.7493
  0.0000    0.0000    0.0000    0.0000    0.0000    0.0000    0.7493    0.7493    0.7493    0.7493
  0.0000    0.0000    0.0000    0.0000    0.0000    0.0000    0.6304    0.6304    0.6304    0.6304
 -0.0236   -0.0236   -0.0236   -0.0236   -0.0236   -0.0236    0.0004    0.0004    0.0004    0.0004
  0.0004    0.0004    0.0004    0.0004    0.0004    0.0004   -0.0236   -0.0236   -0.0236   -0.0236
  0.6304    0.6304    0.6304    0.6304    0.6304    0.6304    0.0000    0.0000    0.0000    0.0000
  0.7493    0.7493    0.7493    0.7493    0.7493    0.7493    0.0000    0.0000    0.0000    0.0000
  0.7493    0.7493    0.7493    0.7493    0.7493    0.7493    0.0000    0.0000    0.0000    0.0000
  0.8682    0.8682    0.8682    0.8682    0.8682    0.8682    0.0000    0.0000    0.0000    0.0000
  0.8682    0.8682    0.8682    0.8682    0.8682    0.8682    0.0000    0.0000    0.0000    0.0000
  0.9871    0.9871    0.9871    0.9871    0.9871    0.9871    0.0000    0.0000    0.0000    0.0000
  0.9871    0.9871    0.9871    0.9871    0.9871    0.9871    0.0000    0.0000    0.0000    0.0000
  1.1059    1.1059    1.1059    1.1059    1.1059    1.1059    0.0000    0.0000    0.0000    0.0000
```

Figure 10.16: Sigma values for the Two-Hinged Arch with modified input data, load condition 4. Unit of measurement [Pa].

- Higher stability of the structure. The buckling load factor provided by the Fem analysis is not shown, but previous analysis validated this behaviour.

Disadvantages of the increasing of the input value

- Slightly higher value of the bending moment to fold the MadFlex for both for the Three-Hinged Arch and the Two-Hinged one for the load condition 4.

$\mathbf{N}^{\circ}_{disc}$	1	2	3	4	5	6	7	8	9	10
$\mathbf{M}_{3H}$[Nm]	1417	1417	1417	1417	1417	1417	1417	1417	1417	1417
$\mathbf{M}_{2H}$[Nm]	1417	1417	1417	1417	1417	1417	-1417	-1417	-1417	-1417

Thickness of each layer

Rigid skin (Carbon)			
Item	**Original Value**	**Modified Value**	**Unit**
Thickness of each ply	0.20	0.25	mm

Advantages of increasing the input values

- Lower deformation of the structure under the load condition 3, both for the Three-Hinged Arch and the Two-Hinged one.

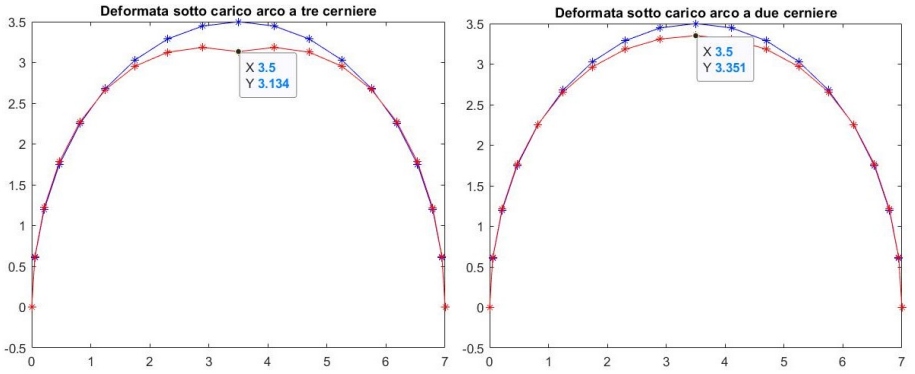

Figure 10.17: Vertical displacement of the Three-Hinged Arch (on the left) and the Two-Hinged Arch (on the right) with modified input data, load condition 3. Unit of measurement of both the axes [m].

- Lower values of compression stress in the rigid skin (carbon) both for the Three-Hinged Arch and the Two-Hinged one for the load condition 3. The

material work cases are shown below for both structures. W_{3H} refers to the Three-Hinged Arch while W_{2H} to the Two-Hinged one.

$\mathbf{N}^{\circ}_{disc}$	1	2	3	4	5	6	7	8	9	10
$\mathbf{WC}_{3H}$	8	6	6	6	6	6	6	6	6	8
$\mathbf{WC}_{2H}$	8	6	6	6	6	6	2	2	2	2

```
 1.0e+08 *

Columns 1 through 12

  0.0000    2.0854    3.3933    3.7464    3.3788    2.5670    1.5893    0.6939    0.0745    0.0000
  0.0000    2.0734    3.3745    3.7260    3.3603    2.5529    1.5804    0.6897    0.0736    0.0000
  0.0000    0.0021    0.0034    0.0037    0.0034    0.0026    0.0016    0.0007    0.0001    0.0000
  0.0000    0.0021    0.0034    0.0037    0.0033    0.0025    0.0016    0.0007    0.0001    0.0000
  0.0000    2.0613    3.3558    3.7055    3.3419    2.5387    1.5714    0.6854    0.0726    0.0000
  0.0000    2.0493    3.3370    3.6850    3.3234    2.5246    1.5625    0.6812    0.0716    0.0000
  0.0000    0.0020    0.0033    0.0037    0.0033    0.0025    0.0016    0.0007    0.0001    0.0000
  0.0000    0.0020    0.0033    0.0037    0.0033    0.0025    0.0016    0.0007    0.0001    0.0000
 -0.0066    0.0012    0.0020    0.0022    0.0020    0.0015    0.0009    0.0004    0.0000   -0.0030
 -0.0001   -0.0009   -0.0014   -0.0015   -0.0013   -0.0010   -0.0007   -0.0004   -0.0001   -0.0001
 -0.0063   -0.0457   -0.0671   -0.0721   -0.0649   -0.0503   -0.0329   -0.0172   -0.0063   -0.0029
 -0.0048   -0.0461   -0.0677   -0.0728   -0.0656   -0.0508   -0.0333   -0.0174   -0.0064   -0.0022
 -0.2254   -2.1466   -3.1530   -3.3910   -3.0528   -2.3636   -1.5485   -0.8077   -0.2972   -0.1033
 -0.1582   -2.1670   -3.1847   -3.4256   -3.0841   -2.3875   -1.5637   -0.8149   -0.2988   -0.0725
 -0.0034   -0.0465   -0.0684   -0.0736   -0.0663   -0.0513   -0.0336   -0.0175   -0.0064   -0.0016
 -0.0020   -0.0470   -0.0691   -0.0743   -0.0669   -0.0518   -0.0339   -0.0177   -0.0065   -0.0009
 -0.0909   -2.1873   -3.2164   -3.4603   -3.1153   -2.4114   -1.5788   -0.8220   -0.3004   -0.0417
 -0.0236   -2.2076   -3.2481   -3.4949   -3.1465   -2.4353   -1.5940   -0.8292   -0.3020   -0.0108
```

Figure 10.18: Sigma values for the Three-Hinged Arch with modified input data, load condition 3. Unit of measurement [Pa].

```
 1.0e+08 *

Columns 1 through 12

  0.0000    1.6725    2.5800    2.5576    1.8504    0.7455   -0.3750   -1.2380   -1.8238   -2.0307
  0.0000    1.6626    2.5655    2.5432    1.8399    0.7408   -0.3729   -1.2262   -1.8055   -2.0100
  0.0000    0.0017    0.0026    0.0025    0.0018    0.0007   -0.0080   -0.0263   -0.0388   -0.0432
  0.0000    0.0017    0.0026    0.0025    0.0018    0.0007   -0.0080   -0.0261   -0.0384   -0.0427
  0.0000    1.6527    2.5510    2.5289    1.8294    0.7362   -0.3708   -1.2145   -1.7871   -1.9894
  0.0000    1.6428    2.5365    2.5146    1.8188    0.7315   -0.3686   -1.2027   -1.7688   -1.9687
  0.0000    0.0016    0.0025    0.0025    0.0018    0.0007   -0.0079   -0.0258   -0.0380   -0.0423
  0.0000    0.0016    0.0025    0.0025    0.0018    0.0007   -0.0079   -0.0256   -0.0376   -0.0418
 -0.0066    0.0010    0.0015    0.0015    0.0011    0.0004   -0.0002   -0.0005   -0.0008   -0.0009
 -0.0001   -0.0008   -0.0011   -0.0011   -0.0008   -0.0004    0.0001    0.0007    0.0012    0.0013
 -0.0063   -0.0387   -0.0534   -0.0521   -0.0392   -0.0196    0.0001    0.0012    0.0020    0.0022
 -0.0048   -0.0391   -0.0539   -0.0526   -0.0395   -0.0197    0.0001    0.0012    0.0020    0.0022
 -0.2254   -1.8192   -2.5082   -2.4483   -1.8409   -0.9193    0.1074    1.2185    1.9707    2.2361
 -0.1582   -1.8359   -2.5327   -2.4725   -1.8587   -0.9272    0.1086    1.2254    1.9816    2.2483
 -0.0034   -0.0394   -0.0544   -0.0531   -0.0399   -0.0199    0.0001    0.0012    0.0020    0.0022
 -0.0020   -0.0398   -0.0549   -0.0536   -0.0403   -0.0201    0.0001    0.0012    0.0020    0.0023
 -0.0909   -1.8526   -2.5573   -2.4967   -1.8765   -0.9351    0.1099    1.2324    1.9924    2.2605
 -0.0236   -1.8694   -2.5818   -2.5209   -1.8943   -0.9430    0.1112    1.2394    2.0032    2.2727
```

Figure 10.19: Sigma values for the Two-Hinged Arch with modified input data, load condition 3. Unit of measurement [Pa].

- Lower values of tensile stress in the rigid skin (carbon) both for the Three-Hinged Arch and the Two-Hinged one for the load condition 4.

N°_{disc}	1	2	3	4	5	6	7	8	9	10
$\mathbf{WC}_{3H}$	7	7	7	7	7	7	7	7	7	7
$\mathbf{W}_{2H}$	7	7	7	7	7	7	3	3	3	3

```
  1.0e+08 *

Columns 1 through 12

  0.0000    0.0000    0.0000    0.0000    0.0000    0.0000    0.0000    0.0000    0.0000    0.0000
  0.0000    0.0000    0.0000    0.0000    0.0000    0.0000    0.0000    0.0000    0.0000    0.0000
  0.0000    0.0000    0.0000    0.0000    0.0000    0.0000    0.0000    0.0000    0.0000    0.0000
  0.0000    0.0000    0.0000    0.0000    0.0000    0.0000    0.0000    0.0000    0.0000    0.0000
  0.0000    0.0000    0.0000    0.0000    0.0000    0.0000    0.0000    0.0000    0.0000    0.0000
  0.0000    0.0000    0.0000    0.0000    0.0000    0.0000    0.0000    0.0000    0.0000    0.0000
  0.0000    0.0000    0.0000    0.0000    0.0000    0.0000    0.0000    0.0000    0.0000    0.0000
  0.0000    0.0000    0.0000    0.0000    0.0000    0.0000    0.0000    0.0000    0.0000    0.0000
 -0.0237   -0.0237   -0.0237   -0.0237   -0.0237   -0.0237   -0.0237   -0.0237   -0.0237   -0.0237
  0.0003    0.0003    0.0003    0.0003    0.0003    0.0003    0.0003    0.0003    0.0003    0.0003
  0.0146    0.0146    0.0146    0.0146    0.0146    0.0146    0.0146    0.0146    0.0146    0.0146
  0.0195    0.0195    0.0195    0.0195    0.0195    0.0195    0.0195    0.0195    0.0195    0.0195
  1.0063    1.0063    1.0063    1.0063    1.0063    1.0063    1.0063    1.0063    1.0063    1.0063
  1.2567    1.2567    1.2567    1.2567    1.2567    1.2567    1.2567    1.2567    1.2567    1.2567
  0.0243    0.0243    0.0243    0.0243    0.0243    0.0243    0.0243    0.0243    0.0243    0.0243
  0.0291    0.0291    0.0291    0.0291    0.0291    0.0291    0.0291    0.0291    0.0291    0.0291
  1.5071    1.5071    1.5071    1.5071    1.5071    1.5071    1.5071    1.5071    1.5071    1.5071
  1.7576    1.7576    1.7576    1.7576    1.7576    1.7576    1.7576    1.7576    1.7576    1.7576
```

Figure 10.20: Sigma values for the Three-Hinged Arch with modified input data, load condition 4. Unit of measure [Pa].

```
  1.0e+08 *

Columns 1 through 12

  0.0000    0.0000    0.0000    0.0000    0.0000    0.0000    1.7576    1.7576    1.7576    1.7576
  0.0000    0.0000    0.0000    0.0000    0.0000    0.0000    1.5071    1.5071    1.5071    1.5071
  0.0000    0.0000    0.0000    0.0000    0.0000    0.0000    0.0291    0.0291    0.0291    0.0291
  0.0000    0.0000    0.0000    0.0000    0.0000    0.0000    0.0243    0.0243    0.0243    0.0243
  0.0000    0.0000    0.0000    0.0000    0.0000    0.0000    1.2567    1.2567    1.2567    1.2567
  0.0000    0.0000    0.0000    0.0000    0.0000    0.0000    1.0063    1.0063    1.0063    1.0063
  0.0000    0.0000    0.0000    0.0000    0.0000    0.0000    0.0195    0.0195    0.0195    0.0195
  0.0000    0.0000    0.0000    0.0000    0.0000    0.0000    0.0146    0.0146    0.0146    0.0146
 -0.0237   -0.0237   -0.0237   -0.0237   -0.0237   -0.0237    0.0003    0.0003    0.0003    0.0003
  0.0003    0.0003    0.0003    0.0003    0.0003    0.0003   -0.0237   -0.0237   -0.0237   -0.0237
  0.0146    0.0146    0.0146    0.0146    0.0146    0.0146    0.0000    0.0000    0.0000    0.0000
  0.0195    0.0195    0.0195    0.0195    0.0195    0.0195    0.0000    0.0000    0.0000    0.0000
  1.0063    1.0063    1.0063    1.0063    1.0063    1.0063    0.0000    0.0000    0.0000    0.0000
  1.2567    1.2567    1.2567    1.2567    1.2567    1.2567    0.0000    0.0000    0.0000    0.0000
  0.0243    0.0243    0.0243    0.0243    0.0243    0.0243    0.0000    0.0000    0.0000    0.0000
  0.0291    0.0291    0.0291    0.0291    0.0291    0.0291    0.0000    0.0000    0.0000    0.0000
  1.5071    1.5071    1.5071    1.5071    1.5071    1.5071    0.0000    0.0000    0.0000    0.0000
  1.7576    1.7576    1.7576    1.7576    1.7576    1.7576    0.0000    0.0000    0.0000    0.0000
```

Figure 10.21: Sigma values for the Two-Hinged Arch with modified input data, load condition 4. Unit of measure [Pa].

- Higher critical buckling stress of wrinkling provided only by the first empirical formula. The second formula does not show this increment because it does not depend on the thickness of the skin.
  - First empirical formula (sigma _b1): 2.3238e+08,

  - Second empirical formula (sigma _b2): 3.0124e+08.

- Higher stability of the structure. The buckling load factor provided by the Fem analysis is not shown, but previous analysis validated this behaviour.

Disadvantages of increasing the input values

- Slightly higher value of the bending moment to fold the MadFlex for both for the Three-Hinged Arch and the Two-Hinged one for the load condition 4.

$\mathbf{N}^{\circ}_{disc}$	1	2	3	4	5	6	7	8	9	10
$\mathbf{M}_{3H}$[Nm]	1436	1436	1436	1436	1436	1436	1436	1436	1436	1436
$\mathbf{M}_{2H}$[Nm]	1436	1436	1436	1436	1436	1436	-1436	-1436	-1436	-1436

- Slightly higher mass of the habitat.

10.2.2 Foam

Longitudinal Elastic Modulus in traction and in compression

Foam			
Item	**Original Value**	**Modified Value**	**Unit**
Tensile Elastic Modulus	60	180	MPa

Advantages of increasing the input values

- Lower deformation of the structure under the load condition 3, both for the Three-Hinged Arch and the Two-Hinged one.

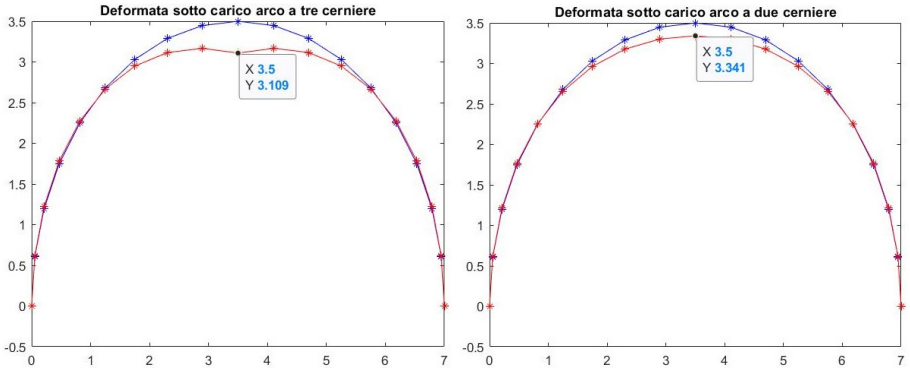

Figure 10.22: Vertical displacement of the Three-Hinged Arch (on the left) and the Two-Hinged Arch (on the right) with modified input data, load condition 3. Unit of measurement of both the axes [m].

- Higher critical buckling stress of wrinkling. Its increase can be easily understood observing the empirical formula of critical buckling stress of wrinkling in Chapter 5 and 9.
  - First empirical formula (sigma _b1): 2.6882e+08,
  - Second empirical formula (sigma _b2): 3.5760e+08.
- Higher stability of the structure. The buckling load factor provided by the Fem analysis is not shown, but previous analysis validated this behaviour.

Disadvantages of increasing the input values

- Higher values of tensile and compression stress in the foam both for the Three-Hinged Arch (Figure 10.23) and the Two-Hinged one (Figure 10.24) for the load condition 3.

$\mathbf{N}^{\circ}_{disc}$	1	2	3	4	5	6	7	8	9	10
$\mathbf{WC}_{3H}$	8	6	6	6	6	6	6	6	6	8
$\mathbf{WC}_{2H}$	8	6	6	6	6	6	2	2	2	2

```
 1.0e+08 *

Columns 1 through 12

  0.0000    2.0384    3.3071    3.6488    3.2906    2.5012    1.5510    0.6809    0.0791    0.0000
  0.0000    2.0253    3.2869    3.6267    3.2707    2.4860    1.5413    0.6763    0.0780    0.0000
  0.0000    0.0020    0.0033    0.0036    0.0033    0.0025    0.0015    0.0007    0.0001    0.0000
  0.0000    0.0020    0.0033    0.0036    0.0033    0.0025    0.0015    0.0007    0.0001    0.0000
  0.0000    2.0122    3.2666    3.6046    3.2508    2.4707    1.5316    0.6717    0.0768    0.0000
  0.0000    1.9992    3.2464    3.5825    3.2309    2.4555    1.5219    0.6670    0.0757    0.0000
  0.0000    0.0020    0.0032    0.0036    0.0032    0.0025    0.0015    0.0007    0.0001    0.0000
  0.0000    0.0020    0.0032    0.0036    0.0032    0.0024    0.0015    0.0007    0.0001    0.0000
 -0.0066    0.0036    0.0058    0.0064    0.0058    0.0044    0.0027    0.0012    0.0001   -0.0030
 -0.0002   -0.0035   -0.0051   -0.0055   -0.0050   -0.0038   -0.0025   -0.0013   -0.0005   -0.0001
 -0.0050   -0.0562   -0.0827   -0.0890   -0.0801   -0.0620   -0.0406   -0.0211   -0.0077   -0.0023
 -0.0043   -0.0566   -0.0833   -0.0897   -0.0807   -0.0625   -0.0409   -0.0212   -0.0077   -0.0020
 -0.2018   -2.6335   -3.8783   -4.1740   -3.7580   -2.9081   -1.9024   -0.9881   -0.3580   -0.0925
 -0.1698   -2.6512   -3.9057   -4.2039   -3.7849   -2.9287   -1.9155   -0.9944   -0.3595   -0.0778
 -0.0036   -0.0570   -0.0839   -0.0903   -0.0813   -0.0629   -0.0411   -0.0214   -0.0077   -0.0017
 -0.0030   -0.0573   -0.0845   -0.0909   -0.0819   -0.0634   -0.0414   -0.0215   -0.0078   -0.0014
 -0.1378   -2.6689   -3.9331   -4.2338   -3.8118   -2.9493   -1.9286   -1.0007   -0.3610   -0.0632
 -0.1058   -2.6866   -3.9605   -4.2636   -3.8387   -2.9700   -1.9418   -1.0069   -0.3626   -0.0485
```

Figure 10.23: Sigma values for the Three-Hinged Arch with modified input data, load condition 3. Unit of measurement [Pa].

```
 1.0e+08 *

Columns 1 through 12

  0.0000    1.6376    2.5177    2.4947    1.8069    0.7330   -0.4506   -1.5083   -2.2261   -2.4796
  0.0000    1.6268    2.5020    2.4792    1.7955    0.7279   -0.4486   -1.4981   -2.2103   -2.4618
  0.0000    0.0016    0.0025    0.0025    0.0018    0.0007   -0.0096   -0.0322   -0.0475   -0.0529
  0.0000    0.0016    0.0025    0.0025    0.0018    0.0007   -0.0096   -0.0320   -0.0471   -0.0525
  0.0000    1.6160    2.4862    2.4637    1.7841    0.7228   -0.4466   -1.4879   -2.1945   -2.4441
  0.0000    1.6052    2.4705    2.4482    1.7727    0.7176   -0.4447   -1.4776   -2.1787   -2.4263
  0.0000    0.0016    0.0025    0.0024    0.0018    0.0007   -0.0096   -0.0317   -0.0468   -0.0521
  0.0000    0.0016    0.0025    0.0024    0.0018    0.0007   -0.0095   -0.0315   -0.0465   -0.0517
 -0.0066    0.0029    0.0044    0.0044    0.0032    0.0013   -0.0006   -0.0020   -0.0029   -0.0032
 -0.0002   -0.0029   -0.0041   -0.0040   -0.0030   -0.0015    0.0002    0.0021    0.0034    0.0039
 -0.0050   -0.0476   -0.0657   -0.0642   -0.0482   -0.0240    0.0001    0.0012    0.0019    0.0022
 -0.0043   -0.0479   -0.0662   -0.0646   -0.0486   -0.0241    0.0001    0.0012    0.0019    0.0022
 -0.2018   -2.2290   -3.0815   -3.0091   -2.2604   -1.1233    0.1115    1.1867    1.9147    2.1715
 -0.1698   -2.2435   -3.1028   -3.0301   -2.2759   -1.1303    0.1130    1.1943    1.9264    2.1847
 -0.0036   -0.0482   -0.0667   -0.0651   -0.0489   -0.0243    0.0001    0.0012    0.0019    0.0022
 -0.0030   -0.0485   -0.0671   -0.0655   -0.0492   -0.0244    0.0001    0.0012    0.0019    0.0022
 -0.1378   -2.2581   -3.1240   -3.0510   -2.2913   -1.1372    0.1144    1.2018    1.9381    2.1978
 -0.1058   -2.2727   -3.1453   -3.0719   -2.3067   -1.1441    0.1159    1.2094    1.9498    2.2109
```

Figure 10.24: Sigma values for the Two-Hinged Arch with modified input data, load condition 3. Unit of measurement [Pa].

- Higher value of the bending moment to fold the MadFlex for both the Three-Hinged Arch and the Two-Hinged one for the load condition 4.

  Work cases for load condition 4 are shown in the following tables:

$\mathbf{N}^{\circ}_{disc}$	1	2	3	4	5	6	7	8	9	10
$\mathbf{WC}_{3H}$	7	7	7	7	7	7	7	7	7	7
$\mathbf{WC}_{2H}$	7	7	7	7	7	7	3	3	3	3

N°_{disc}	1	2	3	4	5	6	7	8	9	10
$\mathbf{M}_{3H}$[Nm]	3927	3927	3927	3927	3927	3927	3927	3927	3927	3927
$\mathbf{M}_{2H}$[Nm]	3927	3927	3927	3927	3927	3927	-3927	-3927	-3927	-3927

- Higher values of tensile and compression stress in the foam both for the Three-Hinged Arch (Figures 10.25) and the Two-Hinged one (10.26) for the load condition 4.

```
  1.0e+08 *

Columns 1 through 12

   0.0000    0.0000    0.0000    0.0000    0.0000    0.0000    0.0000    0.0000    0.0000    0.0000
   0.0000    0.0000    0.0000    0.0000    0.0000    0.0000    0.0000    0.0000    0.0000    0.0000
   0.0000    0.0000    0.0000    0.0000    0.0000    0.0000    0.0000    0.0000    0.0000    0.0000
   0.0000    0.0000    0.0000    0.0000    0.0000    0.0000    0.0000    0.0000    0.0000    0.0000
   0.0000    0.0000    0.0000    0.0000    0.0000    0.0000    0.0000    0.0000    0.0000    0.0000
   0.0000    0.0000    0.0000    0.0000    0.0000    0.0000    0.0000    0.0000    0.0000    0.0000
   0.0000    0.0000    0.0000    0.0000    0.0000    0.0000    0.0000    0.0000    0.0000    0.0000
   0.0000    0.0000    0.0000    0.0000    0.0000    0.0000    0.0000    0.0000    0.0000    0.0000
  -0.0671   -0.0671   -0.0671   -0.0671   -0.0671   -0.0671   -0.0671   -0.0671   -0.0671   -0.0671
   0.0049    0.0049    0.0049    0.0049    0.0049    0.0049    0.0049    0.0049    0.0049    0.0049
   0.0789    0.0789    0.0789    0.0789    0.0789    0.0789    0.0789    0.0789    0.0789    0.0789
   0.0828    0.0828    0.0828    0.0828    0.0828    0.0828    0.0828    0.0828    0.0828    0.0828
   4.2814    4.2814    4.2814    4.2814    4.2814    4.2814    4.2814    4.2814    4.2814    4.2814
   4.4818    4.4818    4.4818    4.4818    4.4818    4.4818    4.4818    4.4818    4.4818    4.4818
   0.0866    0.0866    0.0866    0.0866    0.0866    0.0866    0.0866    0.0866    0.0866    0.0866
   0.0905    0.0905    0.0905    0.0905    0.0905    0.0905    0.0905    0.0905    0.0905    0.0905
   4.6821    4.6821    4.6821    4.6821    4.6821    4.6821    4.6821    4.6821    4.6821    4.6821
   4.8825    4.8825    4.8825    4.8825    4.8825    4.8825    4.8825    4.8825    4.8825    4.8825
```

Figure 10.25: Sigma values for the Three-Hinged Arch with modified input data, load condition 4. Unit of measurement [Pa].

```
  1.0e+08 *

Columns 1 through 12

   0.0000    0.0000    0.0000    0.0000    0.0000    0.0000    4.8825    4.8825    4.8825    4.8825
   0.0000    0.0000    0.0000    0.0000    0.0000    0.0000    4.6821    4.6821    4.6821    4.6821
   0.0000    0.0000    0.0000    0.0000    0.0000    0.0000    0.0905    0.0905    0.0905    0.0905
   0.0000    0.0000    0.0000    0.0000    0.0000    0.0000    0.0866    0.0866    0.0866    0.0866
   0.0000    0.0000    0.0000    0.0000    0.0000    0.0000    4.4818    4.4818    4.4818    4.4818
   0.0000    0.0000    0.0000    0.0000    0.0000    0.0000    4.2814    4.2814    4.2814    4.2814
   0.0000    0.0000    0.0000    0.0000    0.0000    0.0000    0.0828    0.0828    0.0828    0.0828
   0.0000    0.0000    0.0000    0.0000    0.0000    0.0000    0.0789    0.0789    0.0789    0.0789
  -0.0671   -0.0671   -0.0671   -0.0671   -0.0671   -0.0671    0.0049    0.0049    0.0049    0.0049
   0.0049    0.0049    0.0049    0.0049    0.0049    0.0049   -0.0671   -0.0671   -0.0671   -0.0671
   0.0789    0.0789    0.0789    0.0789    0.0789    0.0789    0.0000    0.0000    0.0000    0.0000
   0.0828    0.0828    0.0828    0.0828    0.0828    0.0828    0.0000    0.0000    0.0000    0.0000
   4.2814    4.2814    4.2814    4.2814    4.2814    4.2814    0.0000    0.0000    0.0000    0.0000
   4.4818    4.4818    4.4818    4.4818    4.4818    4.4818    0.0000    0.0000    0.0000    0.0000
   0.0866    0.0866    0.0866    0.0866    0.0866    0.0866    0.0000    0.0000    0.0000    0.0000
   0.0905    0.0905    0.0905    0.0905    0.0905    0.0905    0.0000    0.0000    0.0000    0.0000
   4.6821    4.6821    4.6821    4.6821    4.6821    4.6821    0.0000    0.0000    0.0000    0.0000
   4.8825    4.8825    4.8825    4.8825    4.8825    4.8825    0.0000    0.0000    0.0000    0.0000
```

Figure 10.26: Sigma values for the Two-Hinged Arch with modified input data, load condition 4. Unit of measurement [Pa].

Advantages of the decreasing of the input value It can be convenient to slightly decrease the longitudinal elastic modulus for the following reasons:

- to obtain lower tensile and compression stresses in foam when the structure has to withstand load condition 3 in order to satisfy the foam's sturdiness criteria.
- to obtain lower tensile and compression stresses in foam when the structure has to withstand load condition 4 in order to satisfy the foam's sturdiness criteria.

Thickness of the Foam

Foam			
Item	**Original Value**	**Modified Value**	**Unit**
Thickness of the foam	60	80	mm

Advantages of increasing the input values

- Lower deformation of the structure under the load condition 3, both for the Three-Hinged Arch and the Two-Hinged one.

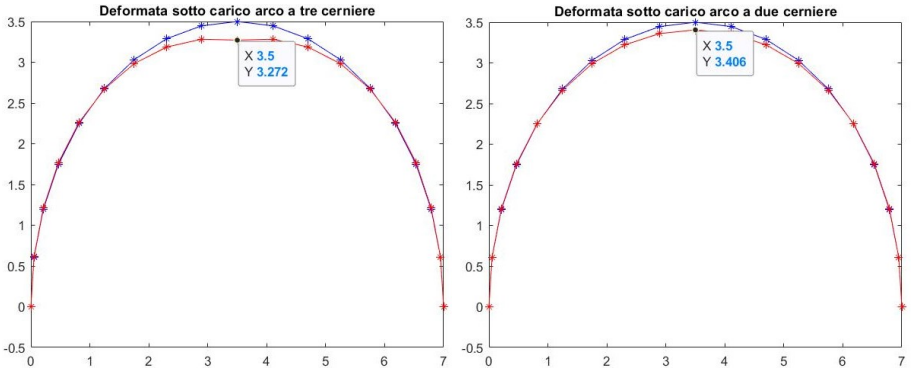

Figure 10.27: Vertical displacement of the Three-Hinged Arch (on the left) and the Two-Hinged Arch (on the right) with modified input data, load condition 3. Unit of measurement of both the axes [m].

- Lower values of tensile and compression stress in the foam, both for the Three-Hinged Arch (Figure 10.28) and the Two-Hinged one (Figure 10.29) for the load condition 3. The material work cases are shown below for both structures.

$\mathbf{N}^{\circ}_{disc}$	1	2	3	4	5	6	7	8	9	10
$\mathbf{WC}_{3H}$	8	6	6	6	6	6	6	6	6	8
$\mathbf{WC}_{2H}$	8	6	6	6	6	6	2	2	2	2

- Higher stability of the structure. The buckling load factor provided by the Fem analysis is not shown, but previous analysis validated this behaviour.

```
 1.0e+08 *

Columns 1 through 12

  0.0000    1.4875    2.4712    2.7419    2.4736    1.8727    1.1467    0.4810    0.0202    0.0000
  0.0000    1.4800    2.4595    2.7291    2.4621    1.8639    1.1412    0.4784    0.0196    0.0000
  0.0000    0.0015    0.0025    0.0027    0.0025    0.0019    0.0011    0.0005    0.0000    0.0000
  0.0000    0.0015    0.0024    0.0027    0.0025    0.0019    0.0011    0.0005    0.0000    0.0000
  0.0000    1.4725    2.4479    2.7164    2.4507    1.8551    1.1356    0.4757    0.0190    0.0000
  0.0000    1.4650    2.4362    2.7037    2.4392    1.8463    1.1300    0.4731    0.0184    0.0000
  0.0000    0.0015    0.0024    0.0027    0.0024    0.0018    0.0011    0.0005    0.0000    0.0000
  0.0000    0.0015    0.0024    0.0027    0.0024    0.0018    0.0011    0.0005    0.0000    0.0000
 -0.0049    0.0009    0.0015    0.0016    0.0015    0.0011    0.0007    0.0003    0.0000   -0.0023
 -0.0001   -0.0009   -0.0013   -0.0014   -0.0013   -0.0010   -0.0007   -0.0004   -0.0001   -0.0000
 -0.0050   -0.0449   -0.0652   -0.0699   -0.0629   -0.0488   -0.0322   -0.0171   -0.0067   -0.0023
 -0.0043   -0.0451   -0.0655   -0.0702   -0.0632   -0.0491   -0.0324   -0.0172   -0.0068   -0.0020
 -0.2009   -2.1010   -3.0495   -3.2690   -2.9423   -2.2835   -1.5062   -0.8005   -0.3145   -0.0921
 -0.1706   -2.1111   -3.0653   -3.2862   -2.9579   -2.2954   -1.5138   -0.8041   -0.3153   -0.0782
 -0.0037   -0.0453   -0.0658   -0.0706   -0.0635   -0.0493   -0.0325   -0.0173   -0.0068   -0.0017
 -0.0030   -0.0456   -0.0662   -0.0710   -0.0639   -0.0496   -0.0327   -0.0174   -0.0068   -0.0014
 -0.1403   -2.1213   -3.0811   -3.3034   -2.9734   -2.3073   -1.5213   -0.8077   -0.3162   -0.0643
 -0.1100   -2.1314   -3.0969   -3.3207   -2.9889   -2.3192   -1.5289   -0.8113   -0.3170   -0.0504
```

Figure 10.28: Sigma values for the Three-Hinged Arch with modified input data, load condition 3. Unit of measurement [Pa].

```
 1.0e+08 *

Columns 1 through 12

  0.0000    1.1782    1.8620    1.8512    1.3286    0.5082   -0.3924   -1.1880   -1.7283   -1.9191
  0.0000    1.1720    1.8529    1.8423    1.3221    0.5052   -0.3913   -1.1821   -1.7192   -1.9088
  0.0000    0.0012    0.0019    0.0018    0.0013    0.0005   -0.0084   -0.0254   -0.0369   -0.0410
  0.0000    0.0012    0.0018    0.0018    0.0013    0.0005   -0.0084   -0.0253   -0.0367   -0.0408
  0.0000    1.1659    1.8439    1.8334    1.3155    0.5023   -0.3902   -1.1763   -1.7100   -1.8986
  0.0000    1.1597    1.8348    1.8245    1.3090    0.4994   -0.3891   -1.1704   -1.7009   -1.8883
  0.0000    0.0012    0.0018    0.0018    0.0013    0.0005   -0.0084   -0.0251   -0.0365   -0.0406
  0.0000    0.0012    0.0018    0.0018    0.0013    0.0005   -0.0083   -0.0250   -0.0363   -0.0403
 -0.0049    0.0007    0.0011    0.0011    0.0008    0.0003   -0.0002   -0.0005   -0.0008   -0.0008
 -0.0001   -0.0008   -0.0011   -0.0010   -0.0008   -0.0004    0.0000    0.0005    0.0009    0.0010
 -0.0050   -0.0383   -0.0521   -0.0508   -0.0384   -0.0196    0.0000    0.0009    0.0014    0.0016
 -0.0043   -0.0385   -0.0524   -0.0510   -0.0385   -0.0197    0.0000    0.0009    0.0015    0.0017
 -0.2009   -1.7908   -2.4386   -2.3759   -1.7942   -0.9151    0.0400    0.8831    1.4537    1.6550
 -0.1706   -1.7991   -2.4508   -2.3879   -1.8030   -0.9191    0.0408    0.8874    1.4605    1.6625
 -0.0037   -0.0386   -0.0526   -0.0513   -0.0387   -0.0197    0.0000    0.0009    0.0015    0.0017
 -0.0030   -0.0388   -0.0529   -0.0516   -0.0389   -0.0198    0.0000    0.0009    0.0015    0.0017
 -0.1403   -1.8075   -2.4631   -2.3999   -1.8119   -0.9230    0.0416    0.8918    1.4672    1.6701
 -0.1100   -1.8158   -2.4753   -2.4120   -1.8208   -0.9270    0.0424    0.8961    1.4739    1.6777
```

Figure 10.29: Sigma values for the Two-Hinged Arch with modified input data, load condition 3. Unit of measurement [Pa].

Disadvantages of increasing the input values

- Higher values of tensile and compression stress in the foam, both for the Three-Hinged Arch (Figure 10.30) and the Two-Hinged one (Figure 10.31) for the load condition 4.

$\mathbf{N}^{\circ}_{disc}$	1	2	3	4	5	6	7	8	9	10
$\mathbf{WC}_{3H}$	7	7	7	7	7	7	7	7	7	7
$\mathbf{W}_{2H}$	7	7	7	7	7	7	3	3	3	3

```
1.0e+08 *

Columns 1 through 10

  0.0000    0.0000    0.0000    0.0000    0.0000    0.0000    0.0000    0.0000    0.0000    0.0000
  0.0000    0.0000    0.0000    0.0000    0.0000    0.0000    0.0000    0.0000    0.0000    0.0000
  0.0000    0.0000    0.0000    0.0000    0.0000    0.0000    0.0000    0.0000    0.0000    0.0000
  0.0000    0.0000    0.0000    0.0000    0.0000    0.0000    0.0000    0.0000    0.0000    0.0000
  0.0000    0.0000    0.0000    0.0000    0.0000    0.0000    0.0000    0.0000    0.0000    0.0000
  0.0000    0.0000    0.0000    0.0000    0.0000    0.0000    0.0000    0.0000    0.0000    0.0000
  0.0000    0.0000    0.0000    0.0000    0.0000    0.0000    0.0000    0.0000    0.0000    0.0000
  0.0000    0.0000    0.0000    0.0000    0.0000    0.0000    0.0000    0.0000    0.0000    0.0000
 -0.0310   -0.0310   -0.0310   -0.0310   -0.0310   -0.0310   -0.0310   -0.0310   -0.0310   -0.0310
  0.0010    0.0010    0.0010    0.0010    0.0010    0.0010    0.0010    0.0010    0.0010    0.0010
  0.0474    0.0474    0.0474    0.0474    0.0474    0.0474    0.0474    0.0474    0.0474    0.0474
  0.0512    0.0512    0.0512    0.0512    0.0512    0.0512    0.0512    0.0512    0.0512    0.0512
  2.6506    2.6506    2.6506    2.6506    2.6506    2.6506    2.6506    2.6506    2.6506    2.6506
  2.8510    2.8510    2.8510    2.8510    2.8510    2.8510    2.8510    2.8510    2.8510    2.8510
  0.0551    0.0551    0.0551    0.0551    0.0551    0.0551    0.0551    0.0551    0.0551    0.0551
  0.0590    0.0590    0.0590    0.0590    0.0590    0.0590    0.0590    0.0590    0.0590    0.0590
  3.0513    3.0513    3.0513    3.0513    3.0513    3.0513    3.0513    3.0513    3.0513    3.0513
  3.2517    3.2517    3.2517    3.2517    3.2517    3.2517    3.2517    3.2517    3.2517    3.2517
```

Figure 10.30: Sigma values for the Three-Hinged Arch with modified input data, load condition 4. Unit of measurement [Pa].

```
1.0e+08 *

Columns 1 through 10

  0.0000    0.0000    0.0000    0.0000    0.0000    0.0000    3.2517    3.2517    3.2517    3.2517
  0.0000    0.0000    0.0000    0.0000    0.0000    0.0000    3.0513    3.0513    3.0513    3.0513
  0.0000    0.0000    0.0000    0.0000    0.0000    0.0000    0.0590    0.0590    0.0590    0.0590
  0.0000    0.0000    0.0000    0.0000    0.0000    0.0000    0.0551    0.0551    0.0551    0.0551
  0.0000    0.0000    0.0000    0.0000    0.0000    0.0000    2.8510    2.8510    2.8510    2.8510
  0.0000    0.0000    0.0000    0.0000    0.0000    0.0000    2.6506    2.6506    2.6506    2.6506
  0.0000    0.0000    0.0000    0.0000    0.0000    0.0000    0.0512    0.0512    0.0512    0.0512
  0.0000    0.0000    0.0000    0.0000    0.0000    0.0000    0.0474    0.0474    0.0474    0.0474
 -0.0310   -0.0310   -0.0310   -0.0310   -0.0310   -0.0310    0.0010    0.0010    0.0010    0.0010
  0.0010    0.0010    0.0010    0.0010    0.0010    0.0010   -0.0310   -0.0310   -0.0310   -0.0310
  0.0474    0.0474    0.0474    0.0474    0.0474    0.0474    0.0000    0.0000    0.0000    0.0000
  0.0512    0.0512    0.0512    0.0512    0.0512    0.0512    0.0000    0.0000    0.0000    0.0000
  2.6506    2.6506    2.6506    2.6506    2.6506    2.6506    0.0000    0.0000    0.0000    0.0000
  2.8510    2.8510    2.8510    2.8510    2.8510    2.8510    0.0000    0.0000    0.0000    0.0000
  0.0551    0.0551    0.0551    0.0551    0.0551    0.0551    0.0000    0.0000    0.0000    0.0000
  0.0590    0.0590    0.0590    0.0590    0.0590    0.0590    0.0000    0.0000    0.0000    0.0000
  3.0513    3.0513    3.0513    3.0513    3.0513    3.0513    0.0000    0.0000    0.0000    0.0000
  3.2517    3.2517    3.2517    3.2517    3.2517    3.2517    0.0000    0.0000    0.0000    0.0000
```

Figure 10.31: Sigma values for the Two-Hinged Arch with modified input data, load condition 4. Unit of measurement [Pa].

- Lower critical buckling stress of wrinkling provided only by the first empirical formula. The second formula does not show this increment because it does not depend on the thickness of the skin.
  - First empirical formula (sigma _b1): 1.8e+08,
  - Second empirical formula (sigma _b2): 3.0124e+08.
- Higher value of the bending moment to fold the MadFlex for both the Three-Hinged Arch and the Two-Hinged one for the load condition 4.
- Higher mass of the habitat.

$\mathbf{N}^{\circ}_{disc}$	1	2	3	4	5	6	7	8	9	10
$\mathbf{M}_{3H}$[Nm]	3287	3287	3287	3287	3287	3287	3287	3287	3287	3287
$\mathbf{M}_{2H}$[Nm]	3287	3287	3287	3287	3287	3287	-3287	-3287	-3287	-3287

Advantages of the decreasing of the input value It can be convenient to slightly decrease the longitudinal elastic modulus to have a lower value of the stresses developed by the foam for the load condition 4 in order to satisfy the foam's sturdiness criteria.

10.2.3 Flexible skin (Dyneema)

For ease of reading, the following paragraph will contain a qualitative dissertation rather than quantitative one.

Increase of the Longitudinal Elastic Modulus in traction and in compression

Advantages of increasing the input values

- Lower deformation of the structure under the load condition 3, both for the Three-Hinged Arch and the Two-Hinged one.
- Higher stability of the structure. The buckling load factor provided by the Fem analysis is not shown, but previous analysis validated this behaviour.

Disadvantages of increasing the input values

- Higher values of tensile stress in the flexible skin (Dyneema) both for the Three-Hinged Arch and the Two-Hinged one for the load condition 3.

Comments about the unmentioned items

- Critical buckling stress of wrinkling for the rigid skin. The flexible skin does not influence this phenomenon, in fact mechanical and geometrical properties of the flexible skin are not included in the empirical formulas.
- Compression stresses in the flexible skin for load condition 4. The quantitative comparison is not reported because of its lack of meaning. To know the real value of the compression stresses, a in-depth Fem analysis would have to be carried out. It is impossible to evaluate this phenomenon with the employed global analytical model.
- Value of the bending moment. Similar problems arise for this value.

Layering optimization

Flexible skin (Dyneema)			
Item	**Original Value**	**Modified Value**	**Unit**
Fiber orientations	[90 0 90 0]	[-30 30 -30 30]	Degree

Advantages of changing the fibers' orientation

- Lower deformation of the structure under the load condition 3, both for the Three-Hinged Arch and the Two-Hinged one.
- More homogeneous tensile stress values in the rigid skin for load condition 3, avoiding critical stresses in some layers (the previous one with 0° of orientation) and involving all layers to withstand the load both for the Three-Hinged Arch and for the Two-Hinged one.

- More homogeneous compression stress values in the rigid skin for load condition 4 avoiding critical stresses in some layers and involving all layers to withstand the load. This happens both for the Three-Hinged Arch and for the Two-Hinged one.
- Higher stability of the structure. The buckling load factor provided by the Fem analysis is not shown, but previous analysis validated this behaviour.

Comments about the unmentioned items The reasons are the same ones reported in the previous paragraph.

Increase of the thickness of each layer

Advantages of increasing the input values

- Lower deformation of the structure under the load condition 3, both for the Three-Hinged Arch and the Two-Hinged one.
- Lower values of tensile stress in the flexible skin (Dyneema) both for the Three-Hinged Arch and the Two-Hinged one for the load condition 3. The material work cases are shown below for both structures.
- Higher stability of the structure. The buckling load factor provided by the Fem analysis is not shown, but previous analysis validated this behaviour.

Disadvantages of increasing the input values

- Slightly higher mass of the habitat.

Comments about the unmentioned items The reasons are the same ones reported in the previous paragraph.

Load condition 2 was not included in this dissertation because, as mentioned in Chapter 7, "a 101.4-kPa internal pressure is capable of supporting 40 m of soil on the Moon, assuming a soil density of 1.6 g per cubic centimetre" [34]. Therefore this is not a critical load condition also because the pressure load reduces the bending moment introduced by the regolith load.

10.3 Critical requirements and solving methods

This section summarizes and lists the requirements whose satisfaction generated the most critical issues. As mentioned by the title also the solving methods are reported. The latter are based on the considerations of the sections above. As mentioned, each variation of the input value can have both advantages and disadvantages, therefore each solution generates new problems that are also shown in this section.

Sturdiness criteria for the rigid skin (carbon) for load condition 3

The first main issue is exceedingly high compression stresses developed by the carbon especially in the outer layers of the material. These stresses appear at about $\pm 45^{\circ}$ along the arch span when the structure has to withstand the load condition 3. As mentioned by chapter 5 the stresses are multiplied by a SF of 4 and the maximum compression stresses must not exceed the critical wrinkling stress. The applied solution and the consequent issues are:

1. Increase the thickness of each ply. This choice leads to the increase of the critical buckling stress of wrinkling, but it also leads to:
   (a) Higher value of the bending moment to reach the same radius of curvature in the folded configuration and therefore higher stresses in the carbon layers when they have to withstand the load condition 4 (the second principal issue of this section). If the following choice is to decrease the bending moment, the consequence is a smaller radius of curvature of the habitat in the folded configuration and therefore a higher volume occupied by the structure inside the launcher. However, decreasing the bending moment is necessary because its previous value cannot be reached by the machinery employed to bend the habitat or by the device to keep it in the folded configuration or to avoid critical stresses in the rigid skin for the load condition 4.
2. Layering optimization. This does not lead to any subsequent issue.
3. Slight decrease of the longitudinal elastic modulus of the rigid skin. However this solution leads to:
   (a) Higher deformation of the structure;
   (b) Lower stability of the structure;
   (c) Lower critical buckling stress of wrinkling.
4. Increasing the longitudinal elastic modulus of the rigid skin augments the critical buckling stress of wrinkling. This stress is calculated through the two empirical formulas (sigma_b1 and sigma_b2). However, this solution leads to:
   (a) Higher stresses in the rigid skin for both the analysed structures for load condition 3. However, coupled with a layering optimization it could be a good solution;

   (b) Higher stresses in the rigid skin for both the analysed structures for load condition 4 (the main issue of this section). The previous consideration about layering is also valid for this point;

   (c) Higher bending moment to keep the same radius of curvature in the folded configuration. This solution links this issue to the consideration about the volume occupied by the structure inside the launcher and to the critical stresses of the rigid skin for load condition 4 expressed in (1.a).

5. Considering the empirical formulas about critical buckling stress of wrinkling, a solution could be to employ a foam with a higher elastic modulus in compression. However this leads to:

   (a) Higher stresses in the foam for both the analysed structures for load condition 3;

   (b) Higher stresses in the foam for both the analysed structures for load condition 4 (the third main issue of this section);

   (c) Higher bending moment to keep the same radius of curvature in the folded configuration. This is also linked to the consideration expressed about the volume occupied by the structure inside the launcher (1.a).

6. Considering the first empirical formula, a solution could be decreasing the thickness of the foam. However this solution leads to:

   (a) Higher deformation of the structure;

   (b) Higher stresses in the foam for both analysed structures for load condition 3.

7. Considering the second empirical formula, a solution could be increasing the shear modulus of the foam. It has no consequences if the other mechanical properties of the foam remain constant, however this is unlikely to happen.

Sturdiness criteria for the rigid skin (carbon) for load condition 4

The second main issue is exceedingly high tensile stresses developed by the carbon, especially in the outer layers of the material. Those occur when the structures have to be folded in the store configuration. As mentioned by chapter 5 the stresses are multiplied by a SF of 4 and the maximum tensile stresses must not exceed the ultimate tensile strength of the rigid skin (carbon). The applied solution and the consequent issues are:

1. Decrease the radius of curvature for the habitat in the stored configuration, therefore the bending moment which the structure has to withstand. However this solution leads to:

   (a) higher volume occupied by the structure inside the launcher.

2. Solution 1,2 and 3 mentioned in the previous paragraph about the first issue.

Sturdiness criteria for the foam for load condition 4

The third main issue is exceedingly high tensile and compression stresses developed by the foam when the structures have to be folded in the store configuration. The stresses are not multiplied by a SF of 4 and the maximum tensile and compression stresses must not exceed the relative ultimate tensile and compression strength of the foam. The applied solution and the consequent issues are:

1. Solution 1 mentioned in the previous paragraph about the second issue.
2. Decrease the tensile and compression elastic modulus of the foam. However this leads to:
   (a) higher deformation of the structure;
   (b) lower stability of the structure;
   (c) lower critical buckling stress of wrinkling (the first main issue of this section).
3. Remove some wedges in the foam at equally spaced intervals to create notches in order avoid the contact of the lateral side of the foam until the structure reaches the desired radius of curvature. This allows to avoid high values of compression stresses which can exceed the ultimate compression strength of the foam. Figure 10.32 shows the previously mentioned concept. It is already implemented in all the MadFLex types with high thickness of the foam.

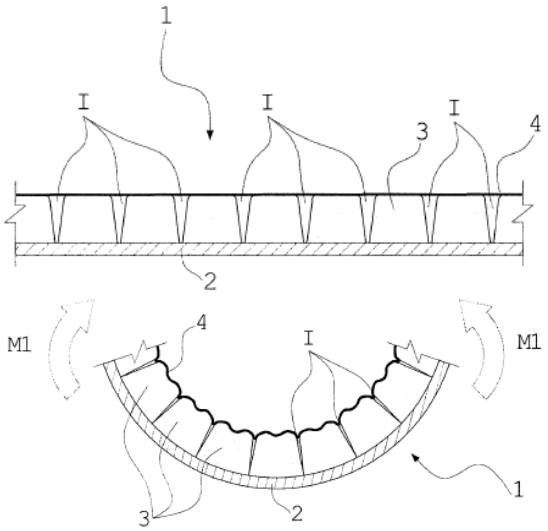

Figure 10.32: Sigma values for the Two-Hinged Arch with modified input data, load condition 4. Unit of measure [Pa]

What can be understood from this section is that each of the main issues is linked with the others in a non-linear manner, therefore the resolution of the global problem is an iterative process. A balance between all the input values is needed to satisfy all the imposed requirements.

Chapter 11

Preliminary design, The MadFLex Hab

This Chapter shows the preliminary design developed at the end of the preliminary study phase and it is the suitable conclusion of this Thesis. Chapter starts showing the features of the habitat and the mechanical and geometrical properties of the MadFlex used to develop it. After these initial informations, a dissertation about the satisfaction of the requirements is also provided by this Chapter. With great satisfaction it is possible to affirm that all the requirements imposed at the beginning of the preliminary study, and shown in Chapter 5, are fully satisfied. Moreover, already existing materials are used in the preliminary design in order to make it not a simple academic exercise but a first step towards something that can be achieved for real.

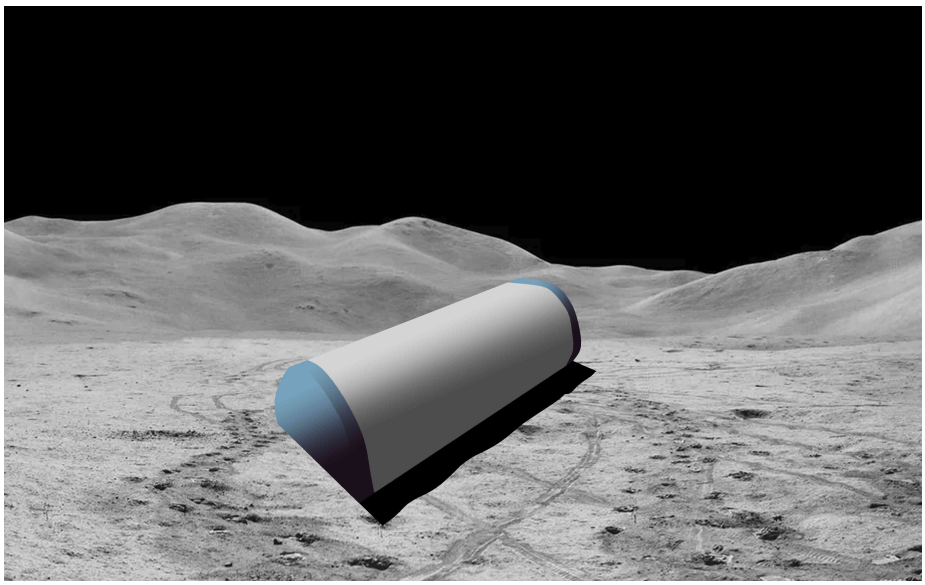

Figure 11.1: Preliminary design, The MadFLex Hab

11.1 Features of habitat and mechanical and geometrical properties of the MadFlex

As mentioned in the title, this section shows the features of the habitat and the mechanical and geometrical properties of the MadFlex able to satisfy all the requirements imposed at the beginning of this project. The MadFlex is a composite material panel, with a layered structure, particularly a sandwich-like structure, therefore it is composed by two skins and a core. The mechanical properties of each layer are shown below (for a further knowledge of MadFLex refer to Chapter 6)

Table 11.1: Geometric feature

Geometrical features		
Item	**Value**	**Unit**
Arch radius	3.5	m
Thickness of the regolith cover	2.5	m
g _l	1.635	m/s^2
Section width (b)	0.5	m
N (N° discretization points)	19	

Mechanical properties and thickness of each layer are the following:

Rigid skin (IM Carbon T1100G (Delta Preg®), fiber Torayca®) [61]		
Item	**Value**	**Unit**
Fiber orientation	[30 -30 30 -30]	degree
Thickness for every ply	0.28	mm
Tensile Longitudinal Elastic Modulus	324	GPa
Compression Longitudinal Elastic Modulus	291 (*)	GPa
Transversal Elastic Modulus	2.9 (*)	GPa
Shear Modulus	5.5 (*)	GPa
Poisson's ratio	0.3 (*)	
Density	$1.79 \cdot 10^3$	Kg/m^3
Ultimate tensile strength	6600	MPa

Foam (Rohacell®, 110 WF [62])		
Item	**Value**	**Unit**
Thickness of the foam	80	mm
Tensile Longitudinal Elastic Modulus	180	MPa
Compression Longitudinal Elastic Modulus	90 (*)	MPa
Shear Modulus	70	GPa
Density	110	Kg/m^3
Ultimate tensile strength	3.7	MPa
Ultimate compression strength	3.6	MPa

Flexible skin (Dyneema® sk62)		
Item	**Value**	**Unit**
Fiber orientation	[-30 30 -30 30]	degree
Thickness for every ply	0.5	mm
Tensile Longitudinal Elastic Modulus	100	GPa
Compression Longitudinal Elastic Modulus	0.1 (**)	Pa
Transversal Elastic Modulus	0.1 (*)	GPa
Shear Modulus	0.2 (*)	GPa
Poisson's ratio	0.05 (*)	
Density	$0.98 \cdot 10^3$ (*)	Kg/m^3
Ultimate tensile strength	3300	MPa

(*) Value not provided by data sheets and inserted by the Thesis student in agreement with that shown by material with same mechanical properties.

(**) Value inserts by the Thesis student in order to simulate the wrinkling phenomenon of the flexible skin describe in Chapter 6

Load condition	
Item	**Description**
Load condition	Semi-circular cover of regolith (shape of the operative condition)

11.2 Displacement and stresses for the Three analysed load conditions

This section shows the results obtained from the analysis of the chosen Preliminary design through the Matlab® script and their validation with the FEM analysis. Features of the habitat and mechanical properties of the MadFlex mentioned above are the input data of it. The results are classified and shown in the order analysed by the Matlab® script. Therefore the first ones are the results obtained by the load condition 3, than by load condition 2 and in conclusion by load condition 4. The following list resumes the meaning of the load condition:

1. Internal pressure of 1 atm only.
2. Internal pressure of 1 atm plus regolith cover load: It is the nominal operative load which the structure must withstand during its entire operative life.
3. Regolith cover load only. It is the most critical load condition due the lack of the internal pressure, which has a mitigating effect on the bending moment induced by regolith. For this reason the largest displacements of the habitat top is expected in this load condition.
4. Load used to keep the habitat in folded configuration. This load condition provides the greatest limitation about the curvature of the habitat in the this configuration. The higher stresses in the foam are expected under this load.

The first load condition is not analysed because it is the less critical.
The meaning of the table about the Work Cases developed by the material or how to understand the results in the tables about the stress is explained at the beginning of Chapter 10.

11.2.1 Load condition 3, Regolith load only

Three-Hinged Arch

Displacement of the Three-Hinged Arch This paragraph shows the results obtained by the script and by the Fem for the vertical displacement of the Three-Hinged Arch.

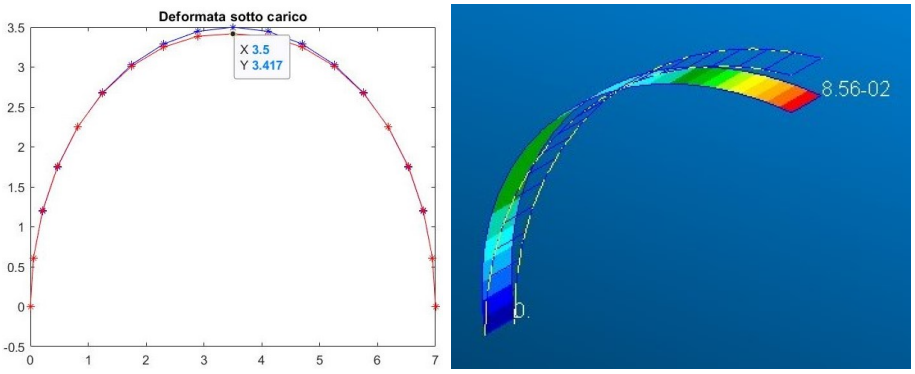

Figure 11.2: Vertical displacement of the Three-Hinged Arch. Script solution on the left (unit of measurement of both the axes [m]), Fem solution on the right.

Considerations:

- Script solution: The blue curve identifies the not deformed structure in the figure, while the red curve the deformed one. Value shows in the box is the height reached by the structure under the mentioned loads and is expressed in [m].
  The displacement of the apex of the arch is: 0.0832 [m],
- Fem solution: the result shown in the figure is expressed in [m] and it represents the vertical displacement because the constraint imposed at the right end avoids the horizontal displacement.

Work Case of the Three-Hinged Arch The following table shows the material Work Cases developed by the Three-Hinged Arch in the discretization point for the load condition 3. Due to the fact that the structure is symmetrical, only the left part of the arch including the apex of it is shown in the table.

$\mathbf{N}^{\circ}_{disc}$	1	2	3	4	5	6	7	8	9	10
$\mathbf{WC}_{3H}$	8	6	6	6	6	6	6	6	6	8

Stresses of the Three-Hinged Arch Figure 11.3 shows the stresses developed by the structure in the discretization points in which the arch is analysed. Each column is referred to a single discretization point, while each couple of rows is referred to the stresses developed by each material layer in the upper and lower side. The foam is considered as a single layer. The first row represents the upper layer of the skin facing outwards, while the last one the lower layer of the skin facing inwards. The reference for outward and inward is the Arch seen from the front.
The stresses developed by the carbon layers are highlighted in green, the ones developed by the foam in yellow and the ones developed by the Dyneema in red.

1.0e+08 *

Columns 1 through 10

-0.0075	0.2981	0.4955	0.5499	0.4961	0.3755	0.2299	0.0963	0.0039	-0.0035
-0.0075	0.2947	0.4903	0.5441	0.4909	0.3716	0.2274	0.0951	0.0036	-0.0034
-0.0075	0.2947	0.4903	0.5441	0.4909	0.3716	0.2274	0.0951	0.0036	-0.0034
-0.0075	0.2914	0.4850	0.5384	0.4857	0.3676	0.2249	0.0940	0.0034	-0.0034
-0.0075	0.2914	0.4850	0.5384	0.4857	0.3676	0.2249	0.0940	0.0034	-0.0034
-0.0074	0.2880	0.4797	0.5326	0.4805	0.3636	0.2224	0.0928	0.0031	-0.0034
-0.0074	0.2880	0.4797	0.5326	0.4805	0.3636	0.2224	0.0928	0.0031	-0.0034
-0.0074	0.2847	0.4745	0.5269	0.4753	0.3597	0.2199	0.0916	0.0028	-0.0034
-0.0044	0.0009	0.0015	0.0017	0.0015	0.0011	0.0007	0.0003	0.0000	-0.0020
-0.0001	-0.0008	-0.0012	-0.0013	-0.0011	-0.0009	-0.0006	-0.0003	-0.0001	-0.0000
-0.1196	-0.7587	-1.1005	-1.1796	-1.0617	-0.8240	-0.5437	-0.2893	-0.1140	-0.0548
-0.0910	-0.7643	-1.1094	-1.1892	-1.0704	-0.8307	-0.5479	-0.2912	-0.1144	-0.0417
-0.0910	-0.7643	-1.1094	-1.1892	-1.0704	-0.8307	-0.5479	-0.2912	-0.1144	-0.0417
-0.0624	-0.7699	-1.1182	-1.1989	-1.0791	-0.8373	-0.5522	-0.2932	-0.1148	-0.0286
-0.0624	-0.7699	-1.1182	-1.1989	-1.0791	-0.8373	-0.5522	-0.2932	-0.1148	-0.0286
-0.0339	-0.7756	-1.1270	-1.2085	-1.0878	-0.8440	-0.5564	-0.2952	-0.1153	-0.0155
-0.0339	-0.7756	-1.1270	-1.2085	-1.0878	-0.8440	-0.5564	-0.2952	-0.1153	-0.0155
-0.0053	-0.7812	-1.1358	-1.2181	-1.0965	-0.8507	-0.5606	-0.2971	-0.1157	-0.0024

Columns 11 through 19

0.0039	0.0963	0.2299	0.3755	0.4961	0.5499	0.4955	0.2981	-0.0075
0.0036	0.0951	0.2274	0.3716	0.4909	0.5441	0.4903	0.2947	-0.0075
0.0036	0.0951	0.2274	0.3716	0.4909	0.5441	0.4903	0.2947	-0.0075
0.0034	0.0940	0.2249	0.3676	0.4857	0.5384	0.4850	0.2914	-0.0075
0.0034	0.0940	0.2249	0.3676	0.4857	0.5384	0.4850	0.2914	-0.0075
0.0031	0.0928	0.2224	0.3636	0.4805	0.5326	0.4797	0.2880	-0.0074
0.0031	0.0928	0.2224	0.3636	0.4805	0.5326	0.4797	0.2880	-0.0074
0.0028	0.0916	0.2199	0.3597	0.4753	0.5269	0.4745	0.2847	-0.0074
0.0000	0.0003	0.0007	0.0011	0.0015	0.0017	0.0015	0.0009	-0.0044
-0.0001	-0.0003	-0.0006	-0.0009	-0.0011	-0.0013	-0.0012	-0.0008	-0.0001
-0.1140	-0.2893	-0.5437	-0.8240	-1.0617	-1.1796	-1.1005	-0.7587	-0.1196
-0.1144	-0.2912	-0.5479	-0.8307	-1.0704	-1.1892	-1.1094	-0.7643	-0.0910
-0.1144	-0.2912	-0.5479	-0.8307	-1.0704	-1.1892	-1.1094	-0.7643	-0.0910
-0.1148	-0.2932	-0.5522	-0.8373	-1.0791	-1.1989	-1.1182	-0.7699	-0.0624
-0.1148	-0.2932	-0.5522	-0.8373	-1.0791	-1.1989	-1.1182	-0.7699	-0.0624
-0.1153	-0.2952	-0.5564	-0.8440	-1.0878	-1.2085	-1.1270	-0.7756	-0.0339
-0.1153	-0.2952	-0.5564	-0.8440	-1.0878	-1.2085	-1.1270	-0.7756	-0.0339
-0.1157	-0.2971	-0.5606	-0.8507	-1.0965	-1.2181	-1.1358	-0.7812	-0.0053

Figure 11.3: Stresses of the Three-Hinged Arch, load condition 3. Unit of measurement [Pa].

The stresses calculated with the FEM are not shown due the difficulty to display them in the thesis.

Stability of the Three-Hinged Arch The stability analysis is carried out through the FEM analysis. The following image shows the first buckling defor-

mation shape. The buckling load factor provided by the FEM is 6.898 therefore this structure is not in buckling and it is highly stable.

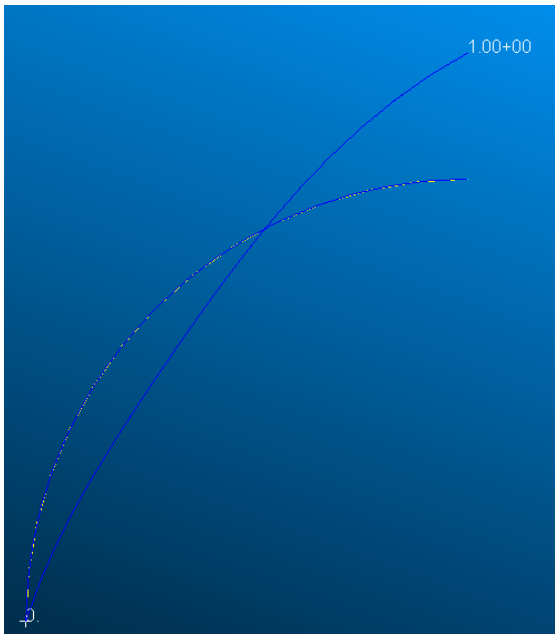

Figure 11.4: First buckling deformation shape of the Three-Hinged Arch.

Two-Hinged Arch

Displacement of the Two-Hinged Arch This paragraph shows the results obtained by the script and by the Fem for the vertical displacement of the Two-Hinged Arch.

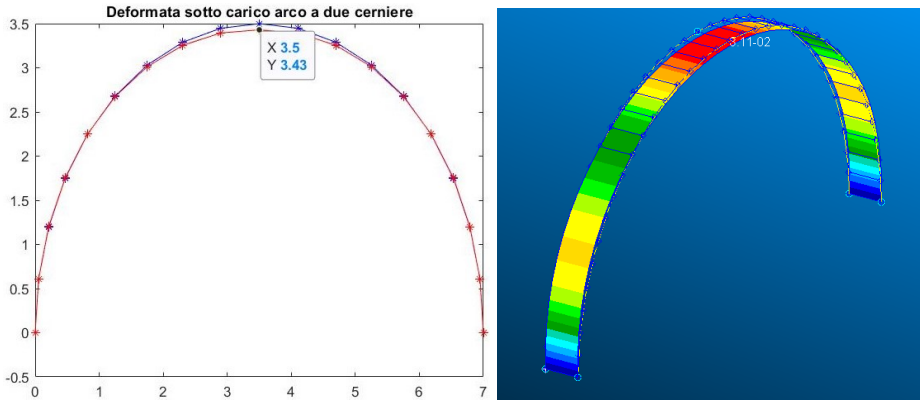

Figure 11.5: Vertical displacement of the Two-Hinged Arch. Script solution on the left (unit of measurement of both the axes [m]), Fem solution on the right.

Consideration:

- Script solution: The blue curve identifies the not deformed structure in the figure, while the red curve the deformed one. Value shows in the box is the height reached by the structure under the mentioned loads and is expressed in [m].
  The displacement of the apex of the arch is: 0.0702 [m],
- Fem solution: the result shown in the figure is expressed in [m] and it represents the vertical displacement because the structure is symmetrical.
  The displacement of the apex of the arch is: 0.0811 [m].

Work Case of the Two-Hinged Arch The following table shows the material Work Cases developed by the Two-Hinged Arch in the discretization point for the load condition 3.

$\mathbf{N}^{\circ}_{disc}$	1	2	3	4	5	6	7	8	9	10
$\mathbf{WC}_{2H}$	8	6	6	6	6	6	6	6	2	2

Stresses of the Two-Hinged Arch Figure 11.7 shows the stresses developed by the structure in the discretization points in which the arch is analysed. Informations to understand the results shown by the following table are the same mentioned for the Three-Hinged Arch.
The stresses developed by the carbon layers are highlighted in green, the ones developed by the foam in yellow and the ones developed by the Dyneema in red. The stress calculated with the FEM are not shown due the difficulty to display them in the thesis.

Stability of the Two-Hinged Arch The stability analysis is carried out through the FEM analysis. The following image shows the first buckling deformation shape. The buckling load factor provided by the FEM is 1.549 therefore this structure is not in buckling and it is stable.

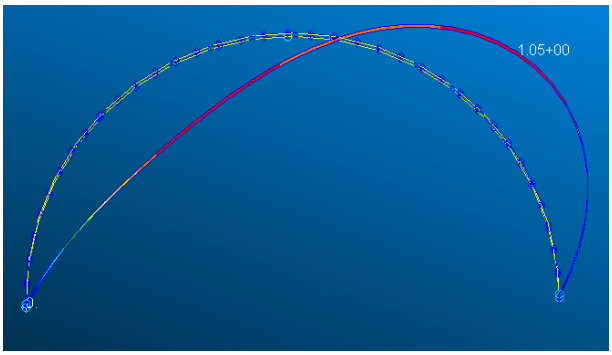

Figure 11.6: First buckling deformation shape of the Three-Hinged Arch.

1.0e+08 *

Columns 1 through 10

-0.0075	0.2807	0.4613	0.4998	0.4317	0.2988	0.1431	0.0021	-0.1713	-0.2343
-0.0075	0.2775	0.4563	0.4945	0.4271	0.2955	0.1414	0.0019	-0.1704	-0.2328
-0.0075	0.2775	0.4563	0.4945	0.4271	0.2955	0.1414	0.0019	-0.1704	-0.2328
-0.0075	0.2743	0.4514	0.4892	0.4226	0.2923	0.1398	0.0016	-0.1694	-0.2312
-0.0075	0.2743	0.4514	0.4892	0.4226	0.2923	0.1398	0.0016	-0.1694	-0.2312
-0.0074	0.2711	0.4465	0.4840	0.4180	0.2891	0.1381	0.0014	-0.1685	-0.2297
-0.0074	0.2711	0.4465	0.4840	0.4180	0.2891	0.1381	0.0014	-0.1685	-0.2297
-0.0074	0.2679	0.4415	0.4787	0.4134	0.2859	0.1365	0.0011	-0.1675	-0.2282
-0.0044	0.0009	0.0014	0.0015	0.0013	0.0009	0.0004	0.0000	-0.0002	-0.0002
-0.0001	-0.0008	-0.0011	-0.0012	-0.0010	-0.0007	-0.0004	-0.0001	0.0001	0.0002
-0.1196	-0.7273	-1.0388	-1.0893	-0.9456	-0.6857	-0.3874	-0.1196	0.0343	0.0698
-0.0910	-0.7327	-1.0471	-1.0981	-0.9533	-0.6911	-0.3902	-0.1200	0.0348	0.0707
-0.0910	-0.7327	-1.0471	-1.0981	-0.9533	-0.6911	-0.3902	-0.1200	0.0348	0.0707
-0.0624	-0.7380	-1.0553	-1.1069	-0.9609	-0.6965	-0.3930	-0.1205	0.0354	0.0716
-0.0624	-0.7380	-1.0553	-1.1069	-0.9609	-0.6965	-0.3930	-0.1205	0.0354	0.0716
-0.0339	-0.7434	-1.0636	-1.1158	-0.9686	-0.7019	-0.3957	-0.1209	0.0360	0.0725
-0.0339	-0.7434	-1.0636	-1.1158	-0.9686	-0.7019	-0.3957	-0.1209	0.0360	0.0725
-0.0053	-0.7487	-1.0718	-1.1246	-0.9762	-0.7073	-0.3985	-0.1213	0.0365	0.0734

Columns 11 through 19

-0.1713	0.0021	0.1431	0.2988	0.4317	0.4998	0.4613	0.2807	-0.0075
-0.1704	0.0019	0.1414	0.2955	0.4271	0.4945	0.4563	0.2775	-0.0075
-0.1704	0.0019	0.1414	0.2955	0.4271	0.4945	0.4563	0.2775	-0.0075
-0.1694	0.0016	0.1398	0.2923	0.4226	0.4892	0.4514	0.2743	-0.0075
-0.1694	0.0016	0.1398	0.2923	0.4226	0.4892	0.4514	0.2743	-0.0075
-0.1685	0.0014	0.1381	0.2891	0.4180	0.4840	0.4465	0.2711	-0.0074
-0.1685	0.0014	0.1381	0.2891	0.4180	0.4840	0.4465	0.2711	-0.0074
-0.1675	0.0011	0.1365	0.2859	0.4134	0.4787	0.4415	0.2679	-0.0074
-0.0002	0.0000	0.0004	0.0009	0.0013	0.0015	0.0014	0.0009	-0.0044
0.0001	-0.0001	-0.0004	-0.0007	-0.0010	-0.0012	-0.0011	-0.0008	-0.0001
0.0343	-0.1196	-0.3874	-0.6857	-0.9456	-1.0893	-1.0388	-0.7273	-0.1196
0.0348	-0.1200	-0.3902	-0.6911	-0.9533	-1.0981	-1.0471	-0.7327	-0.0910
0.0348	-0.1200	-0.3902	-0.6911	-0.9533	-1.0981	-1.0471	-0.7327	-0.0910
0.0354	-0.1205	-0.3930	-0.6965	-0.9609	-1.1069	-1.0553	-0.7380	-0.0624
0.0354	-0.1205	-0.3930	-0.6965	-0.9609	-1.1069	-1.0553	-0.7380	-0.0624
0.0360	-0.1209	-0.3957	-0.7019	-0.9686	-1.1158	-1.0636	-0.7434	-0.0339
0.0360	-0.1209	-0.3957	-0.7019	-0.9686	-1.1158	-1.0636	-0.7434	-0.0339
0.0365	-0.1213	-0.3985	-0.7073	-0.9762	-1.1246	-1.0718	-0.7487	-0.0053

Figure 11.7: Stresses of the Two-Hinged Arch, load condition 3. Unit of measurement [Pa].

11.2.2 Load condition 4, Load to keep the habitat in folded configuration

This paragraph shows the work case developed by the material, needed bending moment and stresses to reach a curvature radius of 3 m.

Three-Hinged Arch

Work case of the Three-Hinged Arch The following table shows the material Work Cases developed by the Two-Hinged Arch in the discretization point for the load condition 4.

$\mathbf{N}^{\circ}_{disc}$	1	2	3	4	5	6	7	8	9	10
$\mathbf{WC}_{3H}$	7	7	7	7	7	7	7	7	7	7

Bending moment to keep Three-Hinged in folded configuration The needed bending moment for each discretization point that has to be applied to keep the habitat in folded configuration with a 3 m radius of curvature is shown below.

N°_{disc}	1	2	3	4	5	6	7	8	9	10
M_{3H}[Nm]	2874	5289	5289	5289	5289	5289	5289	5289	5289	2874

Stresses of the Three-Hinged Arch Figure 11.8 shows the stresses developed by the structure in the discretization points in which the arch is analysed. The stresses developed by the carbon layers are highlighted in green, the ones developed by the foam in yellow and the ones developed by the Dyneema in red.

1.0e+08 *

Columns 1 through 10

-0.0217	-0.0399	-0.0399	-0.0399	-0.0399	-0.0399	-0.0399	-0.0399	-0.0399	-0.0217
-0.0216	-0.0397	-0.0397	-0.0397	-0.0397	-0.0397	-0.0397	-0.0397	-0.0397	-0.0216
-0.0216	-0.0397	-0.0397	-0.0397	-0.0397	-0.0397	-0.0397	-0.0397	-0.0397	-0.0216
-0.0214	-0.0394	-0.0394	-0.0394	-0.0394	-0.0394	-0.0394	-0.0394	-0.0394	-0.0214
-0.0214	-0.0394	-0.0394	-0.0394	-0.0394	-0.0394	-0.0394	-0.0394	-0.0394	-0.0214
-0.0213	-0.0392	-0.0392	-0.0392	-0.0392	-0.0392	-0.0392	-0.0392	-0.0392	-0.0213
-0.0213	-0.0392	-0.0392	-0.0392	-0.0392	-0.0392	-0.0392	-0.0392	-0.0392	-0.0213
-0.0212	-0.0389	-0.0389	-0.0389	-0.0389	-0.0389	-0.0389	-0.0389	-0.0389	-0.0212
-0.0254	-0.0467	-0.0467	-0.0467	-0.0467	-0.0467	-0.0467	-0.0467	-0.0467	-0.0254
0.0007	0.0013	0.0013	0.0013	0.0013	0.0013	0.0013	0.0013	0.0013	0.0007
0.7299	1.3432	1.3432	1.3432	1.3432	1.3432	1.3432	1.3432	1.3432	0.7299
0.8247	1.5178	1.5178	1.5178	1.5178	1.5178	1.5178	1.5178	1.5178	0.8247
0.8247	1.5178	1.5178	1.5178	1.5178	1.5178	1.5178	1.5178	1.5178	0.8247
0.9196	1.6923	1.6923	1.6923	1.6923	1.6923	1.6923	1.6923	1.6923	0.9196
0.9196	1.6923	1.6923	1.6923	1.6923	1.6923	1.6923	1.6923	1.6923	0.9196
1.0145	1.8669	1.8669	1.8669	1.8669	1.8669	1.8669	1.8669	1.8669	1.0145
1.0145	1.8669	1.8669	1.8669	1.8669	1.8669	1.8669	1.8669	1.8669	1.0145
1.1093	2.0415	2.0415	2.0415	2.0415	2.0415	2.0415	2.0415	2.0415	1.1093

Columns 11 through 19

-0.0399	-0.0399	-0.0399	-0.0399	-0.0399	-0.0399	-0.0399	-0.0399	-0.0217
-0.0397	-0.0397	-0.0397	-0.0397	-0.0397	-0.0397	-0.0397	-0.0397	-0.0216
-0.0397	-0.0397	-0.0397	-0.0397	-0.0397	-0.0397	-0.0397	-0.0397	-0.0216
-0.0394	-0.0394	-0.0394	-0.0394	-0.0394	-0.0394	-0.0394	-0.0394	-0.0214
-0.0394	-0.0394	-0.0394	-0.0394	-0.0394	-0.0394	-0.0394	-0.0394	-0.0214
-0.0392	-0.0392	-0.0392	-0.0392	-0.0392	-0.0392	-0.0392	-0.0392	-0.0213
-0.0392	-0.0392	-0.0392	-0.0392	-0.0392	-0.0392	-0.0392	-0.0392	-0.0213
-0.0389	-0.0389	-0.0389	-0.0389	-0.0389	-0.0389	-0.0389	-0.0389	-0.0212
-0.0467	-0.0467	-0.0467	-0.0467	-0.0467	-0.0467	-0.0467	-0.0467	-0.0254
0.0013	0.0013	0.0013	0.0013	0.0013	0.0013	0.0013	0.0013	0.0007
1.3432	1.3432	1.3432	1.3432	1.3432	1.3432	1.3432	1.3432	0.7299
1.5178	1.5178	1.5178	1.5178	1.5178	1.5178	1.5178	1.5178	0.8247
1.5178	1.5178	1.5178	1.5178	1.5178	1.5178	1.5178	1.5178	0.8247
1.6923	1.6923	1.6923	1.6923	1.6923	1.6923	1.6923	1.6923	0.9196
1.6923	1.6923	1.6923	1.6923	1.6923	1.6923	1.6923	1.6923	0.9196
1.8669	1.8669	1.8669	1.8669	1.8669	1.8669	1.8669	1.8669	1.0145
1.8669	1.8669	1.8669	1.8669	1.8669	1.8669	1.8669	1.8669	1.0145
2.0415	2.0415	2.0415	2.0415	2.0415	2.0415	2.0415	2.0415	1.1093

Figure 11.8: Stresses of the Three-Hinged Arch, load condition 4. Unit of measurement [Pa].

Two-Hinged Arch

Work case of the Two-Hinged Arch The following table shows the material Work Cases developed by the Two-Hinged Arch in the discretization point for the load condition 4.

$\mathbf{N}^{\circ}_{disc}$	1	2	3	4	5	6	7	8	9	10
$\mathbf{WC}_{2H}$	7	7	7	7	7	7	7	7	3	3

Bending moment to keep Two-Hinged in folded configuration The needed bending moment for each discretization point that has to be applied to keep the habitat in folded configuration with a radius of curvature of 3 m is shown below.

$\mathbf{N}^{\circ}_{disc}$	1	2	3	4	5	6	7	8	9	10
$\mathbf{M}_{3H}$[Nm]	2874	5289	5289	5289	5289	5289	5289	5289	-5289	-5289

Stresses of the Two-Hinged Arch Figure 11.10 shows the stresses developed by the structure in the discretization points in which the arch is analysed. The stresses developed by the carbon layers are highlighted in green, the ones developed by the foam in yellow and the ones developed by the Dyneema in red.

11.2.3 Load condition 2, Internal pressure plus regolith load

Three-Hinged-Arch

Displacement of the Three-Hinged Arch This paragraph shows the results obtained by the script and by the Fem for the vertical displacement of the Three-Hinged Arch.

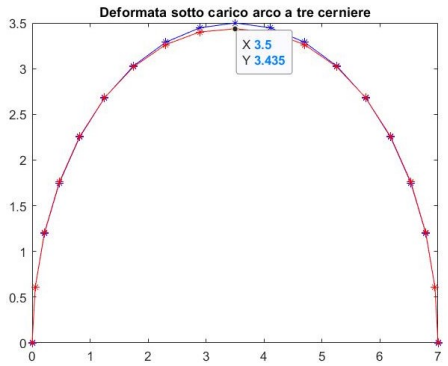

Figure 11.9: Vertical displacement of the Three-Hinged Arch. Script solution. Unit of measurement of both the axes [m].

Consideration:

- Script solution: The blue curve identifies the not deformed structure in the figure, while the red curve the deformed one. Value shows in the box is the height reached by the structure under the mentioned loads and is expressed in [m].
  The displacement of the apex of the arch is: 0.0649 [m],

- Fem solution: The result provided by the FEM is not shown because the value obtained are different from the one calculated with the script. Moreover, the displacement obtained by the FEM for the apex of Three-Hinged Arch is also smaller than the one obtained for the Two-Hinged Arch.

1.0e+08 *

Columns 1 through 10

-0.0217	-0.0399	-0.0399	-0.0399	-0.0399	-0.0399	-0.0399	-0.0399	2.0415	2.0415
-0.0216	-0.0397	-0.0397	-0.0397	-0.0397	-0.0397	-0.0397	-0.0397	1.8669	1.8669
-0.0216	-0.0397	-0.0397	-0.0397	-0.0397	-0.0397	-0.0397	-0.0397	1.8669	1.8669
-0.0214	-0.0394	-0.0394	-0.0394	-0.0394	-0.0394	-0.0394	-0.0394	1.6923	1.6923
-0.0214	-0.0394	-0.0394	-0.0394	-0.0394	-0.0394	-0.0394	-0.0394	1.6923	1.6923
-0.0213	-0.0392	-0.0392	-0.0392	-0.0392	-0.0392	-0.0392	-0.0392	1.5178	1.5178
-0.0213	-0.0392	-0.0392	-0.0392	-0.0392	-0.0392	-0.0392	-0.0392	1.5178	1.5178
-0.0212	-0.0389	-0.0389	-0.0389	-0.0389	-0.0389	-0.0389	-0.0389	1.3432	1.3432
-0.0254	-0.0467	-0.0467	-0.0467	-0.0467	-0.0467	-0.0467	-0.0467	0.0013	0.0013
0.0007	0.0013	0.0013	0.0013	0.0013	0.0013	0.0013	0.0013	-0.0467	-0.0467
0.7299	1.3432	1.3432	1.3432	1.3432	1.3432	1.3432	1.3432	-0.0389	-0.0389
0.8247	1.5178	1.5178	1.5178	1.5178	1.5178	1.5178	1.5178	-0.0392	-0.0392
0.8247	1.5178	1.5178	1.5178	1.5178	1.5178	1.5178	1.5178	-0.0392	-0.0392
0.9196	1.6923	1.6923	1.6923	1.6923	1.6923	1.6923	1.6923	-0.0394	-0.0394
0.9196	1.6923	1.6923	1.6923	1.6923	1.6923	1.6923	1.6923	-0.0394	-0.0394
1.0145	1.8669	1.8669	1.8669	1.8669	1.8669	1.8669	1.8669	-0.0397	-0.0397
1.0145	1.8669	1.8669	1.8669	1.8669	1.8669	1.8669	1.8669	-0.0397	-0.0397
1.1093	2.0415	2.0415	2.0415	2.0415	2.0415	2.0415	2.0415	-0.0399	-0.0399

Columns 11 through 19

2.0415	-0.0399	-0.0399	-0.0399	-0.0399	-0.0399	-0.0399	-0.0399	-0.0217
1.8669	-0.0397	-0.0397	-0.0397	-0.0397	-0.0397	-0.0397	-0.0397	-0.0216
1.8669	-0.0397	-0.0397	-0.0397	-0.0397	-0.0397	-0.0397	-0.0397	-0.0216
1.6923	-0.0394	-0.0394	-0.0394	-0.0394	-0.0394	-0.0394	-0.0394	-0.0214
1.6923	-0.0394	-0.0394	-0.0394	-0.0394	-0.0394	-0.0394	-0.0394	-0.0214
1.5178	-0.0392	-0.0392	-0.0392	-0.0392	-0.0392	-0.0392	-0.0392	-0.0213
1.5178	-0.0392	-0.0392	-0.0392	-0.0392	-0.0392	-0.0392	-0.0392	-0.0213
1.3432	-0.0389	-0.0389	-0.0389	-0.0389	-0.0389	-0.0389	-0.0389	-0.0212
0.0013	-0.0467	-0.0467	-0.0467	-0.0467	-0.0467	-0.0467	-0.0467	-0.0254
-0.0467	0.0013	0.0013	0.0013	0.0013	0.0013	0.0013	0.0013	0.0007
-0.0389	1.3432	1.3432	1.3432	1.3432	1.3432	1.3432	1.3432	0.7299
-0.0392	1.5178	1.5178	1.5178	1.5178	1.5178	1.5178	1.5178	0.8247
-0.0392	1.5178	1.5178	1.5178	1.5178	1.5178	1.5178	1.5178	0.8247
-0.0394	1.6923	1.6923	1.6923	1.6923	1.6923	1.6923	1.6923	0.9196
-0.0394	1.6923	1.6923	1.6923	1.6923	1.6923	1.6923	1.6923	0.9196
-0.0397	1.8669	1.8669	1.8669	1.8669	1.8669	1.8669	1.8669	1.0145
-0.0397	1.8669	1.8669	1.8669	1.8669	1.8669	1.8669	1.8669	1.0145
-0.0399	2.0415	2.0415	2.0415	2.0415	2.0415	2.0415	2.0415	1.1093

Figure 11.10: Stresses of the Two-Hinged Arch, load condition 4. Unit of measurement [Pa].

Work Case of the Three-Hinged Arch The following table shows the material Work Cases developed by the Three-Hinged Arch in the discretization

point for the load condition 2. Due to the fact that the structure is symmetrical, only the left part of the arch including the apex of it is shown in the table.

$\mathbf{N}^{\circ}_{disc}$	1	2	3	4	5	6	7	8	9	10
$\mathbf{WC}_{3H}$	5	5	5	5	5	5	5	5	5	5

Stresses of the Three-Hinged Arch Figure 11.12 shows the stresses developed by the structure in the discretization points in which the arch is analysed. Informations to understand the results shown by the following table are the same mentioned for the Three-Hinged Arch.
The stresses developed by the carbon layers are highlighted in green, the ones developed by the foam in yellow and the ones developed by the Dyneema in red.

1.0e+08 *

Columns 1 through 10

0.7879	1.1512	1.3494	1.4040	1.3500	1.2289	1.0827	0.9485	0.8557	0.8227
0.7857	1.1455	1.3420	1.3960	1.3426	1.2227	1.0778	0.9450	0.8531	0.8204
0.7857	1.1455	1.3420	1.3960	1.3426	1.2227	1.0778	0.9450	0.8531	0.8204
0.7835	1.1399	1.3345	1.3881	1.3352	1.2165	1.0730	0.9415	0.8505	0.8180
0.7835	1.1399	1.3345	1.3881	1.3352	1.2165	1.0730	0.9415	0.8505	0.8180
0.7813	1.1343	1.3270	1.3801	1.3277	1.2102	1.0682	0.9380	0.8478	0.8157
0.7813	1.1343	1.3270	1.3801	1.3277	1.2102	1.0682	0.9380	0.8478	0.8157
0.7790	1.1286	1.3195	1.3722	1.3203	1.2040	1.0634	0.9344	0.8452	0.8134
0.0025	0.0036	0.0042	0.0044	0.0042	0.0038	0.0034	0.0030	0.0027	0.0026
0.0014	0.0007	0.0004	0.0003	0.0004	0.0007	0.0009	0.0012	0.0014	0.0014
1.4041	0.7533	0.4090	0.3296	0.4485	0.6880	0.9704	1.2268	1.4033	1.4661
1.4000	0.7428	0.3951	0.3148	0.4347	0.6764	0.9615	1.2202	1.3984	1.4618
1.4000	0.7428	0.3951	0.3148	0.4347	0.6764	0.9615	1.2202	1.3984	1.4618
1.3959	0.7324	0.3812	0.3001	0.4210	0.6648	0.9525	1.2137	1.3935	1.4574
1.3959	0.7324	0.3812	0.3001	0.4210	0.6648	0.9525	1.2137	1.3935	1.4574
1.3917	0.7219	0.3674	0.2853	0.4072	0.6533	0.9436	1.2071	1.3887	1.4531
1.3917	0.7219	0.3674	0.2853	0.4072	0.6533	0.9436	1.2071	1.3887	1.4531
1.3876	0.7114	0.3535	0.2705	0.3935	0.6417	0.9346	1.2006	1.3838	1.4488

Columns 11 through 19

0.8557	0.9485	1.0827	1.2289	1.3500	1.4040	1.3494	1.1512	0.7879
0.8531	0.9450	1.0778	1.2227	1.3426	1.3960	1.3420	1.1455	0.7857
0.8531	0.9450	1.0778	1.2227	1.3426	1.3960	1.3420	1.1455	0.7857
0.8505	0.9415	1.0730	1.2165	1.3352	1.3881	1.3345	1.1399	0.7835
0.8505	0.9415	1.0730	1.2165	1.3352	1.3881	1.3345	1.1399	0.7835
0.8478	0.9380	1.0682	1.2102	1.3277	1.3801	1.3270	1.1343	0.7813
0.8478	0.9380	1.0682	1.2102	1.3277	1.3801	1.3270	1.1343	0.7813
0.8452	0.9344	1.0634	1.2040	1.3203	1.3722	1.3195	1.1286	0.7790
0.0027	0.0030	0.0034	0.0038	0.0042	0.0044	0.0042	0.0036	0.0025
0.0014	0.0012	0.0009	0.0007	0.0004	0.0003	0.0004	0.0007	0.0014
1.4033	1.2268	0.9704	0.6880	0.4485	0.3296	0.4090	0.7533	1.4041
1.3984	1.2202	0.9615	0.6764	0.4347	0.3148	0.3951	0.7428	1.4000
1.3984	1.2202	0.9615	0.6764	0.4347	0.3148	0.3951	0.7428	1.4000
1.3935	1.2137	0.9525	0.6648	0.4210	0.3001	0.3812	0.7324	1.3959
1.3935	1.2137	0.9525	0.6648	0.4210	0.3001	0.3812	0.7324	1.3959
1.3887	1.2071	0.9436	0.6533	0.4072	0.2853	0.3674	0.7219	1.3917
1.3887	1.2071	0.9436	0.6533	0.4072	0.2853	0.3674	0.7219	1.3917
1.3838	1.2006	0.9346	0.6417	0.3935	0.2705	0.3535	0.7114	1.3876

Figure 11.11: Stresses of the Three-Hinged Arch, load condition 2. Unit of measurement [Pa].

Stability of the Three-Hinged Arch Even if the the FEM analysis about the displacement of the structure provides different results from the ones of Matlab script, the stability analysis is shown because the result is only qualitative and not affected by this type of errors (these ones about the displacement). The buckling load factor provided is negative and this means that the buckling arising is impossible.

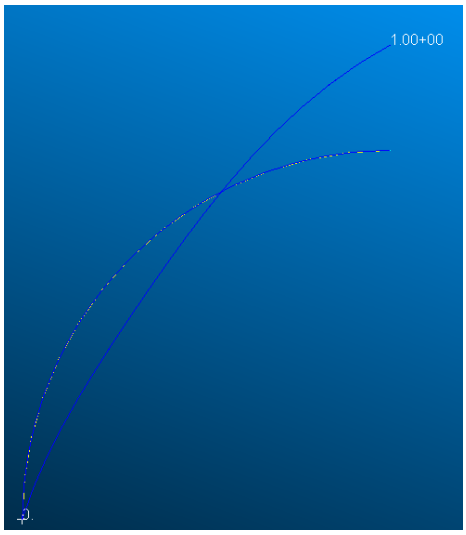

Figure 11.12: First buckling deformation shape of the Three-Hinged Arch.

Two-Hinged Arch

Displacement of the Two-Hinged Arch This paragraph shows the results obtained by the script and by the Fem for the vertical displacement of the Two-Hinged Arch.

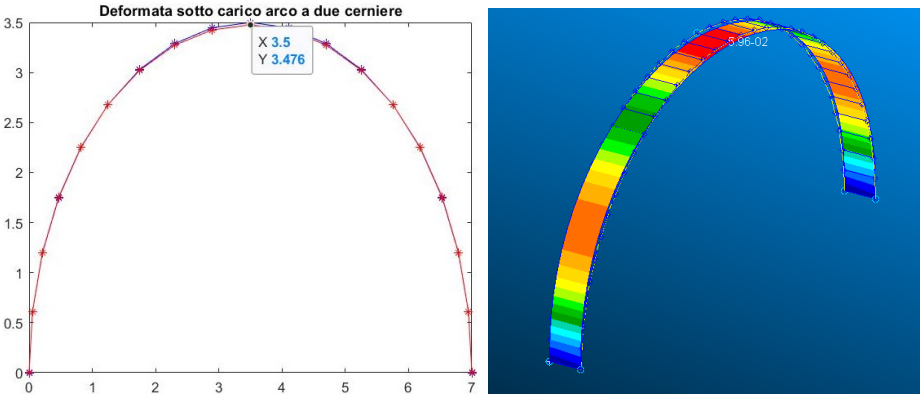

Figure 11.13: Vertical displacement of the Two-Hinged Arch. Script solution on the left (unit of measurement of both the axes [m]), Fem solution on the right.

Consideration:

- Script solution: The blue curve identifies the not deformed structure in the figure, while the red curve the deformed one. Value shows in the box is the height reached by the structure under the mentioned loads and is expressed in [m].
  The displacement of the apex of the arch is: 0.0239 [m],
- Fem solution: the result shown in the figure is expressed in [m] and it represents the vertical displacement of the apex of the arch because the structure is symmetrical. The displacement is: 0.0596 [m],

In this analysis the result provided by the FEM does not coincide with the one obtained by the Matlab script.

Work Case of the Two-Hinged Arch The following table shows the material Work Cases developed by the Two-Hinged Arch in the discretization point for the load condition 3.

$\mathbf{N}^{\circ}_{disc}$	1	2	3	4	5	6	7	8	9	10
$\mathbf{WC}_{2H}$	5	5	5	5	5	5	5	5	1	1

Stresses of the Two-Hinged Arch Figure 11.15 shows the stresses developed by the structure in the discretization points in which the arch is analysed. Informations to understand the results shown by the following table are the same mentioned for the Three-Hinged Arch.
The stresses developed by the carbon layers are highlighted in green, the ones developed by the foam in yellow and the ones developed by the Dyneema in red. The stresses calculated with the FEM are not shown due the difficulty to display them in the thesis.

Stability of the Two-Hinged Arch Even if the the FEM analysis about the displacement of the structure provides different results from the ones of Matlab script, the stability analysis is shown because the result is only qualitative and not affected by this type of errors (these ones about the displacement). The buckling load factor provided is negative and this means that the buckling arising is impossible.

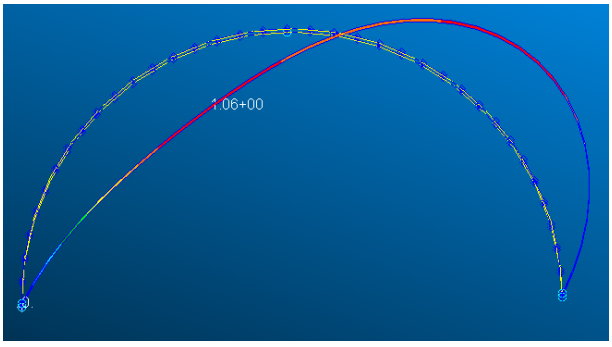

Figure 11.14: First buckling deformation shape of the Three-Hinged Arch.

1.0e+08 *

Columns 1 through 10

0.7879	1.0908	1.2306	1.2302	1.1265	0.9626	0.7816	0.6219	0.8808	0.8103
0.7857	1.0857	1.2242	1.2239	1.1212	0.9589	0.7797	0.6215	0.8905	0.8208
0.7857	1.0857	1.2242	1.2239	1.1212	0.9589	0.7797	0.6215	0.8905	0.8208
0.7835	1.0807	1.2178	1.2176	1.1159	0.9552	0.7777	0.6210	0.9003	0.8312
0.7835	1.0807	1.2178	1.2176	1.1159	0.9552	0.7777	0.6210	0.9003	0.8312
0.7813	1.0756	1.2115	1.2112	1.1106	0.9515	0.7757	0.6206	0.9100	0.8416
0.7813	1.0756	1.2115	1.2112	1.1106	0.9515	0.7757	0.6206	0.9100	0.8416
0.7790	1.0705	1.2051	1.2049	1.1053	0.9478	0.7737	0.6201	0.9197	0.8521
0.0025	0.0034	0.0038	0.0038	0.0035	0.0030	0.0025	0.0020	0.0009	0.0008
0.0014	0.0008	0.0006	0.0006	0.0008	0.0011	0.0015	0.0017	0.0036	0.0037
1.4041	0.8624	0.6239	0.6437	0.8523	1.1692	1.5144	1.8171	1.1164	1.1558
1.4000	0.8529	0.6121	0.6320	0.8424	1.1623	1.5107	1.8162	1.1216	1.1614
1.4000	0.8529	0.6121	0.6320	0.8424	1.1623	1.5107	1.8162	1.1216	1.1614
1.3959	0.8435	0.6003	0.6202	0.8326	1.1554	1.5071	1.8154	1.1268	1.1670
1.3959	0.8435	0.6003	0.6202	0.8326	1.1554	1.5071	1.8154	1.1268	1.1670
1.3917	0.8341	0.5884	0.6085	0.8227	1.1485	1.5034	1.8146	1.1321	1.1726
1.3917	0.8341	0.5884	0.6085	0.8227	1.1485	1.5034	1.8146	1.1321	1.1726
1.3876	0.8247	0.5766	0.5968	0.8129	1.1416	1.4997	1.8137	1.1373	1.1782

Columns 11 through 19

0.8808	0.6219	0.7816	0.9626	1.1265	1.2302	1.2306	1.0908	0.7879
0.8905	0.6215	0.7797	0.9589	1.1212	1.2239	1.2242	1.0857	0.7857
0.8905	0.6215	0.7797	0.9589	1.1212	1.2239	1.2242	1.0857	0.7857
0.9003	0.6210	0.7777	0.9552	1.1159	1.2176	1.2178	1.0807	0.7835
0.9003	0.6210	0.7777	0.9552	1.1159	1.2176	1.2178	1.0807	0.7835
0.9100	0.6206	0.7757	0.9515	1.1106	1.2112	1.2115	1.0756	0.7813
0.9100	0.6206	0.7757	0.9515	1.1106	1.2112	1.2115	1.0756	0.7813
0.9197	0.6201	0.7737	0.9478	1.1053	1.2049	1.2051	1.0705	0.7790
0.0009	0.0020	0.0025	0.0030	0.0035	0.0038	0.0038	0.0034	0.0025
0.0036	0.0017	0.0015	0.0011	0.0008	0.0006	0.0006	0.0008	0.0014
1.1164	1.8171	1.5144	1.1692	0.8523	0.6437	0.6239	0.8624	1.4041
1.1216	1.8162	1.5107	1.1623	0.8424	0.6320	0.6121	0.8529	1.4000
1.1216	1.8162	1.5107	1.1623	0.8424	0.6320	0.6121	0.8529	1.4000
1.1268	1.8154	1.5071	1.1554	0.8326	0.6202	0.6003	0.8435	1.3959
1.1268	1.8154	1.5071	1.1554	0.8326	0.6202	0.6003	0.8435	1.3959
1.1321	1.8146	1.5034	1.1485	0.8227	0.6085	0.5884	0.8341	1.3917
1.1321	1.8146	1.5034	1.1485	0.8227	0.6085	0.5884	0.8341	1.3917
1.1373	1.8137	1.4997	1.1416	0.8129	0.5968	0.5766	0.8247	1.3876

Figure 11.15: Stresses of the Two-Hinged Arch, load condition 2. Unit of measurement [Pa].

11.3 Consideration about the structure of the habitat with the floor

Until now the habitat structure is analysed as an arch whose ends are fixed in the desired positions through infinite stiff constraints (hinges) which avoid the movement of the ends along the horizontal and vertical directions keeping them fixed at the established distance. In reality, infinite stiff constraints do not exist and the task to keep the ends at the desired distance is carried out by the floor of the habitat. The not infinite flexural stiffness of the floor allows therefore the movement of the ends letting the possibility to the habitat to reach shape similar to the one shown in figure 11.16 when it has to withstand the load condition 2. It is important to remember that load condition 2 is the one that the structure has to withstand for most of his life. Moreover an excessive curvature of the floor can lead to the instability of the habitat on the lunar soil and the consequent difficulty to place equipments and walk on it.

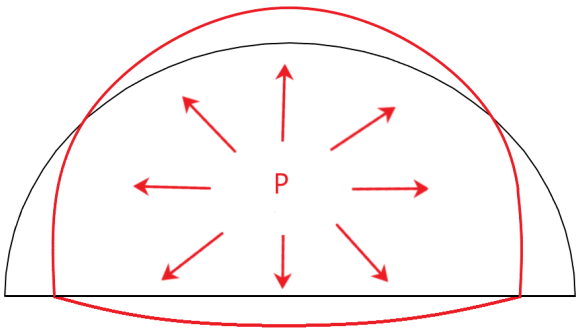

Figure 11.16: Not deformed structure is shown in black and the deformed one in red.

Flexural stiffness of the floor

Analysing the overall structure with FEM, the value of the flexural stiffness of the floor is related to the displacement of the central point of the it and the apex of the arch. An aluminum beam is used to simulate the floor and three different values of flexural stiffness are developed by increasing the thickness of the plate and keeping constant the elastic modulus (71 GPa). The obtained results are summarized in following table and shown in the figure 11.17 through a graph to understand their trend.

Plate Thickness [mm]	150	250	350
EI [Nm^2]	$9.9844 \cdot 10^6$	$4.62244 \cdot 10^7$	$1.2684 \cdot 10^8$
Maximum displacement of the floor [m]	$1.51 \cdot 10^{-1}$	$3.32 \cdot 10^{-2}$	$\simeq 0$
Displacement of the apex of the arch [m]	$8.76 \cdot 10^{-1}$	$8.76 \cdot 10^{-2}$	$\simeq 0$

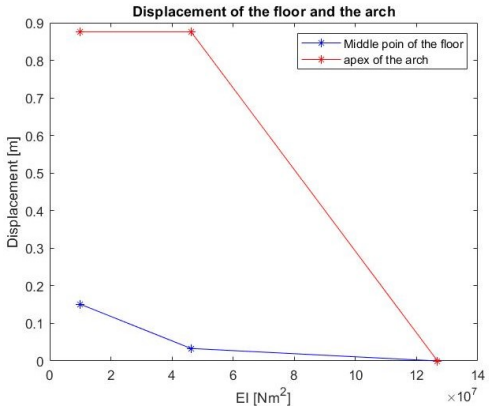

Figure 11.17: Trend of the displacement of the apex of the arch and the central point of the floor referred to the flexural stiffness of the latter.

A flexural stiffness between $4.62244 \cdot 10^7$ and $1.2684 \cdot 10^8$ is needed to reach an acceptable displacement of the floor. The question is: how can it be possible to reach these values without using an aluminum plate or the MadFLex?
The MadFLex can not be used due to the orientation required by this load condition. It has to be oriented with the carbon layer facing inwards the habitat and the Dyneema facing outwards in order to exploit its higher flexural stiffness. However, if this configuration is optimal for the previously mentioned load condition, it avoids to fold the habitat in the stored configuration, which establish the easy folding upwards of the floor. The solution proposed is to employ materials with a snap through. This behaviour is shown for example by the objects in figure 11.18.

Figure 11.18: reflective bracelet

This type of instability is due to the geometry of the section, coupled with the mechanical properties of it. The section is able to become flat thanks to the elasticity of the material which allows the section deformation without breaking. This behaviour can also be shown by a thermoformed MadFlex with a low curvature thanks to the small elasticity of the carbon layer.

The idea is to create a floor by placing this object along the module transversal direction. In this configuration each object connects one lateral part of the habitat with the other one, obtaining a 90° between it and the habitat. All the elements in the stored configuration are flat, while they reach the curved configuration once the habitat is deployed. The latter configuration avoids the upwards floor inflection. Moreover, the bending moment supported by the elements can be increased by blocking the snap of the section with a high punctual resistance foam.

Other solutions

If the required flexural stiffness can not be reached through the solutions mentioned before other two proposals are shown below:

- The easiest solution is to accept higher deformation of the habitat's floor and create a curved base, using the regolith, to keep the habitat in the right position and avoiding the lateral instability. By applying this idea, another solution has to be provided to create an internal flat floor.
- Fix the lateral side of the habitat in a way similar to the one used for the tent but with a more sophisticated mechanism. By applying this solution and assuming the displacement of the anchoring systems equal to zero, the floor deformation depends only on the reaction offered by the lunar soil. Displacement of the central point of the floor is shown in the next table for different value of hypothetical compression stiffness of the regolith. The compression stiffness of the regolith is simulated in the FEM through 0D element (ground spring).

spring stiffness [N/m]	10^3	10^4	10^5	10^6
Displacement of the floor central point [m]	1.84	1.08	0.193	0.0169

11.4 Satisfaction of the Requirements

This section represents the conclusion of the Thesis and provides a comparison between the features of the primary design and the results obtained by the structural analysis with the requirements imposed at the beginning of the preliminary study (Chapter 6). Its aim is to verify the satisfaction of the requirements and provide the conclusive consideration about them.
The mentioned considerations are reported below with the same order shown by the relative requirements in Chapter 5.

11.4.1 Architectural requirement

Needed habitable volume per person

The required free volume per person (available free space which not includes occupied volume by equipments or secondary structure) is 120 m^3. Applying the consideration explained in the paragraph "Total Needed floor area per person" (Chapter 5) which considers the shape assumed by the free space similar to a parallelepiped one and a 20% of the floor area occupied by equipments, each habitat can ensure the required free space for 1.3 person (in numerical terms). Therefore a Moon base constituted by 4 semi-cylindrical modules (without considering the dome needed for their connection) is able to accommodate five astronauts for long duration missions.

Height of the habitat

As shown by the table 11.1 the height of the preliminary design is 3.5 m and therefore the requirement is satisfied.

Length of the Habitat

Only a slice of 0.5 m of structure is consider in the structural analysis in order to apply the Allen beam theory, therefore the effects due to the load conditions along the longitudinal direction of the habitat is not considered. Even if a in-depth analysis it is needed, the structure can be considered as the sum of 18 slices of 0.5 m wide, reaching the required length. Therefore the requirement can be satisfied.

Total Needed floor area per person

The estimate provided by the paragraph "Needed habitable volume per person" are based on the method adopted to calculate the needed floor area per person. Therefore, the number of people that a habitat can accommodate ensuring the required free floor area of 40 m^2 per person is the same mentioned in the previous chapter: 1.3 people. Also for this paragraph the consideration about a Moon base composed by 4 semi-cylindrical module is valid. The base is able to accommodate five astronauts for long duration missions.

Habitat shape

The preliminary design's geometry coupled with the MadFlex orientation along the thickness for both the analysed structure (Three-Hinged Arch and Two-

Hinged one) allows the folding of the structure. This feature can be extended to the semi-cylindrical habitat, thanks to its single curvature and to the dome with the limitation explained in section 8.4. Therefore the imposed requirement about the deployment of the module is satisfied. The possible shapes assumed by both of the structures in the folding configuration are shown below. The floor is represented by the blue curve, while the arch in MadFlex with the black one.

- Three-Hinged Arch

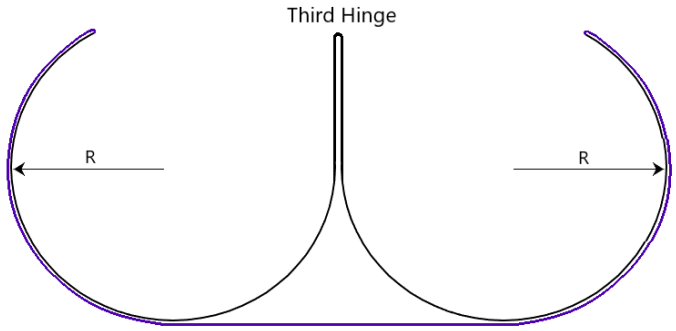

Figure 11.19: Shape assumed by the Three-Hinged Arch in the folding configuration

It is characterized by a cusp where the third hinge is located.

- Two-Hinged Arch

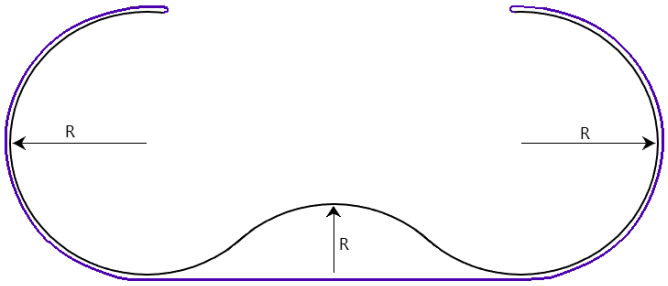

Figure 11.20: Shape assumed by the Two-Hinged Arch in the folding configuration

The previously shown figures have only a qualitative purpose. The shape assumed by the structure in the folding configuration depends mainly by the radius of curvature allowed by the foam. This because the stress developed by the foam in the folding configuration for the imposed radius must not exceed the ultimate tensile and compression strength of it (Sturdiness criterion of the foam). This question is examined in the structural requirement paragraph.

11.4.2 Environmental requirement (ECLS)

Internal pressure

How to generate and maintain a dual-gas oxygen-nitrogen atmosphere inside the habitat with the right proportion (proportion are mentioned in Chapter 5) was not subject of analysis of this Thesis. However the presence of an internal pressure 1 atm ($1.013 \cdot 10^5$ Pa) is considered as a load condition in the preliminary structural analysis.

Temperature and Humidity

Requirement not analysed in this Thesis

Noise and vibration

Requirement not analysed in this Thesis

Ventilation

Requirement not analysed in this Thesis

Ionizing radiation

The protection of the astronauts from the ionizing radiation, keeping their level inside the habitat under the value mentioned in the tables , and is considered in the preliminary design. The requirement is satisfied by applying a 2.5 m thickness regolith cover above the habitat in accordance with the study mentioned in Chapter 4.

11.4.3 Structural requirements)

Safety Factor

A Safety Factor equal to 4 is applied for load condition 2 and 3. It is not applied for the load condition 4 because the needed bending moment to fold the habitat in the stored configuration is known (it depends from the desired radius of curvature and the flexural stiffness of the MadFlex) and the thickness of each layer is established from the analysis of load condition 3.

Load condition

Load conditions 2, 3 and 4 mentioned by this requirement are analysed while load condition 1 is not considered because it is less critical than the others.

Sturdiness criterion

The satisfaction of the sturdiness criterion is analysed for each load conditions and for each layer of the MadFlex.

- **Load condition 2**, internal pressure plus regolith load.

  - **Flexible skin (Dyneema)**: Tensile stresses of the flexible skin multiplied by a SF equal to 4 are lower than the ultimate tensile strength of the Dyneema. The previous consideration is valid for both the Three-Hinged Arc and the Two-Hinged one. The flexible skin sturdiness criterion is satisfied,
  - **Foam**: Tensile stresses of the foam multiplied by a SF equal to 4 are lower than its ultimate tensile strength. The previous consideration is valid for both the Three-Hinged Arc and the Two-Hinged one. The foam sturdiness criterion is satisfied,
  - **Rigid skin (Carbon)**: Tensile stresses of the rigid skin multiplied by a SF equal to 4 are lower than the ultimate tensile strength of the carbon. The previous consideration is valid for both the Three-Hinged Arc and the Two-Hinged one. The rigid skin sturdiness criterion is satisfied.

- **Load condition 3**, internal pressure plus regolith load.
  - **Flexible skin (Dyneema)**: Tensile stresses of the flexible skin multiplied by a SF equal to 4 are lower than the ultimate tensile strength of the Dyneema. The previous consideration is valid for both the Three-Hinged Arc and the Two-Hinged one. The flexible skin sturdiness criterion is satisfied,
  - **Foam**: Tensile and compression stresses of the foam multiplied by a SF equal to 4 are lower than the relative ultimate tensile and compression strength of the material. The previous consideration is valid for both the Three-Hinged Arc and the Two-Hinged one. The foam sturdiness criterion is satisfied,
  - **Rigid skin (Carbon)**: Compression stresses of the rigid skin multiplied by a SF equal to 4 are lower than the critical buckling stress of wrinkling provided by the second empirical formula. As mentioned by the requirement is sufficient that the compression stresses are lower than only one of the formulas, therefore the requirement is satisfied.

- **Load condition 4**, Load to keep the habitat in the folded configuration. The established curvature radius for this analysis is 3 m. Figures 11.19 and 11.20 show the meaning of the curvature radius with the "R" terms.
  - **Flexible skin (Dyneema)**: As mentioned by the requirement "When compressed, Dyneema layers in the MadFlex, reach the buckling condition, therefore no compressive Sturdiness requirement is needed."
  - **Foam**: Tensile stresses of the foam are lower than the relative ultimate compression strength of the material both for the the Three-Hinged Arc and the Two-Hinged one. However even if the established radius of curvature is high, compression stresses of the foam are not lower than the relative ultimate compression strength of the material. The solutions to solve these issues are explained in the section 10.3:
  - **Rigid skin (Carbon)**: Tensile stresses of the rigid skin multiplied by a SF equal to 4 are lower than the ultimate tensile strength of the carbon. The previous consideration is valid for both the Three-Hinged Arc and the Two-Hinged one. The rigid skin sturdiness criterion is satisfied.

11.4.4 Stiffness requirements

Considerations about the two sub-requirements.

- The displacements of both the analysed structures allow a residual habitat height of 3.417 m for the Three-Hinged Arch and 3.43 m for the Two-Hinged one. The previous heights are great enough to allow the movement of the astronauts inside the module when an accidental or planned depressurization happens and avoid the sliding or the regolith bags above it. Therefore the first sub-requirement is satisfied.
- A flexural stiffness between $4.62244 \cdot 10^7$ and $1.2684 \cdot 10^8$ is needed to reach acceptable displacement of the floor.

11.4.5 External environmental requirements

Regolith abrasion

Considerations about the two sub-requirements.

- Both the analysed structures show the flexible skin (Dyneema) facing outwards for the overall surface of the arch's vault (Three-Hinged Arch) or part of it (Two-Hinged Arch) in order to optimize the Madflex orientation when structures have to withstand load condition 3. The previous orientation does not satisfy the first sub-requirement. Therefore as mentioned by section 8.4 an additional coverage in MadFlex, with carbon facing outwards is needed to protect the flexible layer from abrasion phenomena.
- To satisfy the requirement about the habitat deployability a MadFlex floor with the rigid skin facing downwards has to be employed. The previous configuration satisfies also the second sub-requirement of this section.

Vibration

Requirement not analysed in this Thesis

11.4.6 Payload requirements

Faring diameter

Results obtained to answer at this requirement are provided by the structural analysis carry out for the load condition 4. As mentioned in the paragraph about the "Sturdiness criterion" for load condition 4, the established radius of curvature in the analysis is 3 m. With the previous value the total length of the habitat (higher dimension of the folded habitat section) is around 6 m for the Three-Hinged Arch and 6.5 m for the Two-Hinged one. However as also mentioned before the compressive stresses in the foam exceed the ultimate compression strength of the chosen material, therefore the solution explained in section 10.3 for the foam has to be adopted. Employing the previously mentioned solution the radius of curvature of the habitat can also be lower. The latter consideration could lead at the possibility to store more than one module in the same transversal plane of the faring. An in-depth analysis is needed to understand how it would be possible to place more than one module on the same transversal plane of the faring.

Fairing height

Considering the data reported in the requirement explanation:

1. SLS block 1B cargo can accommodate 2 modules 9 meters long,
2. SLS block 1B cargo can accommodate 2 modules 9 meters long,
3. SLS block 2 can accommodate 3 modules 9 meters long.

Fairing volume

The satisfaction of the requirement is based on the radius of curvature reached by each habitat. However if the two previous requirements are satisfied also this can have the same status.

Maximum transportable mass

The proper mass of the preliminary design and the one of each material, which MadFlex is composed, is shown below:

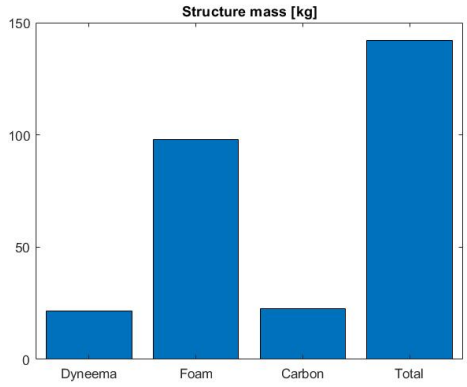

Figure 11.21: Overall mass of the structure and the one of each material

At the previous masses have to be added the mass of the floor, not considered in the analysis. Its contribution can be approximatively 2/3 of the total mass of the habitat. However the overall mass of the structure (142 kg), adding also the floor (94.6 kg), is very low (236.6 kg). Therefore:

- The SLS block 1 cargo can ideally transport 114 habitats without considering equipments for habitat pressurization and deployment,
- The SLS block 1B cargo can ideally transport 177 habitats without considering equipments for habitat pressurization and deployment,
- The SLS block 2 can ideally transport 194 habitats without considering equipments for habitat pressurization and deployment,

What can be understood from the previous data is that the major limiting factor is the volume occupied by the habitat in the folding position an therefore the radius of curvature that is possible to reach in the folded configuration.

Vibration

Requirement not analysed in this Thesis

11.4.7 Thermal protection requirement

Thickness of regolith shield

As shown by the table 11.1 the thickness of the regolith cover is 2.5 m therefore the requirement is satisfied.

11.4.8 Micro-meteorites protection requirements

Thickness of regolith shield

As mentioned in the next paragraph the radiation protection requirement is satisfied therefore also this requirement is satisfied.

11.4.9 Radiation protection requirements

Thickness of regolith shield

As shown by the table 11.1 the thickness of the regolith cover is 2.5 m therefore the requirement is satisfied.

11.4.10 Summary of Requirements

Architectural requirements			
Item	**Requirement**	**Status**	**Notes**
Volume per person	120 m^3	Satisfied	Each habitat can ensure the required free space for 1.3 person
Habitat height (radius)	3.5 m	Satisfied	
Habitat length	9 m	Satisfied	
Floor area per person	40 m^2	Satisfied	Each habitat can ensure the required free floor area for 1.3 person
Habitat shape	Habitat must be deployable	Satisfied	

Environmental requirement (ECLS)			
Item	**Requirement**	**Status**	**Notes**
Internal pressure	1 atm ($1.013 \cdot 10^5$ Pa) dual-gas atmosphere (oxygen (21%, nitrogen)	not analysed	Presence of an internal pressure of 1 atm ($1.013 \cdot 10^5$ Pa) is consider as a load condition
Temperature	22.2°C - 23.9°C (72°F - 75°F) (295,35 K - 297,05 K)	not analysed	
Humidity	60% relative humidity (corresponding to approximately 0.2 psi of water vapour pressure)	not analysed	
Noise	$<$ 50 dB	not analysed	

Ventilation	Forced ventilation is required with an air flow rates of 0.08-0.2 m / s.	not analysed	
Ionizing radiation	See tables in paragraph 5.2.5	Satisfied	By applying a 2.5 m thickness regolith cover above the habitat

Structural requirements

Item	Requirement	Status	Notes
Safety Factor	4	Applied	for load conditions 2 and 3
Load conditions	1. Internal pressure only; 2. Internal pressure plus regolith cover load; 3. Regolith cover load only; 4. Load used to keep the habitat in folded. configuration.	Satisfied	Load condition 1 is not considered because it is less critical than the other.
Sturdiness criterion	Internal stresses of the structure generated by the ultimate loads, must be lower than the ultimate strength of each material of which the structure is composed.	Satisfied	Completely satisfied if solutions mentioned in section 10.3 are applied

Stiffness criterion	• Arch: Under the ultimate load, the deformation of the structure must allow the movement of the astronauts in it and avoid the sliding of the regolith bags, compromising the radiation shielding. • Tie of the Arch: It must have an adequate stiffness to avoid an excessive deformation of habitat floor under ultimate load proper of second load condition.	Satisfied	

External environmental requirements			
Item	**Requirement**	**Status**	**Notes**
Regolith abrasion	• Vault of the structure: The MadFLex layer in contact with the regolith, placed on the top of the habitat, must be the rigid one because it is more resistant to abrasive phenomena caused by regolith. • Floor of the structure: The MadFlex layer facing downwards must be the rigid one because of its high abrasive and punctual resistance.	Satisfied	To satisfy the first sub-requirement an additional coverage in MadFlex, with carbon facing outwards is needed to protect the flexible layer from abrasion phenomena.

Vibration	Vibrations produced by the movement of astronauts inside the habitat or by the payloads and equipments must be mitigated, avoiding their transmission at the regolith bags since movement of the latter can produce laceration and degradation in the bags and structure below.	not analysed	

Payload requirements			
Item	**Requirement**	**Status**	**Notes**
faring diameter	7.5 m (24.6 ft) or 9.1 m (29.9 ft)	Satisfied	By applying to the foam the solutions explain in section 10.3 lower radious of curvature can be reached and more than one module can be stored on the same transversal plane of the faring .
Fairing height	19,1 m (62.7 ft) or 27,4 m (90 ft)	Satisfied	
Fairing volume	1. SLS block 1 cargo: 229.9 m^3 (8118 ft^3); 2. SLS block 1B cargo: 621.1 m^3 (21930 ft^3); 3. SLS block 2: 988 m^3 (34910 ft^3).	Satisfied	See the consideration in the relative paragraph

Maximum transportable mass	1. SLS block 1 cargo: 27 t (59.5k lbs); 2. SLS block 1B cargo: 42 t (92.5k lbs); 3. SLS block 2: 46 t (101.4k lbs) [56].	Satisfied	The main limiting factor is the volume occupied by the habitat
Vibrations	Resonance frequencies of the payload must be far from the ones generated by the launcher and atmospheric phenomena.	not analysed	

Thermal protection requirements

Item	Requirement	Status	Notes
Thickness of regolith shield	50 to 100 cm	Satisfied	

Micro-meteorites protection requirements

Item	Requirement	Status	Notes
Thickness of regolith shield	If the habitat is protected from radiation, it will be adequately protected for micrometeorite damages	Satisfied	

Radiation protection requirements

Item	Requirement	Status	Notes
Thickness of regolith shield	2.5 m of regolith cover would be sufficient to keep the annual dose of radiation at 5 rem	Satisfied	

Appendix A

This appendix shows the First script.

```
%Structural preliminar analysis

clc
close all
clear all

%Dati
r=3.5; %raggio habitat[m]
s_r=2.5; % s_r spessore regolite [m]
g_l=9.81/6; % acccellerazione di gravita' della luna [
    m/s^2]
b=0.5; %profondita' dell'arco, lunghezza habitat [m]
rho_r=1600; % densita' regolite [kg/m^3]
N=19; %numero punti della discretizzazione SOLO NUMERI
     DISPARI, sia per calcolo sollecitazioni che PLV
N_theta=100; % numero punti usati per creare grafico
    dopo intermoplazione, per maggiore definizione
SF=4; % safety factor preso da "Structural Design of a
     Lunar Habitat"


%Calcolo aree regolite

% sistema di riferimento cartesiano con asse x
    parallelo ad apertura
% dell'arco e y ortogonale ad esso.

r_r=r+s_r; % r_r raggio regolite

% calcolo i punti di disxcretizzazione come
    equidistanziati lungo linea
% media dell'arco, lungo ds dunque
theta_disc=linspace(0,pi,N); % discretizzo in modo da
    avere angoli equispaziati
p_disc=fliplr(r*cos(theta_disc)); %p punti di
    discretizzazione che vanno da -r ad r, centrato in
    0 per integrale funzione, semicerchio
```

```
d_theta=diff(theta_disc); % angolo di distanza fra i
    vari punti
theta_int=theta_disc(1:end-1)+d_theta(1)/2; % angoli
    di interpolazion/integrazione, dove andranno poi
    collocati i carichi equivalenti dei carichi
    cncentrati
p_int=fliplr(r*cos(theta_int)); %punti reativi agli
    angoli precedenti

% calcolo punti per sistema di riferimento posizionato
    nell'estremo
% sinistro dell'arco e dunque da 0 a 2r
x_disc=r-r*cos(theta_disc);
y_disc=r*sin(theta_disc);
ds_disc=r*theta_disc;
phi_int=(pi/2-theta_int);
d_ds_disc=diff(ds_disc);

%stessa cosa per i punti di interpolazione/
    integrazione
x_int=r-r*cos(theta_int);
y_int=r*sin(theta_int);
ds_int=r*theta_int;
phi_disc=(pi/2-theta_disc);

%calcolo area di ugni trapezio di discretizzazione
f=@(x) sqrt(r.^2-x.^2);
g=@(x) sqrt(r_r.^2-x.^2);

for k=1:length(p_disc)-1
    in_r(k)=integral(g,p_disc(k),p_disc(k+1)); %
        integrali semi circonfernza con regolite
    in(k)=integral(f,p_disc(k),p_disc(k+1)); %
        integrali semi circonfernza senza regolite
    in_a(k)=in_r(k)-in(k); %area di ogni trapezio
        della discretizzazione
end

%Calcolo forza esercitata di ogni rapezio di regolite
    nella discretizzazione
P_car_int= in_a*b*rho_r*g_l;   %carico puntuale
    discretizzato agente nei punti di interpolazione
    int [N]

%Calcolo funzione del carico punti interpolazione,
    centrali nell'intervallo di interpolazione
theta_t=linspace(0,pi,N_theta);
dss=r*theta_t;
p_xx=fliplr(r*cos(theta_t));
```

```
c=polyfit(p_int,P_car_int,length(p_int)-1);
p_yy=polyval(c,p_xx);

% c=polyfit(ds_int,P_car_int,length(p_int)-1);
% p_yy=polyval(c,dss);

figure(1)
plot(p_xx,p_yy,'b')

%calcolo reazioni vincolari con carichi distribuiti
   effettivi della
%discretizzazione e seguendo principio esposto nel
   libro Theory of Arched
%Structures pag 57

%Calcolo delle reazioni vincolari verticali dell'arco.
    Rferendoci al metodo
%della trave di sostituzione o riferimento, le
   reazioni verticali dell'arco sono pari
%a quelle della trave e dato che siamo in un caso di
   simmetria dei carichi
%esse sono uguali e pari a meta' del carico verticale
   dell'arco. pag 58
%libro citato prima.

Va=sum(P_car_int)/2;
Vb=Va;

% alternativa che porta allo stesso risultato
% Vb=(P_car_int*x_int')/(2*r);
% Va=Vb;

% Calcolo delle reazioni vincolari orizzontali
   equazione di equilibrio
% ausiliaria su cerniera all'apice dell'arco

M_c1=0; %momento in c, riferimento a teoria pag 58
   libro
for k=1:N/2 %lo calcolo solo fino ad N/2, cioe' il
   numero intero prima della meta', in quanto l'arco e
   ' caricato simmetricamente
    M_c1=M_c1+P_car_int(k)*p_int(k);
end
M_c=M_c1+Va*r;
Ha=M_c/r;
Hb=-Ha;

%CALCOLO CARATTERISTICHE SOLLECITAZIONE
%momento flettente
```

```
for k=1:length(ds_disc)-2
    M(k)=Va*x_disc(k+1)-P_car_int(1:k)*(x_disc(k+1)-
        x_int(1:k))'-Ha*y_disc(k+1);
end
M=[0,M,0];
Myy=spline(ds_disc,M,dss);
M_int=spline(ds_disc,M,ds_int);

figure(2)
plot(dss,Myy,'b',ds_disc,M,'*',ds_int,M_int,'*')
title('Diagramma del Momento flettente')

%SFORZO DI TAGLIO

for k=1:length(ds_disc)-1
   T(k)=(Va-sum(P_car_int(1:k)))*cos(phi_disc(k+1))-Ha
      *sin(phi_disc(k+1));
end

T=[-Ha,T];
Tyy=spline(ds_disc,T,dss);
T_int=spline(ds_disc,T,ds_int);

figure(3)
plot(dss,Tyy,'b',ds_disc,T,'*',ds_int,T_int,'*')
title('Diagramma del Taglio')

%SFORZO NORMALE

for k=1:length(ds_disc)-1
   N_s(k)=-(Va-sum(P_car_int(1:k)))*sin(phi_disc(k+1))
      -Ha*cos(phi_disc(k+1));
end

N_s=[-Va,N_s];
N_syy=spline(ds_disc,N_s,dss);
N_s_int=spline(ds_disc,N_s,ds_int);

figure(4)
plot(dss,N_syy,'b',ds_disc,N_s,'*',ds_int,N_s_int,'*')
title('Diagramma dello Sforzo Normale')

%% CALCOLO MATRICI DI RIGIDEZZA A,B,D,At MADFLEX
clc

%Dati strati madflex
%sistema di riferimento con x lungo larghezza piastra
   e y lungo profondita'
%Dati strato di carbonio
```

```
theta_c=[30 -30 30 -30]; % [gradi] inserire l'
    orientamento delle fibre
s_c=[0.28 0.28 0.28 0.28]*10^-3; % [m] inserire
    spessore singoli strati, il numero di componenti
    nel vettore theta deve coincidere con il numero di
    questo
E_Lc_t= 324*10^9; % [N/m^2] modulo elastico
    longitudinale a TRAZIONE delle fibre
E_Lc_c= E_Lc_t/100*90 ; % [N/m^2] modulo elastico
    longitudinale a COMPRESSIONE delle fibre, 10%
    minore di quello a trazione
E_Tc=2.9*10^9; % [N/m^2] modulo elastico nella
    direzione trasversale alle fibre
G_LTc= 5.5*10^9; % [N/m^2] modulo elastico di taglio
    direzione xy
ni_LTc=0.3; % modulo di poisson
rho_c=1.79*10^3; %[kg/m^3] densita' del carbonio
sigma_rc_t=6.6*10^9; % [Pa] sigma di rottura del
    carbonio a trazione

%Dati strato schiuma (Rohacell 110 WF)
theta_s=0; % [gradi]
s_s=80*10^-3; % [m] spessore schiuma
E_s_t=180*10^6; % [N/m^2] modulo elastico a TRAZIONE
    schiuma
E_s_c=(180/164*82.3)*10^6; % [N/m^2] modulo elastico a
     COMPRESSIONE schiuma
G_s=70*10^6; % [N/m^2] modulo elastico di taglio
rho_s=110; % densita' della schiuma [kg/m^3]
sigma_rs_t=3.7*10^6; % [Pa] sigam di rottura della
    schiuma a trazione
sigma_rs_c=3.6*10^6; % [Pa] sigma di rottura della
    schiuma a compressione

%Dati stato di dyneema
theta_d=[-30 30 -30 30]; % [gradi] inserire l'
    orientamento delle fibre
s_d=[0.5 0.5 0.5 0.5]*10^-3; % [m] inserire spessore
    singoli strati, il numero di componenti nel vettore
     theta deve coincidere con il numero di questo
E_Ld_t= 100*10^9; % [N/m^2] modulo elastico
    longitudinale a TRAZIONE delle fibre
E_Ld_c= 0.1; % [N/m^2] modulo elastico longitudinale a
     COMPRESSIONE delle fibre preso nullo
E_Td=0.1*10^9; % [N/m^2] modulo elastico nella
    direzione trasversale alle fibre
G_LTd= 0.2*10^9; % [N/m^2] modulo elastico di taglio
    direzione xy
ni_LTd=0.05; % modulo di poisson
rho_d=0.98*10^3; %[kg/m^3] densita' del dyneema
```

```
sigma_rd_t=3.3*10^9; % [Pa] sigma di rottura del
    dyneema a trazione


% calcolo hs per materiale normale con carbonio su
    faccia superiore
hst_1=[s_c s_s s_d]; %vettore spessore strati
hs_f1=sum(hst_1); %vettore spessore totale degli
    strati
hsi_1=-hs_f1/2; %posizione faccia inferiore composito
    con assi centrati al centro dello spessore
hss_1=hs_f1/2; %posizione faccia superiore composito
    con assi centrati al centro dello spessore

for k=1:length(hst_1)
    hs_f1(k+1)=hs_f1(k)-hst_1(k);
end

hs_f1=hs_f1+hsi_1;
hs_1=fliplr(hs_f1);

% calcolo hs per materiale ribaltato con carbonio su
    faccia inferiore
hst_2=fliplr([s_c s_s s_d]); %vettore spessore strati
hs_f2=sum(hst_2); %vettore spessore totale degli
    strati
hsi_2=-hs_f2/2; %posizione faccia inferiore composito
    con assi centrati al centro dello spessore
hss_2=hs_f2/2; %posizione faccia superiore composito
    con assi centrati al centro dello spessore

for k=1:length(hst_2)
    hs_f2(k+1)=hs_f2(k)-hst_2(k);
end

hs_f2=hs_f2+hsi_2;
hs_2=fliplr(hs_f2);


% CASO 1) carbonio TRAZIONATO (faccia superiore),
    dyneema TRAZIONATO (faccia inferiore).
% CASO 2) carbonio COMPRESSO  (faccia superiore),
    dyneema TRAZIONATO (faccia inferiore).
% CASO 3) carbonio TRAZIONATO (faccia superiore),
    dyneema COMPRESSO  (faccia inferiore).
% CASO 4) carbonio COMPRESSO  (faccia superiore),
    dyneema COMPRESSO  (faccia inferiore).
% CASO 5) dyneema TRAZIONATO (faccia superiore),
    carbonio TRAZIONATO (faccia inferiore).
```

```
% CASO 6) dyneema TRAZIONATO (faccia superiore),
    carbonio COMPRESSO  (faccia inferiore).
% CASO 7) dyneema COMPRESSO  (faccia superiore),
    carbonio TRAZIONATO (faccia inferiore).
% CASO 8) dyneema COMPRESSO  (faccia superiore),
    carbonio COMPRESSO  (faccia inferiore).

hs=[hs_1' hs_1' hs_1' hs_1' hs_2' hs_2' hs_2' hs_2'];

theta=[flipud(pi/180*[theta_c theta_s theta_d]')
    flipud(pi/180*[theta_c theta_s theta_d]') flipud(pi
    /180*[theta_c theta_s theta_d]') flipud(pi/180*[
    theta_c theta_s theta_d]')...
              pi/180*[theta_c theta_s theta_d]'
                        pi/180*[theta_c theta_s
                  theta_d]'        pi/180*[theta_c
                  theta_s theta_d]'          pi/180*[
                  theta_c theta_s theta_d]'];

E_L=[flipud([E_Lc_t*ones(1,length(theta_c)) E_s_t*ones
    (1,length(theta_s)) E_Ld_t*ones(1,length(theta_d))
    ]')...
      flipud([E_Lc_c*ones(1,length(theta_c)) E_s_t*ones
         (1,length(theta_s)) E_Ld_t*ones(1,length(
         theta_d))]')...
      flipud([E_Lc_t*ones(1,length(theta_c)) E_s_t*ones
         (1,length(theta_s)) E_Ld_c*ones(1,length(
         theta_d))]')...
      flipud([E_Lc_c*ones(1,length(theta_c)) E_s_c*ones
         (1,length(theta_s)) E_Ld_c*ones(1,length(
         theta_d))]')...
             [E_Lc_t*ones(1,length(theta_c)) E_s_t*ones
                (1,length(theta_s)) E_Ld_t*ones(1,
                length(theta_d))]'...
             [E_Lc_c*ones(1,length(theta_c)) E_s_t*ones
                (1,length(theta_s)) E_Ld_t*ones(1,
                length(theta_d))]'...
             [E_Lc_t*ones(1,length(theta_c)) E_s_t*ones
                (1,length(theta_s)) E_Ld_c*ones(1,
                length(theta_d))]'...
             [E_Lc_c*ones(1,length(theta_c)) E_s_c*ones
                (1,length(theta_s)) E_Ld_c*ones(1,
                length(theta_d))]'];


E_T=[flipud([E_Tc*ones(1,length(theta_c)) E_s_t*ones
    (1,length(theta_s)) E_Td*ones(1,length(theta_d))]')
    ...
      flipud([E_Tc*ones(1,length(theta_c)) E_s_t*ones
         (1,length(theta_s)) E_Td*ones(1,length(theta_d
```

```
        ))]')...
     flipud([E_Tc*ones(1,length(theta_c)) E_s_t*ones
        (1,length(theta_s)) E_Td*ones(1,length(theta_d
        ))]')...
     flipud([E_Tc*ones(1,length(theta_c)) E_s_c*ones
        (1,length(theta_s)) E_Td*ones(1,length(theta_d
        ))]')...
            [E_Tc*ones(1,length(theta_c)) E_s_t*ones
               (1,length(theta_s)) E_Td*ones(1,length(
               theta_d))]'...
            [E_Tc*ones(1,length(theta_c)) E_s_t*ones
               (1,length(theta_s)) E_Td*ones(1,length(
               theta_d))]'...
            [E_Tc*ones(1,length(theta_c)) E_s_t*ones
               (1,length(theta_s)) E_Td*ones(1,length(
               theta_d))]'...
            [E_Tc*ones(1,length(theta_c)) E_s_c*ones
               (1,length(theta_s)) E_Td*ones(1,length(
               theta_d))]'];


G_LT=[flipud([G_LTc*ones(1,length(theta_c)) G_s*ones
   (1,length(theta_s)) G_LTd*ones(1,length(theta_d))
   ]')...
      flipud([G_LTc*ones(1,length(theta_c)) G_s*ones
         (1,length(theta_s)) G_LTd*ones(1,length(
         theta_d))]')...
      flipud([G_LTc*ones(1,length(theta_c)) G_s*ones
         (1,length(theta_s)) G_LTd*ones(1,length(
         theta_d))]')...
      flipud([G_LTc*ones(1,length(theta_c)) G_s*ones
         (1,length(theta_s)) G_LTd*ones(1,length(
         theta_d))]')...
            [G_LTc*ones(1,length(theta_c)) G_s*ones
               (1,length(theta_s)) G_LTd*ones(1,
               length(theta_d))]'...
            [G_LTc*ones(1,length(theta_c)) G_s*ones
               (1,length(theta_s)) G_LTd*ones(1,
               length(theta_d))]'...
            [G_LTc*ones(1,length(theta_c)) G_s*ones
               (1,length(theta_s)) G_LTd*ones(1,
               length(theta_d))]'...
            [G_LTc*ones(1,length(theta_c)) G_s*ones
               (1,length(theta_s)) G_LTd*ones(1,
               length(theta_d))]'];


ni_LT=[flipud([ni_LTc*ones(1,length(theta_c)) 0*ones
   (1,length(theta_s)) ni_LTd*ones(1,length(theta_d))
   ]')...
```

```
        flipud([ni_LTc*ones(1,length(theta_c)) 0*ones
            (1,length(theta_s)) ni_LTd*ones(1,length(
            theta_d))]')...
        flipud([ni_LTc*ones(1,length(theta_c)) 0*ones
            (1,length(theta_s)) ni_LTd*ones(1,length(
            theta_d))]')...
        flipud([ni_LTc*ones(1,length(theta_c)) 0*ones
            (1,length(theta_s)) ni_LTd*ones(1,length(
            theta_d))]')...
                [ni_LTc*ones(1,length(theta_c)) 0*ones
                    (1,length(theta_s)) ni_LTd*ones(1,
                    length(theta_d))]'...
                [ni_LTc*ones(1,length(theta_c)) 0*ones
                    (1,length(theta_s)) ni_LTd*ones(1,
                    length(theta_d))]'...
                [ni_LTc*ones(1,length(theta_c)) 0*ones
                    (1,length(theta_s)) ni_LTd*ones(1,
                    length(theta_d))]'...
                [ni_LTc*ones(1,length(theta_c)) 0*ones
                    (1,length(theta_s)) ni_LTd*ones(1,
                    length(theta_d))]'];

for x=1:size(E_L,2)

ni_TL(:,x)=ni_LT(:,x).*E_T(:,x)./E_L(:,x);

A_1=zeros(3,3);
B_1=zeros(3,3);
D_1=zeros(3,3);

for k=1:size(theta,1)
Qp=[E_L(k,x)/(1-ni_LT(k,x)*ni_TL(k,x))        ni_LT(k,x
    )*E_T(k,x)/(1-ni_LT(k,x)*ni_TL(k,x))    0
     ni_LT(k,x)*E_T(k,x)/(1-ni_LT(k,x)*ni_TL(k,x))
         E_T(k,x)/(1-ni_LT(k,x)*ni_TL(k,x))      0
              0                          0
                  G_LT(k,x)];

lambda_k=[   (cos(theta(k,x)))^2       (sin(theta(k,x)
    ))^2           2*cos(theta(k,x))*sin(theta(k,x))
             (sin(theta(k,x)))^2       (cos(theta(k,x))
                )^2          -2*cos(theta(k,x))*sin(
                theta(k,x))
          -cos(theta(k,x))*sin(theta(k,x))  cos(theta(k
             ,x))*sin(theta(k,x))  (cos(theta(k,x)))
             ^2-(sin(theta(k,x)))^2];

Qk= inv(lambda_k)*Qp*(inv(lambda_k))';

cA=hs(k+1,x)-hs(k,x);
```

```
cB=0.5*(hs(k+1,x)^2-hs(k,x)^2);
cD=1/3*(hs(k+1,x)^3-hs(k,x)^3);

A_1=A_1+cA*Qk;
B_1=B_1+cB*Qk;
D_1=D_1+cD*Qk;

end

A(x)=A_1(1,1);
B(x)=B_1(1,1);
D(x)=D_1(1,1);

%matrici di rigidezza non per unita' di lunghezza
   poiche' moltiplicate per
%profondita'
A_nu(x)=A(x)*b;
B_nu(x)=B(x)*b;
D_nu(x)=D(x)*b;

%calcolo del centroide
y_c(x)=B(x)/A(x);

%nuove posizioni degli strati rispetto al centroide
hs_c(:,x)=hs(:,x)-y_c(x);

%Matrici di rigidezza relative al centroide
A_1c=zeros(3,3); %con c agiunto si indica le matrici
   rispetto al centroide
B_1c=zeros(3,3);
D_1c=zeros(3,3);

for k=1:size(theta,1)
Qp=[E_L(k,x)/(1-ni_LT(k,x)*ni_TL(k,x))        ni_LT(k,x
   )*E_T(k,x)/(1-ni_LT(k,x)*ni_TL(k,x))    0
    ni_LT(k,x)*E_T(k,x)/(1-ni_LT(k,x)*ni_TL(k,x))
       E_T(k,x)/(1-ni_LT(k,x)*ni_TL(k,x))       0
            0                          0
               G_LT(k,x)];

lambda_k=[   (cos(theta(k,x)))^2       (sin(theta(k,x)
   ))^2            2*cos(theta(k,x))*sin(theta(k,x))
            (sin(theta(k,x)))^2       (cos(theta(k,x))
               )^2           -2*cos(theta(k,x))*sin(
               theta(k,x))
         -cos(theta(k,x))*sin(theta(k,x))  cos(theta(k
            ,x))*sin(theta(k,x))  (cos(theta(k,x)))
            ^2-(sin(theta(k,x)))^2];

Qk= inv(lambda_k)*Qp*(inv(lambda_k))';
```

```
cA=hs_c(k+1,x)-hs_c(k,x);
cB=0.5*(hs_c(k+1,x)^2-hs_c(k,x)^2);
cD=1/3*(hs_c(k+1,x)^3-hs_c(k,x)^3);

A_1c=A_1c+cA*Qk;
B_1c=B_1c+cB*Qk;
D_1c=D_1c+cD*Qk;

end

A_c(x)=A_1c(1,1);
B_c(x)=B_1c(1,1); % solo B_1c(1,1) viene nullo, giusto
    in quanto il centroide non l'abbiamo trovato
   dividendo tutta la matrice B per A
D_c(x)=D_1c(1,1);

%matrici di rigidezza non per unita' di lunghezza
   poiche' moltiplicate per
%profondita'

A_cnu(x)=A_c(x)*b;
B_cnu(x)=B_c(x)*b;
D_cnu(x)=D_c(x)*b;

end


% Calcolo della matrice At per la rigidezza al taglio
   secondo Allen non per
% unita' di lunghezza
d_allen=hst_1(length(theta_c)+length(s_s))+sum(s_c)/2+
   sum(s_d)/2;
At_nu=G_s*d_allen^2*b/s_s;


%% CALCOLO DELLE TENSIONI SU FACCIA SUPERIORE ED
   INFERIORE
clc

% la convenzione del sistema di riferimento usata ora
   nel calcolo delle
% epsilon e sigma e' diversa dalla precedente. Ora si
   ha x nella direzione
% dell'asse della trave, y entrante nel foglio e z
   rivolta verso l'alto. Ne
% consegue che se il momento prima era negativo, per
   avere lo stesso
% effetto ora deve essere positivo, lo sforzo normale
   rimane invariato in
```

```
% questa nuova convenzione.

N_s_es=N_s;
M_es=-M;

hs_f=flipud(hs);
theta_f=flipud(theta);
E_L_f=flipud(E_L); %le colonne identificano i casi
   mentre le righe i moduli elastici assunti dai
   materiali nel caso considerato, strato superiore
   prime 4 colonne carbonio, poi dyneema, foam sempre
   su 5 riga, faccia inferiore dyneema per prime 4
   colonne poi carbonio
E_T_f=flipud(E_T);
G_LT_f=flipud(G_LT);
ni_LT_f=flipud(ni_LT);
ni_TL_f=flipud(ni_TL);

hs_es=zeros(size(hs_f,1)+size(hs_f,1)-2,size(hs_f,2));
    %posizione degli strati per calcolo delle epsilo e
    sigma
hs_es([1 3:2:end-1 end],:)=hs_f;
hs_es(2:2:end-2,:)=hs_f(2:end-1,:);
Qk1_1_es=zeros(size(hs_f,1)+size(hs_f,1)-2,1);
Aree=[hst_1' hst_1' hst_1' hst_1' hst_2' hst_2' hst_2'
    hst_2']*b;
hs_fmedia=(hs_f(1:end-1,:)+hs_f(2:end,:))/2;

toll_sigma=10^1; %tolleranza minima voluta tra la
   somma di tutti i valori delle sigma sommate tra di
   loro al ciclo precedente con quelle del ciclo
   appena effettuato
t_it_max=3; %numero di cicli massimo che si vuole
   avere nel ciclo di calcolo dei casi, epsilon e
   sigma
j_is=1*ones(1,length(x_disc)); %compilando j assumera
   sulle colonne indicate da k, il caso che la
   stazione assumera' alla prossima iterazione e sulle
    righe i valori assunti da j nelle varie iterazioni

flag=0; %NON TOCCARE QUESTI VALORI
flag_rib=zeros(1,length(x_disc)); %NON TOCCARE QUESTI
   VALORI flag relativo al ribaltamento di ogni
   sezione, se assume valore uno l'ordine dei
   materiali e' stato ribaltato
t=1;    %NON TOCCARE QUESTI VALORI
sigma_old=zeros(size(hs_es,1),length(x_disc)); %NON
   TOCCARE QUESTI VALORI
n_it_max_rib=1; %NON TOCCARE QUESTI VALORI, numero
   massimo di cicli che si vuole avere per ribaltare
```

```
    il materiale al fine di sfruttare il dinema in
    trazione e carbonio in compressione, ne basta
    solitamente uno.

% ciclo piu' esterno che gestisce il ribaltamento del
    materiale per
% sfruttare il dynema attivo e quindi in trazione.
    NECESSARIO FARE SEMPRE
% RUN in quanto calcella le informazioni precedenti
    con clear alle close
% all, E NON RUN SECTION, in quanto la funzione fliplr
     potrebbe creare dei
% problemi nei cicli for
for n_rib=1:(n_it_max_rib+1)

% ciclo che gestisce il calcolo in modo iterativo dei
    casi effettivi in cui
% lavora il materiale, le epsilon e le sigma in esso
    secondo il modello
% della trave di timoshenko
% while t<t_it_max+1 && flag==0
while t<t_it_max+1 && flag==0

for x=1:length(x_disc)
Mat=[A_nu(j_is(t,x)) B_nu(j_is(t,x))
     B_nu(j_is(t,x)) D_nu(j_is(t,x))]; %matrice
Car=[N_s_es(x) M_es(x)]'; %vettore dei carichi nel
    punto della discretizzazione
epsilon_0k(:,x)=Mat\Car; %vettore con epsilon_0 e la
    curvatura k

%k come indice per il ciclo indica il punto in cui il
    ciclo sta calcolando
%gli stress, cioe' i punti scritti come x_disc

epsilon(:,x)=epsilon_0k(1,x)+hs_es(:,j_is(t,x)).*
    epsilon_0k(2,x);

Qk1_1=zeros(size(theta_f,1),1);

for z=1:size(theta_f,1)
Qp1_es=[E_L_f(z,j_is(t,x))/(1-ni_LT_f(z,j_is(t,x))*
    ni_TL_f(z,j_is(t,x)))        ni_LT_f(z,j_is(t,x))*
    E_T_f(z,j_is(t,x))/(1-ni_LT_f(z,j_is(t,x))*ni_TL_f(
    z,j_is(t,x)))    0
     ni_LT_f(z,j_is(t,x))*E_T_f(z,j_is(t,x))/(1-ni_LT_f
         (z,j_is(t,x))*ni_TL_f(z,j_is(t,x)))     E_T_f(z
         ,j_is(t,x))/(1-ni_LT_f(z,j_is(t,x))*ni_TL_f(z,
         j_is(t,x)))      0
```

```
            0                          0
                G_LT_f(z,j_is(t,x))];

lambda_k1_es=[   (cos(theta_f(z,j_is(t,x))))^2       (
   sin(theta_f(z,j_is(t,x))))^2           2*cos(
   theta_f(z,j_is(t,x)))*sin(theta_f(z,j_is(t,x)))
            (sin(theta_f(z,j_is(t,x))))^2       (cos(
               theta_f(z,j_is(t,x))))^2          -2*
               cos(theta_f(z,j_is(t,x)))*sin(theta_f(z
               ,j_is(t,x)))
         -cos(theta_f(z,j_is(t,x)))*sin(theta_f(z,j_is
            (t,x)))  cos(theta_f(z,j_is(t,x)))*sin(
            theta_f(z,j_is(t,x)))  (cos(theta_f(z,j_is
            (t,x))))^2-(sin(theta_f(z,j_is(t,x))))^2];

Qk1_es= inv(lambda_k1_es)*Qp1_es*(inv(lambda_k1_es))';
Qk1_1(z,1)=Qk1_es(1,1);

end

Qk1_1_es(1:2:end-1,1)=Qk1_1;  % Qk1_1 modificata per
   poter essere moltiplicata alle epsilon che nascono
   dal vettore hs_es cioe' epsilon modificato che le
   posizioni intermedie duplicate per fare la media
   delle sigma.
Qk1_1_es(2:2:end,1)=Qk1_1;

sigma(:,x)=epsilon(:,x).*Qk1_1_es;
sigma_m(:,x)=(sigma(1:2:end-1,x)+sigma(2:2:end,x))/2;
   %calcolo delle sigma medie a coppie

if flag_rib==0
sigma_mm(1,x)=(sigma_m(1,x)+sigma_m(length(theta_c),x)
   )/2; % calcolo delle sigma medie a coppie delle
   coppie per ciclo di if
sigma_mm(2,x)=(sigma_m(end,x)+sigma_m(end-length(
   theta_d)+1,x))/2;
else
sigma_mm(1,x)=(sigma_m(1,x)+sigma_m(length(theta_d),x)
   )/2; % calcolo delle sigma medie a coppie delle
   coppie per ciclo di if
sigma_mm(2,x)=(sigma_m(end,x)+sigma_m(end-length(
   theta_c)+1,x))/2;
end

N_strati(:,x)=sigma_m(:,x).*Aree(:,j_is(t,x));
N_ris=sum(N_strati,1);
N_err(t,x)=abs(N_s_es(x)-N_ris(x));
```

```
% correzione per nel calcolo della risultante del
    momento, si cerca a quale altezza si trova la sigma
     media calcolata per avere la z precisa e non
    quella media cioe' zero.
% m_sigma_foam(1,x)=-hst(length(theta_c)+1)/(sigma(2*
    length(theta_c)+2,x)+sigma(2*length(theta_c)+1,x));
     %calcolo pendenza retta nel foam
% z_m_foam(1,x)=m_sigma_foam(1,x)*(sigma_m(length(
    theta_c)+1,x)-sigma(2*length(theta_c)+1,x))+hs_es(
    length(theta_c)+1); % z della sigma media nel foam
% hs_fmedia_f=hs_fmedia;
% hs_fmedia_f(length(theta_c)+1)=z_m_foam(1,x); % hs
    media flirpata con inserimento della z del foam
%nel caso qualcosa fosse sbagliato cancellare
    ragoinamenti sul foam e riportare hs_fmedia_f ad
    hs_fmedia

M_strati(:,x)=sigma_m(:,x).*Aree(:,j_is(t,x)).*
    hs_fmedia(:,j_is(t,x));
M_ris=sum(M_strati,1);
M_err(t,x)=abs(M_es(x)-M_ris(x));

if sigma_mm(1,x)>=0 && sigma_mm(2,x)>=0
     if flag_rib(x)==0
        j_is(t+1,x)=1;
     else
        j_is(t+1,x)=5;
     end
else
     if sigma_mm(1,x)<0 && sigma_mm(2,x)>0
          if flag_rib(x)==0
             j_is(t+1,x)=2;
          else
             j_is(t+1,x)=7;
          end
     else
          if sigma_mm(1,x)>0 && sigma_mm(2,x)<0
               if flag_rib(x)==0
                  j_is(t+1,x)=3;
               else
                  j_is(t+1,x)=6;
               end
          else
               if sigma_mm(1,x)<=0 && sigma_mm(2,x)<=0
                  if flag_rib(x)==0
                      j_is(t+1,x)=4;
                   else
                      j_is(t+1,x)=8;
                   end
               else
```

```
            end
        end
    end
end

end

if abs(sum(sum(sigma,1),2)-sum(sum(sigma_old),2))>
   toll_sigma
       t=t+1;
       sigma_old=sigma;
    else
        flag=1; %il flag=1 fa uscire fuori dal ciclo,
           indica cioe' quando si e' raggiunto il
           livello di accuratezza voluto
        t=t+1;
    end

end

% Salvataggio delle vecchie variabili per incominciare
    il ciclo di
% ribaltamento dell'ordine del materiale
j_old=j_is;
j_is=zeros(1,length(x_disc));
sigma_ris=sigma;

% Ciclo ribaltamento ordine materiale
for x_interno=1:length(x_disc)

if j_old(end,x_interno)==1
   %nulla
   j_is(1,x_interno)=1;
else
    if j_old(end,x_interno)==2
    %nulla
    j_is(1,x_interno)=2;
    else
        if j_old(end,x_interno)==3
           % scrivi j relativa al nuovo caso ribaltato
           j_is(1,x_interno)=6;
           flag_rib(x_interno)=1;
        else
            if j_old(end,x_interno)==4
                if x_interno<=ceil(N/2)
                    if j_old(end,x_interno+1)==3
                       % scrivi j relativa al nuovo
                           caso ribaltato
                       j_is(1,x_interno)=8;
                       flag_rib(x_interno)=1;
```

```
                    else
                        j_is(1,x_interno)=4;
                    end
                else
                    if j_old(end,x_interno-1)==3
                        % scrivi j relativa al nuovo
                            caso ribaltato
                        j_is(1,x_interno)=8;
                        flag_rib(x_interno)=1;
                    else
                        j_is(1,x_interno)=4;
                    end
                end
            else

            end
        end
    end
end

end

flag=0; %NON TOCCARE QUESTI VALORI
t=1;    %NON TOCCARE QUESTI VALORI
sigma_old=zeros(size(hs_es,1),length(x_disc)); %NON
    TOCCARE QUESTI VALORI

end


% j_old
% j
% N_err
% M_err
% epsilon_0k
% sigma
% flag
% flag_rib

j_is=j_old;
sigma_ris;
flag_rib_is=flag_rib;

% figure(5)
% plot(epsilon,hs_es(:,j(end,:)),'-*')
% title('Andamento delle epsilon')
%
% figure(6)
% plot(sigma(:,1),hs_es(:,j(end,1)),'-*')
% title('Andamento delle sigma')
```

```
%
% figure(7)
% plot(sigma_m(:,1),hs_fmedia(:,j(end,1)),'-*')
% title('Andamento delle sigma medie')

%% CALCOLO SPOSTAMENTI ARCO A TRE CERNIERE CON PLV
clc

% con r si indicheranno le caratteristiche di
   sollecitazione del sistema reale (r)
% con u si indicheranno le caratteristiche di
   sollecitazione del sistema unitario o fittizio,
   cioe' con carico unitario (u)

ds_plv=zeros(1,length(ds_disc)+length(ds_int));
ds_plv(1:2:end)=ds_disc;
ds_plv(2:2:end-1)=ds_int;

d_ds_plv=diff(ds_plv);
d_ds_int=diff(ds_int);

x_plv=zeros(1,length(x_disc)+length(x_int));
x_plv(1:2:end)=x_disc;
x_plv(2:2:end-1)=x_int;

y_plv=zeros(1,length(y_disc)+length(y_int));
y_plv(1:2:end)=y_disc;
y_plv(2:2:end-1)=y_int;

phi_plv=zeros(1,length(phi_disc)+length(phi_int));
phi_plv(1:2:end)=phi_disc;
phi_plv(2:2:end-1)=phi_int;

M_plv_r=zeros(1,length(M)+length(M_int));
M_plv_r(1:2:end)=M;
M_plv_r(2:2:end-1)=M_int;

% figure(8)
% plot(ds_plv,M_plv_r,'-*')
% title('Momento flettente')

T_plv_r=zeros(1,length(T)+length(T_int));
T_plv_r(1:2:end)=T;
T_plv_r(2:2:end-1)=T_int;

% figure(9)
% plot(ds_plv,T_plv_r,'-*')
% title('Taglio')

N_s_plv_r=zeros(1,length(N_s)+length(N_s_int));
```

```
N_s_plv_r(1:2:end)=N_s;
N_s_plv_r(2:2:end-1)=N_s_int;

% figure(10)
% plot(ds_plv,N_s_plv_r,'-*')
% title('Taglio')

% calcolo delle reazioni vincolari e caratteristiche
   del sistema unitario
% per forze unitarie poste in ds_disc

%k indica le posizioni delle forze unitarie lungo l'
   apertura dell'arco e
%collocate in ds_disc

for k=1:length(ds_disc)
%calcolo reazioni vincolari verticali
    Vb_plv_u(k,1)=1*x_disc(k)/(2*r);
    Va_plv_u(k,1)=1-Vb_plv_u(k,1);

%calcolo reazioni vincolari orizzontali
 if k<length(x_disc)/2
    H_plv_u(k,1)=(Va_plv_u(k,1)*r-1*abs(r-x_disc(k)))/
       r;
 else
    H_plv_u(k,1)=(Vb_plv_u(k,1)*r-1*abs(r-x_disc(k)))/
       r;
 end

%calcolo caratteristiche di sollecitazione
    %Momento
    for J=1:length(ds_plv)-2
    if x_plv(J+1)-x_disc(k)>0
    M_plv_u(J)=Va_plv_u(k,1)*x_plv(J+1)-1*(x_plv(J+1)-
       x_disc(k))-H_plv_u(k,1)*y_plv(J+1); %le J
       indicano le colonne e salvano i valori per ogni
        sezione dell'arco in x_disc, le k sono le
       righe che indicano il variare della forza
       unitaria nelle x_int
    else
    M_plv_u(J)=Va_plv_u(k,1)*x_plv(J+1)-H_plv_u(k,1)*
       y_plv(J+1);
    end

    end
    M_plv1_u(k,:)=[0,M_plv_u,0];

 %Sforzo di taglio

    for J=1:length(ds_plv)-1
```

```
        if x_plv(J+1)-x_disc(k)>0
        T_plv_u(J)=(Va_plv_u(k,1)-1)*cos(phi_plv(J+1))
            -H_plv_u(k,1)*sin(phi_plv(J+1));
        else
        T_plv_u(J)=Va_plv_u(k,1)*cos(phi_plv(J+1))-
            H_plv_u(k,1)*sin(phi_plv(J+1));
        end
    end
    T_plv1_u(k,:)=[-H_plv_u(k,1),T_plv_u];

  %Sforzo normale

    for J=1:length(ds_plv)-1
        if x_plv(J+1)-x_disc(k)>=0
        N_s_plv_u(J)=-(Va_plv_u(k,1)-1)*sin(phi_plv(J
            +1))-H_plv_u(k,1)*cos(phi_plv(J+1));
        else
        N_s_plv_u(J)=-Va_plv_u(k,1)*sin(phi_plv(J+1))-
            H_plv_u(k,1)*cos(phi_plv(J+1));
        end
    end

    N_s_plv1_u(k,:)=[-Va_plv_u(k,1),N_s_plv_u];


 % Calcolo del plv
for J=1:length(ds_disc)-2
    caso=j_is(end,J+1);

    % Contributo PLV Momento
    w_M=d_ds_plv(1)/(2*D_cnu(caso))*[1; 2; 1];
    I_t_M(k,J)=[M_plv_r(2+(J-1)*2)*M_plv1_u(k,2+(J-1)
        *2) M_plv_r(3+(J-1)*2)*M_plv1_u(k,3+(J-1)*2)
        M_plv_r(4+(J-1)*2)*M_plv1_u(k,4+(J-1)*2)]*w_M;

    % Contributo PLV Taglio
    w_T=d_ds_plv(1)/(2*5/6*At_nu)*[1; 2; 1];
    I_t_T(k,J)=[T_plv_r(2+(J-1)*2)*T_plv1_u(k,2+(J-1)
        *2) T_plv_r(3+(J-1)*2)*T_plv1_u(k,3+(J-1)*2)
        T_plv_r(4+(J-1)*2)*T_plv1_u(k,4+(J-1)*2)]*w_T;

    % Contributo PLV Sforzo Normale
    w_N_s=d_ds_plv(1)/(2*A_cnu(caso))*[1; 2; 1];
    I_t_N_s(k,J)=[N_s_plv_r(2+(J-1)*2)*N_s_plv1_u(k
        ,2+(J-1)*2) N_s_plv_r(3+(J-1)*2)*N_s_plv1_u(k
        ,3+(J-1)*2) N_s_plv_r(4+(J-1)*2)*N_s_plv1_u(k
        ,4+(J-1)*2)]*w_N_s;

end
    % Contributo PLV Momento
```

```
    w_i_M=d_ds_plv(1)/(2*D_cnu(j_is(end,1)))*[1; 1];
    I_t_i_M(k,1)=[M_plv_r(1)*M_plv1_u(k,1) M_plv_r(2)*
        M_plv1_u(k,2)]*w_i_M;

    w_f_M=d_ds_plv(1)/(2*D_cnu(j_is(end,end)))*[1; 1];
    I_t_f_M(k,1)=[M_plv_r(end-1)*M_plv1_u(k,end-1)
        M_plv_r(end)*M_plv1_u(k,end)]*w_f_M;

    % Contributo PLV Taglio
    w_i_T=d_ds_plv(1)/(2*5/6*At_nu)*[1; 1];
    I_t_i_T(k,1)=[T_plv_r(1)*T_plv1_u(k,1) T_plv_r(2)*
        T_plv1_u(k,2)]*w_i_T;

    w_f_T=d_ds_plv(1)/(2*5/6*At_nu)*[1; 1];
    I_t_f_T(k,1)=[T_plv_r(end-1)*T_plv1_u(k,end-1)
        T_plv_r(end)*T_plv1_u(k,end)]*w_f_T;

    % Contributo PLV Sforzo Normale
    w_i_N_s=d_ds_plv(1)/(2*A_cnu(j_is(end,1)))*[1; 1];
    I_t_i_N_s(k,1)=[N_s_plv_r(1)*N_s_plv1_u(k,1)
        N_s_plv_r(2)*N_s_plv1_u(k,2)]*w_i_N_s;

    w_f_N_s=d_ds_plv(1)/(2*A_cnu(j_is(end,end)))*[1;
        1];
    I_t_f_N_s(k,1)=[N_s_plv_r(end-1)*N_s_plv1_u(k,end
        -1) N_s_plv_r(end)*N_s_plv1_u(k,end)]*w_f_N_s;


It_tot_M(k,1)=sum([I_t_i_M(k,1) I_t_M(k,:) I_t_f_M(k
    ,1)]);
It_tot_T(k,1)=sum([I_t_i_T(k,1) I_t_T(k,:) I_t_f_T(k
    ,1)]);
It_tot_N_s(k,1)=sum([I_t_i_N_s(k,1) I_t_N_s(k,:)
    I_t_f_N_s(k,1)]);

 end

It_tot_M;
It_tot_T;
It_tot_N_s;

%calcolo di quanto e' la percentuale dello spostamento
     dovuta al taglio
%rispetto al momento preso come 100%
perc_contributo_taglio=100/max(It_tot_M)*max(It_tot_T)
    ;
perc_contributo_s_normale=100/max(It_tot_M)*max(
    It_tot_N_s);

It_tot=sum([It_tot_M It_tot_T It_tot_N_s],2);
```

```
y_spost=y_disc-It_tot';

figure(11)
plot(ds_plv,M_plv1_u(ceil(N/2),:),'-*')
title('Diagramma del Momento flettente per sistema
   unitario (u)')

figure(12)
plot(ds_plv,T_plv1_u(ceil(N/2),:),'-*')
title('Diagramma del Taglio per sistema unitario (u)')

figure(13)
plot(ds_plv,N_s_plv1_u(ceil(N/2),:),'-*')
title('Diagramma dello Sforzo Normale per sistema
   unitario (u)')

figure(14)
plot(x_disc,y_disc,'b-*',x_disc,y_spost,'r-*')
title('Deformata sotto carico')


%% Calcolo soluzione iperstatica
clc

%Divido l'arco in due semiarchi ed inserisco in ognuno
    una coppia
%concentrata all'estremita' libera di verso opposto e
   congruente con la
%convenzione posistiva del momento.

%calcolo reazioni vincolari verticali
Vb_ip_1=0;
Va_ip_1=0;

%calcolo reazioni vincolari orizzontali
Ha_ip_1=-1/r;
Hb_ip_1=1/r;

%calcolo caratteristiche di sollecitazione
%Momento
    for J=1:length(x_plv)-2
        M_ip_1(J)=-Ha_ip_1*y_plv(J+1); %le J indicano
           le colonne e salvano i valori per ogni
           sezione dell'arco in x_disc, le k sono le
           righe che indicano il variare della forza
           unitaria nelle x_int
    end

     M_ip1_1=[0,M_ip_1,0];
```

```
figure(15)
plot(ds_plv,M_ip1_1,'-*')
title('Diagramma del Momento flettente per sistema
    unitario (1)')

%Sforzo di taglio

    for J=1:length(x_plv)-1
        T_ip_1(J)=-Ha_ip_1*sin(phi_plv(J+1));
    end

    T_ip1_1=[-Ha_ip_1,T_ip_1];

figure(16)
plot(ds_plv,T_ip1_1,'-*')
title('Diagramma del Taglio per sistema unitario (1)')

%Sforzo normale

    for J=1:length(x_plv)-1
        N_s_ip_1(J)=-Ha_ip_1*cos(phi_plv(J+1));
    end

    N_s_ip1_1=[-Va_ip_1,N_s_ip_1];

figure(17)
plot(ds_plv,N_s_ip1_1,'-*')
title('Diagramma dello Sforzo Normale per sistema
    unitario (1)')

% Calcolo (M(0)*M(1))/EI

%  calcolo il numeratore della frazione per trovare l'
    incognita
%  iperstatica X, simila a formula 5.43 in calcolo
    spostamenti
%  iperstatiche 05 di fondamenti di mecchanica
    strutturale

for J=1:length(ds_disc)-2 %tolgo due casi di cui uno
    presente su un semi intervallo iniziale e l'altro
    sul semi intervallo finale
    caso=j_is(end,J+1);

    % Contributo PLV Momento
    w_M=d_ds_plv(1)/(2*D_cnu(caso))*[1; 2; 1];
    It_ip_M_num(J)=[M_plv_r(2+(J-1)*2)*M_ip1_1(2+(J-1)
        *2) M_plv_r(3+(J-1)*2)*M_ip1_1(3+(J-1)*2)
        M_plv_r(4+(J-1)*2)*M_ip1_1(4+(J-1)*2)]*w_M;
```

```
    % Contributo PLV Taglio
    w_T=d_ds_plv(1)/(2*5/6*At_nu)*[1; 2; 1];
    It_ip_T_num(J)=[T_plv_r(2+(J-1)*2)*T_ip1_1(2+(J-1)
       *2) T_plv_r(3+(J-1)*2)*T_ip1_1(3+(J-1)*2)
       T_plv_r(4+(J-1)*2)*T_ip1_1(4+(J-1)*2)]*w_T;

    % Contributo PLV Sforzo Normale
    w_N_s=d_ds_plv(1)/(2*A_cnu(caso))*[1; 2; 1];
    It_ip_N_s_num(J)=[N_s_plv_r(2+(J-1)*2)*N_s_ip1_1
       (2+(J-1)*2) N_s_plv_r(3+(J-1)*2)*N_s_ip1_1(3+(J
       -1)*2) N_s_plv_r(4+(J-1)*2)*N_s_ip1_1(4+(J-1)
       *2)]*w_N_s;

end

% Contributo PLV Momento
wi_M=d_ds_plv(1)/(2*D_cnu(j_is(end,1)))*[1; 1];
It_iM_ip_num=[M_plv_r(1)*M_ip1_1(1) M_plv_r(2)*M_ip1_1
   (2)]*wi_M;

wf_M=d_ds_plv(1)/(2*D_cnu(j_is(end,end)))*[1; 1];
It_fM_ip_num=[M_plv_r(end-1)*M_ip1_1(end-1) M_plv_r(
   end)*M_ip1_1(end)]*wf_M;

% Contributo PLV Taglio
wi_T=d_ds_plv(1)/(2*5/6*At_nu)*[1; 1];
It_iT_ip_num=[T_plv_r(1)*T_ip1_1(1) T_plv_r(2)*T_ip1_1
   (2)]*wi_T;

wf_T=d_ds_plv(1)/(2*5/6*At_nu)*[1; 1];
It_fT_ip_num=[T_plv_r(end-1)*T_ip1_1(end-1) T_plv_r(
   end)*T_ip1_1(end)]*wf_T;

% Contributo PLV Sforzo Normale
wi_N_s=d_ds_plv(1)/(2*A_cnu(j_is(end,1)))*[1; 1];
It_iN_s_ip_num=[N_s_plv_r(1)*N_s_ip1_1(1) N_s_plv_r(2)
   *N_s_ip1_1(2)]*wi_N_s;

wf_N_s=d_ds_plv(1)/(2*A_cnu(j_is(end,end)))*[1; 1];
It_fN_s_ip_num=[N_s_plv_r(end-1)*N_s_ip1_1(end-1)
   N_s_plv_r(end)*N_s_ip1_1(end)]*wf_N_s;


It_tot_M_ip_num=sum([It_iM_ip_num   It_ip_M_num
   It_fM_ip_num]);
It_tot_T_ip_num=sum([It_iT_ip_num   It_ip_T_num
   It_fT_ip_num]);
It_tot_N_s_ip_num=sum([It_iN_s_ip_num   It_ip_N_s_num
     It_fN_s_ip_num]);
```

```
%calcolo di quanto e' la percentuale dello spostamento
    dovuta al taglio
%rispetto al momento preso come 100%
perc_contributo_taglio_num=100/It_tot_M_ip_num*
   It_tot_T_ip_num;
perc_contributo_s_normale_num=100/It_tot_M_ip_num*
   It_tot_N_s_ip_num;

It_tot_ip_num=sum([It_tot_M_ip_num It_tot_T_ip_num
   It_tot_N_s_ip_num],2);



%  calcolo il denominatore della frazione per trovare
   l'incognita iperstatica X
for J=1:length(ds_disc)-2 %tolgo due casi di cui uno
   presente su un semi intervallo iniziale e l'altro
   sul semi intervallo finale
    caso=j_is(end,J+1);

    % Contributo PLV Momento
    w_M=d_ds_plv(1)/(2*D_cnu(caso))*[1; 2; 1];
    It_ip_M_den(J)=[M_ip1_1(2+(J-1)*2)*M_ip1_1(2+(J-1)
       *2) M_ip1_1(3+(J-1)*2)*M_ip1_1(3+(J-1)*2)
       M_ip1_1(4+(J-1)*2)*M_ip1_1(4+(J-1)*2)]*w_M;

    % Contributo PLV Taglio
    w_T=d_ds_plv(1)/(2*5/6*At_nu)*[1; 2; 1];
    It_ip_T_den(J)=[T_ip1_1(2+(J-1)*2)*T_ip1_1(2+(J-1)
       *2) T_ip1_1(3+(J-1)*2)*T_ip1_1(3+(J-1)*2)
       T_ip1_1(4+(J-1)*2)*T_ip1_1(4+(J-1)*2)]*w_T;

    % Contributo PLV Sforzo Normale
    w_N_s=d_ds_plv(1)/(2*A_cnu(caso))*[1; 2; 1];
    It_ip_N_s_den(J)=[N_s_ip1_1(2+(J-1)*2)*N_s_ip1_1
       (2+(J-1)*2) N_s_ip1_1(3+(J-1)*2)*N_s_ip1_1(3+(J
       -1)*2) N_s_ip1_1(4+(J-1)*2)*N_s_ip1_1(4+(J-1)
       *2)]*w_N_s;

end

% Contributo PLV Momento
wi_M=d_ds_plv(1)/(2*D_cnu(j_is(end,1)))*[1; 1];
It_iM_ip_den=[M_ip1_1(1)*M_ip1_1(1) M_ip1_1(2)*M_ip1_1
   (2)]*wi_M;

wf_M=d_ds_plv(1)/(2*D_cnu(j_is(end,end)))*[1; 1];
It_fM_ip_den=[M_ip1_1(end-1)*M_ip1_1(end-1) M_ip1_1(
   end)*M_ip1_1(end)]*wf_M;
```

```
% Contributo PLV Taglio
wi_T=d_ds_plv(1)/(2*5/6*At_nu)*[1; 1];
It_iT_ip_den=[T_ip1_1(1)*T_ip1_1(1) T_ip1_1(2)*T_ip1_1
    (2)]*wi_T;

wf_T=d_ds_plv(1)/(2*5/6*At_nu)*[1; 1];
It_fT_ip_den=[T_ip1_1(end-1)*T_ip1_1(end-1) T_ip1_1(
    end)*T_ip1_1(end)]*wf_T;

% Contributo PLV Sforzo Normale
wi_N_s=d_ds_plv(1)/(2*A_cnu(j_is(end,1)))*[1; 1];
It_iN_s_ip_den=[N_s_ip1_1(1)*N_s_ip1_1(1) N_s_ip1_1(2)
    *N_s_ip1_1(2)]*wi_N_s;

wf_N_s=d_ds_plv(1)/(2*A_cnu(j_is(end,end)))*[1; 1];
It_fN_s_ip_den=[N_s_ip1_1(end-1)*N_s_ip1_1(end-1)
    N_s_ip1_1(end)*N_s_ip1_1(end)]*wf_N_s;


It_tot_M_ip_den=sum([It_iM_ip_den   It_ip_M_den
    It_fM_ip_den]);
It_tot_T_ip_den=sum([It_iT_ip_den   It_ip_T_den
    It_fT_ip_den]);
It_tot_N_s_ip_den=sum([It_iN_s_ip_den   It_ip_N_s_den
     It_fN_s_ip_den]);

perc_contributo_taglio_den=100/It_tot_M_ip_den*
    It_tot_T_ip_den;
perc_contributo_s_normale_den=100/It_tot_M_ip_den*
    It_tot_N_s_ip_den;

It_tot_ip_den=sum([It_tot_M_ip_den It_tot_T_ip_den
    It_tot_N_s_ip_den],2);

X=-It_tot_ip_num/It_tot_ip_den;


% calcolo delle reazioni vincolari della travatura
    iperstatica attraverso
% la relazione Ha=Ha(0)+X*Ha(1)

%reazioni vincolari vericali
Vb_ip=Vb+X*Vb_ip_1;
Va_ip=Va+X*Va_ip_1;

%reazioni vincolari orizzontali
Ha_ip=Ha+X*Ha_ip_1;
Hb_ip=Hb+X*Hb_ip_1;

%diagramma momento flettente
```

```
M_ip=M_plv_r+X*M_ip1_1;

figure(18)
plot(ds_plv,M_ip,'-*')
title('Diagramma del Momento flettente per arco a due
    cerniere')

%diagramma taglio
T_ip=T_plv_r+X*T_ip1_1;

figure(19)
plot(ds_plv,T_ip,'-*')
title('Diagramma del taglio per arco a due cerniere')

%diagramma di sforzo normale
N_s_ip=N_s_plv_r+X*N_s_ip1_1;

figure(20)
plot(ds_plv,N_s_ip,'-*')
title('Diagramma dello sforzo normale per arco a due
    cerniere')


%% Calcolo delle sigma nell'arco iperstatico a due
    cerniere
clc

% epsilon e sigma e' diversa dalla precedente. Ora si
    ha x nella direzione
% dell'asse della trave, y entrante nel foglio e z
    rivolta verso l'alto. Ne
% consegue che se il momento prima era negativo, per
    avere lo stesso
% effetto ora deve essere positivo, lo sforzo normale
    rimane invariato in
% questoa nuova convenzione.

N_s_es_ip=N_s_ip(1:2:end);
M_es_ip=-M_ip(1:2:end);

hs_f=flipud(hs);
theta_f=flipud(theta);
E_L_f=flipud(E_L); %le colonne identificano i casi
    mentre le righe i moduli elastici assunti dai
    materiali nel caso considerato, strato superiore
    prime 4 colonne carbonio, poi dyneema, foam sempre
    su 5 riga, faccia inferiore dyneema per prime 4
    colonne poi carbonio
E_T_f=flipud(E_T);
G_LT_f=flipud(G_LT);
```

```
ni_LT_f=flipud(ni_LT);
ni_TL_f=flipud(ni_TL);

hs_es=zeros(size(hs_f,1)+size(hs_f,1)-2,size(hs_f,2));
    %posizione degli strati per calcolo delle epsilo e
    sigma
hs_es([1 3:2:end-1 end],:)=hs_f;
hs_es(2:2:end-2,:)=hs_f(2:end-1,:);
Qk1_1_es=zeros(size(hs_f,1)+size(hs_f,1)-2,1);
Aree=[hst_1' hst_1' hst_1' hst_1' hst_2' hst_2' hst_2'
    hst_2']*b;
hs_fmedia=(hs_f(1:end-1,:)+hs_f(2:end,:))/2;

toll_sigma=10^1; %tolleranza minima voluta tra la
   somma di tutti i valori delle sigma sommate tra di
   loro al ciclo precedente con quelle del ciclo
   appena effettuato
t_it_max=3; %numero di cicli massimo che si vuole
   avere nel ciclo di calcolo dei casi, epsilon e
   sigma
j_ip=1*ones(1,length(x_disc)); %compilando j assumera
   sulle colonne indicate da k, il caso che la
   stazione assumera' alla prossima iterazione e sulle
    righe i valori assunti da j nelle varie iterazioni

flag=0; %NON TOCCARE QUESTI VALORI
flag_rib=zeros(1,length(x_disc)); %NON TOCCARE QUESTI
   VALORI flag relativo al ribaltamento di ogni
   sezione, se assume valore uno l'ordine dei
   materiali e' stato ribaltato
t=1;    %NON TOCCARE QUESTI VALORI
sigma_old=zeros(size(hs_es,1),length(x_disc)); %NON
   TOCCARE QUESTI VALORI
n_it_max_rib=1; %NON TOCCARE QUESTI VALORI, numero
   massimo di cicli che si vuole avere per ribaltare
   il materiale al fine di sfruttare il dinema in
   trazione e carbonio in compressione, ne basta
   solitamente uno.

% ciclo piu' esterno che gestisce il ribaltamento del
   materiale per
% sfruttare il dynema attivo e quindi in trazione.
   NECESSARIO FARE SEMPRE
% RUN in quanto calcella le informazioni precedenti
   con clear alle close
% all, E NON RUN SECTION, in quanto la funzione fliplr
    potrebbe creare dei
% problemi nei cicli for
for n_rib=1:(n_it_max_rib+1)
```

```
% ciclo che gestisce il calcolo in modo iterativo dei
   casi effettivi in cui
% lavora il materiale, le epsilon e le sigma in esso
   secondo il modello
% della trave di timoshenko
% while t<t_it_max+1 && flag==0
while t<t_it_max+1 && flag==0

for x=1:length(x_disc)
Mat=[A_nu(j_ip(t,x)) B_nu(j_ip(t,x))
     B_nu(j_ip(t,x)) D_nu(j_ip(t,x))]; %matrice
Car=[N_s_es_ip(x) M_es_ip(x)]'; %vettore dei carichi
   nel punto della discretizzazione
epsilon_0k_ip(:,x)=Mat\Car; %vettore con epsilon_0 e
   la curvatura k

%k come indice per il ciclo indica il punto in cui il
   ciclo sta calcolando
%gli stress, cioe' i punti scritti come x_disc

epsilon_ip(:,x)=epsilon_0k_ip(1,x)+hs_es(:,j_ip(t,x))
   .*epsilon_0k_ip(2,x);

Qk1_1=zeros(size(theta_f,1),1);

for z=1:size(theta_f,1)
Qp1_es=[E_L_f(z,j_ip(t,x))/(1-ni_LT_f(z,j_ip(t,x))*
   ni_TL_f(z,j_ip(t,x)))       ni_LT_f(z,j_ip(t,x))*
   E_T_f(z,j_ip(t,x))/(1-ni_LT_f(z,j_ip(t,x))*ni_TL_f(
   z,j_ip(t,x)))    0
    ni_LT_f(z,j_ip(t,x))*E_T_f(z,j_ip(t,x))/(1-ni_LT_f
       (z,j_ip(t,x))*ni_TL_f(z,j_ip(t,x)))     E_T_f(z
       ,j_ip(t,x))/(1-ni_LT_f(z,j_ip(t,x))*ni_TL_f(z,
       j_ip(t,x)))      0
            0                          0
               G_LT_f(z,j_ip(t,x))];

lambda_k1_es=[   (cos(theta_f(z,j_ip(t,x))))^2       (
   sin(theta_f(z,j_ip(t,x))))^2           2*cos(
   theta_f(z,j_ip(t,x)))*sin(theta_f(z,j_ip(t,x)))
            (sin(theta_f(z,j_ip(t,x))))^2       (cos(
               theta_f(z,j_ip(t,x))))^2          -2*
               cos(theta_f(z,j_ip(t,x)))*sin(theta_f(z
               ,j_ip(t,x)))
         -cos(theta_f(z,j_ip(t,x)))*sin(theta_f(z,j_ip
            (t,x)))  cos(theta_f(z,j_ip(t,x)))*sin(
            theta_f(z,j_ip(t,x)))  (cos(theta_f(z,j_ip
            (t,x))))^2-(sin(theta_f(z,j_ip(t,x))))^2];

Qk1_es= inv(lambda_k1_es)*Qp1_es*(inv(lambda_k1_es))';
```

```
Qk1_1(z,1)=Qk1_es(1,1);

end

Qk1_1_es(1:2:end-1,1)=Qk1_1;  % Qk1_1 modificata per
    poter essere moltiplicata alle epsilon che nascono
    dal vettore hs_es cioe' epsilon modificato che le
    posizioni intermedie duplicate per fare la media
    delle sigma.
Qk1_1_es(2:2:end,1)=Qk1_1;

sigma_ip(:,x)=epsilon_ip(:,x).*Qk1_1_es;
sigma_m_ip(:,x)=(sigma_ip(1:2:end-1,x)+sigma_ip(2:2:
    end,x))/2; %calcolo delle sigma medie a coppie

if flag_rib==0
sigma_mm_ip(1,x)=(sigma_m_ip(1,x)+sigma_m_ip(length(
    theta_c),x))/2; % calcolo delle sigma medie a
    coppie delle coppie per ciclo di if
sigma_mm_ip(2,x)=(sigma_m_ip(end,x)+sigma_m_ip(end-
    length(theta_d)+1,x))/2;
else
sigma_mm_ip(1,x)=(sigma_m_ip(1,x)+sigma_m_ip(length(
    theta_d),x))/2; % calcolo delle sigma medie a
    coppie delle coppie per ciclo di if
sigma_mm_ip(2,x)=(sigma_m_ip(end,x)+sigma_m_ip(end-
    length(theta_c)+1,x))/2;
end

N_strati_ip(:,x)=sigma_m_ip(:,x).*Aree(:,j_ip(t,x));
N_ris_ip=sum(N_strati_ip,1);
N_err_ip(t,x)=abs(N_s_es_ip(x)-N_ris_ip(x));

% correzione per nel calcolo della risultante del
    momento, si cerca a quale  altezzo si trova la
    sigma media calcolata per avere la z precisa e non
    quella media cioe' zero.
% m_sigma_foam(1,x)=-hst(length(theta_c)+1)/(sigma(2*
    length(theta_c)+2,x)+sigma(2*length(theta_c)+1,x));
     %calcolo pendenza retta nel foam
% z_m_foam(1,x)=m_sigma_foam(1,x)*(sigma_m(length(
    theta_c)+1,x)-sigma(2*length(theta_c)+1,x))+hs_es(
    length(theta_c)+1); % z della sigma media nel foam
% hs_fmedia_f=hs_fmedia;
% hs_fmedia_f(length(theta_c)+1)=z_m_foam(1,x); % hs
    media flirpata con inserimento della z del foam
%nel caso qualcosa fosse sbagliato cancellare
    ragoinamenti sul foam e riportare hs_fmedia_f ad
    hs_fmedia
```

```
M_strati_ip(:,x)=sigma_m_ip(:,x).*Aree(:,j_ip(t,x)).*
    hs_fmedia(:,j_ip(t,x));
M_ris_ip=sum(M_strati_ip,1);
M_err_ip(t,x)=abs(M_es_ip(x)-M_ris_ip(x));

if sigma_mm_ip(1,x)>=0 && sigma_mm_ip(2,x)>=0
    if flag_rib(x)==0
       j_ip(t+1,x)=1;
    else
       j_ip(t+1,x)=5;
    end
else
    if sigma_mm_ip(1,x)<0 && sigma_mm_ip(2,x)>0
        if flag_rib(x)==0
           j_ip(t+1,x)=2;
        else
           j_ip(t+1,x)=7;
        end
    else
        if sigma_mm_ip(1,x)>0 && sigma_mm_ip(2,x)<0
            if flag_rib(x)==0
               j_ip(t+1,x)=3;
            else
               j_ip(t+1,x)=6;
            end
        else
            if sigma_mm_ip(1,x)<=0 && sigma_mm_ip(2,x)
               <=0
               if flag_rib(x)==0
                   j_ip(t+1,x)=4;
                else
                   j_ip(t+1,x)=8;
                end
            else
            end
        end
    end
end

end

if abs(sum(sum(sigma_ip,1),2)-sum(sum(sigma_old),2))>
    toll_sigma
       t=t+1;
       sigma_old=sigma_ip;
    else
        flag=1; %il flag=1 fa uscire fuori dal ciclo,
           indica cioe' quando si e' raggiunto il
           livello di accuratezza voluto
        t=t+1;
```

```
    end

end

% Salvataggio delle vecchie variabili per incominciare
    il ciclo di
% ribaltamento dell'ordine del materiale
j_old_ip=j_ip;
j_ip=zeros(1,length(x_disc));
sigma_ris_ip=sigma_ip;

% Ciclo ribaltamento ordine materiale nel caso di
   momento negativo secondo
% vecchia convenzione e positivo ora
for x_interno=1:length(x_disc)

% if M_es_ip(x_interno)>=0
    if j_old_ip(end,x_interno)==1
       %nulla
       j_ip(1,x_interno)=1;
    else
        if j_old_ip(end,x_interno)==2
        %nulla
        j_ip(1,x_interno)=2;
        else
            if j_old_ip(end,x_interno)==3
               % scrivi j relativa al nuovo caso
                  ribaltato
               j_ip(1,x_interno)=6;
               flag_rib(x_interno)=1;
            else
                if j_old_ip(end,x_interno)==4
                    if x_interno<=ceil(N/2)
                        if j_old_ip(end,x_interno+1)
                           ==3
                           % scrivi j relativa al
                              nuovo caso ribaltato
                           j_ip(1,x_interno)=8;
                           flag_rib(x_interno)=1;
                        else
                           j_ip(1,x_interno)=4;
                        end
                    else
                        if j_old_ip(end,x_interno-1)
                           ==3
                           % scrivi j relativa al
                              nuovo caso ribaltato
                           j_ip(1,x_interno)=8;
                           flag_rib(x_interno)=1;
                        else
```

```
                            j_ip(1,x_interno)=4;
                        end
                    end
                else
                    j_ip(1,x_interno)=j_old_ip(end,
                        x_interno);
                end
            end
        end
    end
% else
%     j_ip(1,x_interno)=j_old_ip(end,x_interno);
% end
end

flag=0; %NON TOCCARE QUESTI VALORI
t=1;    %NON TOCCARE QUESTI VALORI
sigma_old=zeros(size(hs_es,1),length(x_disc)); %NON
    TOCCARE QUESTI VALORI

end


% j_old_ip
% j_ip
% N_err_ip
% M_err_ip
% epsilon_0k_ip
% sigma_ip
% flag
% flag_rib

j_ip=j_old_ip;
sigma_ris_ip;
flag_rib_ip=flag_rib;

%% Calcolo spostamento dell'iperstatica
% come sistema reale prendo l'arco a due cerniere gia'
    risolto in precedenza
% in quanto iperstatico, mentre come sistema u il
    sistema di carichi
% unitari gia' utilizzato per calcolare lo spostamento
    dell'arco a tre
% cerniere.

% In primo luogo, il sistema (r) e' iperstatico per
    cui va risolto a sua volta mediante il PLV per
    ottenere le
% relative caratteristiche di sollecitazione. Quanto
    al sistema (u), a rigore anche questo dovrebbe
```

```
    essere
% iperstatico dato che ha gli stessi vincoli del
    sistema (r) ma un solo carico unitario
    corrispondente allo
% spostamento incognito. Va pero' ricordato che nella
    (5.7) il sistema (u) e' quello fittizio per cui e'
% necessario che sia solo equilibrato e non
    necessariamente congruente. Per (u) si puo' allora
    scegliere
% una condizione di vincolo non reale ma piu' semplice
     e isostatica, per esempio eliminando proprio il
% vincolo sovrabbondante

for k=1:length(ds_disc)

% Calcolo del plv
    % la sigla che accompagna tutte le variabili '
       ip_sp' significa 'iperstatica_spostamento'
for J=1:length(ds_disc)-2
    caso=j_ip(end,J+1);

    % Contributo PLV Momento
    w_M=d_ds_plv(1)/(2*D_cnu(caso))*[1; 2; 1];
    It_M_ip_sp(k,J)=[M_ip(2+(J-1)*2)*M_plv1_u(k,2+(J
       -1)*2) M_ip(3+(J-1)*2)*M_plv1_u(k,3+(J-1)*2)
       M_ip(4+(J-1)*2)*M_plv1_u(k,4+(J-1)*2)]*w_M;

    % Contributo PLV Taglio
    w_T=d_ds_plv(1)/(2*5/6*At_nu)*[1; 2; 1];
    It_T_ip_sp(k,J)=[T_ip(2+(J-1)*2)*T_plv1_u(k,2+(J
       -1)*2) T_ip(3+(J-1)*2)*T_plv1_u(k,3+(J-1)*2)
       T_ip(4+(J-1)*2)*T_plv1_u(k,4+(J-1)*2)]*w_T;

    % Contributo PLV Sforzo Normale
    w_N_s=d_ds_plv(1)/(2*A_cnu(caso))*[1; 2; 1];
    It_N_s_ip_sp(k,J)=[N_s_ip(2+(J-1)*2)*N_s_plv1_u(k
       ,2+(J-1)*2) N_s_ip(3+(J-1)*2)*N_s_plv1_u(k,3+(J
       -1)*2) N_s_ip(4+(J-1)*2)*N_s_plv1_u(k,4+(J-1)
       *2)]*w_N_s;

end

    % Contributo PLV Momento
    wi_M=d_ds_plv(1)/(2*D_cnu(j_ip(end,1)))*[1; 1];
    It_iM_ip_sp(k,1)=[M_ip(1)*M_plv1_u(k,1) M_ip(2)*
       M_plv1_u(k,2)]*wi_M;

    wf_M=d_ds_plv(1)/(2*D_cnu(j_ip(end,end)))*[1; 1];
    It_fM_ip_sp(k,1)=[M_ip(end-1)*M_plv1_u(k,end-1)
       M_ip(end)*M_plv1_u(k,end)]*wf_M;
```

```
    % Contributo PLV Taglio
    wi_T=d_ds_plv(1)/(2*5/6*At_nu)*[1; 1];
    It_iT_ip_sp(k,1)=[T_ip(1)*T_plv1_u(k,1) T_ip(2)*
        T_plv1_u(k,2)]*wi_T;

    wf_T=d_ds_plv(1)/(2*5/6*At_nu)*[1; 1];
    It_fT_ip_sp(k,1)=[T_ip(end-1)*T_plv1_u(k,end-1)
        T_ip(end)*T_plv1_u(k,end)]*wf_T;

    % Contributo PLV Sforzo Normale
    wi_N_s=d_ds_plv(1)/(2*A_cnu(j_ip(end,1)))*[1; 1];
    It_iN_s_ip_sp(k,1)=[N_s_ip(1)*N_s_plv1_u(k,1)
        N_s_ip(2)*N_s_plv1_u(k,2)]*wi_N_s;

    wf_N_s=d_ds_plv(1)/(2*A_cnu(j_ip(end,end)))*[1;
        1];
    It_fN_s_ip_sp(k,1)=[N_s_ip(end-1)*N_s_plv1_u(k,end
        -1) N_s_ip(end)*N_s_plv1_u(k,end)]*wf_N_s;


    It_tot_M_ip_sp(k,1)=sum([It_iM_ip_sp(k,1)
        It_M_ip_sp(k,:) It_fM_ip_sp(k,1)]);
    It_tot_T_ip_sp(k,1)=sum([It_iT_ip_sp(k,1)
        It_T_ip_sp(k,:) It_fT_ip_sp(k,1)]);
    It_tot_N_s_ip_sp(k,1)=sum([It_iN_s_ip_sp(k,1)
        It_N_s_ip_sp(k,:) It_fN_s_ip_sp(k,1)]);

end

It_tot_M_ip_sp;
It_tot_T_ip_sp;
It_tot_N_s_ip_sp;

%calcolo di quanto e' la percentuale dello spostamento
    dovuta al taglio
%rispetto al momento preso come 100%
perc_contributo_taglio_ip_sp=100/max(It_tot_M_ip_sp)*
    max(It_tot_T_ip_sp);
perc_contributo_s_normale_ip_sp=100/max(It_tot_M_ip_sp
    )*max(It_tot_N_s_ip_sp);

It_tot_ip_sp=sum([It_tot_M_ip_sp It_tot_T_ip_sp
    It_tot_N_s_ip_sp],2);
y_spost_ip=y_disc-It_tot_ip_sp';


figure(21)
plot(x_disc,y_disc,'b-*',x_disc,y_spost_ip,'r-*')
title('Deformata sotto carico arco a due cerniere')
```

```
%%
clc
% calcolo sigma di arrotolamento nell'isostatica
% convenzione, momento posistivo se asse del momento
    uscente dal foglio

% Spiegazione del processo
% 1) ribalto il vettore j_is dei casi diventando
    j_curv_is in modo da avere
% le rigidezze per il materiale piegato dal lato
    flessibile

% 2) calcolo la sigma e vado a convergenza trovando i
    veri casi che si
% hanno nel materiale nel caso arrotolato

% 3) Ricalcolo il momento con il nuovo j_curv_is

% il madflex va piegato dalla parte flesibile, quindi
    inverto il materiale
% nel senso opposto

for x=1:length(x_disc)

if j_is(end,x)==1
   j_curv_is(1,x)=4;
else
    if j_is(end,x)==2
       j_curv_is(1,x)=3;
    else
        if j_is(end,x)==3
           j_curv_is(1,x)=2;
        else
            if j_is(end,x)==4
               j_curv_is(1,x)=j_is(end,x);
            else
                if j_is(end,x)==5
                   j_curv_is(1,x)=8;
                else
                    if j_is(end,x)==6
                       j_curv_is(1,x)=7;
                    else
                        if j_is(end,x)==7
                           j_curv_is(1,x)=6;
                        else
                            j_curv_is(1,x)=j_is(end,x)
                                ;
                        end
```

```
                    end
                end
            end
        end
    end
end

end

j_curv_es_is=j_curv_is;

% calcolo del momento necessario per ottenere un certo
    raggio per
% l'isostatica, arco a tre cerniere

r_curv=(0.5:0.5:3.5); % raggio di curvatura
for k=1:length(r_curv)
    for J=1:length(x_disc)
        caso_curv=j_curv_is(end,J);
        M_curv_is(k,J)=D_cnu(caso_curv)/r_curv(k); % [
            Nm] matrice del momento per la curvatura,
            che lungo la riga tiene conto del momento
            per ogni x_disc, mentre sulle righe
            variando il raggio voluto
    end
end

figure(22)
plot(x_disc,M_curv_is,'-*')
legend('raggio 0.5 m','raggio 1 m','raggio 1.5 m','
   raggio 2 m','raggio 2.5 m','raggio 3 m','raggio 3.5
    m')
title('Momento relativo a curvatura arco 3C [Nm]')

% calcolo della coppia di forze necessarie per
   ottenere quel raggio con
% l'applicazione delle due forze a quella distanza.
   Dunque calcolo di F/2

F_curv_is=(1./r_curv)'.*M_curv_is;

figure(23)
plot(x_disc,F_curv_is,'-*')
legend('raggio 0.5 m','raggio 1 m','raggio 1.5 m','
   raggio 2 m','raggio 2.5 m','raggio 3 m','raggio 3.5
    m')
title('Forza relativa a curvatura arco 3C [N]')

% SCEGLIERE IL MOEMENTO CHE SI VUOLE ANALIZZARE per il
    calcolo delle sigma
```

```
% nel materiale, in altre parole il numero indicante
    la posizione della r
% di arrotolamento voluto nel vettore r_curv

N_r_curv_is=6; % solito =3

% calcolo delle sigma all'interno del materiale
    generate dal'arrotolamento
% nel verso flessibile del materiale per ISOSTATICA

% la convenzione del sistema di riferimento usata or
    nel calcolo delle
% epsilon e sigma e' diversa dalla precedente. Ora si
    ha x nella direzione
% dell'asse della trave, y entrante nel foglio e z
    rivolta verso l'alto. Ne
% consegue che se il momento prima era negativo, per
    avere lo stesso
% effetto ora deve essere positivo, lo sforzo normale
    rimane invariato in
% questoa nuova convenzione.

N_s_es_curv=zeros(1,N);
M_es_curv=-M_curv_is(N_r_curv_is,:);

hs_f=flipud(hs);
theta_f=flipud(theta);
E_L_f=flipud(E_L); %le colonne identificano i casi
    mentre le righe i moduli elastici assunti dai
    materiali nel caso considerato, strato superiore
    prime 4 colonne carbonio, poi dyneema, foam sempre
    su 5 riga, faccia inferiore dyneema per prime 4
    colonne poi carbonio
E_T_f=flipud(E_T);
G_LT_f=flipud(G_LT);
ni_LT_f=flipud(ni_LT);
ni_TL_f=flipud(ni_TL);

hs_es=zeros(size(hs_f,1)+size(hs_f,1)-2,size(hs_f,2));
    %posizione degli strati per calcolo delle epsilo e
    sigma
hs_es([1 3:2:end-1 end],:)=hs_f;
hs_es(2:2:end-2,:)=hs_f(2:end-1,:);
Qk1_1_es=zeros(size(hs_f,1)+size(hs_f,1)-2,1);
Aree=[hst_1' hst_1' hst_1' hst_1' hst_2' hst_2' hst_2'
    hst_2']*b;
hs_fmedia=(hs_f(1:end-1,:)+hs_f(2:end,:))/2;

toll_sigma=10^1; %tolleranza minima voluta tra la
    somma di tutti i valori delle sigma sommate tra di
```

```
   loro al ciclo precedente con quelle del ciclo
   appena effettuato
t_it_max=3; %numero di cicli massimo che si vuole
   avere nel ciclo di calcolo dei casi, epsilon e
   sigma

flag=0; %NON TOCCARE QUESTI VALORI
t=1;    %NON TOCCARE QUESTI VALORI
sigma_old=zeros(size(hs_es,1),length(x_disc)); %NON
   TOCCARE QUESTI VALORI


% ciclo che gestisce il calcolo in modo iterativo dei
   casi effettivi in cui
% lavora il materiale, le epsilon e le sigma in esso
   secondo il modello
% della trave di timoshenko
% while t<t_it_max+1 && flag==0
while t<t_it_max+1 && flag==0

for x=1:length(x_disc)
Mat=[A_nu(j_curv_es_is(t,x)) B_nu(j_curv_es_is(t,x))
     B_nu(j_curv_es_is(t,x)) D_nu(j_curv_es_is(t,x))];
         %matrice
Car=[N_s_es_curv(x) M_es_curv(x)]'; %vettore dei
   carichi nel punto della discretizzazione
epsilon_0k_curv(:,x)=Mat\Car; %vettore con epsilon_0 e
    la curvatura k

%k come indice per il ciclo indica il punto in cui il
   ciclo sta calcolando
%gli stress, cioe' i punti scritti come x_disc

epsilon_curv(:,x)=epsilon_0k_curv(1,x)+hs_es(:,
   j_curv_es_is(t,x)).*epsilon_0k_curv(2,x);

Qk1_1=zeros(size(theta_f,1),1);

for z=1:size(theta_f,1)
Qp1_es=[E_L_f(z,j_curv_es_is(t,x))/(1-ni_LT_f(z,
   j_curv_es_is(t,x))*ni_TL_f(z,j_curv_es_is(t,x)))
         ni_LT_f(z,j_curv_es_is(t,x))*E_T_f(z,
   j_curv_es_is(t,x))/(1-ni_LT_f(z,j_curv_es_is(t,x))*
   ni_TL_f(z,j_curv_es_is(t,x)))    0
    ni_LT_f(z,j_curv_es_is(t,x))*E_T_f(z,j_curv_es_is(
       t,x))/(1-ni_LT_f(z,j_curv_es_is(t,x))*ni_TL_f(z
       ,j_curv_es_is(t,x)))     E_T_f(z,j_curv_es_is(t
       ,x))/(1-ni_LT_f(z,j_curv_es_is(t,x))*ni_TL_f(z,
       j_curv_es_is(t,x)))      0
```

```
            0                          0
                G_LT_f(z,j_curv_es_is(t,x))];

lambda_k1_es=[   (cos(theta_f(z,j_curv_es_is(t,x))))^2
          (sin(theta_f(z,j_curv_es_is(t,x))))^2
             2*cos(theta_f(z,j_curv_es_is(t,x)))*sin(
   theta_f(z,j_curv_es_is(t,x)))
          (sin(theta_f(z,j_curv_es_is(t,x))))^2
                    (cos(theta_f(z,j_curv_es_is(t,x))
             ))^2          -2*cos(theta_f(z,
             j_curv_es_is(t,x)))*sin(theta_f(z,
             j_curv_es_is(t,x)))
        -cos(theta_f(z,j_curv_es_is(t,x)))*sin(
             theta_f(z,j_curv_es_is(t,x)))  cos(theta_f
             (z,j_curv_es_is(t,x)))*sin(theta_f(z,
             j_curv_es_is(t,x)))  (cos(theta_f(z,
             j_curv_es_is(t,x))))^2-(sin(theta_f(z,
             j_curv_es_is(t,x))))^2];

Qk1_es= inv(lambda_k1_es)*Qp1_es*(inv(lambda_k1_es))';
Qk1_1(z,1)=Qk1_es(1,1);

end

Qk1_1_es(1:2:end-1,1)=Qk1_1;  % Qk1_1 modificata per
   poter essere moltiplicata alle epsilon che nascono
   dal vettore hs_es cioe' epsilon modificato che le
   posizioni intermedie duplicate per fare la media
   delle sigma.
Qk1_1_es(2:2:end,1)=Qk1_1;

sigma_curv(:,x)=epsilon_curv(:,x).*Qk1_1_es;
sigma_m_curv(:,x)=(sigma_curv(1:2:end-1,x)+sigma_curv
   (2:2:end,x))/2; %calcolo delle sigma medie a coppie

if flag_rib_is==0
sigma_mm_curv(1,x)=(sigma_m_curv(1,x)+sigma_m_curv(
   length(theta_c),x))/2; % calcolo delle sigma medie
   a coppie delle coppie per ciclo di if
sigma_mm_curv(2,x)=(sigma_m_curv(end,x)+sigma_m_curv(
   end-length(theta_d)+1,x))/2;
else
sigma_mm_curv(1,x)=(sigma_m_curv(1,x)+sigma_m_curv(
   length(theta_d),x))/2; % calcolo delle sigma medie
   a coppie delle coppie per ciclo di if
sigma_mm_curv(2,x)=(sigma_m_curv(end,x)+sigma_m_curv(
   end-length(theta_c)+1,x))/2;
end
```

```
N_strati_curv(:,x)=sigma_m_curv(:,x).*Aree(:,
    j_curv_es_is(t,x));
N_ris_curv=sum(N_strati_curv,1);
N_err_curv(t,x)=abs(N_s_es_curv(x)-N_ris_curv(x));

% correzione per nel calcolo della risultante del
    momento, si cerca a quale  altezzo si trova la
    sigma media calcolata per avere la z precisa e non
    quella media cioe' zero.
% m_sigma_foam(1,x)=-hst(length(theta_c)+1)/(sigma(2*
    length(theta_c)+2,x)+sigma(2*length(theta_c)+1,x));
     %calcolo pendenza retta nel foam
% z_m_foam(1,x)=m_sigma_foam(1,x)*(sigma_m(length(
    theta_c)+1,x)-sigma(2*length(theta_c)+1,x))+hs_es(
    length(theta_c)+1); % z della sigma media nel foam
% hs_fmedia_f=hs_fmedia;
% hs_fmedia_f(length(theta_c)+1)=z_m_foam(1,x); % hs
    media flirpata con inserimento della z del foam
%nel caso qualcosa fosse sbagliato cancellare
    ragoinamenti sul foam e riportare hs_fmedia_f ad
    hs_fmedia

M_strati_curv(:,x)=sigma_m_curv(:,x).*Aree(:,
    j_curv_es_is(t,x)).*hs_fmedia(:,j_curv_es_is(t,x));
M_ris_curv=sum(M_strati_curv,1);
M_err_curv(t,x)=abs(M_es_curv(x)-M_ris_curv(x));

if sigma_mm_curv(1,x)>=0 && sigma_mm_curv(2,x)>=0
     if flag_rib_is(x)==0
        j_curv_es_is(t+1,x)=1;
     else
        j_curv_es_is(t+1,x)=5;
     end
else
     if sigma_mm_curv(1,x)<0 && sigma_mm_curv(2,x)>0
          if flag_rib_is(x)==0
             j_curv_es_is(t+1,x)=2;
          else
             j_curv_es_is(t+1,x)=7;
          end
     else
          if sigma_mm_curv(1,x)>0 && sigma_mm_curv(2,x)
              <0
               if flag_rib_is(x)==0
                  j_curv_es_is(t+1,x)=3;
               else
                  j_curv_es_is(t+1,x)=6;
               end
          else
```

```
            if sigma_mm_curv(1,x)<=0 && sigma_mm_curv
               (2,x)<=0
               if flag_rib_is(x)==0
                   j_curv_es_is(t+1,x)=4;
                else
                   j_curv_es_is(t+1,x)=8;
                end
            else
            end
        end
    end
end

end

    if abs(sum(sum(sigma_curv,1),2)-sum(sum(sigma_old)
       ,2))>toll_sigma
       t=t+1;
       sigma_old=sigma_curv;
    else
        flag=1; %il flag=1 fa uscire fuori dal ciclo,
           indica cioe' quando si e' raggiunto il
           livello di accuratezza voluto
        t=t+1;
    end

end

% j_curv_es_is
% N_err_curv
% M_err_curv
% epsilon_0k_curv
% sigma_curv
% flag
% flag_rib_is

% calcolo del momento necessario per ottenere un certo
    raggio per
% l'isostatica, arco a tre cerniere

    for J=1:length(x_disc)
        caso_curv=j_curv_es_is(end-1,J);
        M_curv_es_is(J)=D_cnu(caso_curv)/r_curv(
           N_r_curv_is); % [Nm] matrice del momento
           per la curvatura, che lungo la riga tiene
           conto del momento per ogni x_disc, mentre
           sulle righe variando il raggio voluto
    end

figure(24)
```

```
plot(x_disc,M_curv_es_is,'-*')
title('Momento relativo a curvatura arco 3C raggio
    selez [Nm]')

% calcolo della coppia di forze necessarie per
    ottenere quel raggio con
% l'applicazione delle due forze a quella distanza.
    Dunque calcolo di F/2

F_curv_es_is=(1/r_curv(N_r_curv_is))'.*M_curv_es_is;

figure(25)
plot(x_disc,F_curv_es_is,'-*')
title('Forza relativa a curvatura arco raggio selez 3C
    [N]')


%%
clc

% calcolo del momento necessario per ottenere un certo
    raggio per
% l'iperstatica, arco a due cerniere

for x=1:length(x_disc)

if j_ip(end,x)==1
   j_curv_ip(1,x)=4;
else
    if j_ip(end,x)==2
       j_curv_ip(1,x)=3;
    else
        if j_ip(end,x)==3
           j_curv_ip(1,x)=2;
        else
            if j_ip(end,x)==4
               j_curv_ip(1,x)=j_ip(end,x);
            else
                if j_ip(end,x)==5
                   j_curv_ip(1,x)=8;
                else
                    if j_ip(end,x)==6
                       j_curv_ip(1,x)=7;
                    else
                        if j_ip(end,x)==7
                           j_curv_ip(1,x)=6;
                        else
                            j_curv_ip(1,x)=j_ip(end,x)
                                ;
                        end
```

```
                    end
                end
            end
        end
    end
end

end

j_curv_es_ip=j_curv_ip;

for k=1:length(r_curv)
    for J=1:length(x_disc)
        caso_curv=j_curv_ip(end,J);
        if -1*M_es_ip(J)<=0
        M_curv_ip(k,J)=D_cnu(caso_curv)/r_curv(k); %
           matrice del momento per la curvatura, che
           lungo la riga tiene conto del momento per
           ogni x_disc, mentre sulle righe variando il
            raggio voluto
        else
        M_curv_ip(k,J)=-D_cnu(caso_curv)/r_curv(k); %
           matrice del momento per la curvatura, che
           lungo la riga tiene conto del momento per
           ogni x_disc, mentre sulle righe variando il
            raggio voluto
        end
    end
end

figure(26)
plot(x_disc,M_curv_ip,'-*')
legend('raggio 0.5 m','raggio 1 m','raggio 1.5 m','
   raggio 2 m','raggio 2.5 m','raggio 3 m','raggio 3.5
    m')
title('Momento relativo a curvatura arco 2C [Nm]')

% calcolo della coppia di forze necessarie per
   ottenere quel raggio con
% l'applicazione delle due forze a quella distanza.
   Dunque calcolo di F/2

F_curv_ip=(1./r_curv)'.*M_curv_ip;

figure(27)
plot(x_disc,F_curv_ip,'-*')
legend('raggio 0.5 m','raggio 1 m','raggio 1.5 m','
   raggio 2 m','raggio 2.5 m','raggio 3 m','raggio 3.5
    m')
title('Forza relativa a curvatura arco 2C [N]')
```

```
% SCEGLIERE IL MOEMENTO CHE SI VUOLE ANALIZZARE per il
    calcolo delle sigma
% nel materiale, in altre parole il numero indicante
   la posizione della r
% di arrotolamento voluto nel vettore r_curv

N_r_curv_ip=6;

% la convenzione del sistema di riferimento usata or
   nel calcolo delle
% epsilon e sigma e' diversa dalla precedente. Ora si
   ha x nella direzione
% dell'asse della trave, y entrante nel foglio e z
   rivolta verso l'alto. Ne
% consegue che se il momento prima era negativo, per
   avere lo stesso
% effetto ora deve essere positivo, lo sforzo normale
   rimane invariato in
% questoa nuova convenzione.

N_s_es_ip_curv=zeros(1,N);
M_es_ip_curv=-M_curv_ip(N_r_curv_ip,:);

hs_f=flipud(hs);
theta_f=flipud(theta);
E_L_f=flipud(E_L); %le colonne identificano i casi
   mentre le righe i moduli elastici assunti dai
   materiali nel caso considerato, strato superiore
   prime 4 colonne carbonio, poi dyneema, foam sempre
   su 5 riga, faccia inferiore dyneema per prime 4
   colonne poi carbonio
E_T_f=flipud(E_T);
G_LT_f=flipud(G_LT);
ni_LT_f=flipud(ni_LT);
ni_TL_f=flipud(ni_TL);

hs_es=zeros(size(hs_f,1)+size(hs_f,1)-2,size(hs_f,2));
    %posizione degli strati per calcolo delle epsilo e
    sigma
hs_es([1 3:2:end-1 end],:)=hs_f;
hs_es(2:2:end-2,:)=hs_f(2:end-1,:);
Qk1_1_es=zeros(size(hs_f,1)+size(hs_f,1)-2,1);
Aree=[hst_1' hst_1' hst_1' hst_1' hst_2' hst_2' hst_2'
    hst_2']*b;
hs_fmedia=(hs_f(1:end-1,:)+hs_f(2:end,:))/2;

toll_sigma=10^1; %tolleranza minima voluta tra la
   somma di tutti i valori delle sigma sommate tra di
   loro al ciclo precedente con quelle del ciclo
```

```
   appena effettuato
t_it_max=3; %numero di cicli massimo che si vuole
   avere nel ciclo di calcolo dei casi, epsilon e
   sigma

flag=0; %NON TOCCARE QUESTI VALORI
t=1;    %NON TOCCARE QUESTI VALORI
sigma_old=zeros(size(hs_es,1),length(x_disc)); %NON
   TOCCARE QUESTI VALORI


% ciclo che gestisce il calcolo in modo iterativo dei
   casi effettivi in cui
% lavora il materiale, le epsilon e le sigma in esso
   secondo il modello
% della trave di timoshenko
% while t<t_it_max+1 && flag==0
while t<t_it_max+1 && flag==0

for x=1:length(x_disc)
Mat=[A_nu(j_curv_es_ip(t,x)) B_nu(j_curv_es_ip(t,x))
     B_nu(j_curv_es_ip(t,x)) D_nu(j_curv_es_ip(t,x))];
         %matrice
Car=[N_s_es_ip_curv(x) M_es_ip_curv(x)]'; %vettore dei
    carichi nel punto della discretizzazione
epsilon_0k_ip_curv(:,x)=Mat\Car; %vettore con
   epsilon_0 e la curvatura k

%k come indice per il ciclo indica il punto in cui il
   ciclo sta calcolando
%gli stress, cioe' i punti scritti come x_disc

epsilon_ip_curv(:,x)=epsilon_0k_ip_curv(1,x)+hs_es(:,
   j_curv_es_ip(t,x)).*epsilon_0k_ip_curv(2,x);

Qk1_1=zeros(size(theta_f,1),1);

for z=1:size(theta_f,1)
Qp1_es=[E_L_f(z,j_curv_es_ip(t,x))/(1-ni_LT_f(z,
   j_curv_es_ip(t,x))*ni_TL_f(z,j_curv_es_ip(t,x)))
         ni_LT_f(z,j_curv_es_ip(t,x))*E_T_f(z,
   j_curv_es_ip(t,x))/(1-ni_LT_f(z,j_curv_es_ip(t,x))*
   ni_TL_f(z,j_curv_es_ip(t,x)))    0
    ni_LT_f(z,j_curv_es_ip(t,x))*E_T_f(z,j_curv_es_ip(
       t,x))/(1-ni_LT_f(z,j_curv_es_ip(t,x))*ni_TL_f(z
       ,j_curv_es_ip(t,x)))     E_T_f(z,j_curv_es_ip(t
       ,x))/(1-ni_LT_f(z,j_curv_es_ip(t,x))*ni_TL_f(z,
       j_curv_es_ip(t,x)))      0
            0                          0
                G_LT_f(z,j_curv_es_ip(t,x))];
```

```
lambda_k1_es=[   (cos(theta_f(z,j_curv_es_ip(t,x))))^2
          (sin(theta_f(z,j_curv_es_ip(t,x))))^2
             2*cos(theta_f(z,j_curv_es_ip(t,x)))*sin(
   theta_f(z,j_curv_es_ip(t,x)))
            (sin(theta_f(z,j_curv_es_ip(t,x))))^2
                     (cos(theta_f(z,j_curv_es_ip(t,x))
               ))^2          -2*cos(theta_f(z,
               j_curv_es_ip(t,x)))*sin(theta_f(z,
               j_curv_es_ip(t,x)))
         -cos(theta_f(z,j_curv_es_ip(t,x)))*sin(
            theta_f(z,j_curv_es_ip(t,x)))  cos(theta_f
            (z,j_curv_es_ip(t,x)))*sin(theta_f(z,
            j_curv_es_ip(t,x)))  (cos(theta_f(z,
            j_curv_es_ip(t,x))))^2-(sin(theta_f(z,
            j_curv_es_ip(t,x))))^2];

Qk1_es= inv(lambda_k1_es)*Qp1_es*(inv(lambda_k1_es))';
Qk1_1(z,1)=Qk1_es(1,1);

end

Qk1_1_es(1:2:end-1,1)=Qk1_1;  % Qk1_1 modificata per
   poter essere moltiplicata alle epsilon che nascono
   dal vettore hs_es cioe' epsilon modificato che le
   posizioni intermedie duplicate per fare la media
   delle sigma.
Qk1_1_es(2:2:end,1)=Qk1_1;

sigma_ip_curv(:,x)=epsilon_ip_curv(:,x).*Qk1_1_es;
sigma_m_ip_curv(:,x)=(sigma_ip_curv(1:2:end-1,x)+
   sigma_ip_curv(2:2:end,x))/2; %calcolo delle sigma
   medie a coppie

if flag_rib_ip==0
sigma_mm_ip_curv(1,x)=(sigma_m_ip_curv(1,x)+
   sigma_m_ip_curv(length(theta_c),x))/2; % calcolo
   delle sigma medie a coppie delle coppie per ciclo
   di if
sigma_mm_ip_curv(2,x)=(sigma_m_ip_curv(end,x)+
   sigma_m_ip_curv(end-length(theta_d)+1,x))/2;
else
sigma_mm_ip_curv(1,x)=(sigma_m_ip_curv(1,x)+
   sigma_m_ip_curv(length(theta_d),x))/2; % calcolo
   delle sigma medie a coppie delle coppie per ciclo
   di if
sigma_mm_ip_curv(2,x)=(sigma_m_ip_curv(end,x)+
   sigma_m_ip_curv(end-length(theta_c)+1,x))/2;
end
```

```
N_strati_ip_curv(:,x)=sigma_m_ip_curv(:,x).*Aree(:,
    j_curv_es_ip(t,x));
N_ris_ip_curv=sum(N_strati_ip_curv,1);
N_err_ip_curv(t,x)=abs(N_s_es_ip_curv(x)-N_ris_ip_curv
    (x));

% correzione per nel calcolo della risultante del
    momento, si cerca a quale  altezzo si trova la
    sigma media calcolata per avere la z precisa e non
    quella media cioe' zero.
% m_sigma_foam(1,x)=-hst(length(theta_c)+1)/(sigma(2*
    length(theta_c)+2,x)+sigma(2*length(theta_c)+1,x));
     %calcolo pendenza retta nel foam
% z_m_foam(1,x)=m_sigma_foam(1,x)*(sigma_m(length(
    theta_c)+1,x)-sigma(2*length(theta_c)+1,x))+hs_es(
    length(theta_c)+1); % z della sigma media nel foam
% hs_fmedia_f=hs_fmedia;
% hs_fmedia_f(length(theta_c)+1)=z_m_foam(1,x); % hs
    media flirpata con inserimento della z del foam
%nel caso qualcosa fosse sbagliato cancellare
    ragoinamenti sul foam e riportare hs_fmedia_f ad
    hs_fmedia

M_strati_ip_curv(:,x)=sigma_m_ip_curv(:,x).*Aree(:,
    j_curv_es_ip(t,x)).*hs_fmedia(:,j_curv_es_ip(t,x));
M_ris_ip_curv=sum(M_strati_ip_curv,1);
M_err_ip_curv(t,x)=abs(M_es_ip_curv(x)-M_ris_ip_curv(x
    ));

if sigma_mm_ip_curv(1,x)>=0 && sigma_mm_ip_curv(2,x)
    >=0
     if flag_rib_ip(x)==0
        j_curv_es_ip(t+1,x)=1;
     else
        j_curv_es_ip(t+1,x)=5;
     end
else
     if sigma_mm_ip_curv(1,x)<0 && sigma_mm_ip_curv(2,x
         )>0
          if flag_rib_ip(x)==0
             j_curv_es_ip(t+1,x)=2;
          else
             j_curv_es_ip(t+1,x)=7;
          end
     else
          if sigma_mm_ip_curv(1,x)>0 && sigma_mm_ip_curv
              (2,x)<0
               if flag_rib_ip(x)==0
                  j_curv_es_ip(t+1,x)=3;
               else
```

```
                j_curv_es_ip(t+1,x)=6;
            end
        else
            if sigma_mm_ip_curv(1,x)<=0 &&
               sigma_mm_ip_curv(2,x)<=0
               if flag_rib_ip(x)==0
                   j_curv_es_ip(t+1,x)=4;
                else
                   j_curv_es_ip(t+1,x)=8;
                end
            else
            end
        end
    end
end

end

if abs(sum(sum(sigma_ip_curv,1),2)-sum(sum(sigma_old)
   ,2))>toll_sigma
       t=t+1;
       sigma_old=sigma_ip_curv;
    else
        flag=1; %il flag=1 fa uscire fuori dal ciclo,
           indica cioe' quando si e' raggiunto il
           livello di accuratezza voluto
        t=t+1;
    end

end

% j_curv_es_ip
% N_err_ip_curv
% M_err_ip_curv
% epsilon_0k_ip_curv
% sigma_ip_curv
% flag
% flag_rib_ip


    for J=1:length(x_disc)
        caso_curv=j_curv_es_ip(end-1,J);
        if -1*M_es_ip(J)<=0
        M_curv_es_ip(J)=D_cnu(caso_curv)/r_curv(
           N_r_curv_ip); % matrice del momento per la
           curvatura, che lungo la riga tiene conto
           del momento per ogni x_disc, mentre sulle
           righe variando il raggio voluto
        else
```

```
        M_curv_es_ip(J)=-D_cnu(caso_curv)/r_curv(
            N_r_curv_ip); % matrice del momento per la
            curvatura, che lungo la riga tiene conto
            del momento per ogni x_disc, mentre sulle
            righe variando il raggio voluto
        end
    end


figure(28)
plot(x_disc,M_curv_es_ip,'-*')
title('Momento relativo a curvatura arco 2C raggio
    selez [Nm]')

F_curv_es_ip=(1/r_curv(N_r_curv_ip))'.*M_curv_es_ip;

figure(29)
plot(x_disc,F_curv_es_ip,'-*')
title('Forza relativa a curvatura arco raggio selez 2C
    [N]')


%% Stima dei pesi dell'habitat
clc

W_d=pi*((r+sum(s_d))^2-r^2)*b*rho_d;  % [kg] peso del
    dyneema
W_s=pi*((r+sum(s_d)+s_s)^2-(r+sum(s_d))^2)*b*rho_s; %
    [kg] peso della schiuma
W_c=pi*((r+sum(s_d)+s_s+sum(s_c))^2-(r+sum(s_d)+s_s)
    ^2)*b*rho_c;  % [kg] peso del carbonio

W_tot=W_d+W_s+W_c; % [kg] peso totale della struttura

figure(30)
bar(reordercats(categorical({'Dyneema','Foam','Carbon'
    ,'Total'}),{'Dyneema','Foam','Carbon','Total'}),[
    W_d W_s W_c W_tot])
title('Structure weight')

%% Calcolo sigma di bukling per carbonio
clc

% Load condition 3
%verifica sigma carbonio in compressione

% 1) Prima tipologia di calcolo
sigma_b1=2/3*(E_Lc_c*E_s_c*sum(s_c)/s_s)^0.5; % primo
    metodo di calcolo della sigma di wrinkling del
    carbonio
```

```
% 2) Seconda tipologia di calcolo
sigma_b2=0.5*(E_Lc_c*E_s_c*G_s)^(1/3); % % secondo
    metodo di calcolo della sigma di wrinkling del
    carbonio


Mat_b1_sigma_is=sigma*SF<-sigma_b1; % controllo sigma
    in struttura isostatica con sigma minima ottenuta
    da 1) di wrinkling per carbonio in compressione
Mat_b2_sigma_is=sigma*SF<-sigma_b2; % controllo sigma
    in struttura isostatica con sigma minima ottenuta
    da 2) di wrinkling per carbonio in compressione

Mat_b1_sigma_ip=sigma_ip*SF<-sigma_b1; % controllo
    sigma in struttura iperstatica con sigma minima
    ottenuta da 1) di wrinkling per carbonio in
    compressione
Mat_b2_sigma_ip=sigma_ip*SF<-sigma_b2; % controllo
    sigma in struttura iperstatica con sigma minima
    ottenuta da 2) di wrinkling per carbonio in
    compressione


% ATTENZIONE usabile solo se numeri di strati del
    carbonio coincidono con quelli del dyneema
% Per isostatica
Mat_foam_traz_is=sigma(2*length(s_c)+1,:)*SF>
    sigma_rs_t;
Mat_foam_comp_is=sigma(2*length(s_c)+2,:)*SF<-
    sigma_rs_c;


% controllo sigma dyneema in trazione
Mat_dyneema_traz_is=sigma*SF>sigma_rd_t; % isostatica,
     verifica sigma dyneema trazione

Mat_dyneema_traz_ip=sigma_ip*SF>sigma_rd_t; %
    iperstatica, verifica sigma dyneema trazione


% Load condition 4
% verifica sigma carbonio in trazione
Mat_carb_traz_is=sigma_curv>sigma_rc_t; % isostatica,
    verifica sigma carbonio trazione

Mat_carb_traz_ip=sigma_ip_curv>sigma_rc_t; %
    iperstatica, verifica sigma carbonio trazione

%verifica carbonio in compressione
```

```
Mat_b1_sigma_curv=sigma_curv<-sigma_b1; % controllo
    sigma in struttura isostatica in configurazione
    arrotolata con sigma minima ottenuta da 1) di
    wrinkling per carbonio in compressione
Mat_b2_sigma_curv=sigma_curv<-sigma_b2; % controllo
    sigma in isostatica iperstatica in configurazione
    arrotolata con sigma minima ottenuta da 2) di
    wrinkling per carbonio in compressione

Mat_b1_sigma_ip_curv=sigma_ip_curv<-sigma_b1; %
    controllo sigma in struttura iperstatica in
    configurazione arrotolata con sigma minima ottenuta
     da 1) di wrinkling per carbonio in compressione
Mat_b2_sigma_ip_curv=sigma_ip_curv<-sigma_b2; %
    controllo sigma in struttura iperstatica in
    configurazione arrotolata con sigma minima ottenuta
     da 2) di wrinkling per carbonio in compressione

% ATTENZIONE usabile solo se numeri di strati del
    carbonio coincidono con quelli del dyneema
% Per isostatica

% verisica su foam in compressione e trazione
Mat_foam_comp_curv=sigma_curv(2*length(s_c)+1,:)<-
    sigma_rs_c;
Mat_foam_traz_curv=sigma_curv(2*length(s_c)+2,:)>
    sigma_rs_t;
% neanche arrivando ad avere un diametro di 5 metri si
     riesce ad avere le
% sigma di compressione della schiuma al di sotto di
    quelle massime


%% Struttura completa
clc

% calcolo degli spostamenti della struttura completa
    considerando:
% 1) carico di regolite
% 2) pressione interna
% 3) peso della struttura stessa
% 4) peso di una persona al suo interno

% Creiamo una discretizzazione uniforma per la tie
    dell'arco
x_tie_disc=linspace(0,2*r,N);
x_tie_diff=diff(x_tie_disc);
x_tie_int=x_tie_disc(1:end-1)+x_tie_diff(1)/2;
```

```
% 1) calcolo della forza discretizzata introdotta
    dalla pressione
% parte relativa all'arco
pressure=1.01325*10^5; % [Pa] pressione atmosferica al
     livello del mare, 1 atm
F_pressure_ds=pressure*d_ds_disc*b; % [N] forza
    esercitata dalla pressione
theta_int_f=fliplr(theta_int); % ribalto il vettore
    theta
F_pressure_arc_x=F_pressure_ds.*cos(theta_int_f); %
    scomposizione della forza esercitata dalla
    pressione lungo l'asse x
F_pressure_arc_y=F_pressure_ds.*sin(theta_int_f); %
    scomposizione della forza esercitata dalla
    pressione lungo l'asse y

% parte relativa alla trave, tie
F_pressure_tie_y=pressure*x_tie_diff*b; % [N] forza
    esercitata dalla pressione sulla trave in direzione
     y


% 2) peso della struttura stesso
% parte relativa all'arco
F_tot_ds_y=W_tot/(N-1)*ones(1,N-1)*g_l; % [N] peso
    della struttura distribuito nei vari segmentini, ha
     componente solo in y

% parte relativa alla trave, tie
% per ora lo tralasciamo


% 3) peso della persona
N_el_man=ceil(1/18*(N))-1; % numero di elementi su cui
     viene distribuito il peso della persona
% per ora lo tralasciamo


% Carichi totali agenti sulla struttura
% Per arco
F_arc_tot_x=F_pressure_arc_x; % totale delle forze
    agenti lungo x sull'arco
F_arc_tot_y=P_car_int+F_tot_ds_y-F_pressure_arc_y; %
    totale delle forze agenti lungo y sull'arco

%per trave
F_tie_tot_y=F_pressure_tie_y; % totale delle forze
    agenti lungo y sulla trave, tie
```

Appendix B

This appendix shows the Second script.

```
%Structural preliminar analysis

clc
close all
clear all

%Dati
r=3.5; %raggio habitat[m]
s_r=2.5; % s_r spessore regolite [m]
g_l=9.81/6; % acccellerazione di gravita' della luna [
   m/s^2]
b=0.5; %profondita' dell'arco, lunghezza habitat [m]
rho_r=1600; % densita' regolite [kg/m^3]
N=19; %numero punti della discretizzazione SOLO NUMERI
    DISPARI, sia per calcolo sollecitazioni che PLV
N_theta=100; % numero punti usati per creare grafico
   dopo intermoplazione, per maggiore definizione
SF=4; % safety factor preso da "Structural Design of a
    Lunar Habitat"

%Inserire valori presi da script
   Calcoli_strutturali_18a
F_arc_tot_y=10^4*[-0.2372   -0.7165   -1.1850
   -1.6246   -2.0183   -2.3516   -2.6123   -2.7913
   -2.8824   -2.8824   -2.7913   -2.6123...
                -2.3516   -2.0183   -1.6246
                   -1.1850   -0.7165   -0.2372];   %
                   carico puntuale discretizzato
                   agente nei punti di
                   interpolazione int [N]

F_arc_tot_x=10^4*[ -3.0830   -2.9893   -2.8048
   -2.5351   -2.1884   -1.7751   -1.3079   -0.8010
   -0.2697    0.2697    0.8010    1.3079...
                  1.7751    2.1884    2.5351
                     2.8048    2.9893    3.0830];  %
                      carico agente in x:int in
```

```
                    direzione x [N]

j_is=[8     6     6     6     6     6     6     6
   6     8     6     6     6     6     6     6     6
       6     8]; %compilando j assumera sulle colonne
   indicate da k, il caso che la stazione assumera'
   alla prossima iterazione e sulle righe i valori
   assunti da j nelle varie iterazioni
flag_rib_is=[1     1     1     1     1     1     1
       1     1     1     1     1     1     1     1
       1     1     1     1];

j_ip=[8     6     6     6     6     6     6     6
   2     2     2     6     6     6     6     6     6
       6     8];
flag_rib_ip=[ 1     1     1     1     1     1     1
       1     0     0     0     1     1     1     1
       1     1     1     1];

%Calcolo aree regolite

% sistema di riferimento cartesiano con asse x
   parallelo ad apertura
% dell'arco e y ortogonale ad esso.

r_r=r+s_r; % r_r raggio regolite

% calcolo i punti di disxcretizzazione come
   equidistanziati lungo linea
% media dell'arco, lungo ds dunque
theta_disc=linspace(0,pi,N); % discretizzo in modo da
   avere angoli equispaziati
p_disc=fliplr(r*cos(theta_disc)); %p punti di
   discretizzazione che vanno da -r ad r, centrato in
   0 per integrale funzione, semicerchio

d_theta=diff(theta_disc); % angolo di distanza fra i
   vari punti
theta_int=theta_disc(1:end-1)+d_theta(1)/2; % angoli
   di interpolazion/integrazione, dove andranno poi
   collocati i carichi equivalenti dei carichi
   cncentrati
p_int=fliplr(r*cos(theta_int)); %punti reativi agli
   angoli precedenti

% calcolo punti per sistema di riferimento posizionato
    nell'estremo
% sinistro dell'arco e dunque da 0 a 2r
x_disc=r-r*cos(theta_disc);
y_disc=r*sin(theta_disc);
```

```
ds_disc=r*theta_disc;
phi_int=(pi/2-theta_int);
d_ds_disc=diff(ds_disc);

%stessa cosa per i punti di interpolazione/
   integrazione
x_int=r-r*cos(theta_int);
y_int=r*sin(theta_int);
ds_int=r*theta_int;
phi_disc=(pi/2-theta_disc);

%Calcolo funzione del carico punti interpolazione,
   centrali nell'intervallo di interpolazione
theta_t=linspace(0,pi,N_theta);
dss=r*theta_t;
p_xx=fliplr(r*cos(theta_t));
c=polyfit(p_int,F_arc_tot_y,length(p_int)-1);
p_yy=polyval(c,p_xx);

% c=polyfit(ds_int,P_car_int,length(p_int)-1);
% p_yy=polyval(c,dss);

figure(1)
plot(p_xx,p_yy,'b')

%calcolo reazioni vincolari con carichi distribuiti
   effettivi della
%discretizzazione e seguendo principio esposto nel
   libro Theory of Arched
%Structures pag 57

%Calcolo delle reazioni vincolari verticali dell'arco.
    Rferendoci al metodo
%dellatrave di sostituzione o riferimento, le reazioni
    verticali dell'arco sono pari
%a quelle della trave e dato che siamo in un caso di
   simmetria dei carichi
%esse sono uguali e pari a meta' del carico verticale
   dell'arco. pag 58
%libro citato prima.

% alternativa che porta allo stesso risultato
Vb=(F_arc_tot_y*x_int'+F_arc_tot_x*y_int')/(2*r);
Va=Vb;

% Calcolo delle reazioni vincolari orizzontali
   equazione di equilibrio
% ausiliaria su cerniera all'apice dell'arco
```

```
M_c1=0; %momento in c, riferimento a teoria pag 58
    libro
for k=1:N/2 %lo calcolo solo fino ad N/2, cioe' il
    numero intero prima della meta', in quanto l'arco e
    ' caricato simmetricamente
     M_c1=M_c1+F_arc_tot_y(k)*p_int(k)-F_arc_tot_x(k)*(
         r-y_int(k));
end
M_c=M_c1+Va*r;
Ha=M_c/r;
Hb=-sum(F_arc_tot_x)-Ha;

%CALCOLO CARATTERISTICHE SOLLECITAZIONE
%momento flettente

for k=1:length(ds_disc)-1
     M(k)=Va*x_disc(k+1)-F_arc_tot_y(1:k)*(x_disc(k+1)-
         x_int(1:k))'-F_arc_tot_x(1:k)*(y_disc(k+1)-
         y_int(1:k))'-Ha*y_disc(k+1);
end
M=[0,M];
Myy=spline(ds_disc,M,dss);
M_int=spline(ds_disc,M,ds_int);

figure(2)
plot(dss,Myy,'b',ds_disc,M,'*',ds_int,M_int,'*')
title('Diagramma del Momento flettente')

%SFORZO DI TAGLIO

for k=1:length(ds_disc)-1
    T(k)=(Va-sum(F_arc_tot_y(1:k)))*cos(phi_disc(k+1))
        -(Ha+sum(F_arc_tot_x(1:k)))*sin(phi_disc(k+1));
end

T=[-Ha,T];
Tyy=spline(ds_disc,T,dss);
T_int=spline(ds_disc,T,ds_int);

figure(3)
plot(dss,Tyy,'b',ds_disc,T,'*',ds_int,T_int,'*')
title('Diagramma del Taglio')

%SFORZO NORMALE

for k=1:length(ds_disc)-1
    N_s(k)=-(Va-sum(F_arc_tot_y(1:k)))*sin(phi_disc(k
        +1))-(Ha+sum(F_arc_tot_x(1:k)))*cos(phi_disc(k
        +1));
end
```

```
N_s=[-Va,N_s];
N_syy=spline(ds_disc,N_s,dss);
N_s_int=spline(ds_disc,N_s,ds_int);

figure(4)
plot(dss,N_syy,'b',ds_disc,N_s,'*',ds_int,N_s_int,'*')
title('Diagramma dello Sforzo Normale')

%% CALCOLO MATRICI DI RIGIDEZZA A,B,D,At MADFLEX
clc

%Dati strati madflex
%sistema di riferimento con x lungo larghezza piastra
   e y lungo profondita'
%Dati strato di carbonio
theta_c=[30 -30 30 -30]; % [gradi] inserire l'
   orientamento delle fibre
s_c=[0.28 0.28 0.28 0.28]*10^-3; % [m] inserire
   spessore singoli strati, il numero dicomponenti nel
    vettore theta deve coincidere con il numero di
   questo
E_Lc_t= 324*10^9; % [N/m^2] modulo elastico
   longitudinale a TRAZIONE delle fibre
E_Lc_c= E_Lc_t/100*90 ; % [N/m^2] modulo elastico
   longitudinale a COMPRESSIONE delle fibre, 10%
   minore di quello a trazione
E_Tc=2.9*10^9; % [N/m^2] modulo elastico nella
   direzione trasversale alle fibre
G_LTc= 5.5*10^9; % [N/m^2] modulo elastico di taglio
   direzione xy
ni_LTc=0.3; % modulo di poisson
rho_c=1.79*10^3; %[kg/m^3] densita' del carbonio
sigma_rc_t=6.6*10^9; % [Pa] sigma di rottura del
   carbonio a trazione

%Dati strato schiuma (Rohacell 110 WF)
theta_s=0; % [gradi]
s_s=80*10^-3; % [m] spessore schiuma
E_s_t=180*10^6; % [N/m^2] modulo elastico a TRAZIONE
   schiuma
E_s_c=(180/164*82.3)*10^6; % [N/m^2] modulo elastico a
    COMPRESSIONE schiuma
G_s=70*10^6; % [N/m^2] modulo elastico di taglio
rho_s=110; % Densita' della schiuma [kg/m^3]
sigma_rs_t=3.7*10^6; % [Pa] sigam di rottura della
   schiuma a trazione
sigma_rs_c=3.6*10^6; % [Pa] sigma di rottura della
   schiuma a compressione
```

```
%Dati stato di dyneema
theta_d=[-30 30 -30 30]; % [gradi] inserire l'
    orientamento delle fibre
s_d=[0.5 0.5 0.5 0.5]*10^-3; % [m] inserire spessore
    singoli strati, il numero dicomponenti nel vettore
    theta deve coincidere con il numero di questo
E_Ld_t= 100*10^9; % [N/m^2] modulo elastico
    longitudinale a TRAZIONE delle fibre
E_Ld_c= 0.1; % [N/m^2] modulo elastico longitudinale a
     COMPRESSIONE delle fibre preso nullo
E_Td=0.1*10^9; % [N/m^2] modulo elastico nella
    direzione trasversale alle fibre
G_LTd= 0.2*10^9; % [N/m^2] modulo elastico di taglio
    direzione xy
ni_LTd=0.05; % modulo di poisson
rho_d=0.98*10^3; %[kg/m^3] densita' del dyneema
sigma_rd_t=3.3*10^9; % [Pa] sigma di rottura del
    dyneema a trazione


% calcolo hs per materiale normale con carbonio su
    faccia superiore
hst_1=[s_c s_s s_d]; %vettore spessore strati
hs_f1=sum(hst_1); %vettore spessore totale degli
    strati
hsi_1=-hs_f1/2; %posizione faccia inferiore composito
    con assi centrati al centro dello spessore
hss_1=hs_f1/2; %posizione faccia superiore composito
    con assi centrati al centro dello spessore

for k=1:length(hst_1)
    hs_f1(k+1)=hs_f1(k)-hst_1(k);
end

hs_f1=hs_f1+hsi_1;
hs_1=fliplr(hs_f1);

% calcolo hs per materiale ribaltato con carbonio su
    faccia inferiore
hst_2=fliplr([s_c s_s s_d]); %vettore spessore strati
hs_f2=sum(hst_2); %vettore spessore totale degli
    strati
hsi_2=-hs_f2/2; %posizione faccia inferiore composito
    con assi centrati al centro dello spessore
hss_2=hs_f2/2; %posizione faccia superiore composito
    con assi centrati al centro dello spessore

for k=1:length(hst_2)
    hs_f2(k+1)=hs_f2(k)-hst_2(k);
end
```

```
hs_f2=hs_f2+hsi_2;
hs_2=fliplr(hs_f2);


% CASO 1) carbonio TRAZIONATO (faccia superiore),
   dyneema TRAZIONATO (faccia inferiore).
% CASO 2) carbonio COMPRESSO  (faccia superiore),
   dyneema TRAZIONATO (faccia inferiore).
% CASO 3) carbonio TRAZIONATO (faccia superiore),
   dyneema COMPRESSO  (faccia inferiore).
% CASO 4) carbonio COMPRESSO  (faccia superiore),
   dyneema COMPRESSO  (faccia inferiore).
% CASO 5) dyneema TRAZIONATO (faccia superiore),
   carbonio TRAZIONATO (faccia inferiore).
% CASO 6) dyneema TRAZIONATO (faccia superiore),
   carbonio COMPRESSO  (faccia inferiore).
% CASO 7) dyneema COMPRESSO  (faccia superiore),
   carbonio TRAZIONATO (faccia inferiore).
% CASO 8) dyneema COMPRESSO  (faccia superiore),
   carbonio COMPRESSO  (faccia inferiore).

hs=[hs_1' hs_1' hs_1' hs_1' hs_2' hs_2' hs_2' hs_2'];

theta=[flipud(pi/180*[theta_c theta_s theta_d]')
   flipud(pi/180*[theta_c theta_s theta_d]') flipud(pi
   /180*[theta_c theta_s theta_d]') flipud(pi/180*[
   theta_c theta_s theta_d]')...
              pi/180*[theta_c theta_s theta_d]'
                        pi/180*[theta_c theta_s
                  theta_d]'        pi/180*[theta_c
                  theta_s theta_d]'          pi/180*[
                  theta_c theta_s theta_d]'];

E_L=[flipud([E_Lc_t*ones(1,length(theta_c)) E_s_t*ones
   (1,length(theta_s)) E_Ld_t*ones(1,length(theta_d))
   ]')...
     flipud([E_Lc_c*ones(1,length(theta_c)) E_s_t*ones
        (1,length(theta_s)) E_Ld_t*ones(1,length(
        theta_d))]')...
     flipud([E_Lc_t*ones(1,length(theta_c)) E_s_t*ones
        (1,length(theta_s)) E_Ld_c*ones(1,length(
        theta_d))]')...
     flipud([E_Lc_c*ones(1,length(theta_c)) E_s_c*ones
        (1,length(theta_s)) E_Ld_c*ones(1,length(
        theta_d))]')...
            [E_Lc_t*ones(1,length(theta_c)) E_s_t*ones
               (1,length(theta_s)) E_Ld_t*ones(1,
               length(theta_d))]'...
```

```
            [E_Lc_c*ones(1,length(theta_c)) E_s_t*ones
               (1,length(theta_s)) E_Ld_t*ones(1,
               length(theta_d))]'...
            [E_Lc_t*ones(1,length(theta_c)) E_s_t*ones
               (1,length(theta_s)) E_Ld_c*ones(1,
               length(theta_d))]'...
            [E_Lc_c*ones(1,length(theta_c)) E_s_c*ones
               (1,length(theta_s)) E_Ld_c*ones(1,
               length(theta_d))]'];


E_T=[flipud([E_Tc*ones(1,length(theta_c)) E_s_t*ones
   (1,length(theta_s)) E_Td*ones(1,length(theta_d))]')
   ...
     flipud([E_Tc*ones(1,length(theta_c)) E_s_t*ones
        (1,length(theta_s)) E_Td*ones(1,length(theta_d
        ))]')...
     flipud([E_Tc*ones(1,length(theta_c)) E_s_t*ones
        (1,length(theta_s)) E_Td*ones(1,length(theta_d
        ))]')...
     flipud([E_Tc*ones(1,length(theta_c)) E_s_c*ones
        (1,length(theta_s)) E_Td*ones(1,length(theta_d
        ))]')...
            [E_Tc*ones(1,length(theta_c)) E_s_t*ones
               (1,length(theta_s)) E_Td*ones(1,length(
               theta_d))]'...
            [E_Tc*ones(1,length(theta_c)) E_s_t*ones
               (1,length(theta_s)) E_Td*ones(1,length(
               theta_d))]'...
            [E_Tc*ones(1,length(theta_c)) E_s_t*ones
               (1,length(theta_s)) E_Td*ones(1,length(
               theta_d))]'...
            [E_Tc*ones(1,length(theta_c)) E_s_c*ones
               (1,length(theta_s)) E_Td*ones(1,length(
               theta_d))]'];


G_LT=[flipud([G_LTc*ones(1,length(theta_c)) G_s*ones
   (1,length(theta_s)) G_LTd*ones(1,length(theta_d))
   ]')...
      flipud([G_LTc*ones(1,length(theta_c)) G_s*ones
         (1,length(theta_s)) G_LTd*ones(1,length(
         theta_d))]')...
      flipud([G_LTc*ones(1,length(theta_c)) G_s*ones
         (1,length(theta_s)) G_LTd*ones(1,length(
         theta_d))]')...
      flipud([G_LTc*ones(1,length(theta_c)) G_s*ones
         (1,length(theta_s)) G_LTd*ones(1,length(
         theta_d))]')...
```

```
            [G_LTc*ones(1,length(theta_c)) G_s*ones
               (1,length(theta_s)) G_LTd*ones(1,
               length(theta_d))]'...
            [G_LTc*ones(1,length(theta_c)) G_s*ones
               (1,length(theta_s)) G_LTd*ones(1,
               length(theta_d))]'...
            [G_LTc*ones(1,length(theta_c)) G_s*ones
               (1,length(theta_s)) G_LTd*ones(1,
               length(theta_d))]'...
            [G_LTc*ones(1,length(theta_c)) G_s*ones
               (1,length(theta_s)) G_LTd*ones(1,
               length(theta_d))]'];


ni_LT=[flipud([ni_LTc*ones(1,length(theta_c)) 0*ones
   (1,length(theta_s)) ni_LTd*ones(1,length(theta_d))
   ]')...
       flipud([ni_LTc*ones(1,length(theta_c)) 0*ones
          (1,length(theta_s)) ni_LTd*ones(1,length(
          theta_d))]')...
       flipud([ni_LTc*ones(1,length(theta_c)) 0*ones
          (1,length(theta_s)) ni_LTd*ones(1,length(
          theta_d))]')...
       flipud([ni_LTc*ones(1,length(theta_c)) 0*ones
          (1,length(theta_s)) ni_LTd*ones(1,length(
          theta_d))]')...
           [ni_LTc*ones(1,length(theta_c)) 0*ones
              (1,length(theta_s)) ni_LTd*ones(1,
              length(theta_d))]'...
           [ni_LTc*ones(1,length(theta_c)) 0*ones
              (1,length(theta_s)) ni_LTd*ones(1,
              length(theta_d))]'...
           [ni_LTc*ones(1,length(theta_c)) 0*ones
              (1,length(theta_s)) ni_LTd*ones(1,
              length(theta_d))]'...
           [ni_LTc*ones(1,length(theta_c)) 0*ones
              (1,length(theta_s)) ni_LTd*ones(1,
              length(theta_d))]'];

for x=1:size(E_L,2)

ni_TL(:,x)=ni_LT(:,x).*E_T(:,x)./E_L(:,x);

A_1=zeros(3,3);
B_1=zeros(3,3);
D_1=zeros(3,3);

for k=1:size(theta,1)
Qp=[E_L(k,x)/(1-ni_LT(k,x)*ni_TL(k,x))        ni_LT(k,x
   )*E_T(k,x)/(1-ni_LT(k,x)*ni_TL(k,x))    0
```

```
    ni_LT(k,x)*E_T(k,x)/(1-ni_LT(k,x)*ni_TL(k,x))
       E_T(k,x)/(1-ni_LT(k,x)*ni_TL(k,x))      0
            0                          0
               G_LT(k,x)];

lambda_k=[   (cos(theta(k,x)))^2       (sin(theta(k,x)
   ))^2           2*cos(theta(k,x))*sin(theta(k,x))
            (sin(theta(k,x)))^2       (cos(theta(k,x))
               )^2          -2*cos(theta(k,x))*sin(
               theta(k,x))
         -cos(theta(k,x))*sin(theta(k,x))  cos(theta(k
            ,x))*sin(theta(k,x))  (cos(theta(k,x)))
            ^2-(sin(theta(k,x)))^2];

Qk= inv(lambda_k)*Qp*(inv(lambda_k))';

cA=hs(k+1,x)-hs(k,x);
cB=0.5*(hs(k+1,x)^2-hs(k,x)^2);
cD=1/3*(hs(k+1,x)^3-hs(k,x)^3);

A_1=A_1+cA*Qk;
B_1=B_1+cB*Qk;
D_1=D_1+cD*Qk;

end

A(x)=A_1(1,1);
B(x)=B_1(1,1);
D(x)=D_1(1,1);

%matrici di rigidezza non per unita' di lunghezza
   poiche' moltiplicate per
%profondita'
A_nu(x)=A(x)*b;
B_nu(x)=B(x)*b;
D_nu(x)=D(x)*b;

%calcolo del centroide
y_c(x)=B(x)/A(x);

%nuove posizioni degli strati rispetto al centroide
hs_c(:,x)=hs(:,x)-y_c(x);

%Matrici di rigidezza relative al centroide
A_1c=zeros(3,3); %con c agiunto si indica le matrici
   rispetto al centroide
B_1c=zeros(3,3);
D_1c=zeros(3,3);

for k=1:size(theta,1)
```

```
Qp=[E_L(k,x)/(1-ni_LT(k,x)*ni_TL(k,x))        ni_LT(k,x
   )*E_T(k,x)/(1-ni_LT(k,x)*ni_TL(k,x))     0
    ni_LT(k,x)*E_T(k,x)/(1-ni_LT(k,x)*ni_TL(k,x))
       E_T(k,x)/(1-ni_LT(k,x)*ni_TL(k,x))       0
            0                          0
               G_LT(k,x)];

lambda_k=[   (cos(theta(k,x)))^2        (sin(theta(k,x)
   ))^2            2*cos(theta(k,x))*sin(theta(k,x))
            (sin(theta(k,x)))^2        (cos(theta(k,x))
               )^2           -2*cos(theta(k,x))*sin(
               theta(k,x))
         -cos(theta(k,x))*sin(theta(k,x))  cos(theta(k
            ,x))*sin(theta(k,x))  (cos(theta(k,x)))
            ^2-(sin(theta(k,x)))^2];

Qk= inv(lambda_k)*Qp*(inv(lambda_k))';

cA=hs_c(k+1,x)-hs_c(k,x);
cB=0.5*(hs_c(k+1,x)^2-hs_c(k,x)^2);
cD=1/3*(hs_c(k+1,x)^3-hs_c(k,x)^3);

A_1c=A_1c+cA*Qk;
B_1c=B_1c+cB*Qk;
D_1c=D_1c+cD*Qk;

end

A_c(x)=A_1c(1,1);
B_c(x)=B_1c(1,1); % solo B_1c(1,1) viene nullo, giusto
    in quanto il centroide non l'abbiamo trovato
   dividendo tutta la matrice B per A
D_c(x)=D_1c(1,1);

%matrici di rigidezza non per unita' di lunghezza
   poiche' moltiplicate per
%profondita'

A_cnu(x)=A_c(x)*b;
B_cnu(x)=B_c(x)*b;
D_cnu(x)=D_c(x)*b;

end


% Calcolo della matrice At per la rigidezza al taglio
   secondo Allen non per
% unita' di lunghezza
d_allen=hst_1(length(theta_c)+length(s_s))+sum(s_c)/2+
   sum(s_d)/2;
```

```
At_nu=G_s*d_allen^2*b/s_s;


%% CALCOLO DELLE TENSIONI SU FACCIA SUPERIORE ED
   INFERIORE
clc

% la convenzione del sistema di riferimento usata or
   nel calcolo delle
% epsilon e sigma e' diversa dalla precedente. Ora si
   ha x nella direzione
% dell'asse della trave, y entrante nel foglio e z
   rivolta verso l'alto. Ne
% consegue che se il momento prima era negativo, per
   avere lo stesso
% effetto ora deve essere positivo, lo sforzo normale
   rimane invariato in
% questoa nuova convenzione.

N_s_es=N_s;
M_es=-M;

hs_f=flipud(hs);
theta_f=flipud(theta);
E_L_f=flipud(E_L); %le colonne identificano i casi
   mentre le righe i moduli elastici assunti dai
   materiali nel caso considerato, strato superiore
   prime 4 colonne carbonio, poi dyneema, foam sempre
   su 5 riga, faccia inferiore dyneema per prime 4
   colonne poi carbonio
E_T_f=flipud(E_T);
G_LT_f=flipud(G_LT);
ni_LT_f=flipud(ni_LT);
ni_TL_f=flipud(ni_TL);

hs_es=zeros(size(hs_f,1)+size(hs_f,1)-2,size(hs_f,2));
    %posizione degli strati per calcolo delle epsilo e
    sigma
hs_es([1 3:2:end-1 end],:)=hs_f;
hs_es(2:2:end-2,:)=hs_f(2:end-1,:);
Qk1_1_es=zeros(size(hs_f,1)+size(hs_f,1)-2,1);
Aree=[hst_1' hst_1' hst_1' hst_1' hst_2' hst_2' hst_2'
    hst_2']*b;
hs_fmedia=(hs_f(1:end-1,:)+hs_f(2:end,:))/2;

toll_sigma=10^1; %tolleranza minima voluta tra la
   somma di tutti i valori delle sigma sommate tra di
   loro al ciclo precedente con quelle del ciclo
   appena effettuato
```

```
t_it_max=3; %numero di cicli massimo che si vuole
    avere nel ciclo di calcolo dei casi, epsilon e
    sigma
% j_is=1*ones(1,length(x_disc)); %compilando j
    assumera sulle colonne indicate da k, il caso che
    la stazione assumera' alla prossima iterazione e
    sulle righe i valori assunti da j nelle varie
    iterazioni

flag=0; %NON TOCCARE QUESTI VALORI
% flag_rib_is=zeros(1,length(x_disc)); %NON TOCCARE
    QUESTI VALORI flag relativo al ribaltamento di ogni
     sezione, se assume valore uno l'ordine dei
    materiali e' stato ribaltato
t=1;    %NON TOCCARE QUESTI VALORI
sigma_old=zeros(size(hs_es,1),length(x_disc)); %NON
    TOCCARE QUESTI VALORI

% ciclo che gestisce il calcolo in modo iterativo dei
    casi effettivi in cui
% lavora il materiale, le epsilon e le sigma in esso
    secondo il modello
% della trave di timoshenko
% while t<t_it_max+1 && flag==0
while t<t_it_max+1 && flag==0

for x=1:length(x_disc)
Mat=[A_nu(j_is(t,x)) B_nu(j_is(t,x))
     B_nu(j_is(t,x)) D_nu(j_is(t,x))]; %matrice
Car=[N_s_es(x) M_es(x)]'; %vettore dei carichi nel
    punto della discretizzazione
epsilon_0k(:,x)=Mat\Car; %vettore con epsilon_0 e la
    curvatura k

%k come indice per il ciclo indica il punto in cui il
    ciclo sta calcolando
%gli stress, cioe' i punti scritti come x_disc

epsilon(:,x)=epsilon_0k(1,x)+hs_es(:,j_is(t,x)).*
    epsilon_0k(2,x);

Qk1_1=zeros(size(theta_f,1),1);

for z=1:size(theta_f,1)
Qp1_es=[E_L_f(z,j_is(t,x))/(1-ni_LT_f(z,j_is(t,x))*
    ni_TL_f(z,j_is(t,x)))       ni_LT_f(z,j_is(t,x))*
    E_T_f(z,j_is(t,x))/(1-ni_LT_f(z,j_is(t,x))*ni_TL_f(
    z,j_is(t,x)))    0
     ni_LT_f(z,j_is(t,x))*E_T_f(z,j_is(t,x))/(1-ni_LT_f
         (z,j_is(t,x))*ni_TL_f(z,j_is(t,x)))     E_T_f(z
```

```
        ,j_is(t,x))/(1-ni_LT_f(z,j_is(t,x))*ni_TL_f(z,
        j_is(t,x)))      0
             0                          0
                G_LT_f(z,j_is(t,x))];

lambda_k1_es=[   (cos(theta_f(z,j_is(t,x))))^2       (
   sin(theta_f(z,j_is(t,x))))^2           2*cos(
   theta_f(z,j_is(t,x)))*sin(theta_f(z,j_is(t,x)))
             (sin(theta_f(z,j_is(t,x))))^2       (cos(
                theta_f(z,j_is(t,x))))^2          -2*
                cos(theta_f(z,j_is(t,x)))*sin(theta_f(z
                ,j_is(t,x)))
          -cos(theta_f(z,j_is(t,x)))*sin(theta_f(z,j_is
             (t,x)))  cos(theta_f(z,j_is(t,x)))*sin(
             theta_f(z,j_is(t,x)))  (cos(theta_f(z,j_is
             (t,x))))^2-(sin(theta_f(z,j_is(t,x))))^2];

Qk1_es= inv(lambda_k1_es)*Qp1_es*(inv(lambda_k1_es))';
Qk1_1(z,1)=Qk1_es(1,1);

end

Qk1_1_es(1:2:end-1,1)=Qk1_1;  % Qk1_1 modificata per
   poter essere moltiplicata alle epsilon che nascono
   dal vettore hs_es cioe' epsilon modificato che le
   posizioni intermedie duplicate per fare la media
   delle sigma.
Qk1_1_es(2:2:end,1)=Qk1_1;

sigma(:,x)=epsilon(:,x).*Qk1_1_es;
sigma_m(:,x)=(sigma(1:2:end-1,x)+sigma(2:2:end,x))/2;
   %calcolo delle sigma medie a coppie

if flag_rib_is==0
sigma_mm(1,x)=(sigma_m(1,x)+sigma_m(length(theta_c),x)
   )/2; % calcolo delle sigma medie a coppie delle
   coppie per ciclo di if
sigma_mm(2,x)=(sigma_m(end,x)+sigma_m(end-length(
   theta_d)+1,x))/2;
else
sigma_mm(1,x)=(sigma_m(1,x)+sigma_m(length(theta_d),x)
   )/2; % calcolo delle sigma medie a coppie delle
   coppie per ciclo di if
sigma_mm(2,x)=(sigma_m(end,x)+sigma_m(end-length(
   theta_c)+1,x))/2;
end

N_strati(:,x)=sigma_m(:,x).*Aree(:,j_is(t,x));
N_ris=sum(N_strati,1);
N_err(t,x)=abs(N_s_es(x)-N_ris(x));
```

```
M_strati(:,x)=sigma_m(:,x).*Aree(:,j_is(t,x)).*
    hs_fmedia(:,j_is(t,x));
M_ris=sum(M_strati,1);
M_err(t,x)=abs(M_es(x)-M_ris(x));

if sigma_mm(1,x)>=0 && sigma_mm(2,x)>=0
     if flag_rib_is(x)==0
        j_is(t+1,x)=1;
     else
        j_is(t+1,x)=5;
     end
else
     if sigma_mm(1,x)<0 && sigma_mm(2,x)>0
          if flag_rib_is(x)==0
             j_is(t+1,x)=2;
          else
             j_is(t+1,x)=7;
          end
     else
          if sigma_mm(1,x)>0 && sigma_mm(2,x)<0
               if flag_rib_is(x)==0
                  j_is(t+1,x)=3;
               else
                  j_is(t+1,x)=6;
               end
          else
               if sigma_mm(1,x)<=0 && sigma_mm(2,x)<=0
                  if flag_rib_is(x)==0
                       j_is(t+1,x)=4;
                   else
                       j_is(t+1,x)=8;
                   end
               else
               end
          end
     end
end

end

if abs(sum(sum(sigma,1),2)-sum(sum(sigma_old),2))>
    toll_sigma
        t=t+1;
        sigma_old=sigma;
     else
          flag=1; %il flag=1 fa uscire fuori dal ciclo,
             indica cioe' quando si e' raggiunto il
             livello di accuratezza voluto
          t=t+1;
```

```
    end

end

% j_is
% N_err
% M_err
% epsilon_0k
% sigma
% flag
% flag_rib_is

% figure(5)
% plot(epsilon,hs_es(:,j(end,:)),'-*')
% title('Andamento delle epsilon')
%
% figure(6)
% plot(sigma(:,1),hs_es(:,j(end,1)),'-*')
% title('Andamento delle sigma')
%
% figure(7)
% plot(sigma_m(:,1),hs_fmedia(:,j(end,1)),'-*')
% title('Andamento delle sigma medie')

%% CALCOLO SPOSTAMENTI ARCO A TRE CERNIERE CON PLV
clc

% con r si indicheranno le caratteristiche di
   sollecitazione del sistema reale (r)
% con u si indicheranno le caratteristiche di
   sollecitazione del sistema unitario o fittizio,
   cioe' con carico unitario (u)

ds_plv=zeros(1,length(ds_disc)+length(ds_int));
ds_plv(1:2:end)=ds_disc;
ds_plv(2:2:end-1)=ds_int;

d_ds_plv=diff(ds_plv);
d_ds_int=diff(ds_int);

x_plv=zeros(1,length(x_disc)+length(x_int));
x_plv(1:2:end)=x_disc;
x_plv(2:2:end-1)=x_int;

y_plv=zeros(1,length(y_disc)+length(y_int));
y_plv(1:2:end)=y_disc;
y_plv(2:2:end-1)=y_int;

phi_plv=zeros(1,length(phi_disc)+length(phi_int));
phi_plv(1:2:end)=phi_disc;
```

```
phi_plv(2:2:end-1)=phi_int;

M_plv_r=zeros(1,length(M)+length(M_int));
M_plv_r(1:2:end)=M;
M_plv_r(2:2:end-1)=M_int;

% figure(8)
% plot(ds_plv,M_plv_r,'-*')
% title('Momento flettente')

T_plv_r=zeros(1,length(T)+length(T_int));
T_plv_r(1:2:end)=T;
T_plv_r(2:2:end-1)=T_int;

% figure(9)
% plot(ds_plv,T_plv_r,'-*')
% title('Taglio')

N_s_plv_r=zeros(1,length(N_s)+length(N_s_int));
N_s_plv_r(1:2:end)=N_s;
N_s_plv_r(2:2:end-1)=N_s_int;

% figure(10)
% plot(ds_plv,N_s_plv_r,'-*')
% title('Taglio')

% calcolo delle reazioni vincolari e caratteristiche
   del sistema unitario
% per forze unitarie poste in ds_disc

%k indica le posizioni delle forze unitarie lungo l'
   apertura dell'arco e
%collocate in ds_disc

for k=1:length(ds_disc)
%calcolo reazioni vincolari verticali
    Vb_plv_u(k,1)=1*x_disc(k)/(2*r);
    Va_plv_u(k,1)=1-Vb_plv_u(k,1);

%calcolo reazioni vincolari orizzontali
 if k<length(x_disc)/2
    H_plv_u(k,1)=(Va_plv_u(k,1)*r-1*abs(r-x_disc(k)))/
       r;
 else
    H_plv_u(k,1)=(Vb_plv_u(k,1)*r-1*abs(r-x_disc(k)))/
       r;
 end

%calcolo caratteristiche di sollecitazione
    %Momento
```

```
    for J=1:length(ds_plv)-2
    if x_plv(J+1)-x_disc(k)>0
    M_plv_u(J)=Va_plv_u(k,1)*x_plv(J+1)-1*(x_plv(J+1)-
       x_disc(k))-H_plv_u(k,1)*y_plv(J+1); %le J
       indicano le colonne e salvano i valori per ogni
        sezione dell'arco in x_disc, le k sono le
       righe che indicano il variare della forza
       unitaria nelle x_int
    else
    M_plv_u(J)=Va_plv_u(k,1)*x_plv(J+1)-H_plv_u(k,1)*
       y_plv(J+1);
    end

    end
    M_plv1_u(k,:)=[0,M_plv_u,0];

 %Sforzo di taglio

    for J=1:length(ds_plv)-1
        if x_plv(J+1)-x_disc(k)>0
        T_plv_u(J)=(Va_plv_u(k,1)-1)*cos(phi_plv(J+1))
           -H_plv_u(k,1)*sin(phi_plv(J+1));
        else
        T_plv_u(J)=Va_plv_u(k,1)*cos(phi_plv(J+1))-
           H_plv_u(k,1)*sin(phi_plv(J+1));
        end
    end
    T_plv1_u(k,:)=[-H_plv_u(k,1),T_plv_u];

  %Sforzo normale

    for J=1:length(ds_plv)-1
        if x_plv(J+1)-x_disc(k)>=0
        N_s_plv_u(J)=-(Va_plv_u(k,1)-1)*sin(phi_plv(J
           +1))-H_plv_u(k,1)*cos(phi_plv(J+1));
        else
        N_s_plv_u(J)=-Va_plv_u(k,1)*sin(phi_plv(J+1))-
           H_plv_u(k,1)*cos(phi_plv(J+1));
        end
    end

    N_s_plv1_u(k,:)=[-Va_plv_u(k,1),N_s_plv_u];


 % Calcolo del plv
for J=1:length(ds_disc)-2
    caso=j_is(end,J+1);

    % Contributo PLV Momento
    w_M=d_ds_plv(1)/(2*D_cnu(caso))*[1; 2; 1];
```

```
    I_t_M(k,J)=[M_plv_r(2+(J-1)*2)*M_plv1_u(k,2+(J-1)
        *2) M_plv_r(3+(J-1)*2)*M_plv1_u(k,3+(J-1)*2)
        M_plv_r(4+(J-1)*2)*M_plv1_u(k,4+(J-1)*2)]*w_M;

    % Contributo PLV Taglio
    w_T=d_ds_plv(1)/(2*5/6*At_nu)*[1; 2; 1];
    I_t_T(k,J)=[T_plv_r(2+(J-1)*2)*T_plv1_u(k,2+(J-1)
        *2) T_plv_r(3+(J-1)*2)*T_plv1_u(k,3+(J-1)*2)
        T_plv_r(4+(J-1)*2)*T_plv1_u(k,4+(J-1)*2)]*w_T;

    % Contributo PLV Sforzo Normale
    w_N_s=d_ds_plv(1)/(2*A_cnu(caso))*[1; 2; 1];
    I_t_N_s(k,J)=[N_s_plv_r(2+(J-1)*2)*N_s_plv1_u(k
        ,2+(J-1)*2) N_s_plv_r(3+(J-1)*2)*N_s_plv1_u(k
        ,3+(J-1)*2) N_s_plv_r(4+(J-1)*2)*N_s_plv1_u(k
        ,4+(J-1)*2)]*w_N_s;

end
    % Contributo PLV Momento
    w_i_M=d_ds_plv(1)/(2*D_cnu(j_is(end,1)))*[1; 1];
    I_t_i_M(k,1)=[M_plv_r(1)*M_plv1_u(k,1) M_plv_r(2)*
        M_plv1_u(k,2)]*w_i_M;

    w_f_M=d_ds_plv(1)/(2*D_cnu(j_is(end,end)))*[1; 1];
    I_t_f_M(k,1)=[M_plv_r(end-1)*M_plv1_u(k,end-1)
        M_plv_r(end)*M_plv1_u(k,end)]*w_f_M;

    % Contributo PLV Taglio
    w_i_T=d_ds_plv(1)/(2*5/6*At_nu)*[1; 1];
    I_t_i_T(k,1)=[T_plv_r(1)*T_plv1_u(k,1) T_plv_r(2)*
        T_plv1_u(k,2)]*w_i_T;

    w_f_T=d_ds_plv(1)/(2*5/6*At_nu)*[1; 1];
    I_t_f_T(k,1)=[T_plv_r(end-1)*T_plv1_u(k,end-1)
        T_plv_r(end)*T_plv1_u(k,end)]*w_f_T;

    % Contributo PLV Sforzo Normale
    w_i_N_s=d_ds_plv(1)/(2*A_cnu(j_is(end,1)))*[1; 1];
    I_t_i_N_s(k,1)=[N_s_plv_r(1)*N_s_plv1_u(k,1)
        N_s_plv_r(2)*N_s_plv1_u(k,2)]*w_i_N_s;

    w_f_N_s=d_ds_plv(1)/(2*A_cnu(j_is(end,end)))*[1;
        1];
    I_t_f_N_s(k,1)=[N_s_plv_r(end-1)*N_s_plv1_u(k,end
        -1) N_s_plv_r(end)*N_s_plv1_u(k,end)]*w_f_N_s;


It_tot_M(k,1)=sum([I_t_i_M(k,1) I_t_M(k,:) I_t_f_M(k
    ,1)]);
```

```
It_tot_T(k,1)=sum([I_t_i_T(k,1) I_t_T(k,:) I_t_f_T(k
    ,1)]);
It_tot_N_s(k,1)=sum([I_t_i_N_s(k,1) I_t_N_s(k,:)
    I_t_f_N_s(k,1)]);

 end

It_tot_M
It_tot_T
It_tot_N_s

%calcolo di quanto e' la percentuale dello spostamento
     dovuta al taglio
%rispetto al momento preso come 100%
perc_contributo_taglio=max(It_tot_M)/100*max(It_tot_T)

It_tot=sum([It_tot_M It_tot_T It_tot_N_s],2);
y_spost=y_disc-It_tot';

figure(11)
plot(ds_plv,M_plv1_u(ceil(N/2),:),'-*')
title('Diagramma del Momento flettente per sistema
    unitario (u)')

figure(12)
plot(ds_plv,T_plv1_u(ceil(N/2),:),'-*')
title('Diagramma del Taglio per sistema unitario (u)')

figure(13)
plot(ds_plv,N_s_plv1_u(ceil(N/2),:),'-*')
title('Diagramma dello Sforzo Normale per sistema
    unitario (u)')

figure(14)
plot(x_disc,y_disc,'b-*',x_disc,y_spost,'r-*')
title('Deformata sotto carico arco a tre cerniere')


%% Calcolo soluzione iperstatica
clc

%Divido l'arco in due semiarchi ed inserisco in ognuno
     una coppia
%concentrata all'estremita' libera di verso opposto e
    congruente con la
%convenzione posistiva del momento.

%calcolo reazioni vincolari verticali
Vb_ip_1=0;
Va_ip_1=0;
```

```
%calcolo reazioni vincolari orizzontali
Ha_ip_1=-1/r;
Hb_ip_1=1/r;

%calcolo caratteristiche di sollecitazione
%Momento
    for J=1:length(x_plv)-2
        M_ip_1(J)=-Ha_ip_1*y_plv(J+1); %le J indicano
           le colonne e salvano i valori per ogni
           sezione dell'arco in x_disc, le k sono le
           righe che indicano il variare della forza
           unitaria nelle x_int
    end

     M_ip1_1=[0,M_ip_1,0];

figure(15)
plot(ds_plv,M_ip1_1,'-*')
title('Diagramma del Momento flettente per sistema
   unitario (1)')

%Sforzo di taglio

    for J=1:length(x_plv)-1
        T_ip_1(J)=-Ha_ip_1*sin(phi_plv(J+1));
    end

    T_ip1_1=[-Ha_ip_1,T_ip_1];

figure(16)
plot(ds_plv,T_ip1_1,'-*')
title('Diagramma del Taglio per sistema unitario (1)')

%Sforzo normale

    for J=1:length(x_plv)-1
        N_s_ip_1(J)=-Ha_ip_1*cos(phi_plv(J+1));
    end

    N_s_ip1_1=[-Va_ip_1,N_s_ip_1];

figure(17)
plot(ds_plv,N_s_ip1_1,'-*')
title('Diagramma dello Sforzo Normale per sistema
   unitario (1)')

% Calcolo (M(0)*M(1))/EI
```

```
%  calcolo il numeratore della frazione per trovare l'
   incognita
%  iperstatica X, simila a formula 5.43 in calcolo
   spostamenti
%  iperstatiche 05 di fondamenti di mecchanica
   strutturale

for J=1:length(ds_disc)-2 %tolgo due casi di cui uno
   presente su un semi intervallo iniziale e l'altro
   sul semi intervallo finale
    caso=j_is(end,J+1);

    % Contributo PLV Momento
    w_M=d_ds_plv(1)/(2*D_cnu(caso))*[1; 2; 1];
    It_ip_M_num(J)=[M_plv_r(2+(J-1)*2)*M_ip1_1(2+(J-1)
       *2) M_plv_r(3+(J-1)*2)*M_ip1_1(3+(J-1)*2)
       M_plv_r(4+(J-1)*2)*M_ip1_1(4+(J-1)*2)]*w_M;

    % Contributo PLV Taglio
    w_T=d_ds_plv(1)/(2*5/6*At_nu)*[1; 2; 1];
    It_ip_T_num(J)=[T_plv_r(2+(J-1)*2)*T_ip1_1(2+(J-1)
       *2) T_plv_r(3+(J-1)*2)*T_ip1_1(3+(J-1)*2)
       T_plv_r(4+(J-1)*2)*T_ip1_1(4+(J-1)*2)]*w_T;

    % Contributo PLV Sforzo Normale
    w_N_s=d_ds_plv(1)/(2*A_cnu(caso))*[1; 2; 1];
    It_ip_N_s_num(J)=[N_s_plv_r(2+(J-1)*2)*N_s_ip1_1
       (2+(J-1)*2) N_s_plv_r(3+(J-1)*2)*N_s_ip1_1(3+(J
       -1)*2) N_s_plv_r(4+(J-1)*2)*N_s_ip1_1(4+(J-1)
       *2)]*w_N_s;

end

% Contributo PLV Momento
wi_M=d_ds_plv(1)/(2*D_cnu(j_is(end,1)))*[1; 1];
It_iM_ip_num=[M_plv_r(1)*M_ip1_1(1) M_plv_r(2)*M_ip1_1
   (2)]*wi_M;

wf_M=d_ds_plv(1)/(2*D_cnu(j_is(end,end)))*[1; 1];
It_fM_ip_num=[M_plv_r(end-1)*M_ip1_1(end-1) M_plv_r(
   end)*M_ip1_1(end)]*wf_M;

% Contributo PLV Taglio
wi_T=d_ds_plv(1)/(2*5/6*At_nu)*[1; 1];
It_iT_ip_num=[T_plv_r(1)*T_ip1_1(1) T_plv_r(2)*T_ip1_1
   (2)]*wi_T;

wf_T=d_ds_plv(1)/(2*5/6*At_nu)*[1; 1];
It_fT_ip_num=[T_plv_r(end-1)*T_ip1_1(end-1) T_plv_r(
   end)*T_ip1_1(end)]*wf_T;
```

```
% Contributo PLV Sforzo Normale
wi_N_s=d_ds_plv(1)/(2*A_cnu(j_is(end,1)))*[1; 1];
It_iN_s_ip_num=[N_s_plv_r(1)*N_s_ip1_1(1) N_s_plv_r(2)
   *N_s_ip1_1(2)]*wi_N_s;

wf_N_s=d_ds_plv(1)/(2*A_cnu(j_is(end,end)))*[1; 1];
It_fN_s_ip_num=[N_s_plv_r(end-1)*N_s_ip1_1(end-1)
   N_s_plv_r(end)*N_s_ip1_1(end)]*wf_N_s;


It_tot_M_ip_num=sum([It_iM_ip_num   It_ip_M_num
   It_fM_ip_num]);
It_tot_T_ip_num=sum([It_iT_ip_num   It_ip_T_num
   It_fT_ip_num]);
It_tot_N_s_ip_num=sum([It_iN_s_ip_num   It_ip_N_s_num
     It_fN_s_ip_num]);

%calcolo di quanto e' la percentuale dello spostamento
    dovuta al taglio
%rispetto al momento preso come 100%
perc_contributo_taglio_num=It_tot_M_ip_num/100*
   It_tot_T_ip_num;

It_tot_ip_num=sum([It_tot_M_ip_num It_tot_T_ip_num
   It_tot_N_s_ip_num],2);



%  calcolo il denominatore della frazione per trovare
   l'incognita iperstatica X
for J=1:length(ds_disc)-2 %tolgo due casi di cui uno
   presente su un semi intervallo iniziale e l'altro
   sul semi intervallo finale
    caso=j_is(end,J+1);

    % Contributo PLV Momento
    w_M=d_ds_plv(1)/(2*D_cnu(caso))*[1; 2; 1];
    It_ip_M_den(J)=[M_ip1_1(2+(J-1)*2)*M_ip1_1(2+(J-1)
       *2) M_ip1_1(3+(J-1)*2)*M_ip1_1(3+(J-1)*2)
       M_ip1_1(4+(J-1)*2)*M_ip1_1(4+(J-1)*2)]*w_M;

    % Contributo PLV Taglio
    w_T=d_ds_plv(1)/(2*5/6*At_nu)*[1; 2; 1];
    It_ip_T_den(J)=[T_ip1_1(2+(J-1)*2)*T_ip1_1(2+(J-1)
       *2) T_ip1_1(3+(J-1)*2)*T_ip1_1(3+(J-1)*2)
       T_ip1_1(4+(J-1)*2)*T_ip1_1(4+(J-1)*2)]*w_T;

    % Contributo PLV Sforzo Normale
    w_N_s=d_ds_plv(1)/(2*A_cnu(caso))*[1; 2; 1];
```

```
    It_ip_N_s_den(J)=[N_s_ip1_1(2+(J-1)*2)*N_s_ip1_1
       (2+(J-1)*2) N_s_ip1_1(3+(J-1)*2)*N_s_ip1_1(3+(J
       -1)*2) N_s_ip1_1(4+(J-1)*2)*N_s_ip1_1(4+(J-1)
       *2)]*w_N_s;

end

% Contributo PLV Momento
wi_M=d_ds_plv(1)/(2*D_cnu(j_is(end,1)))*[1; 1];
It_iM_ip_den=[M_ip1_1(1)*M_ip1_1(1) M_ip1_1(2)*M_ip1_1
   (2)]*wi_M;

wf_M=d_ds_plv(1)/(2*D_cnu(j_is(end,end)))*[1; 1];
It_fM_ip_den=[M_ip1_1(end-1)*M_ip1_1(end-1) M_ip1_1(
   end)*M_ip1_1(end)]*wf_M;

% Contributo PLV Taglio
wi_T=d_ds_plv(1)/(2*5/6*At_nu)*[1; 1];
It_iT_ip_den=[T_ip1_1(1)*T_ip1_1(1) T_ip1_1(2)*T_ip1_1
   (2)]*wi_T;

wf_T=d_ds_plv(1)/(2*5/6*At_nu)*[1; 1];
It_fT_ip_den=[T_ip1_1(end-1)*T_ip1_1(end-1) T_ip1_1(
   end)*T_ip1_1(end)]*wf_T;

% Contributo PLV Sforzo Normale
wi_N_s=d_ds_plv(1)/(2*A_cnu(j_is(end,1)))*[1; 1];
It_iN_s_ip_den=[N_s_ip1_1(1)*N_s_ip1_1(1) N_s_ip1_1(2)
   *N_s_ip1_1(2)]*wi_N_s;

wf_N_s=d_ds_plv(1)/(2*A_cnu(j_is(end,end)))*[1; 1];
It_fN_s_ip_den=[N_s_ip1_1(end-1)*N_s_ip1_1(end-1)
   N_s_ip1_1(end)*N_s_ip1_1(end)]*wf_N_s;


It_tot_M_ip_den=sum([It_iM_ip_den   It_ip_M_den
   It_fM_ip_den]);
It_tot_T_ip_den=sum([It_iT_ip_den   It_ip_T_den
   It_fT_ip_den]);
It_tot_N_s_ip_den=sum([It_iN_s_ip_den   It_ip_N_s_den
     It_fN_s_ip_den]);

perc_contributo_taglio_den=It_tot_M_ip_den/100*
   It_tot_T_ip_den;

It_tot_ip_den=sum([It_tot_M_ip_den It_tot_T_ip_den
   It_tot_N_s_ip_den],2);

X=-It_tot_ip_num/It_tot_ip_den;
```

```
% calcolo delle reazioni vincolari della travatura
    iperstatica attraverso
% la relazione Ha=Ha(0)+X*Ha(1)

%reazioni vincolari vericali
Vb_ip=Vb+X*Vb_ip_1;
Va_ip=Va+X*Va_ip_1;

%reazioni vincolari orizzontali
Ha_ip=Ha+X*Ha_ip_1;
Hb_ip=Hb+X*Hb_ip_1;

%diagramma momento flettente
M_ip=M_plv_r+X*M_ip1_1;

figure(18)
plot(ds_plv,M_ip,'-*')
title('Diagramma del Momento flettente per arco a due
    cerniere')

%diagramma taglio
T_ip=T_plv_r+X*T_ip1_1;

figure(19)
plot(ds_plv,T_ip,'-*')
title('Diagramma del taglio per arco a due cerniere')

%diagramma di sforzo normale
N_s_ip=N_s_plv_r+X*N_s_ip1_1;

figure(20)
plot(ds_plv,N_s_ip,'-*')
title('Diagramma dello sforzo normale per arco a due
    cerniere')


%% Calcolo delle sigma nell'arco iperstatico a due
    cerniere
clc

% epsilon e sigma e' diversa dalla precedente. Ora si
    ha x nella direzione
% dell'asse della trave, y entrante nel foglio e z
    rivolta verso l'alto. Ne
% consegue che se il momento prima era negativo, per
    avere lo stesso
% effetto ora deve essere positivo, lo sforzo normale
    rimane invariato in
% questoa nuova convenzione.
```

```
N_s_es_ip=N_s_ip(1:2:end);
M_es_ip=-M_ip(1:2:end);

hs_f=flipud(hs);
theta_f=flipud(theta);
E_L_f=flipud(E_L); %le colonne identificano i casi
    mentre le righe i moduli elastici assunti dai
    materiali nel caso considerato, strato superiore
    prime 4 colonne carbonio, poi dyneema, foam sempre
    su 5 riga, faccia inferiore dyneema per prime 4
    colonne poi carbonio
E_T_f=flipud(E_T);
G_LT_f=flipud(G_LT);
ni_LT_f=flipud(ni_LT);
ni_TL_f=flipud(ni_TL);

hs_es=zeros(size(hs_f,1)+size(hs_f,1)-2,size(hs_f,2));
     %posizione degli strati per calcolo delle epsilo e
     sigma
hs_es([1 3:2:end-1 end],:)=hs_f;
hs_es(2:2:end-2,:)=hs_f(2:end-1,:);
Qk1_1_es=zeros(size(hs_f,1)+size(hs_f,1)-2,1);
Aree=[hst_1' hst_1' hst_1' hst_1' hst_2' hst_2' hst_2'
     hst_2']*b;
hs_fmedia=(hs_f(1:end-1,:)+hs_f(2:end,:))/2;

toll_sigma=10^1; %tolleranza minima voluta tra la
    somma di tutti i valori delle sigma sommate tra di
    loro al ciclo precedente con quelle del ciclo
    appena effettuato
t_it_max=3; %numero di cicli massimo che si vuole
    avere nel ciclo di calcolo dei casi, epsilon e
    sigma
% j_ip=1*ones(1,length(x_disc)); %compilando j
    assumera sulle colonne indicate da k, il caso che
    la stazione assumera' alla prossima iterazione e
    sulle righe i valori assunti da j nelle varie
    iterazioni

flag=0; %NON TOCCARE QUESTI VALORI
% flag_rib_ip=zeros(1,length(x_disc)); %NON TOCCARE
    QUESTI VALORI flag relativo al ribaltamento di ogni
     sezione, se assume valore uno l'ordine dei
    materiali e' stato ribaltato
t=1;    %NON TOCCARE QUESTI VALORI
sigma_old=zeros(size(hs_es,1),length(x_disc)); %NON
    TOCCARE QUESTI VALORI
```

```
% ciclo che gestisce il calcolo in modo iterativo dei
   casi effettivi in cui
% lavora il materiale, le epsilon e le sigma in esso
   secondo il modello
% della trave di timoshenko
% while t<t_it_max+1 && flag==0
while t<t_it_max+1 && flag==0

for x=1:length(x_disc)
Mat=[A_nu(j_ip(t,x)) B_nu(j_ip(t,x))
     B_nu(j_ip(t,x)) D_nu(j_ip(t,x))]; %matrice
Car=[N_s_es_ip(x) M_es_ip(x)]'; %vettore dei carichi
   nel punto della discretizzazione
epsilon_0k_ip(:,x)=Mat\Car; %vettore con epsilon_0 e
   la curvatura k

%k come indice per il ciclo indica il punto in cui il
   ciclo sta calcolando
%gli stress, cioe' i punti scritti come x_disc

epsilon_ip(:,x)=epsilon_0k_ip(1,x)+hs_es(:,j_ip(t,x))
   .*epsilon_0k_ip(2,x);

Qk1_1=zeros(size(theta_f,1),1);

for z=1:size(theta_f,1)
Qp1_es=[E_L_f(z,j_ip(t,x))/(1-ni_LT_f(z,j_ip(t,x))*
   ni_TL_f(z,j_ip(t,x)))       ni_LT_f(z,j_ip(t,x))*
   E_T_f(z,j_ip(t,x))/(1-ni_LT_f(z,j_ip(t,x))*ni_TL_f(
   z,j_ip(t,x)))    0
    ni_LT_f(z,j_ip(t,x))*E_T_f(z,j_ip(t,x))/(1-ni_LT_f
       (z,j_ip(t,x))*ni_TL_f(z,j_ip(t,x)))     E_T_f(z
       ,j_ip(t,x))/(1-ni_LT_f(z,j_ip(t,x))*ni_TL_f(z,
       j_ip(t,x)))      0
            0                          0
               G_LT_f(z,j_ip(t,x))];

lambda_k1_es=[   (cos(theta_f(z,j_ip(t,x))))^2       (
   sin(theta_f(z,j_ip(t,x))))^2           2*cos(
   theta_f(z,j_ip(t,x)))*sin(theta_f(z,j_ip(t,x)))
            (sin(theta_f(z,j_ip(t,x))))^2       (cos(
               theta_f(z,j_ip(t,x))))^2          -2*
               cos(theta_f(z,j_ip(t,x)))*sin(theta_f(z
               ,j_ip(t,x)))
         -cos(theta_f(z,j_ip(t,x)))*sin(theta_f(z,j_ip
            (t,x)))  cos(theta_f(z,j_ip(t,x)))*sin(
            theta_f(z,j_ip(t,x)))  (cos(theta_f(z,j_ip
            (t,x))))^2-(sin(theta_f(z,j_ip(t,x))))^2];

Qk1_es= inv(lambda_k1_es)*Qp1_es*(inv(lambda_k1_es))';
```

```
Qk1_1(z,1)=Qk1_es(1,1);

end

Qk1_1_es(1:2:end-1,1)=Qk1_1;  % Qk1_1 modificata per
   poter essere moltiplicata alle epsilon che nascono
   dal vettore hs_es cioe' epsilon modificato che le
   posizioni intermedie duplicate per fare la media
   delle sigma.
Qk1_1_es(2:2:end,1)=Qk1_1;

sigma_ip(:,x)=epsilon_ip(:,x).*Qk1_1_es;
sigma_m_ip(:,x)=(sigma_ip(1:2:end-1,x)+sigma_ip(2:2:
   end,x))/2; %calcolo delle sigma medie a coppie

if flag_rib_ip==0
sigma_mm_ip(1,x)=(sigma_m_ip(1,x)+sigma_m_ip(length(
   theta_c),x))/2; % calcolo delle sigma medie a
   coppie delle coppie per ciclo di if
sigma_mm_ip(2,x)=(sigma_m_ip(end,x)+sigma_m_ip(end-
   length(theta_d)+1,x))/2;
else
sigma_mm_ip(1,x)=(sigma_m_ip(1,x)+sigma_m_ip(length(
   theta_d),x))/2; % calcolo delle sigma medie a
   coppie delle coppie per ciclo di if
sigma_mm_ip(2,x)=(sigma_m_ip(end,x)+sigma_m_ip(end-
   length(theta_c)+1,x))/2;
end

N_strati_ip(:,x)=sigma_m_ip(:,x).*Aree(:,j_ip(t,x));
N_ris_ip=sum(N_strati_ip,1);
N_err_ip(t,x)=abs(N_s_es_ip(x)-N_ris_ip(x));

M_strati_ip(:,x)=sigma_m_ip(:,x).*Aree(:,j_ip(t,x)).*
   hs_fmedia(:,j_ip(t,x));
M_ris_ip=sum(M_strati_ip,1);
M_err_ip(t,x)=abs(M_es_ip(x)-M_ris_ip(x));

if sigma_mm_ip(1,x)>=0 && sigma_mm_ip(2,x)>=0
    if flag_rib_ip(x)==0
       j_ip(t+1,x)=1;
    else
       j_ip(t+1,x)=5;
    end
else
    if sigma_mm_ip(1,x)<0 && sigma_mm_ip(2,x)>0
        if flag_rib_ip(x)==0
           j_ip(t+1,x)=2;
        else
           j_ip(t+1,x)=7;
```

```
        end
    else
        if sigma_mm_ip(1,x)>0 && sigma_mm_ip(2,x)<0
            if flag_rib_ip(x)==0
               j_ip(t+1,x)=3;
            else
               j_ip(t+1,x)=6;
            end
        else
            if sigma_mm_ip(1,x)<=0 && sigma_mm_ip(2,x)
               <=0
               if flag_rib_ip(x)==0
                   j_ip(t+1,x)=4;
                else
                   j_ip(t+1,x)=8;
                end
            else
            end
        end
    end
end

end

    if abs(sum(sum(sigma_ip,1),2)-sum(sum(sigma_old)
       ,2))>toll_sigma
       t=t+1;
       sigma_old=sigma_ip;
    else
        flag=1; %il flag=1 fa uscire fuori dal ciclo,
           indica cioe' quando si e' raggiunto il
           livello di accuratezza voluto
        t=t+1;
    end

end


% j_old_ip
% j_ip
% N_err_ip
% M_err_ip
% epsilon_0k_ip
% sigma_ip
% flag
% flag_rib_ip

%% Calcolo spostamento dell'iperstatica
% come sistema reale prendo l'arco a due cerniere gia'
    risolto in precedenza
```

```
% in quanto iperstatico, mentre come sistema u il
    sistema di carichi
% unitari gia' utilizzato per calcolare lo spostamento
    dell'arco a tre
% cerniere.

% In primo luogo, il sistema (r) e' iperstatico per
    cui va risolto a sua volta mediante il PLV per
    ottenere le
% relative caratteristiche di sollecitazione. Quanto
    al sistema (u), a rigore anche questo dovrebbe
    essere
% iperstatico dato che ha gli stessi vincoli del
    sistema (r) ma un solo carico unitario
    corrispondente allo
% spostamento incognito. Va pero' ricordato che nella
    (5.7) il sistema (u)
% e' quello fittizio per cui e' necessario che sia
    solo equilibrato e non necessariamente congruente.
% Per (u) si puo' allora scegliere  una condizione di
    vincolo non reale ma piu'
% semplice e isostatica, per esempio eliminando
    proprio il vincolo sovrabbondante

for k=1:length(ds_disc)

% Calcolo del plv
    % la sigla che accompagna tutte le variabili '
       ip_sp' significa 'iperstatica_spostamento'
for J=1:length(ds_disc)-2
    caso=j_ip(end,J+1);

    % Contributo PLV Momento
    w_M=d_ds_plv(1)/(2*D_cnu(caso))*[1; 2; 1];
    It_M_ip_sp(k,J)=[M_ip(2+(J-1)*2)*M_plv1_u(k,2+(J
       -1)*2) M_ip(3+(J-1)*2)*M_plv1_u(k,3+(J-1)*2)
       M_ip(4+(J-1)*2)*M_plv1_u(k,4+(J-1)*2)]*w_M;

    % Contributo PLV Taglio
    w_T=d_ds_plv(1)/(2*5/6*At_nu)*[1; 2; 1];
    It_T_ip_sp(k,J)=[T_ip(2+(J-1)*2)*T_plv1_u(k,2+(J
       -1)*2) T_ip(3+(J-1)*2)*T_plv1_u(k,3+(J-1)*2)
       T_ip(4+(J-1)*2)*T_plv1_u(k,4+(J-1)*2)]*w_T;

    % Contributo PLV Sforzo Normale
    w_N_s=d_ds_plv(1)/(2*A_cnu(caso))*[1; 2; 1];
    It_N_s_ip_sp(k,J)=[N_s_ip(2+(J-1)*2)*N_s_plv1_u(k
       ,2+(J-1)*2) N_s_ip(3+(J-1)*2)*N_s_plv1_u(k,3+(J
       -1)*2) N_s_ip(4+(J-1)*2)*N_s_plv1_u(k,4+(J-1)
       *2)]*w_N_s;
```

```
end

    % Contributo PLV Momento
    wi_M=d_ds_plv(1)/(2*D_cnu(j_ip(end,1)))*[1; 1];
    It_iM_ip_sp(k,1)=[M_ip(1)*M_plv1_u(k,1) M_ip(2)*
        M_plv1_u(k,2)]*wi_M;

    wf_M=d_ds_plv(1)/(2*D_cnu(j_ip(end,end)))*[1; 1];
    It_fM_ip_sp(k,1)=[M_ip(end-1)*M_plv1_u(k,end-1)
        M_ip(end)*M_plv1_u(k,end)]*wf_M;

    % Contributo PLV Taglio
    wi_T=d_ds_plv(1)/(2*5/6*At_nu)*[1; 1];
    It_iT_ip_sp(k,1)=[T_ip(1)*T_plv1_u(k,1) T_ip(2)*
        T_plv1_u(k,2)]*wi_T;

    wf_T=d_ds_plv(1)/(2*5/6*At_nu)*[1; 1];
    It_fT_ip_sp(k,1)=[T_ip(end-1)*T_plv1_u(k,end-1)
        T_ip(end)*T_plv1_u(k,end)]*wf_T;

    % Contributo PLV Sforzo Normale
    wi_N_s=d_ds_plv(1)/(2*A_cnu(j_ip(end,1)))*[1; 1];
    It_iN_s_ip_sp(k,1)=[N_s_ip(1)*N_s_plv1_u(k,1)
        N_s_ip(2)*N_s_plv1_u(k,2)]*wi_N_s;

    wf_N_s=d_ds_plv(1)/(2*A_cnu(j_ip(end,end)))*[1;
        1];
    It_fN_s_ip_sp(k,1)=[N_s_ip(end-1)*N_s_plv1_u(k,end
        -1) N_s_ip(end)*N_s_plv1_u(k,end)]*wf_N_s;


    It_tot_M_ip_sp(k,1)=sum([It_iM_ip_sp(k,1)
        It_M_ip_sp(k,:) It_fM_ip_sp(k,1)]);
    It_tot_T_ip_sp(k,1)=sum([It_iT_ip_sp(k,1)
        It_T_ip_sp(k,:) It_fT_ip_sp(k,1)]);
    It_tot_N_s_ip_sp(k,1)=sum([It_iN_s_ip_sp(k,1)
        It_N_s_ip_sp(k,:) It_fN_s_ip_sp(k,1)]);

end

It_tot_M_ip_sp
It_tot_T_ip_sp
It_tot_N_s_ip_sp

%calcolo di quanto e' la percentuale dello spostamento
    dovuta al taglio
%rispetto al momento preso come 100%
perc_contributo_taglio_ip_sp=max(It_tot_M_ip_sp)/100*
   max(It_tot_T_ip_sp);
```

```
It_tot_ip_sp=sum([It_tot_M_ip_sp It_tot_T_ip_sp
   It_tot_N_s_ip_sp],2);
y_spost_ip=y_disc-It_tot_ip_sp';


figure(21)
plot(x_disc,y_disc,'b-*',x_disc,y_spost_ip,'r-*')
title('Deformata sotto carico arco a due cerniere')
```

Bibliography

[1] F. Ruess, J. Schaenzlin, and H. Benaroya. "Structural Design of a Lunar Habitat.

[2] Schrunk, D. G. (2002). “The Moon: Optimum location for the first industrial scientific base in space.” SPACE 02, ASCE, Reston, Va., 122–128.

[3] Chua, K. M., Yuan, Z., and Johnson, S. W. (1990). “Foundation design of a large diameter radio telescope on the Moon.” SPACE 90, ASCE, Reston, Va., 707–716.

[4] GRANT H. HEIKEN, DAVID T. VANIMAN, BEVAN M. FRENCH. "LUNAR SOURCEBOOK A. User's Guide to the Moon"

[5] Gani B. Ganapathi, Joseph Ferrall, P. K. Seshan. "Lunar Base Habitat Designs: Characterizing the Environment, and Selecting Habitat Designs for Future Trade-offs"

[6] Langseth M. G. Jr., Keihm S. J., and Chute J. L. Jr. (1973) Heat-flow experiment. In Apollo 17 Preliminary Science Report, pp. 9–1 to 9–24. NASA SP-330.

[7] Dalton, C. and Hoffman, E. (1972) "Conceptual Design of a Lunar Colony" NASA Grant Rpt. NGT 44-005-114, NASA, Washington, D.C.

[8] Wikipedia. Internal structure of the Moon

[9] Vondrak, R.R. (1974) "Creation of an Artificial Lunar Atmosphere", Nature, 248, pp. 657-659.

[10] Gurtler C. A. and Grew G. W. (1968). "Meteoroid hazard near Moon". Science, 161, 462–464.

[11] Fechtig H., Hartung J. B., Nagel K., Neukum G., and Storzer D. (1974) "Lunar microcrater studies, derived meteoroid fluxes, and comparison with satellite-borne experiments." Proc. Lunar Sci. Conf. 5th, pp. 2463–2474.

[12] Zook H. A. and Berg O. E. (1975) A source for hyperbolic cosmic dust particles. Planet. Space Sci., 23, 183–203.

[13] Oberst J. and Nakamura Y. (1986) "Distinct meteoroid families identified on the lunar seismograms." Proc. Lunar Planet. Sci. Conf. 17th, in J. Geophys. Res., 91, E769–E773.

[14] Zook H. A. (1975) "The state of meteoritic material on the Moon." Proc. Lunar Sci. Conf.6th, pp. 1653–1672.

[15] Feldman W. C., Ashbridge J. R., Bame S. J., and Gosling J. T. (1977) "Plasma and magnetic fields from the Sun. In The Solar Output and its Variation" (O. R White, ed.), pp. 351− 382. Colorado Assoc. Univ., Boulder.

[16] McGuire R. E., von Rosenvinge T. T., and McDonald F. B. (1986) "The composition of solar energetic particles." Astrophys. J., 301, 938–961.

[17] Pomerantz M. A. and Duggal S. P. (1974) "The sun and cosmic rays". Rev. Geophys. Space Phys., 12, 343–361.

[18] Stafford, T.P. (1991) "America at the Threshold: Report of the Synthesis Group on America's Space Exploration Initiative", NASA, Washington, D.C.

[19] Cohen MM, Benaroya H. "Lunar-base structures." In: Howe AS, Sherwood B, editors. Out of this world, the new field of space architecture. AIAA; 2009.

[20] Claudia Sicignano, "Le strutture Tensegrali e la loro applicazione in Architettura"

[21] Haym Benaroya. "Lunar habitats: A brief overview of issues and concepts"

[22] Stuster J. W (1986) "Space Station Habitability Recommendations Based on a Systematic Comparative Analysts of Analogous Conditions." NASA CR-3943. NASA, Washington, DC. 209 pp.

[23] Kriss J. Kennedy, R.A., TX NASA Johnson Space Center, "Lessons from TransHab, AN ARCHITECT'S EXPERIENCE"

[24] "PAGEOS", https://en.wikipedia.org/wiki/PAGEOS

[25] Wikipedia. "TransHab".

[26] Wikipedia. "The Whipple shield".

[27] Wikipedia. "Bigelow Expandable Activity Module".

[28] Haym Benaroya. "Lunar habitats: A brief overview of issues and concepts"

[29] https://volcanoes.usgs.gov/

[30] Internal structure of the Moon

[31] Blair DM, Chappaz L, Sood R, Milbury C, Melosh HJ, Howell KC, Freed AM. "Determining the structural stability of lunar lava tubes." In: 46th Lunar and Planetary Science Conference; 2015, 2174.pdf.

[32] Burke, J.D. (1985) "Merits of a Lunar Pole Base Location", In Lunar Bases and Space Activities in the 21st. Century, ed. Mendell, W.W., Lunar and Planetary Institute, Houston, TX, p. 77-84.

[33] https://earthsky.org/space/nasa-moon-announcement-monday-october-26-2020-sofia

[34] Roberts. "INFLATABLE HABITATION FOR THE LUNAR BASE". NASAJobnson Space Center Houston TX 77058

[35] Kriss Kennedy. "Horizontal inflatable habitat for SEI"

[36] W. D. Hypes, A. J. Butterfield, C. B. King, G. D. Qualls, W. T. Davis, M. J. Gould, J. E. Nealy, L. C. Simonsen. "CONCEPTS FOR MANNED LUNAR HABITATS". NASA Technical Memorandum 1041.

[37] Harrison, R.A. (1992) "Cylindrical Fabric-Confined Soil Structures", In Engineering, Construction, and Operations in Space III: Proceedings of the Third International Conference,

[38] Benaroya, H., and Ettouney, M. (1992a). “Framework for evaluation of lunar base concepts.” J. Aerosp. Eng., 5(2), 187–198.

[39] Sandra Häuplik-Meusburger, Kürsad Özdemir. "Deployable Lunar Habitation Design"

[40] Bialla, P., Nottke, N., Suzuki, S. (1992) "Genesis : The Creation of a Lunar Base" In Engineering, Construction, and Operations in Space III: Proceedings of the Third International Conference, ed. Sadeh, W.Z., Sture, S., and Miller, R.J., pp. 13-24.

[41] Cliffton, E.W. (1990) "A Fused Regolith Structure", In Engineerinq, Construction, and Operations in Space II: Proceedings of the Second International Conference, ed. Johnson, S.W., Wetzel, J.P., pp. 541-550.

[42] Daga, A.W., Daga, M.A., Wendel, W.R. (1992) "Evolving Concepts of Lunar Architecture: The Potential of Subselene Development" In The Second Conference on Lunar Bases and Space Activities of the 21st. Century, NASA Conference Publication 3166, Vol. i.

[43] John E. Nealy, John W. Wilson, Lawrence W. Townsend. "Solar-Flare Shielding With Regolith at a Lunar-Base Site". Langley Research Center Hampton, Virginia Information

[44] Wilson, John W.; Townsend, Lawrence W.; Chun, Sang Y.; Buck, Warren W.; Khan, Ferdous; and Cucinotta, Frank: "BRYNTRN: A Baryon Transport Computer Code Computation Procedures and Data Base". NASA TM-4037, 1988.

[45] Svestka, "Zdenek: Solar Flares". chapter V. D. Reidel Publ. Co., Inc., c. 1976.

[46] Interaction Depth https://www2.lbl.gov/abc/cosmic/SKliewer/Cosmic Rays/Interaction.htm

[47] NASA-STS-3000, Volume I - Man-Systems Integration Standards, Architecture, Envelope Geometry for Crew Functions.

[48] MADFLEX SAMPLE BOOK, Composite Research s.r.l. Turin, Italy

[49] Achilles Petras Robinson College Cambridge, "Design of Sandwich Structures"

[50] Kriss Kennedy,"Lunar Architecture Team: Phase 2 Habitat Volume Estimation: "Caution When Using Analogs" ".

[51] Kira Bacal, MD, PhD, MPH, "III.1.2 Cabin Environment and EVA Environment"

[52] United States Patent, Patent No .: US 10,583,638 B2, Date of Patent : Mar. 10 , 2020, "PANEL MADE OF COMPOSITE MATERIAL HAVING A LAYERED STRUCTURE"

[53] Linus Fagerberg, "Wrinkling in sandwich panels for marine applications"

[54] "Space Launch System", https://en.wikipedia.org/wiki/Space Launch System

[55] Sharon Jefferies, Tim Collins, Alicia Dwyer Cianciolo, Tara Polsgrove, "Impacts of Launch Vehicle Fairing Size on Human Exploration Architectures"

[56] https://www.nasa.gov/exploration/systems/sls/overview.html

[57] Space engineering, "Environmental control and life support, ECLS"

[58] Igor A. Karnovsky, "Theory of Arched Structures. Strength, Stability, Vibration"

[59] Marco Gherlone, Polytechnic of Turin, Lecture notes of the course "Fundamentals of structural mechanics"

[60] Marco Di Sciuva, Marco Gherlone, Polytechnic of Turin, Lecture notes of the course "Aircraft structures"

[61] Delta Preg CatalogA4_2017Feb_carbonio

[62] Rohacell, https://www.rohacell.com/sites/lists/re/documentshp/rohacell%20wf%20product%20information.pdf

[63] Dyneema_Folder_201611_Gruschwitz_97593

This page intentionally left blank

Acknowledgements

I would like to dedicate this last page of my thesis to those who helped and supported me during this challenging and exciting period of my life.

My heartfelt thanks to my family, not only for their support during the writing process, but also for all the days spent together and especially for giving me the possibility to reach this great achievement. I would like to mention each one of them individually in order to link them forever to this work. Their names are: M. Cumino, M. Padovani, S. Cumino, E. Cumino, R. Padovani, O. Saviane, L. Padovani, B. Bonaudo and D. Cumino.

All my gratitude goes to the Prof. G. Frulla and the Prof. E. Cestino for their constant help even in the most difficult moments.

I must express my gratitude to E. Fossat and N. Giulietti - inventors of the MadFlex and founders of the start-up Composite Research (CoRe) - for giving me the chance to share their dream about the development of deployable habitats.

I also wish to express my deepest gratitude to Alessio Piccolo for all the FEM analyses reported in this work and for sharing with me the hardest moments during this period.

I would like to pay my special regards to C. Bocca, S. Benevenuta, M. Bertocchi, A. Elia, L. Gamerro, E. Cumino, C. Gallo and last but not least S. D'ippolito for their essential help in the correction of this work.

I wish to thank S. Cumino for the drawings in Chapter 8.

Lastly, I would like to acknowledge the community of families "Il filo d'erba" located in Rivalta (To) for their hospitality, and thanks also to my housemates, N. Tassinari and A. Boran in this new adventure, and all of my friends as I could not have completed this dissertation without their support.

Rivalta (To), 7/12/2020.

This page intentionally left blank